Epithelial-mesenchymal interactions in the cornea – development of a novel 3D culture cornea model and progress towards environmental reprogramming of cornea epithelium

Arianna Bianchi

PhD Thesis

Institute of Genetic Medicine

Newcastle University

March 2015

Acknowledgments

First of all I would like to express my special appreciation and gratitude to my supervisor Professor Colin Jahoda, for his time, patience and guidance throughout my PhD, and for inspiring me with creative, new ideas. His advice and teaching have been extremely valuable.

Also I would like to thank my supervisors Professor Majlinda Lako and Professor Helen Arthur for their help and advice and Dr. Sajjad Ahmad for giving me the opportunity to start this PhD in the first place and for his help and support during my first PhD year.

My colleagues at Durham University: Hilary Prescott, Rebecca Lamb, Dr. Mathilde Roger, Dr. Craig Manning and Dr. Aaron Gardner, for their advice, help and friendship.

The IGM colleagues: Dr. Lyle Armstrong, Dr. Oliver Baylis, Dr. Joseph Collin, Dr. Carla Mellough, Dr. Charles Osei-Bempong, Dr. Juliane Muller and Fabio D'Agostino for all their help and support while working in Newcastle.

And last but not least, I would like to thank Cyril Testeniere for his love, patience and support, and a particular big loving thank you goes to my family who has always encouraged and supported me in undertaking my studies and in believing in me. I could not have done it without you!

Abstract

The unmet need for corneal epithelial cells for treating human eye diseases makes the cornea important in the cell therapy field. Additionally cornea tissue engineering has become valuable for clinical use, research, and for creating representative models replacing animals for chemical/drug testing.

This study initially used qPCR to investigate the expression levels of key markers produced by 2D corneal epithelial cell cultures after wounding in a scratch assay. Then an attempt was made to environmentally reprogram human hair follicle keratinocytes into corneal epithelial cells using limbal epithelial stem cell media. Immunohistochemical and qPCR analysis revealed no changes in signature genes but rather a similarity between HFC and LSC's when cultured in LSC's culture conditions.

Attention then focused on developing a novel three-dimensional bilayered spheroid cornea model using hanging drop culture. It is widely accepted that cells in 3D culture more closely mimic their *in vivo* counterparts than 2D cultures, and qPCR and immunofluorescence analysis of 3D spheroids made from cultured rabbit corneal stromal cells revealed that they partially reverted back to a quiescent *in vivo* phenotype. Coating the spheroids with cultured rabbit limbal epithelial cells produced a bilayered model of the cornea. Multiple iterations were produced incorporating variations in media and cell origin, leading to a cornea model that could be maintained for 10 days, expressed appropriate cytokeratins and other corneal markers including Pax6 and that, upregulated the expression of key cornea signature proteins including Aldh1a1 as a result of epithelial-mesenchymal interactions. Preliminary versions of a human bilayered cornea model were then created from equivalent human cell types. Generally this 3D model displays advantages over other *in vitro* cornea equivalents and has potential, but needs further refinement. The methodology was also used to coat stromal spheroids with skin keratinocytes, highlighting the possibility of reprogramming the former into corneal epithelial cells through epithelial-mesenchymal interactions.

Indexes

Main Index

Figure Index

Table Index

Appendix Figures & Tables Index

1. General Introduction

1.1 The Cornea – Structure & Function

The cornea lies at the front of the eye and functions as our window to the world. The transparency of the cornea is crucial for the transmission of light to the retina at the back of the eye which enables visual perception. The cornea is avascular and is composed of five layers: the outermost layer is a non-keratinised stratified epithelium, the Bowman's layer, a highly ordered keratocyte-populated collagenous stroma, Descement's membrane and the inner endothelium which is a cellular monolayer (Secker and Daniels, 2008) (See Fig. 2). The limbus is located between the cornea and conjunctiva, and in humans, is approximately 1.5mm wide. Corneal transparency is dependent on the continuous self-renewal of the corneal epithelium and its self-renewal properties are in turn dependent on the presence of corneal epithelial stem cells (CESCs), also commonly known as limbal stem cells (LSCs), located within the limbal epithelial basal layer.

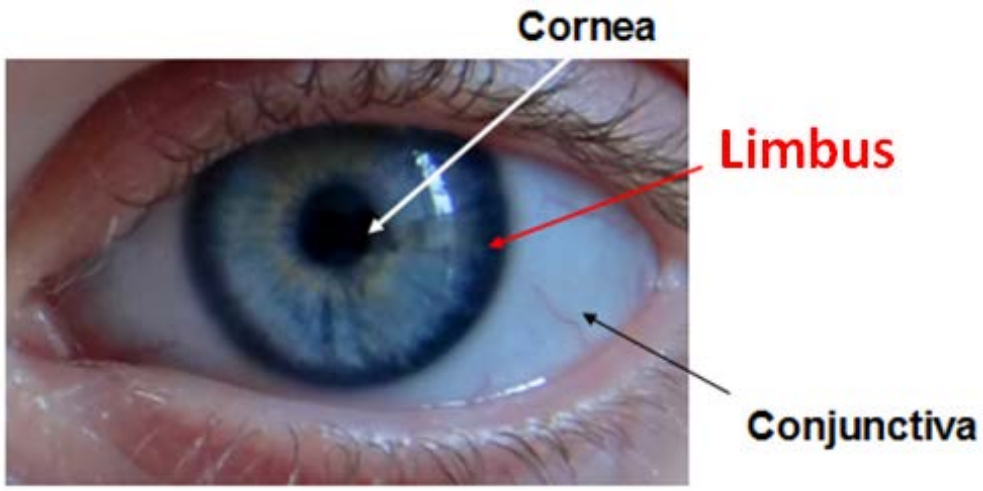

Figure 1: Representation of the cornea, conjunctiva and the limbus. LSCs reside within the limbal basal layer

1.1.1 Human Corneal structure:

a) *Corneal epithelium*. This is approximately 50 to 52µm thick and is usually composed of five to seven layers of organised epithelial cells that consist of a single layer of basal columnar cells in which mitosis occurs, two or three layers of wing cells, and two or three layers of superficial squamous cells. The cells of the corneal epithelium are linked between each other by four types of intercellular junction adhesions: gap junctions, tight junctions, desmosomes and adherens junctions. Gap junctions are found in the basal layers of the corneal epithelium and this enables intercellular transport. Tight junctions can be found in the superficial cell layers and this prevents the penetration of the tear film and its components such as bacteria. Desmosomes are found in the wing cell layers, and adherens junctions in all cell layers. Intercellular junctions are thought to be important for the maintenance of tissue integrity and for the regulations of cellular processes such as migration and differentiation. They also provide a pathway for inside-out and outside-in signal transduction (Edelhauser, 2003).

b) *The Basement Membrane and Bowman's layer*. The corneal epithelial basement membrane rests upon the Bowman's layer, which is an acellular condensation of the outer section of the corneal stroma and mostly consists of collagen fibres (type I and III) and proteoglycans (Edelhauser, 2003).

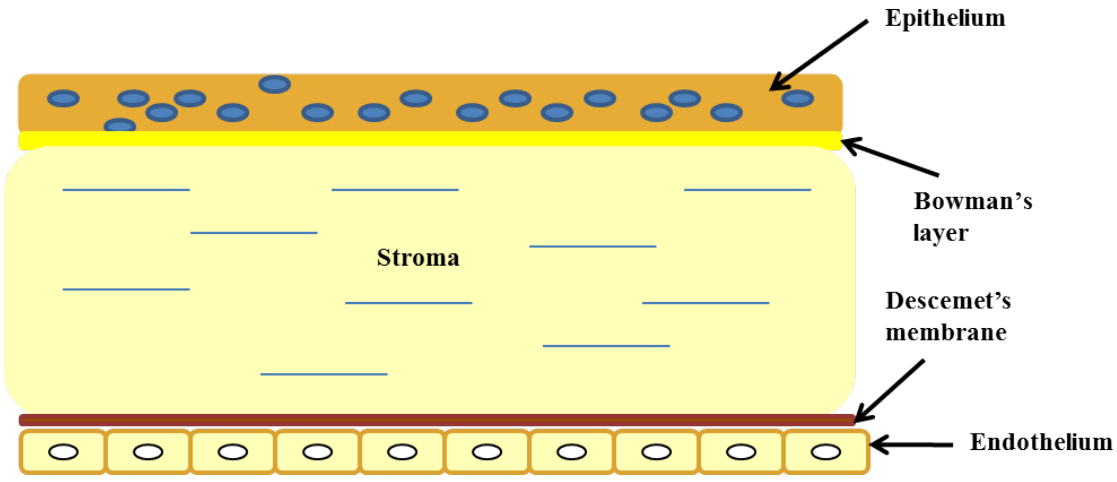

Figure 2: Diagram of a cross section through the human cornea

c) *Corneal stroma*. The stroma constitutes 90% of the corneal thickness and consists of an extracellular matrix that is made up of collagens (type I, V and VI) and proteoglycans. Keratocytes are dispersed within the stroma lying between the collagen lamellae and these secrete components of the stroma that allow for its maintenance and repair (Edelhauser, 2003).

d) *Descement's membrane*. This is a basement membrane of the corneal endothelium. It is mainly composed of collagen type IV and laminin (Edelhauser, 2003).

e) *Corneal endothelium*. This layer is composed of a single layer of hexagonal cells. These cells have an important role in pumping water from the corneal stroma that together with the regular organisation of the collagen lamellae, allows for the corneal transparency (Edelhauser, 2003).

1.2 Corneal Epithelial Stem Cells (CESC's)

1.2.1 Limbal Stem Cells (LSC's)

LSC's are located within the basal layer of the limbal epithelium. The limbal epithelium is a transition zone between the corneal and conjunctival epithelia (Snell, 1998) and is around 10 to 12 cell layers thick. Its main functions are to harbour LSC's and it acts as a physical barrier thus preventing the conjunctival epithelium and its blood vessels from invading the corneal surface, which would otherwise impair the transparency of the cornea and cause visual loss (Dua and Azuara-Blanco, 2000). The presence of anti-angiogenic molecules in the cornea are believed to be one of the reasons why optical transparency is maintained during normal homeostasis. Work by Ambati *et al*., 2006, showed that the soluble vascular endothelial growth factor (VEGF) receptor 1 (also known as sFlt1) is essential for the cornea to remain avascular and that it contribute to the corneal antiangiogenic barrier (Ambati *et al*., 2007).

Being adult stem cells, the unique capacity of limbal stem cells is to self-renew and produce committed progenitors. These progenitors are often referred to as transient amplifying (TA) cells (see Fig. 3). Transient amplifying cells differentiate into the cell

lineages of the tissue of origin and can increase the number of differentiated progeny produced (Pellegrini *et al*., 2009). When LSC's divide asymmetrically, one daughter cell, may leave the niche under specific environmental signals, proliferate, migrate centripetally and become lineage committed i.e. become a transient amplifying cell (Secker and Daniels, 2008; Schlotzer-Schrehardt *et al*., 2007).

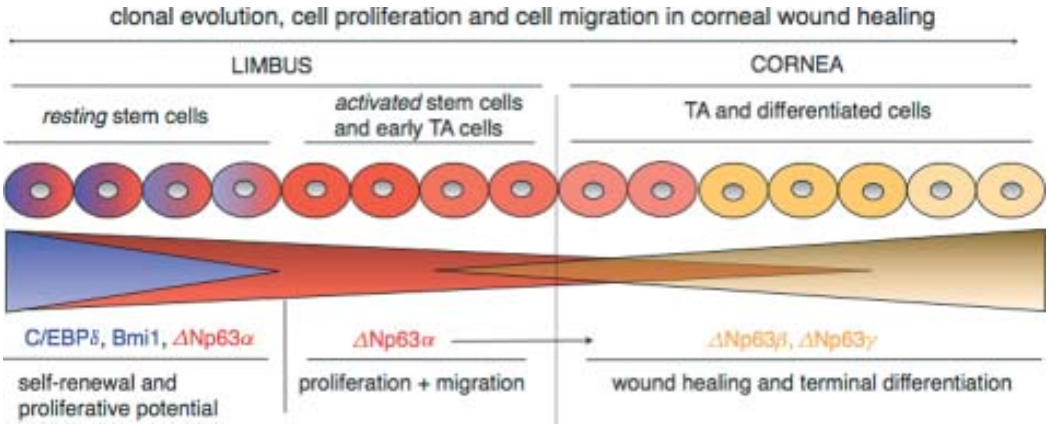

Figure 3: Clonal evolution, cell proliferation and cell migration in corneal wound healing (taken from (Pellegrini *et al*., 2009)).

1.2.1.1 Characteristics

LSCs are slow cycling during homeostasis, relatively undifferentiated within the limbal epithelial basal layer and have been found to have prolonged self-renewal and a high proliferative potential after being activated by wounding or by *in vitro* culture conditions (Thoft and Friend, 1983). As shown in Figure 4, cells migrating from the limbus towards the wounded cornea follow the X, Y, Z hypothesis of the preservation of the corneal epithelium through the proliferation and migration of limbal stem cells, as proposed by Thoft & Friend, 1983.

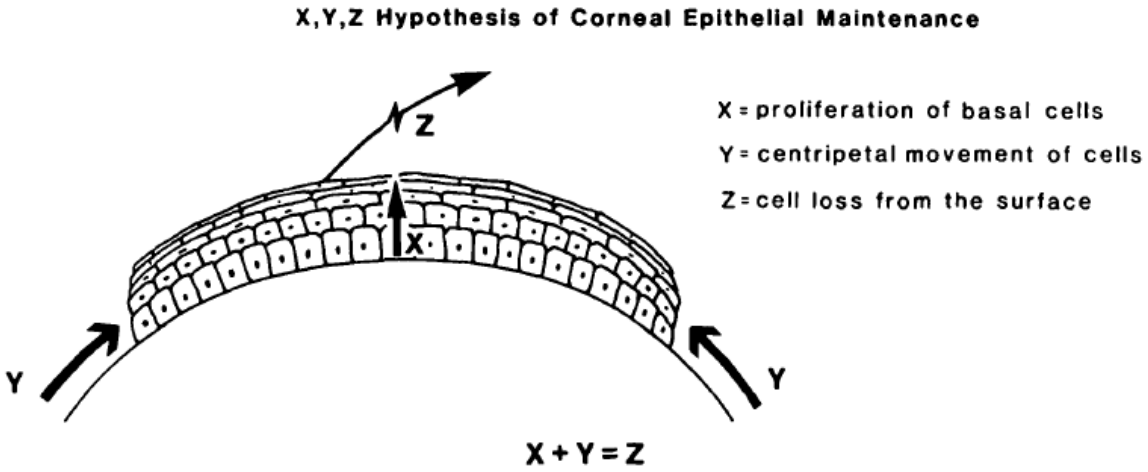

Figure 4: X, Y, Z Hypothesis of Corneal Epithelial Maintenance (taken from (Thoft and Friend, 1983)).

X= proliferation of basal cells, Y= centripetal movement of cells and Z= cell loss from the surface. Corneal epithelial maintenance can therefore be defined by the equation: X+Y=Z. The X, Y, Z hypothesis states that in order for the corneal epithelium to be maintained, cell loss must be balanced by cell replacement.

1.2.1.2 The LSC niche

In order for limbal stem cells to retain their stem-ness and quiescence, they are located within a niche, a specific microenvironment composed of cellular and extracellular components. This niche is believed to prevent limbal stem cell differentiation, therefore regulating their fate. The LSC niche is thought to be located within the palisades of Vogt or limbal crypts (Dua *et al*., 2005). This is an undulating region of increased surface area. Within this proposed niche, LSCs are potentially protected from damaging ultraviolet light by the presence of melanin pigmentation (Goldberg and Bron, 1982). The limbal stem cell niche is highly innervated and vascularised, therefore providing the limbal stem cells with a source of nutrients and growth factors. A number of factors have been proposed to retain cell stem-ness within the limbal stem cell niche, such as signalling pathways present in the limbal epithelial cornea and limbus, such as the Sonic hedgehog, Wnt/β-catenin, TGF-β and Notch signalling pathways. However, it is not known what their precise potential role in the limbal stem cell niche is and this remains to be investigated (Secker and Daniels, 2008). Work by Kulkarni et al., 2010 identified up-regulation of FRZB1, a soluble WNT antagonist found to maintain skin bulge stem cell quiescence and LEF1 and CDH1, molecules involved in WNTβ-catenin signalling

and known to be crucial in maintaining stemness in a number of stem cell populations, to be up-regulated in the limbal epithelial cornea only.

Extracellular matrix components have also been proposed, such as laminin-1,5, α2β2 chains, type IV collagen α1, α2 and α5 chains. These factors were all found within the limbal region. Furthermore, patchy immunolocalisation of laminin γ3 chain, BM40/SPARC and tenancin C were found to co-localise with ABCG2/p63/K19-positive cell clusters, i.e. the putative limbal stem cell markers (Schlotzer-Schrehardt *et al*., 2007). In addition, limbal stem cell adhesion is partly influenced by the presence of limbal stromal fibroblasts that are located in the underlying stroma. Extracellular matrix components have been characterised between the limbal area and the cornea and have been found to be involved in accommodating a stromal microenvironment that supports and maintains LSC's. These components include laminin isoforms, collagen type XII and IV chains and tenascin-C (Schlotzer-Schrehardt *et al*., 2007). Work by Kulkarni et *al*., 2010 performed gene expression profiling of the limbal stroma and found enrichment of various proteins previously reported to be involved in stem cell maintenance in other tissues. These were the tissue metalloproteinase inhibitors (TIMP1, TIMP2), developmetal protein FLII, antioxidants XPA, DUOXI, GFRα4 (a member of the GDNF family) and LMNA a nuclear envelope matrix protein (Kulkarni *et al*., 2010).

Increasing evidence has therefore indicated that limbal stromal cells might act as niche cells, therefore maintaining LSC's phenotype (Li *et al*., 2007). Work by Pinnamaneni and Funderburgh in 2012, described the location of the corneal stromal stem cells being in the anterior limbal stroma and were therefore hypothesised to support LSC's function. More recent work has found that the microvascular net in the limbus together with the limbal stroma regulate and maintain LSCs survival and homeostasis (Huang *et al*., 2015).

1.2.1.3 The Limbal Dogma – Evidence of LSC's location

Evidence supporting the "Limbal Dogma", i.e. that corneal epithelial stem cells reside only in the basal layers of the limbal epithelium, has been identified by various studies. Pigment migration studies in the guinea-pig-eye, by Davanger & Evensen, 1971, is known to possess a pigmented limbal basal epithelial layer. This study showed that when the non-pigmented central corneal epithelium was removed, the cornea healed exhibiting a pigmented epithelium, thus indicating that cells from the limbal region migrated to regenerate the wound site (Davanger & Evensen, 1971).

A second study by Cotsarelis *et* al., 1989, identified the slow cycling nature of cells in the basal epithelium of the limbus. This was achieved by radio-labelling cells in mouse cornea and limbus in the S phase of the cell cycle, using tritiated thymidine. They also showed that wounding the central cornea, these cells were cycling much more rapidly, suggesting the stem cell nature of these cells located in the limbal area.

Other studies supporting the limbal location of CEC's, included the identification of high proliferating human limbal epithelial cells, compared to corneal and conjunctival epithelial cells, when cultured *in vitro*, a common feature of stem cells (Ebato *et al*., 1988); corneal wound healing studies performed in rabbits that showed corneal conjunctivalisation after removal of the limbal epithelium (Chen & Tseng, 1991; Kruse *et al*., 1990; Huang & Tseng, 1991) and corneal regeneration in patients with Limbal Stem Cell Deficiency (LSCD) after a limbal graft (Kenyon & Tseng, 1989), being the first to show the regeneration and therapeutic potential of the limbal epithelium and its stem cells.

Recent work by Majo *et al*., 2008, dismissed the widely accepted limbal dogma by performing ablation and grafting experiments in mice, hypothesising that centripetal limbal cell migration was not occurring in normal circumstances and that oligopotent stem cells spread throughout the ocular surface were responsible for regenerating the mammalian cornea. This study involved the excision of limbal portions of athymic mice by replacing these with β-galactosidase-labelled mice limbal grafts. Results showed that grafted cells were not migrating out of the grafts and towards the centre of the cornea for a long period of time. However, when the recipient mice corneas were wounded, labelled cells were observed to migrate out of the grafts. Additionally, experiments

involving transplantation of corneal tissue from the central cornea into the limbal region of athymic mice, resulting in the full restoration of the cornea, as well as the isolation and *in vitro* expansion of highly proliferative corneal cells, indicated a novel finding whereby stem cells in the cornea were not exclusively located in the limbal region of the corneal epithelium.

The debate about the location of corneal epithelial stem cells has been addressed by the work carried out by Shalom-Feuerstein and co-workers, who used a new mouse model incorporating the increasingly popular multi-coloured confetti reporter transgene combined to tamoxifen-inducible Keratin 14-CreER, allowing to trace limbal and corneal cytokeratin 14 positive cells (Amitai-Lange *et al*., 2015). Results proved the original evidence in favour of the limbal epithelial stem cell hypothesis to be correct and highlighted a novel finding whereby limbal stem cell derived progenitor cells not only possess a significant regenerative ability but that these cells can survive for up to 4 – 5 months (Amitai-Lange *et al*., 2015), which in previous work had not been consistently estimated.

1.2.1.4 Putative positive and negative LSC markers

Ongoing research in the area of limbal stem cell biology has tried to establish limbal stem cell markers in order to identify limbal stem cells and locate their niche. In order to accomplish this, the different expression of a protein marker, or a set of protein markers in the stem cell environments compared to the amount of expression of these markers in more differentiated tissue have to be tested.

Putative markers can be either positive or negative. Positive markers identify the presence and negative markers identify the absence of limbal stem cells.

Integrins (α9 and β1), NGF receptors (TrkA), CD34, CD133, α-enolase, metabolic enzymes, vimentin and Cytokeratin K19, have all been proposed as potential markers for limbal stem cells. However, most of these markers were found to lack limbal stem cell specificity as these were not found in label-retaining-cells following the pulse-chase labelling of all cells with BrdU (bromodeoxyuridine) (Cotsarelis *et al*., 1989).

Positive putative markers such as the *p63* transcription factor and *ABCG2*, an ATP binding cassette, were found to be the most reliable markers for identifying limbal stem cells as these determine the proliferative potential of stem cells in the stratified epithelia (Pellegrini *et al*., 2001).

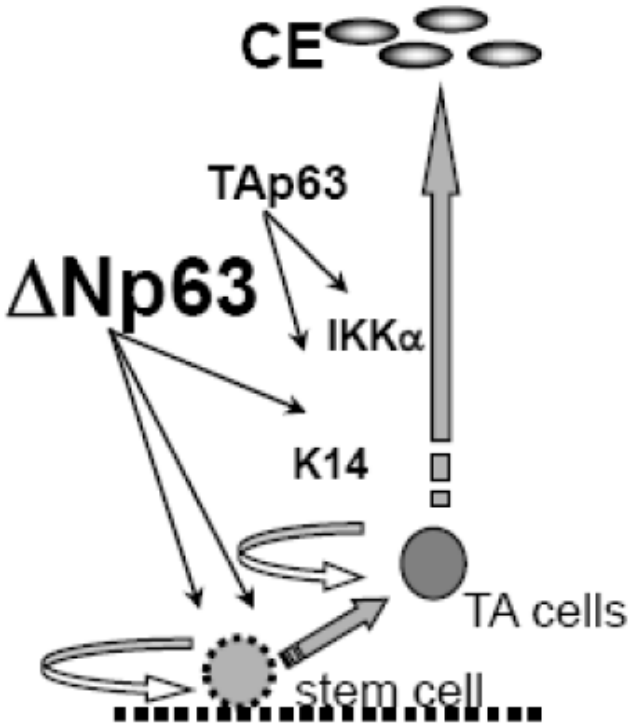

Figure 5: p63 in epithelial development: ΔNp63 expression in stem cells and TAp63 expression in terminally differentiating progenitor cells. Taken and adapted from (Candi *et al*., 2008).

Evidence that *p63* could be used as a positive marker for identifying limbal stem cells, came from a study in 1999 where a *p63* knock-out mice showed lack of all stratified squamous epithelia (Yang *et al*., 1999). *p63* has six isoforms, which fall into two main types dependent on the presence of a transactivation domain (TA). Isoforms lacking this domain are referred to as ΔN. For both isoforms three different C termini named α, β, and γ are generated through alternative splicing (Yang and McKeon, 2000). It was found that *ΔNp63α*, β, and γ are expressed during wound healing and are connected to limbal cell migration and corneal regeneration and differentiation (Di Iorio *et al*., 2006).

ΔNp63α has been described to be the most precise marker for identifying limbal stem cells. In fact, *ΔNp63α* abundance decreases during clonal transition from stem to TA

cell and the protein is absent in TA cells (see Fig. 3). On the other hand, *ΔNp63β* and *ΔNp63γ* are thought to be involved in epithelial differentiation, hence during the regeneration of the cornea (Di Iorio *et al*., 2006).

A second marker for limbal stem cell-identification which has been previously used for identifying bone marrow stem cells, is *ABCG2*, a member of the ATP binding cassette (ABC) transporters. *ABCG2* has been proposed as a universal marker for stem cells (de Paiva *et al*., 2005). The *ABCG2* protein is mainly found in the basal cells of the limbal epithelia, however it is not found in the limbal suprabasal and corneal epithelial. Ongoing research in the area of limbal stem cell biology is still trying to find more specific limbal stem cells markers. Recent work by Ksander *et al*., 2014 has identified a new molecular marker to identify LSC's. This is the ATP-binding cassette, sub-family B, member 5 (ABCB5). Isolated human and murine ABCB5 positive cells from the limbal area, when grafted onto LSC deficient mice, were found to fully restore the cornea. Moreover, these ABCB5 positive cells were expressed on LSC's that were label-retaining in mice and were positive for p63α LSC's in humans (Ksander *et al*., 2014). This work strongly suggests that ABCB5 identifies mammalian LSC's and that this marker could have potential important implications in treating corneal disease.

The CCAAT enhancer binding protein δ (*C/EBPδ*) is a member of the family of the leucine zipper transcription factors and it is involved in a various number of cellular processes such as in the control of proliferation, differentiation, metabolism and inflammation (Johnson, 2005; Ramji and Foka, 2002). *C/EBPδ* has also been found to be implicated in the regulation of limbal stem cells self-renewal as it regulates the cell cycle by generating a G0/G1 arrest (Barbaro *et al*., 2007).

Putative negative markers are markers expressing differentiation genes, as these are not present in limbal stem cells:

- Cytokeratin 3 (*Ck3*), this is a keratin containing intermediate filament and it is a differentiation marker which is not present in limbal stem cells but in all other layers of the corneal epithelium, including the suprabasal layers of the limbal epithelium (Schermer *et al*., 1986).

- Cytokeratin 12 (*Ck12*) is expressed in a similar pattern as Ck3.

- Connexin 43, is an involucrin and is not expressed in LSC but in the nearby basal cell layer. Connexin 43 is a transmembrane protein involved in cell to cell communication. Its expression is associated with development and differentiation.

1.2.1 Culture methods for LSC extraction

The culture of human limbal epithelial cells is important for two reasons: first, it is used for the aim of transplantation in cases of patients suffering of a dysfunction in the limbal stem cells to renew the corneal epithelium, also called limbal stem cell deficiency (LSCD). This is described in the Methods section 2.2.2.1 of Chapter 2. Secondly, the culture of limbal epithelial cells is used to study limbal stem cell properties and to deepen our understanding of limbal stem cell biology (Osei-Bempong *et al*., 2009).

1.2.2.1 Substrate/feeder layer

In order to successfully culture limbal epithelial cells, the use of a substrate or feeder layer is needed. The early use of culturing corneal epithelial cells was unsuccessful due to fibroblast contamination. This is because fibroblasts have a very high proliferation rate and therefore they can outgrow the epithelial cells, thus overtaking the culture. Furthermore, it was very difficult to culture epithelial cultures as these had a limited growth. In 1975, Rheinwald and Green developed a new method of successfully culturing epithelial cells. This was a co-culture of skin epithelial cells with 3T3 fibroblasts (Rheinwald and Green, 1975). 3T3 cells have been originally developed from Swiss mouse embryos and have become a widely used and established cell line of fibroblasts (Todaro and Green, 1963). Prior co-culturing the 3T3 fibroblasts with the epithelial cells, the 3T3's are mitotically inactivated through the addition of mitomycin C or by irradiation. Inactivating the 3T3's is essential for preventing them to overgrow the epithelial cells in culture. The use of 3T3 fibroblasts successfully cultured epithelial cells and in 1977 Sun and Green were the first to show that also corneal epithelial cells could be successfully co-cultured with 3T3 fibroblasts (Sun and Green, 1977). These not only act as a layer on which epithelial cells can attach and start to proliferate, but

they also act as feeder cells, therefore being necessary for epithelial cells maintenance and growth (Osei-Bempong *et al*., 2009).

1.2.2.2 Culture medium

An important factor in the culture of stem cells in general, is the medium in which they are cultured. The medium used to efficiently culture limbal epithelial cells is composed of a basal medium, in this case a 3:1 ratio of low glucose Dulbecco's modification of Eagle's medium (DMEM) and Ham's nutrient mixture F-12, additives and serum. In order to reduce the risk of culture infection, antibiotics such as penicillin and streptomycin or gentamicin, and antifungal agents can be added to the medium. For research purposes the epithelial cells are co-cultured with 3T3 mouse fibroblasts which act as a feeder layer and this is explained further in the Materials & Methods section.

However for human transplantation purposes the epithelial cells can be cultured on an amniotic membrane, as this is a non-animal component, non-immunogenic and does therefore not require the use of immunosuppression (Kruse *et al*., 2000).

The components for the limbal epithelial growth medium are:

- *Ham's nutrient mixture F-12*. The combination of Ham's nutrient with low glucose DMEM has shown to increase epithelial cell expansion *in vitro* (Allen-Hoffmann and Rheinwald, 1984).

- *Hydrocortisone*. This is a steroid hormone that is naturally produced by the adrenal gland and it plays a complex role in the regulation of body functions. One of its main functions is to increase blood sugar through gluconeogenesis. The addition of hydrocortisone in the growth medium has shown to improve epithelial cell growth and morphology when grown in culture (Rheinwald and Green, 1975).

- *Insulin*. The presence of insulin in the growth media reduces the need of using serum in the culture medium. It has been shown that insulin stimulates glucose

transport into cultured cells and also to be important in glycogen synthesis within these cells (Hayashi *et al*., 1978).

- *Tri-iodothyronine*. This is a hormone involved in important metabolic processes. Addition of tri-iodothyronine also reduces the requirement of using serum in the culture medium (Hayashi *et al*., 1978).

- *Adenine*. Adenine has been found to increase and improve the ability of epithelial cells to form colonies (Allen-Hoffmann and Rheinwald, 1984). This is important for the establishment of a confluent epithelial cell culture.

- *Cholera toxin*. This has been shown to stimulate DNA synthesis by increasing cellular cAMP levels (Marcelo, 1979). This is important as this means that the addition of cholera toxin can foster the proliferation of epithelial cells (Green, 1978). Additionally it was shown that cholera toxin contrasts epithelial cells terminal differentiation (Sun and Green, 1976).

- *EGF*. The role of the growth factor EGF in the epithelial cell medium is to stimulate epithelial cell migration, thus avoiding cellular crowding and clumping at the centre of colonies (Rheinwald and Green, 1977). Furthermore, EGF has shown to oppose epithelial cell differentiation in culture, therefore promoting their undifferentiated state. This is especially important in the culture of epithelial cells because in order to study limbal stem cells their undifferentiated preservation is needed (Osei-Bempong *et al*., 2009).

- *Fetal bovine serum/autologous human serum.* Fetal calf needs to be added at a concentration of 10%. For transplantion purposes in humans however, autologous human serum is used when expanding the epithelial cells in culture (Osei-Bempong *et al*., 2009).

1.2.2 Stromal stem cells

The stroma, a collagenous mesenchymal structure, colonizes approximately 90% of the corneal volume. Its first important function is to confer transparency to the cornea and this is achieved by its tightly packed collagen fibrils aligned in a parallel manner (Hogan *et al.*, 1971). Within the stroma a population of neural crest-derived mesenchymal cells called keratocytes can be found, approximately populating 3% of the whole stromal tissue. Keratocytes are quiescent throughout adult life. Having exited the cell cycle during eyelid opening and becoming G0 cells, they can immediately be stimulated following injury to the cornea, becoming motile and changing their phenotype and morphology to mitotically active fibroblasts (Zieske *et al*., 2001; Wilson *et al*., 2002). Stromal fibroblasts are known to express α-smooth muscle actin and develop a fibrotic extracellular matrix (Funderburgh *et al*., 2003; Fini 1999). Due to the morphological nature of the fibroblastic stromal cells that re-populate the wound, the resulting long lasting scar formation within the stroma cause loss of vision (Johnson 1999). More superficial injuries to the cornea, involving only the corneal epithelium, are known to heal without forming scars (Zieske *et al*., 2001). Keratocytes below the wound undergo apoptosis and keratocytes peripheral to the wound migrate to the injury site and replicate.

It has long been believed that the fibroblastic transformation of stromal keratocytes was irreversible. However, recent finding have shown that early passages of stromal cells placed in a 3D multi-cellular construct, were able to reverse their fibroblastic phenotype as well as express differentiated keratocyte characteristics (Ren *et al*., 2008). Funderburgh et al., 2005 identified a Pax6-positive population of progenitors-like cells in the adult corneal stroma that were able to transform into keratocytes. A number of MSC markers were found to be expressed in bovine stromal progenitor cells, such as Bmi1, CD90, CD73, CD166, ABCG2, Fhl1, stem cell factor (kit ligand) and Notch1 (Funderburgh *et al*., 2005). Floating aggregates, also called neurospheres, were found to form when mouse stromal cells were expanded in attachment-free cultures (Yoshida *et al*., 2005; Yoshida *et al*., 2006). When these spheres were plated back into normal culture dishes, expression of keratocan and neural-specific proteins was found, therefore confirming that multipotent adult stem cells were present within the adult stroma. Further work by Du *et al*., 2005, led to the identification of stromal stem cells in the

human cornea by isolating a side population of ABCG2 expressing stromal cells in proximity to the corneal limbus, by cell sorting. When these ABCG2 and Pax6 positive SP cells were cultured in medium containing fibroblast growth factor-2, they lost the expression of these two markers and instead upregulation of keratocyte markers keratocan, aldehyde dehydrogenase 3A1 and keratan sulfate was observed (Du *et al*., 2005).

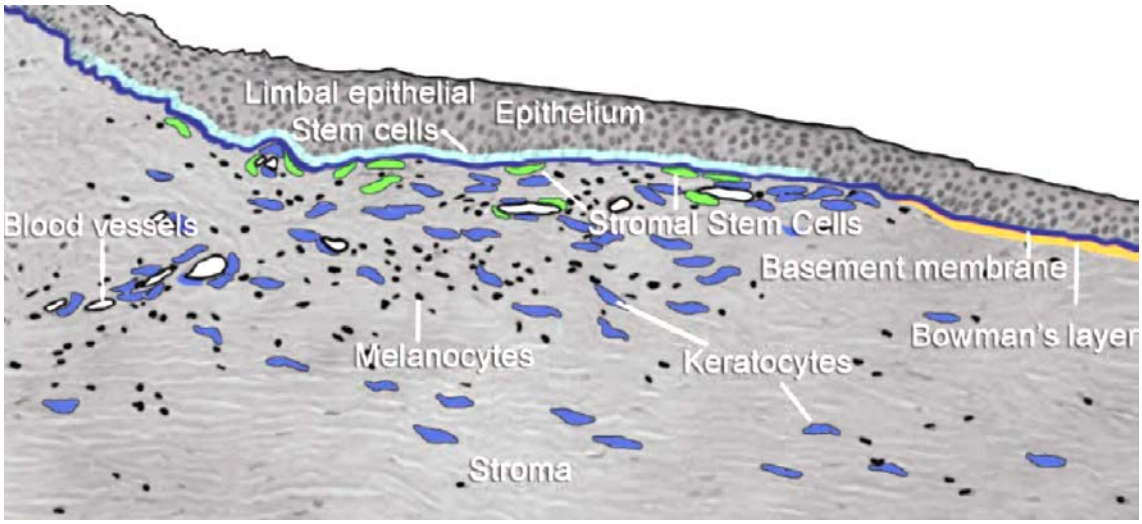

Figure 6: Corneal section showing the limbus and the anatomical and cellular features of the stromal stem cell niche. Image taken from (Pinnamaneni & Funderburgh 2012).

Work by Polisetty *et al*., 2008, identified a mesenchymal cell population (also termed as "niche cells") found in the limbal stroma. Recent work by Branch *et al*., 2012, showed that peripheral and limbal stromal stem cells (PLCSCs) were in fact mesenchymal stem cells and they displayed a trilineage potential and a strong similarity to fetal liver MSCs.

The close proximity of corneal stromal stem cells to the limbal epithelial stem cell niche suggests that interactivity between these two stem cell populations must be taking place. This has been described by Espana *et al*., 2003, where it was shown that the stromal niche controlled the stem cell plasticity of LSCs and by Du *et al*., 2009 who showed that stromal stem cells change their phenotype when injected into the *in vivo* stroma, becoming keratocytes. The latter therefore showed that proximity to the limbal stem cell niche is crucial to the maintenance of un-differentiated stromal stem cells, thus highlighting the symbiotic support and maintenance of the stem cell phenotype between these two stem cell populations and niches. It has also been shown by Bray *et al*., 2012,

that stromal stem cells enhanced limbal epithelial cells proliferation when co-cultured together. Recently, in a study performed by Xie *et al*., 2011, limbal epithelial cells were found to merge with stromal cells in sphere-forming conditions, through the chemokine receptor-mediated signalling pathway, indicating a crucial interaction taking place between the two for optimal stem cell maintenance. A further characteristic of stromal stem cells is their ability to modulate the immune response. Stromal stem cells were shown to have the ability to suppress T-cell-mediated tissue rejection *in vivo* (Du *et al*., 2009), thus making them an interesting therapeutic tool if this feature could also be maintained *in vitro*.

1.3 Limbal Stem Cell Deficiency (LSCD)

According to the WHO statistics, six million individuals worldwide are bilaterally blind from corneal disease and another 135 million have severely impaired vision in both eyes due to the loss of corneal transparency (Majo *et al.*, 2008). One reason for the loss of corneal transparency has been correlated to a defect of the ocular surface to undergo repair and self-renewal and this is due to a condition called limbal stem cell deficiency. The most common causes of limbal stem cell deficiency are due to chemical and thermal injuries to the eye in which limbal stem cells are destroyed. However LSCD can also be caused by LSC's inflammatory destruction due to poorly fitting contact lenses, microbial infections and in Steven-Johnson syndrome (Dua *et al.*, 2000). A less common cause of LSCD is caused by a loss of LSC's due to the inability of the stroma to act as a support. This is found in conditions such as in aniridia.

The consequences of LSCD are conjunctivalisation (See Fig. 7), neovascularisation, chronic inflammation, recurrent erosions, ulceration, stromal scarring and ultimately causing symptoms such as painful vision loss (Dua *et al.*, 2000).

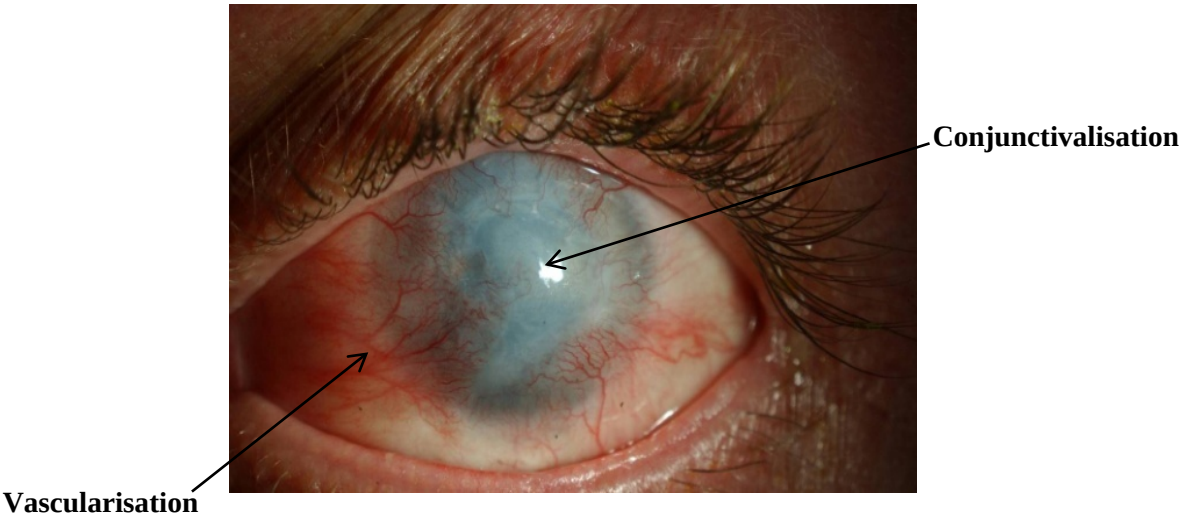

Figure 7: Limbal Stem Cell Deficiency

The image shows a patient with Limbal Stem Cell Deficiency. Vascularisation is the growth of capillaries over the cornea. Conjunctivalisation is the growth of the conjunctiva over the cornea, causing blindness.

1.3.1 Management of LSCD

In order to restore visual function, the corneal epithelium needs to be renewed. In LSCD this does not occur due to damaged or deficient limbal stem cells. Therefore the stem cell population needs to be replaced and this has been traditionally achieved by grafting limbal auto- or allografts. Limbal autografting is a surgical technique that involves transplantation of limbal stem cell tissue (almost 2/3 of the limbal circumference) from the healthy eye of a patient to the affected eye. This technique is therefore only applied in patients with unilateral stem cell deficiency (Sippel, 2001). A more recent technique involves the removal of a $1mm^2$ biopsy from the limbus of the healthy eye and culturing and expanding it *in vitro*. One of the expansion methods that have been most successful has been the culture of a limbal biopsy on an amniotic membrane (AM) that is then sutured back on the LSCD affected eye. This technique has been mostly successful as it has improved visual acuity and has rapidly healed the ocular surface. However, in patients with bilateral LSCD limbal stem cell allografting has to be performed. In this

case the LSC tissue is obtained from a cadaveric or a living donor, therefore requiring the use of immune-suppressants (Sippel, 2001).

The exact cellular and signalling mechanisms that contribute to the activation or re-establishment of the limbal stem cell population are yet not fully understood. One theory states that the application of the amniotic membrane acts as an anti-inflammatory agent, therefore re-activating a number of signalling pathways that are also present during corneal epithelial wound healing. Studies that analysed the amniotic membrane composition found that its basement membrane (BM) contains collagen types I-VII, collagen IV, VII, Ln-1, Ln-5 and fibronectin (Fukuda *et al.*, 1999). It is known that fibronectin and collagen IV and VII stimulate epithelial adhesion and migration (Fujikawa *et al.*, 1984; Murakami *et al.*, 1992). Laminin (Ln) on the other hand plays an important role in corneal epithelial cell adhesion (Kurpakus *et al.*, 1999). The amniotic membrane also contains the most important growth factors that promote wound healing. These are epidermal growth factor (EGF) and keratocyte growth factor (KGF). Moreover, the amniotic membrane has an anti-scarring effect in the treatment of ocular surface disorders due to the inhibition of TGF-β signal transduction (Lee *et al.*, 2000). After amniotic membrane transplantation has been performed, a significant reduction in inflammation has been identified. *In vitro* studies have shown that AM reduces the expression of a number of growth factors and pro-inflammatory cytokines (Solomon *et al.*, 2001). Furthermore, anti-inflammatory cytokines such as interleukin-10 and interleukin-1 receptor antagonist are released in the amniotic membranes's epithelium and stroma. All these effects might be favourable to the growth and differentiation of the cells when used for ocular surface reconstruction. Therefore the AM has been chosen to be a good candidate for culturing limbal stem cells, in order to treat corneal acute chemical burns (Kim *et al.*, 2000; Meller *et al.*, 2000).

In order to identify potentially important proteins in the human amniotic membrane which may be responsible for maintaining LSCs function, proteomic studies were performed (Baharvand *et al.*, 2007). Results showed that limican and mimican/osetoglycin, two members of the proteoglycan (PG) family were among the most abundant proteins found in the amniotic membrane (Baharvand *et al.*, 2007). It is known that proteoglycans of the extracellular matrix are involved in organising collagenous networks and also have cell signalling properties, therefore having an important role in cell growth, differentiation and migration (Baharvand *et al.*, 2007).

1.4 Corneal Wound Healing

The function of the corneal epithelium is to act as a barrier between the continuously changing external environment and the internal surroundings. This function is also highly required for the healthy maintenance of the transparency of the cornea (Suzuki *et al.,* 2003).When the corneal epithelium is damaged by physical, chemical or microbial injuries, the stroma swells, stromal fibroblasts are activated and inflammatory cells are released. This leads to the loss of corneal transparency and integrity and under normal and healthy circumstances the corneal epithelium is quickly repaired and restored as fast as possible (Suzuki *et al.*, 2003).

However, there are certain conditions where the corneal epithelial wound healing process is delayed or even non-functional at all. This may be due to the failure of signalling mechanisms to efficiently stimulate the limbal stem cells to divide and generate progenitor cells, or/and to the complete damage to the niche microenvironment and therefore to a loss of limbal stem cells due to the damage to the limbus (such as in LSCD). This occurs for example in severe chemical burns to the surface of the eye. It is not yet clearly understood what underlying molecular and cellular factors control corneal epithelial wound healing and what the faulty mechanisms are in conditions such as LSCD. For this reason, it is important to deepen the knowledge into what mechanisms underlie corneal epithelial wound healing in order to develop new treatments that can target the underlying cause of corneal epithelial defects. Moreover, stromal scarring is one of the major causes of blindness in the world according to the World Health Organization. Wounds that affect the deeper layers of the stroma are known to cause stromal keratocytes to become motile by producing fibroblastic ECM which cause scar formation in the process of healing the damage. Scar formation and therefore a disruption in the native organization of stromal keratocytes which is known to promote transparency ultimately causes loss of vision. The only way to restore normal function and vision of the cornea is corneal transplantation. Extensive research is taking place with the aim to find a way to treat stromal scarring in the form of topical applications. This has led to the development of *in vitro* wound healing models that can be used to study corneal wound healing biology without the need of using animals, making these more ethically acceptable and relevant to clinical applications for humans.

1.4.1 Wound healing stages

In vivo corneal epithelial wound healing takes place in different stages, that are continuous and overlapping each other. These are known as the a) lag phase, b) the migration of superficial cells to cover the denuded surface, c) cell proliferation and differentiation and d) re-epithelialization. These are described in more detail below.

a) Lag phase

Before any of these stages occur a lag phase takes place during which cells alter their metabolic status (Lu *et al.*, 2001). Also, immediately after corneal epithelial wounding there has been a lack of detection of the mitotic activity within the neighbouring epithelial cells at the wound margin. This is called “mitotic paralysis” (Suzuki *et al.*, 2003).

The lag phase is the time between the injury and the beginning of cell migration. Within this phase a great deal of cellular reorganisation and protein synthesis is taking place (Lu *et al.*, 2001). Important cytoskeletal proteins such as vinculin, actin, talin, and integrin are synthesised, as well as cell surface receptors such as hyaluronan [HA] receptor CD44. Cell migration and wound healing depend greatly on cytoskeletal protein synthesis. Furthermore, cell surface glycolipids and glycoproteins synthesis is also increased.

Surface glycoproteins are believed to be responsible for bidirectional signalling between the extracellular matrix and the cytoskeleton.

b) Migration

Corneal epithelial migration starts after the degradation of the hemidesmosomes and desmosomes. (Gipson *et al.*, 1987; Okada *et al.*, 2001). Hemidesmosomes are integral membrane protein complexes located in the basal cell plasma membrane and their function is to anchor the epithelium to the stroma. A structural component of hemidesmosomes is the α6β4 integrin. This is a signalling molecule known to be involved in the regulation of epithelial cell proliferation. On the other hand, desmosomes link basal, wing, and superficial cells to one another (Edelhauser, 2003). As a result of the degradation of anchoring structures, a focal contact is formed provisionally. However, this is only a momentary attachment complex. During this first

phase the epithelial cells flatten and migrate as one intact sheet in order to cover the wound. This process is also seen as a sliding movement (or sheet like movement as seen in Figure 8) of superficial cells (Lu *et al.*, 2001).

It is believed that the basal and wing cells take part in the creation of the leading edge. Cells from opposite directions of the wound migrate and meet at the centre of the wound to cover the denuded surface.

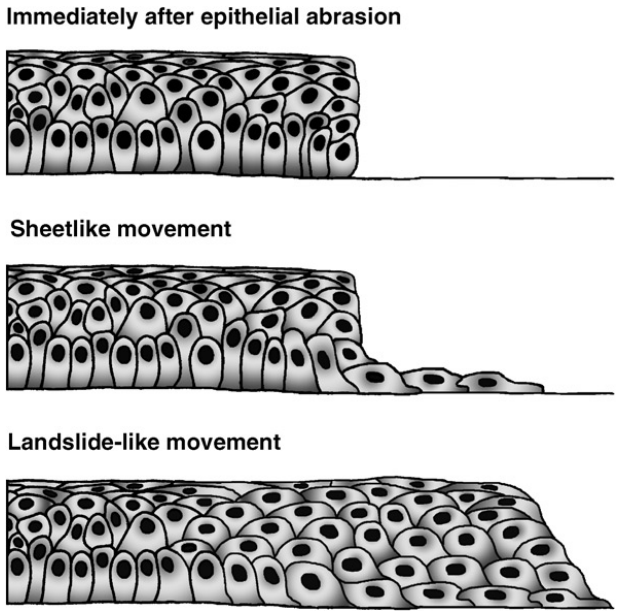

Figure 8: Cell movements in response to injury. After corneal epithelial damage, two types of cell movements occur during wound repair. Taken from (Suzuki *et al.*, 2003).

In vivo studies by Matsuda and co-workers in the rabbit cornea showed that 5 hours after wounding cells start to migrate at a constant rate of 60 – 80 mm/hour until the wound is completely closed (Matsuda *et al.*, 1985). Cell migration is a process that is based on the presence of a complex cytoplasmic array of actin – rich stress fibres. Studies in which these stress fibres were blocked by the inhibition of actin polymerization through the use of Proparacaine (a topical ocular anesthetic), have shown to inhibit epithelial cell migration and adhesion partly due to the alteration of the actin cytoskeleton (Jumblatt and Neufeld, 1981; Lu *et al.*, 2001). On the other hand, cell migration is stimulated by cyclic adenosine 3', 5'-phosphate (cAMP). Levels of cAMP normally increase during migration (Jumblatt and Neufeld, 1981). An *in vitro* study by Kimura and co-workers, has shown that β-Pix (p21-activated kinase [Pak]-interacting

exchange factor) has a role in regulating the formation of these focal adhesions, as well as regulating cell migration by underlying the stimulatory effects of fibronectin (Kimura *et al.*, 2011).

c) Cell proliferation and differentiation

The wounded area is covered by cell layers through the process of flattening and lengthening of cells during the migration phase, i.e. enabling epithelial closure by sliding without a change in the cell number. Cell proliferation on the other hand, actually repopulates the wounded area. The phases of proliferation and migration are separated into distinct compartments: limbal and peripheral epithelial cells display an accentuated proliferative response to wounding. On the other hand, cells close to the migrating epithelium do not proliferate (Chung *et al.*, 1999).

The amount of cell proliferation is strictly dependant on regeneration requirements. Limbal stem cells are slow cycling during homeostasis, relatively undifferentiated within the limbal epithelial basal layer and have been found to have prolonged self-renewal and a high proliferative response to wound healing (Thoft and Friend, 1983). Upon division, LSCs give rise to cycling transient amplifying (TA) cells. These cells are located within the peripheral and central corneal epithelium (See Figure 9). “Young” TA cells with a high division capacity are usually located within the peripheral cornea. On the other hand, more mature TA’s with a lower proliferative capacity are located in the central cornea. Mature TA’s are believed to divide only once before terminally differentiating.

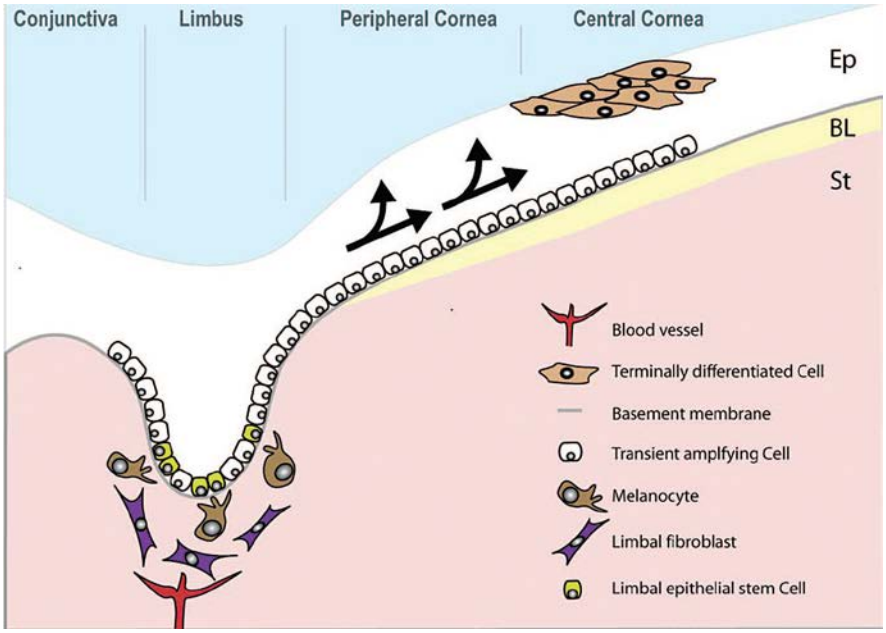

Figure 9: The human limbus. Taken from (Secker and Daniels, 2008).

During homeostasis, TA cells do not always fulfil their capacity of dividing, so stem cell then need to be activated from their normal *in vivo* quiescent state. When the corneal epithelium is stimulated by an injury it can use three different strategies to increase its cell population (Lehrer *et al.*, 1998).

1. The recruitment of more stem cells in order to obtain a higher division frequency, therefore producing more TA cells.

2. Younger TA cells located in the peripheral cornea may act to their fullest replicative potential, thus generating more mature TA cells.

3. The efficiency of TA's replication may be enhanced by shortening the cell cycle time.

All three approaches result in the generation of a higher number of terminally differentiated cells. During homeostasis, cell proliferation and differentiation behaves the same way as during wound healing. However in normal homeostasis, the corneal epithelium is renewed by the continuous centripetal movement of peripheral corneal epithelium towards the centre of the cornea. It is a balance of cell loss that occurs from the anterior movement of basal epithelial cells to the surface and into the tear film. This is also called the X, Y, Z hypothesis by Thoft & Friend and this was explained in section 1.2.1.1 (See Fig. 4).

d) Re-epithelialization

In the third and final phase, the hemidesmosomes are re-formed and synthesis of an extra-cellular matrix and cell reassembly occur. This phase re-establishes the multicellular layers (Lu *et al.,* 2001).

Major players found to be involved during corneal wound healing include cytokines and growth factors found in the tear film and the aqueous fluid such as Cytokines, in particular interleukin-1β, TGF-β1, KGF and HGF. EGF also has been shown to be involved in the wound healing response by facilitating epithelial proliferation (Kitazawa *et al*., 1990). Matrix metalloproteinases such as MMP-2 and MMP-9 have been shown to act as important extracellular-modelling enzymes during wound healing in the cornea. A study by Touhami and co-workers found that the growth factor TrkA was highly expressed in the limbal basal epithelium and this suggests that NGF signalling is beneficial for LSC survival (Touhami *et al.,* 2002). Furthermore, the high number of TGF-β receptors could possibly contribute to the low mitotic activity and the slow cycling characteristic of LSCs (Schlotzer-Schrehardt and Kruse, 2005).

1.5 Cornea Tissue Engineering

The field of transplant surgery has been revolutionised by the *in vitro* engineering of living fabrications used to replace failing and damaged tissues and organs, therefore offering a solution to the constant problem concerning shortage of donor organ or tissue. The conventional method in tissue engineering is the seeding of cells into biodegradable scaffolds. This method has developed clinical products with applications for bone (Vacanti *et al*., 2001), cartilage (Marcacci *et al*., 2005), blood vessels (Poh *et al*., 2005; Shin'oka *et al*., 2001) and heart valves (Veseley 2005). Epithelial tissue engineering commonly uses techniques that use epithelial grafts placed upon various carrier materials such as amniotic membrane, collagen gels and matrices, and fibrin gels. These were successfully used to regenerate epidermis (Pellegrini *et al*., 1999), corneal epithelium (Rama *et al*., 2001) and oral mucosal epithelium (Izumi *et al*., 2003).

Cornea models and equivalents are being created for a variety of purpose including, but not exclusively for a) replacement and transplantation after injury or loss, b) research

models to study the underlying biology and c) for replacing animal models for testing drugs, toxins, treatments and cosmetics. Developed cornea models vary from expanding corneal epithelial cells on the human amniotic membrane, matrices or scaffolds for transplant purpose, to more complex models that may be predominantly cellular or created with biomaterials. 3D culture systems using bioengineered scaffolds have been developed to study collagen biosynthesis and scarring using the three major corneal cell types (epithelial, fibroblasts and endothelial cells) (Dreier *et al*., 2013; Yanez-Soto *et al*., 2013). Ultimately, the development of an artificial cornea that can be used for transplantation is being investigated (Polisetti *et al*., 2013).

1.5.1 Techniques to generate corneal epithelium

Kenyon and Tseng were the first in 1989 to show that transplantation of autologous limbal tissue was able to fully restore the corneal epithelium. Autologous limbal tissue transplantation remains a successful option in patients with unilateral LSCD, however in cases of bilateral LSCD autologous tissue from a donor (living or cadaveric) is needed where immune rejection plays a major risk as well as the risk at causing stem cell failure in the living donor (Angunawela *et al*., 2013). For this reason, *ex vivo* techniques that can expand limbal epithelium *in vitro* from small biopsies for transplantation purpose, are very important.

Ex-vivo expanded limbal stem cell sheets have first shown to be successful to treat patients by Pellegrini *et al*., in 1997. This technique has since been widely used to successfully treat many patients. The basic steps involved in this technique are the isolation of limbal epithelial cells from the biopsy, culturing the cells onto an appropriate substrate and conditions and transplanting the confluent epithelial sheet of cells with its substrate onto the patient's eye. The most commonly used substrate for culturing LSC's has been the human amniotic membrane (HAM) derived from the placenta as this has been found to contain high levels of EGF, KGF, HGF and bFGF, possibly all involved in promoting epithelial proliferation and also epithelium-stromal interactions (Kenyon, 2005). Other substrates such as Fibrin matrices have also been used and have shown to maintain LSC's (Meyer-Blazejewska *et al*., 2010). The fibrin matrix is known to degrade after 24-48 hours and also does not need to be attached to

the patient's eye with sutures as it is naturally adhesive (Rama *et al*., 2001). Moreover, synthetic polymers have also been used. These are substrates that are temperature responsive that can be detached from the culture plates by changing the temperature and have been used for successfully treating LSCD in patients (Sitalakshmi *et al*., 2009; Nishida *et al*., 2004). Other scaffold types include the use of contact lenses onto which to grow LSC's (Di Girolamo *et al*., 2009), scaffolds derived from silk worms cocoons (Chirila *et al*., 2008) and plastic compressed collagen (Levis *et al*., 2010).

Once the limbal epithelial monolayer has grown, the cells are air lifted. This promotes cell proliferation at an air fluid interface and cellular stratification is achieved (Prunieras *et al*., 1983). Some evidence suggests that this technique however promotes cellular squamous metaplasia (Li *et al*., 2008).

However, an unmet need remains for cells that can be used for transplantation in cases of severe and bilateral LSCD and this has led to the search of new sources of cells.

1.6 Transdifferentiation & Reprogramming studies

Alternative cell sources have been explored for treating bilateral LSCD, such as oral mucosal epithelial cells (Nakamura *et al*., 2003) and have proven to be useful, in cases of bilateral LSCD (Nishida *et al*., 2004; Ang *et al*., 2006). Buccal epithelial cells have been found to express mucins and Ck3, both believed to help in their role to treat LSCD, however their cell identity was found to persist over time (Chen *et al*., 2009). Mesenchymal stem cells (Ma *et al*., 2006), embryonic stem cells (Ahmad *et al*., 2007), neural crest-derived stem cell-like cells (Brandl *et al*., 2009) and immature dental pulp stem cells (Gomes *et al*., 2010) have also been proposed for corneal epithelial regeneration. However, no long-term results using these other stem cell sources have been reported until now. A number of studies have shown in animal models that ex-vivo cultured conjunctival tissue transplanted in LSCD affected eyes, was similar to that of the corneal epithelium (Tanioka *et al*., 2006; Scuderi *et al*., 2002). In addition, autologous mesenchymal and induced pluripotent stem cells (IPSCs) therapies could potentially create a vast number of new types of engineered tissue (Rashid *et al*., 2010; Branch *et al*., 2012). A recent study has shown the successful generation of corneal epithelial cells from dermal fibroblast IPSCs (Hayashi *et al*., 2012).

Reprogramming cells using transcription factors has become commonplace since Yamanaka developed iPS cell technology in 2006 in which he found that differentiated cells can be reprogrammed to an embryonic-like state by transfer of nuclear contents into oocytes or by fusion with embryonic stem (ES) cells (Takahashi & Yamanaka, 2006). Nevertheless, other ways of reprogramming cells exist, such as through tissue recombination experiments and through environmental modifications/stimuli.

1.6.1 From skin to cornea

Recently, interest has been drawn to the use of the hair follicle (HF) as an easily accessible source of adult stem cells. Mesenchymal stem cells are harboured within the dermal papilla of the hair follicle, as well as in the connective tissue sheath, and if subjected to specific signals can differentiate into diverse lineages such as hematopoietic, adipogenic, osteogenic, chondrogenic, myogenic, and neurogenic (Lako *et al*., 2002; Jahoda *et al*., 2003; Richardson *et al*., 2005). On the other hand, the bulge region of the outer root sheath (ORS) (see Fig. 10) is believed to store hair follicle stem cells (adult stem cells) of epithelial origin that can differentiate into hair follicles and sebaceous glands under normal physiological conditions, or into epidermis after injury.

Recent studies have shown that hair follicle derived stem cells have the potential to express corneal epithelial markers when placed under specific culture conditions (Blazejewska *et al*., 2009) thus proving they possess a high degree of plasticity and can be pushed to the extremes of lineage boundaries by simply modifying their microenvironment.

Natural trans-differentiation has only shown to occur between closely related cell types (Barrero & Belmonte, 2011). It is known that hair follicle keratinocytes and corneal epithelial cells have a common embryological origin and it has been shown that cells with a similar ontogenesis can undergo trans-differentiation by modulating the microenvironment in which they are placed. However, the work carried out by Blazejewska *et al*., 2009, did not show a long-term establishment of corneal epithelial marker expression.

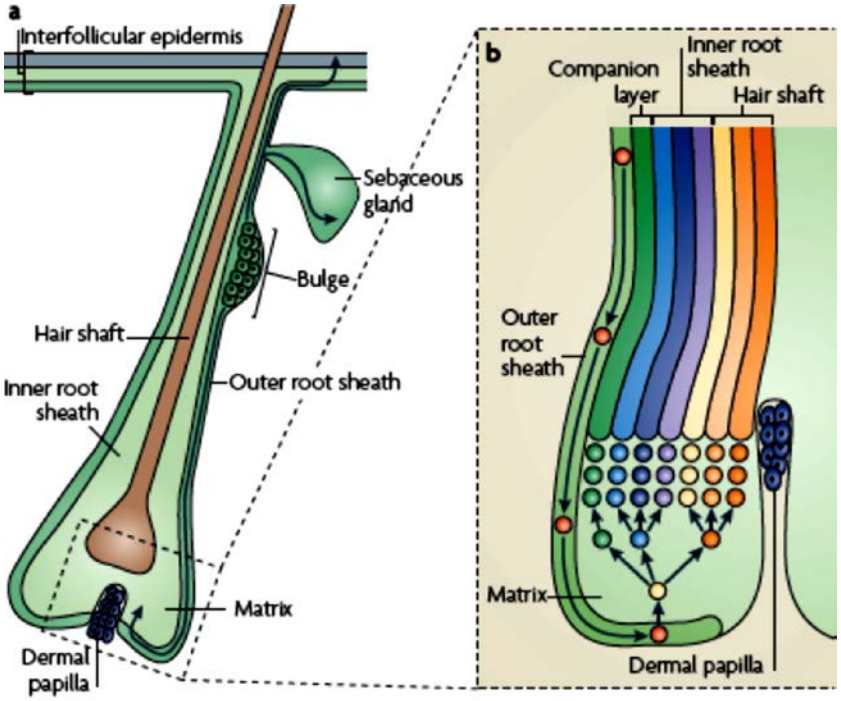

Figure 10: Representative image of a hair follicle showing its main differentiated cell layers. Taken from (Blanpain & Fuchs, 2009).

1.6.2 Using mesenchymal influence for reprogramming purposes

Fibroblasts play a crucial role in the development and maintenance of the extracellular matrix (ECM) in most parts of the human body (Branch *et al*., 2012). The properties of fibroblasts change according to the context in which they are found. For instance, fibroblasts found in a developing tissue compared to those found in adult tissue, as well as those found in wounded tissue compared to those found in unwounded tissue. It is known that in skin for instance, signals from fibroblasts within the underlying dermis are required to form hair follicles in developing epidermis (Fuchs, 2008; Millar, 2002; Yang & Cotsarelis, 2010). This fact not only underlines the importance of fibroblasts of mesenchymal origin in early stages of development but also highlights the fact that a crosstalk between epidermis and dermis exists.

In another study conducted by Collins *et al*., 2011 it was demonstrated that the dermal niche (the mesenchymal niche) that supports the differentiation of the epidermis is extremely plastic as it has the potential of remodelling and reprogramming itself to a

neonatal state in response to external stimuli (such as injury) coming from the epidermis.

In a study conducted by Ferraris *et al*., 2000, adult central corneal cells produced epidermal-like features when placed into close proximity to embryonic dermis, thus not only showing that the corneal epithelial progenitor cells, also called TA (transient amplifying) cells are highly plastic and can be reprogrammed but also that the mesenchymal part of the embryonic skin (dermis) that normally supports the skin epidermis, retains signals that induce corneal epithelial progenitor cells to change their cell identity. Embryonic dermal signals have therefore shown to be able to dedifferentiate adult corneal epithelial cells and differentiate these into epidermal cells. These signals can reactivate developmental regulators within these cells that in turn can facilitate the acquisition of plasticity and therefore the ability to switch cell identity.

The aforementioned studies demonstrate that the dermis that is of mesenchymal origin, influences epithelial differentiation through epithelial - mesenchymal interactions.

In the cornea, a rabbit model of recombined corneal tissue showed that the underlying stroma dictates the plasticity of limbal corneal epithelial differentiation towards the stem cell phenotype, thus proving that an essential cross-talk is taking place between the stroma and the limbus, favouring the stem-cell phenotype (Espana *et al.,* 2003). In response to injury, stromal keratocytes are activated and lose their keratocyte marker expression, gaining fibroblast and myofibroblast scar-forming phenotypes expressing α-smooth muscle actin (Jester *et al*., 1999; Funderburgh *et al*., 2003). Interestingly, this transition is reversible (Kawakita *et al*., 2005; Espana *et al*., 2003), indicating that like the mesenchymal cells in the dermis, also those in the corneal stroma are influenced by their environment and therefore have an adaptive phenotype.

A better understanding of the cross-talk taking place between the stroma and the corneal epithelium during corneal epithelial homeostasis as well as during wound healing could potentially help identify some major signals that could be used *in vitro* to re-program hair follicle keratinocytes and trans-differentiate them into corneal epithelial cells.

A recent study used identified the ability of Pax6 to reprogram rabbit skin epithelial cells into corneal epithelial cells after the former were transduced with Pax6 (Ouyang *et*

al., 2014). These cells were then transplanted back into a LSCD rabbit model and were shown to re-establish a healthy cornea (Ouyang *et al*., 2014).

1.7 Aims of the thesis:

- **Chapter 2:** "A corneal epithelial wound healing model". Here a scratch wound-healing assay was developed in 2D human corneal epithelial primary cultures. There is an unmet need for a cornea wound healing model that can replicate *in vivo* corneal wound healing and replace tests that were formerly performed on animal eyes. The identification of potential mechanisms and up or down-regulated markers during the several stages wound healing could lead to a better understanding of corneal wound healing biology *in vitro* and *in vivo* as well as identifying ways to modulate the wound healing response. Here I studied corneal epithelial stem and progenitor cell roles in wound healing *in vitro*, using qRTPCR to investigate markers known to be involved in the *in vivo* epithelial wound healing response.

- **Chapter 3: "**Environmental reprogramming of skin epidermal cells in a 2D corneal epithelial culture environment". Here I investigated the potential of trans-differentiating hair follicle epithelial cells to corneal epithelial cells by means of environmental reprogramming using limbal epithelial specific culture media. It was hypothesised that due to the common embryonic origin and similar nature of skin epidermal and cornea epithelial cells, environmental modifications could potentially reprogram these into cornea-like epithelial cells. This study involved the use of a set of cornea and skin (ORS) specific markers that were tested using qRTPCR, to indicate any cellular identity loss or acquisition.

- **Chapter 4:** "Establishing an *in vitro* cornea 3D model", initially focussed on reverting stromal keratocytes from an activated fibroblastic phenotype, as found in stromal wound healing and in *in vitro* 2D cultures, to their quiescent *in vivo* phenotype, using a 3D spheroid hanging drop culture method. It was hypothesized that corneal stromal keratocytes placed in the 3D spheroid culture would revert back to a phenotype, more akin to that found *in vivo* and thus provide optimal support for LSC's. A bilayered 3D cornea model was established by adding corneal epithelial around the stromal core. The extent to which it mirrored the cornea in vivo was investigated using various corneal epithelial and stromal markers by immuno-fluorescence and qRTPCR and also

through histological examination core. Both rabbit and human models were created and progressively refined.

- **Chapter 5:** “Reprogramming hDS and skin epithelial cells” involved short studies investigating two potential ways to reprogram human hair follicle dermal sheath and skin epithelial cells into corneal cells. This first study using the transcription factor Glis1 showed some that transfected DS cells up-regulated Pax6 when placed 3D spheroid cultures. The second study used the technique developed in Chapter 4 to establish a chimeric eye/skin model. This comprised corneal stromal keratocytes surrounded by with human skin keratinocytes in a 3D bi-layered sphere. The hypothesis was that the 3D corneal stroma could potentially reprogram skin epithelial cells to corneal epithelial cells.

2 A 2D culture system for a corneal epithelial wound healing model

2.1 Introduction & Aims

A more complete understanding of the mechanisms involved in *in vivo* corneal epithelial wound healing, with the goal of developing better treatments, can be obtained by studying *in vivo* and *in vitro* wound healing models. Because the size, depth and nature of the wound affect the healing mode and result (Lu *et al*., 2001), various wound healing models have been developed.

In vivo models

In vivo models have been widely used and they are great models to study many of the wound types and healing processes. These include circular debridement wounds where the basement membrane on the stroma is kept, whereas keratectomy wounds remove it. Work by Gipson and Kiorpes in 1982 first showed corneal epithelial wound healing occurring by movement of cell sheets. These studies were confirmed by Sta Iglesia and Steep, 2000 by performing debridement wounding in mice. Circular debridement wounds have been found to be ideal to analyse wound healing by quantifying re-epithelialization, re-innervation, cell proliferation rates and innate immune responses. However, debridement wounds in mice have been shown to cause recurrent erosions (Pal-Ghosh *et al*., 2011), while in larger mammals this is found to be very rare, therefore highlighting the fact that corneal wound healing responses differ between species. While debridement wounds can mainly be used to study cell migration rate and recurrent erosions in mice, rotating burr circular wounds are used to study epithelial barrier re-formation and corneal haze by removing the basement membrane. Most studies investigating mechanical corneal wound healing *in vivo*, use this type of wounding method (Ferrington *et al*., 2013; Chinnery *et al*., 2012). The best wound type of choice to study corneal scarring has been manual superficial keratectomy (MSK) that can be performed by using a sharp trephine and photorefractive keratectomy (PRK) by using excimer lasers in mice, rats and rabbits (Mohan *et al*., 2008; Singh et al., 2011; Blanco-Mezquita *et al*., 2011).While these models create corneal scarring, reports have shown that αSMA positive cells are usually transient and disappear (Netto *et al*., 2005; Ruberti and Zieske, 2008) and therefore these models have been reported by several studies to not be useful to study chronic scars that lead to blindness, such as incisional

wounds. These type of wounds re-create the wound healing response of incisions made on corneas during surgery, such as during corneal transplants and refractive surgery. The incisional wounds promote myofibroblast transformation and scarring as a result that remains over time therefore making this a good model type for studying stromal activation after injury. Angiogenesis is studied using a corneal pocket assay, where an incision is made at a certain distance from the limbus and some growth factors contained in a small pellet are inserted underneath the epithelium into the stroma (Kojima *et al*., 2007). This technique can be used in genetically engineered mice where specific mutations in angiogenesis receptors are made in order to study angiogenesis response to certain growth factors. Alternatively suture wounds can be made and these also induce angiogenesis (Amescua *et al*., 2008). A method originally used to diagnose LSCD is impression cytology and is using a filter paper that is applied to the corneal surface and this removes superficial cells, damaging the barrier (Calonge *et al*., 2004; Singh *et al*., 2005). Many studies have used filter papers to study chemical injuries by using these to deliver the chemicals to the cornea. These have been successful at improving the treatment for patients suffering from chemical injuries to the cornea (Fish and Davidson, 2010; Saika, 2007; Javadi *et al*., 2005).

Ex vivo models

Using organ culture models to study corneal wound healing in response to drugs and different injuries has given the opportunity to reduce the number of living animals used, drastically. Studies using this model type have gained insight into the biology of epithelial cell migration (Gipson and Keezer, 1982; Zieske and Gipson, 1986), investigated the role and effect of signalling and growth factors addition to corneal debridement wounds on their re-epithelialization (Ma *et al*., 2011), as well as the effect of drugs (Yamada *et al*., 2004) and cells and bacteria (Wagoner *et al*., 1984). Organ culture systems mostly have been optimized by using serum-free media or reduced serum and by placing the corneas in an air-liquid interface (Stepp *et al*., 1993; Pipparelli *et al*., 2013). Recently, donor human corneas were used in an organ culture system to study corneal scarring (Janin-Manificat *et al*., 2012). Organ culture systems have also been recently used to investigate the ability of a Rho-associated protein inase (ROCK) inhibitor to minimise the loss of endothelial cells in corneas stored for transplantation purpose (Pipparelli *et al*., 2013). Because corneal wound healing *in vivo* is controlled by immune cells, one limitation of the organ culture system is that it lacks a functional

vascular system within the limbus (Stepp *et al*., 2014). It is not clear whether leukocytes residing in organ cultured corneas are involved in the wound healing response as they do *in vivo* (Stepp *et al*., 2014).

Corneal wound healing models using *in vitro* 2D and 3D cultures have been developed as well, in order to study corneal wound healing. 2D cultures have been developed by using cells grown on uncoated or ECM coated culture wells as well as feeder layers (3T3's for example). 3D cultures have been established by growing cells in gels or bioengineered scaffolds. Human primary corneal epithelial cells can be grown in 2D cultures, however these cells differentiate over time, therefore making cell lines a popular choice for this model system as they are less expensive and give a higher reproducibility, such as SV40 transfected (Araki-Sasaki *et al*., 1995), hTCEpi (Robertson *et al*., 2005) and HCLE (Gipson *et al*., 2003). Unfortunately, the proliferation and differentiation of such cell lines are altered as these transform over time. Generating primary corneal epithelial cultures from the mouse has proven more difficult due to its small size, and CEC derived from both mouse and rat are poorly understood and therefore not a preferred choice for studying corneal wound healing *in vitro* (Stepp *et al*., 2014). 3D wound healing models have been used preferentially when studying stromal cells due to their natural three-dimensional conformation found *in vivo*. Stromal cells have therefore been grown in collagen-based matrices to study cell migration (Kim *et al*., 2010; Lakshman and Petroll, 2012). Current limitations when using collagen gels are their protein contamination when performing biochemical tests. A method developed to study quiescent stromal keratocytes has been to grow these cells in serum free medium. This has been found to maintain a keratocyte phenotype *in vitro* similar to that found *in vivo* (Beales *et al*., 1999; Jester *et al*., 1994). Moreover, this method results in a mixture of cells composed of keratocytes and different types of immune cells that also adhere in culture. Immune cells are lost when stromal cells are passaged, thus producing a more homogeneous cell population with a fibroblastic or myofibroblastic phenotype and an increasing αSMA expression (Jester *et al*., 1995; Bernstein *et al*., 2007). 3D culture systems using bioengineered scaffolds have been developed to study collagen biosynthesis and scarring using the three major corneal cell types (epithelial, fibroblasts and endothelial cells) (Dreier *et al*., 2013; Yanez-Soto *et al*., 2013). Ultimately, the development of an artificial cornea that can be used for transplantation is being investigated (Polisetti *et al*., 2013).

Corneal wound healing models grown in 2D on 3T3 feeder cells have not been investigated. Although these cultures do not include the stromal component, it is believed that the 3T3 feeder layer acts as a surrogate, maintaining LSC's proliferation and clonogenicity in culture. In this study a chemical vs. mechanical scratch wound healing assay in a 2D culture system was first compared, using human primary cell cultures grown onto mitotically inactivated 3T3 mouse feeders. Confluent limbal CEC cultures were wounded and key limbal stem cell markers *ΔNp63*, *ABCG2, C/EBPΔ, p63α, p63β* as well as the putative negative markers *Ck12* and $p27^{KIP1}$ and *BimS* were tested at the different stages of the healing process, using qRTPCR.

It was found that *ΔNp63α*, β, and γ are expressed during wound healing and are connected to limbal cell migration and corneal regeneration and differentiation (Di Iorio et al., 2006). For this reason, *ΔNp63*, *p63α* and *p63β* were used in this study to establish whether specific up- or down-regulation was taking place during wound healing *in vitro*, also reflecting the stem cell potential in these cultures. *ΔNp63α* has been described to be the most precise marker for identifying limbal stem cells. In fact, *ΔNp63α* abundance decreases during clonal transition from stem to TA cell and the protein is absent in TA cells. On the other hand, *ΔNp63β* and *ΔNp63γ* are thought to be involved in epithelial differentiation, hence during the regeneration of the cornea (Di Iorio et al., 2006). *ΔNp63* was used as it comprises all three isoforms and because *ΔNp63γ* could not be designed as a primer due to being instable, this way the more general form *ΔNp63* also included the *γ* form.

ABCG2, marker for limbal stem cell-identification which has been previously used for identifying bone marrow stem cells, has been proposed as a universal marker for stem cells (de Paiva *et al*., 2005). The *ABCG2* protein is mainly found in the basal cells of the limbal epithelia, however it is not found in the limbal suprabasal and corneal epithelial. Testing this marker in the wound healing model would assess the type of cells present in the culture during wound healing *in vitro*.

The CCAAT enhancer binding protein δ (*C/EBPδ*) is a member of the family of the leucine zipper transcription factors and it is involved in a various number of cellular processes such as in the control of proliferation, differentiation, metabolism and inflammation (Johnson, 2005; Ramji and Foka, 2002). *C/EBPδ* has also been found to

be implicated in the regulation of limbal stem cells self-renewal as it regulates the cell cycle by generating a G0/G1 arrest (Barbaro *et al*., 2007).

The intermediate filament component *Ck12* plays an important role in maintaining the integrity of the corneal epithelium. It is known that animals that are K12-deficient have a thinner and fragile corneal epithelial layer due to the fact that corneal epithelial cells are not able to attach to the ocular surface (Kao et al., 1996).

Cyclins and cyclin-dependent kinases (CDKs) are known to control cell cycle progression (Sherr and Roberts, 1995). CDK inhibitors (CKIs) regulate cyclin/CDK activity, $p27^{KIP1}$ is one of them (Toyoshima and Hunter, 1994; *Kato et al*., 1994). $p27^{KIP1}$ is found at high levels in quiescent cells and once cells are activated/stimulated and progress through the cell cycle, its presence is much lower (Zieske et al., 2004). Many studies have described the involvement of $p27^{KIP1}$ in corneal epithelial wound healing, especially in regulating of cell proliferation in response to wounding (Yoshida *et al*., 2002). Degradation of $p27^{KIP1}$ by SKp2 has been found to activate proliferation in corneal epithelial cells (Yoshida *et al*., 2002). While TGF-β induces the expression of *p15*, *p21* and $p27^{KIP1}$ CDKIs in epithelial cells (Yue and Mulder, 2001; Hannon and Beach, 1994), it does not affect $p27^{KIP1}$ expression in corneal epithelial cells (Chen *et al*., 2006).

Apoptosis is first observed after injury of the cornea. *BimS* is a member of the pro-apoptotic *Bcl-2* family and was used in this assay to evaluate the amount of cell death taking place after the injury was made and during wound healing. BimS is one of the three isoforms *BimS*, *BimL* and *BimEL*, that are given rise by alternative splicing (O'Connor *et al*., 1998) and that are powerful inducers of apoptosis. *Bcl-2* has been found to play a crucial role in modulating apoptosis in the human cornea *in vivo*, by causing cell desquamation (Yamamoto *et al*., 2001).

Aims of this study

- Establishment of an *in vitro* wound healing scratch assay using the traditional 2D culture system to culture human limbal corneal stem cells.
- At different wound healing stages the expression of specific LSC markers as well as negative markers were tested.

2.2 Materials & Methods

All the experimental procedures carried out in Chapter 1 were conducted in compliance with Newcastle University Health & Safety Policy according to the Control of Substances Hazardous to Health (COSHH) regulations. All tissue culture work was undertaken at Containment Level 2 using standard aseptic techniques.

2.2.1 Materials

All reagents used in this chapter were directly derived from the relevant suppliers and COSHH regulations were respected throughout their usage.

2.2.1.1 Cells

The successful growth and expansion of human limbal stem cells requires specific cell culture conditions and protocols. Limbal stem cells are obtained from human limbal tissue donated for research, obtained from the UK Eye Banks. Cells are released from the tissue by serial trypsinisation to release free epithelial cells in suspension. The culture of limbal stem cells is achieved by plating these on a layer of mitotically inactivated 3T3 J2 cells. The J2 clone of random-bred Swiss mouse 3T3 cells was selected to provide optimal feeder support of keratinocytes. These cells are maintained by weekly passaging when they are 70-90% confluent. All cell cultures discussed in this chapter were maintained at a temperature of 37°C with a humidified gas mixture containing 5% CO_2.

2.2.1.2 Culture Media & tissue culture components

3T3 growth medium required for the culture and growth of 3T3 cells was composed of the following components shown in Table 1.

Reagent	Composition	Supplier
High Glucose DMEM	500ml	Gibco
Adult Bovine Serum	10%	Invitrogen Cat.no. 16170078
100IU/ml Penicillin and 100µg/ml Streptomycin	1%	Gibco

Table 1: Composition of 3T3 culture medium. DMEM = Dulbecco's Modified Eagle's Medium.

Reagent	Composition	Supplier
Low Glucose DMEM	375ml (75%)	Sigma-Aldrich
Ham's F12 Medium	125ml (25%)	Sigma-Aldrich
Fetal Bovine Serum	10%	Sigma-Aldrich
100IU/ml Penicillin and 100µg/ml Streptomycin	1%	Gibco
Hydrocortisone	0.4µg/ml	Sigma-Aldrich
Insulin	5µg/ml	Sigma-Aldrich
Triiodothyronine	1.4ng/ml	Sigma-Aldrich
Adenine	24mg/ml	Sigma-Aldrich
Cholera Toxin	8.4ng/ml	Sigma-Aldrich
Epidermal Growth Factor	10ng/ml	Sigma-Aldrich

Table 2: Composition of Epithelial Culture Medium

Culture media for the growth of human epithelial cells was more complex. The components for the successful expansion of limbal stem cells are listed in Table 2.

All media were prepared under a laminar flow hood and filter sterilised. The media were divided into 50ml centrifuge tubes and refrigerated at 4°C.

Further tissue culture components used are listed in Table 3 below.

Reagent	Supplier
Mitomycin C from *Streptomyces caespitosus*	Sigma-Aldrich
DPBS for tissue culture	Gibco Life Technologies
0.02% EDTA	Sigma-Aldrich
0.05% Trypsin-EDTA	Sigma-Aldrich

Table 3: Tissue culture components

2.2.1.3 Molecular Biology Materials

RNA extraction & Isolation

RNA was extracted using the TRIzol method (described in the Methods section). The following components were used:

- TRIzol [Invitrogen]
- Chloroform [BDH]
- 75% Ethanol
- Isopropyl alcohol [BDH]
- RNase free dH_2O

Reverse Transcription

Reverse transcription was performed using the following reagents:

- DNAse reaction buffer
- DNAse
- STOP solution
- Random Primers
- RNase free dH_2O
- RT Buffer
- dNTPs
- RNAsin
- RTase

All reverse transcription reagents were supplied by Promega.

Primers

Primers were all designed manually and ordered from Eurofins MWG Synthesis.

The primers sequences and annealing temperatures are all listed in Table 4.

Gene	Primer	Sequence (5'-3')	Ta (°C)
ΔNp63	Forward	GAAACGTACAGGCAACAGCA	65
	Reverse	GCTGCTGAGGGTTGATAAGC	
ABCG2	Forward	GCGACCTGCCAATTTCAAATG	65
	Reverse	GACCCTGTTAATCCGTTCGTT	
GAPDH	Forward	TGCACCACCAACTGCTTAGC	53
	Reverse	GGCATGGACTGTGGTCATGAG	
C/EBPΔ	Forward	TTGGGACATAGGAGCGCAAA	55
	Reverse	CGTTTAGCTTCTCTCGCAGT	
Ck12	Forward	GAAGAAGAACCACGAGGATG	53
	Reverse	TCTGCTCAGCGATGGTTTCA	
p27	Forward	AAACTGGGTCAGAGTGAGAG	57.3
	Reverse	TCATCATCCACTTGCAGACC	
p63α	Forward	GAAACGTACACGCAACAGCA	55
	Reverse	GCTGCTGAGGGTTGATAAGC	
p63γ	Forward	GCAGTACCTTCCTCAGCAC	55
	Reverse	CTCCACAAGCTGATTCCTGA	
BimS	Forward	ATGGCAAAGCAACCTTCTGAT	53
	Reverse	GCTCTGTCTGTAGGGAGGTAGG	

Table 4: Primers, their sequences and annealing temperatures (Ta).

Quantitative real-time PCR

Quantitative real-time pcr was performed using the LightCycler Real Time PCR machine [Roche] and by using SYBR Green from Sigma.

2.2.2 Methods

2.2.2.1 Culturing human corneal epithelial cells

Plating 3T3 feeder cells

300,000 3T3 J2 Swiss mouse embryonic fibroblasts were plated in a tissue culture flask of 25cm² size containing 3T3 medium, cultured in an incubator at 37°C. Upon 90% confluence (2-3 days), 3T3 medium was changed and the 3T3 cells were mitotically inactivated through the addition of 10µl of Mitomycin C (MMC)/ 3T3 medium volume (ml). The culture was left in the incubator at 37°C for 2 h. The medium was then removed and disposed appropriately and safely into the MMC waste and the culture was washed 3 times with DPBS. The 3T3 cells were then released from the tissue culture flask through the addition of 0.05% Trypsin-EDTA and a 3 minute incubation at 37°C. The cells were then inspected under phase microscopy and the flask was gently tapped in order to dissolve cell clumps. The trypsin containing the 3T3 cells was pipetted into a 20ml centrifuge tube and centrifuged for 3 minutes at 1,000 revolutions per minute (rpm) with an equivalent balance. The supernatant was removed and the resulting pellet was re-suspended in 3T3 medium. Cell counting was performed in order to quantify the number of cells plated with the final aim to obtain appropriate cultures. This was achieved by using a standard haemocytometer technique and by counting cells in the central square and in the upper left corner and lower right corner. The average number of cells was calculated and this number represented $x10^4$cells/ml. 24,000 cells/cm^2 of plastic were plated, where the radius area of the tissue culture well was calculated and implemented into the formula πr^2. The 3T3 cells were plated in a 4 well plate and incubated at 37°C overnight to be used the next day.

Preparation & culture of limbal corneal epithelial cells

Human limbal tissue was donated for research from UK Eye Banks. Using a pair of sterile forceps, the limbal ring was removed from the transport medium and washed in a DPBS containing well. The limbal ring was dissected into approximately 1mm² pieces using a sterile scalpel and the limbal pieces were exposed to 4 cycles of trypsinisation each lasting no more than 20 minute and incubated at 37°C. After every 10 minute the limbal pieces were agitated using a sterile pipette in order to promote cell detachment from the tissue. After every cycle, the trypsin was transferred into a 25ml centrifuge tube and centrifuged for 3 minute at 1,000 rpm. The supernatant was removed and the resulting pellet was re-suspended in 2ml of limbal medium. The resulting pellets from the 4 trypsinisation cycles were pooled together, the 3T3 medium from the 3T3 cultures was removed and the 2ml cell suspension was divided up equally into 4 wells of a 4-well plate and directly plated on to the 3T3 cultures and incubated at 37°C. The limbal culture medium was changed on the third day, then every other day.

In vitro injury model

The 2ml of limbal cell suspension was plated equally on 4 wells of a 4-well plate. Upon confluence, one well was used as a control and the other 3 wells were wounded. The area that had to be wounded was circled with a marker pen on the outside bottom base of the well, using a circular item (in this case a button for the small 20% size and a two pence coin for the 55% size). The wounded area was approximately 20% or 55% and was achieved using a sterile cotton swab. For the chemical wounding the cotton swab was dipped in 70% ethanol. 1ml of limbal medium was then added to all four cultures and then removed again in order to remove any debris and dead cells. 2ml of fresh media were added to the cultures and these were incubated at 37°C. Pictures of the wound edges were taken at hourly intervals initially and then every day at the same time after having removed 1ml of media and replaced it with 1ml of fresh media. Pictures were taken at phase 1 with magnification 5 and 10 using the phase contrast microscope ZEISS Axio Cam HRC Axiovert 200M.

Pictures were also taken through the use of Nikon BioStation CT. These were taken automatically every 10 minutes and six different positions within the culture well were taken in order to observe wound healing from different angles.

4 cultures were used to test gene expression at different stages of wound healing. The non-wounded culture was used as a control, therefore mimicking gene expression in healthy corneal epithelial cells. The three wounded cultures were tested for gene expression at 3 different stages: immediately after wounding, when the culture was covering 50% of the wound and when the wounded culture was fully healed and confluent. At any of these stages, the feeder cells were removed from the limbal epithelial culture by incubating at room temperature for 30 seconds with 1ml of EDTA. The EDTA solution was pipetted over the base of the culture well in order to ensure removal of all the feeder cells. EDTA was then removed and the culture was incubated at 37°C for 10 minute with 1ml of trypsin. The well's base was then pipetted in a circular motion until clear to ensure that all epithelial cells detached from it. The trypsin was then removed and transferred into a 25ml centrifuge tube and centrifuged for 3 minute at 1,000 rpm. The supernatant was removed and the resulting pellet was re-suspended in Trizol in order to proceed with the RNA extraction method.

2.2.2.2 Molecular Biology

RNA extraction & Isolation

TRIzol is used to isolate total RNA from cells and tissues and it maintains the integrity of RNA while disrupting cells and dissolving cell components.

0.2ml of chloroform was added per 1ml TRIzol reagent to the tested samples. The reaction tube was shaken vigorously for 15 seconds and then centrifuged at 12,000 rpm for 15 minutes at 4°C. The aqueous supernatant was pipetted off and transferred into a fresh eppendorf tube. 0.5ml of isopropyl alcohol was added to the sample containing the aqueous supernatant and was left to incubate at room temperature for 10 minutes. The reaction tube was then centrifuged at 12,000 rpm for 10 minutes at 4°C, the supernatant was removed from the resulting RNA pellet and 1ml of 75% ethanol was added and the reaction tube was vortexed, centrifuged at 7,500 rpm for 5 minutes at 4°C. The supernatant was removed and the pellet was allowed to dry for 10 minutes. The dried pellet was then dissolved in 11µl of dH_2O and the reaction tube incubated for 10 minutes at 60°C. The RNA mixture was then either stored at -80°C or reverse transcription (RT) was performed.

Reverse Transcription

The quantity of RNA extracted was measured using a NanoDrop machine [LabTech International]. The RNA values in ng/µl were converted into µg/µl and the volume in µl was made up to 8µl with dH_20.

Three mastermixes were made up:

1. Mastermix 1 (MM1) was composed of (1x) µl DNAse buffer and (1x) DNAse. (x represents the number of samples tested) 2µl of this mastermix was added into each sample to be tested. The mix was incubated at 37°C for 30 minutes, then 1µl STOP solution was added.

2. Mastermix 2 (MM2) was composed of (1x) Random Primers and (1.5x) dH_2O. 2.5µl of this mix was added to the reaction mix which was then incubated at 70°C for 5 minutes.

3. The third mastermix (MM3) was composed of (5x) RT Buffer, 4(1.25x) dNTPs, (0.5x) RNAsin and (1x) RTase. 11.5µl of this mix was added into each reaction mix tube which was then incubated at 37°C for 60 minutes and then at 99°C for 5 minutes. The last step converts RNA to cDNA and the final mixture was stored on ice ready to be used for the real-time PCR reaction or frozen at -20°C.

Primer Design

Primers were designed by using the National Centre for Biotechnology Information database BLAST website:

http://blast.ncbi.nlm.nih.gov/Blast.cgi?PROGRAM=blastn&BLAST_PROGRAMS=megaBlast&PAGE_TYPE=BlastSearch&SHOW_DEFAULTS=on&LINK_LOC=blasthome.

Forward and reverse sequence primers for quantitative real-time pcr were designed in order to span two different exon sequences in order to avoid genomic contamination. In addition, the primers were designed to be 120 base pairs up-stream and down-stream within the gene and to be approximately 20 base pairs long. The designed primers had a

high T-A's content and their melting temperature (Tm) was around 60°C and this was determined by using the formula Tm = 4(G+C) + 2(A+T).

Quantitative real-time PCR

Real-time PCR was performed in order to detect and quantify gene expression by measuring the DNA sequences of interest compared with a standard reference gene. In this case the reference gene was glyceraldehyde-3-phopshate dehydrogenase (GAPDH). The sequences of the primers tested and the relevant annealing temperatures are described in the Materials section 2.2.1.3.

Real-time PCR was performed using the LightCycler Real Time PCR machine (Roche). The reaction mix was composed of 5µl SYBR Green (Sigma), 0.5µl Forward Primer, 0.5µl Reverse Primer, 3µl dH_2O and 1µl cDNA. 10µl of the mixture was used to fill each capillary tube to be amplified. Each sample was measured in triplicate with GAPDH as the endogenous control and using dH_2O as the negative control.

The tubes were capped and centrifuged at low speed for a couple of minutes to ensure the mix moved to the base of the tube. The capillary tubes were then placed into the LightCycler. The reaction parameters were the following: 95°C for 15 minutes, 50 cycles of 94°C for 15 seconds, primer specific annealing temperature for 30 seconds and 72°C for 20 seconds. Results were analysed using the Comparative Ct Method based on 3 steps: step 1: normalization to endogenous control, step 2: normalization to reference sample and step 3: uses the formula $2^{-\Delta\Delta Ct}$ to calculate fold changes. This analysis method calculates a relative quantification of gene expression.

Statistical Analysis

Data are presented as means and standard deviations. Comparisons between groups were done using ANOVA (Analysis of Variance) assuming a single factor analysis with a confidence level of 95%. $p < 0.05$ was considered significant.

ANOVA is a statistical test used to determine whether the variability between and within more than 2 sets of the tested samples are significantly different. The test is based on the Null Hypothesis.

2.3 Results

2.3.1 Human limbal corneal epithelial cultures

The tissue culture techniques described in the Methods section 2.2.2.1 were successful in establishing limbal corneal epithelial culture growth. The limbal epithelial cells were co-cultured with mitotically inactivated 3T3 mouse fibroblasts. Early growth of limbal epithelial colonies showed classical stem cell appearance, such as containing compact and small homogenous looking cells with large nuclei and a little cytoplasm (see Figure 11).

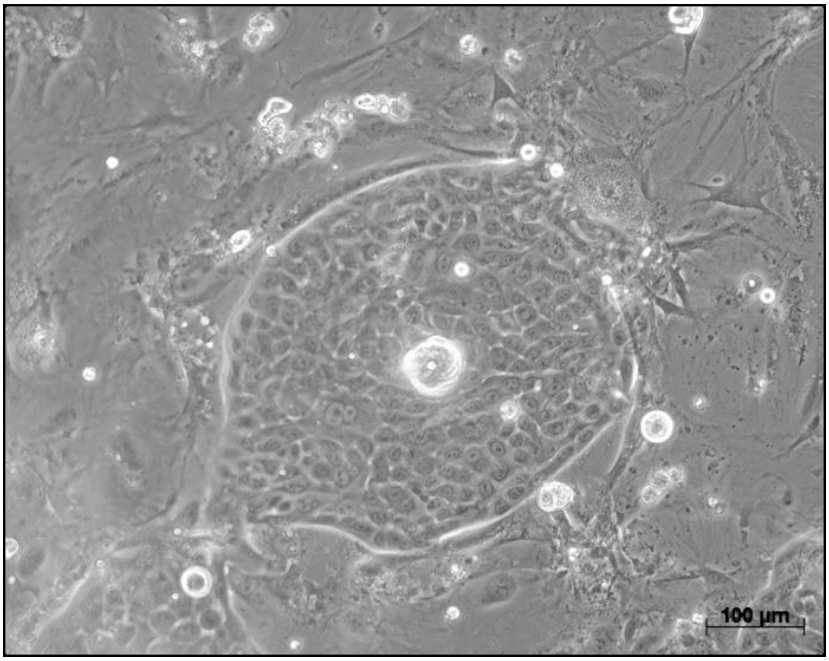

Figure 11: Limbal epithelial co-culture with 3T3 mouse fibroblasts

A phase contrast micrograph of a primary limbal epithelial culture.

Typically, epithelial colonies were noted after 3 days of culture and reached confluence approximately after one week. Figure 11 shows a limbal-epithelial primary culture at day 6 of growth.

2.3.2 An in vitro wound healing model

Once limbal corneal epithelial cultures reached confluence, two different *in vitro* wound healing experiments were performed. The first involved wounding two separate corneal epithelial cultures in different ways: wounding the culture mechanically by 20% of its surface area, and the second wounding it chemically by 20%. The second experiment compared mechanically wounding two cultures by 20% and by 50%.

2.3.2.1 Experiment 1: chemical vs. mechanical wounding

Chemical wounding

A confluent culture in a 6-well plate was centrally wounded with a pointed cotton swab that was dipped in 70% ethanol. The area wounded was approximately 20% of the surface area and the wound took 4 days to heal. Chemical wounding produced a smooth wound margin (see Fig. 12 at day1).

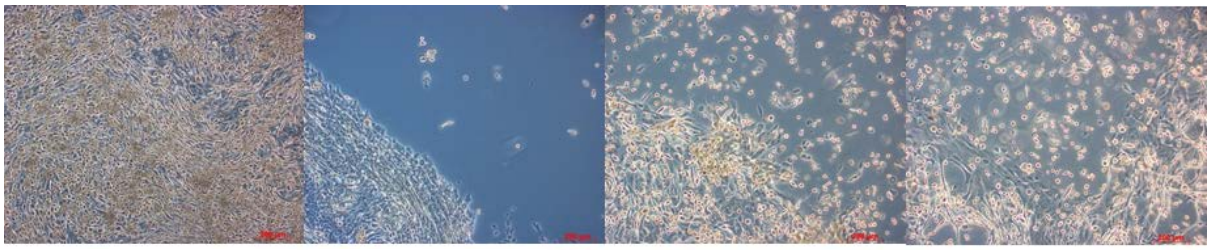

Confluent corneal epithelial culture before wounding took place.

Day 1: chemical wounding.

Day 2: Cell migration and cell proliferation to cover the wound are observable.

Day 3: Cell density at the centre of the wound is increasing.

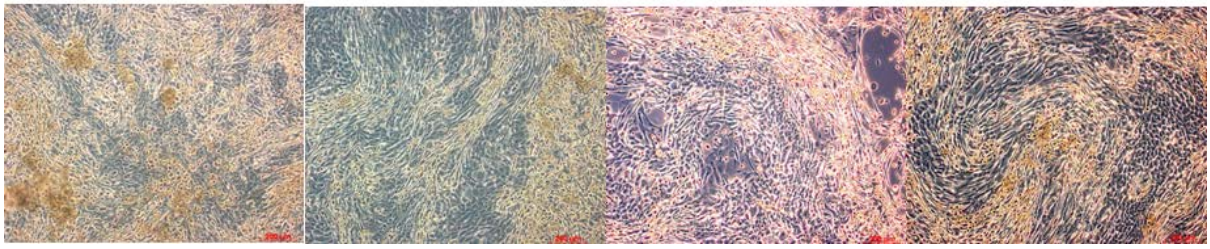

Day 4: wound closure.

Day 5

Day 6

Day 7: Thickening of the cell layer covering the wound.

Figure 12: 20% chemical wounding

Images taken with the phase contrast microscope ZEISS Axio Cam HRC Axiovert. Scale bars: 200µm.

Mechanical wounding

A confluent culture was centrally wounded with a cotton swab by 20% of the well surface area. The wound took 4 days to heal. Mechanical wounding did not produce a smooth wound margin as seen with chemical wounding.

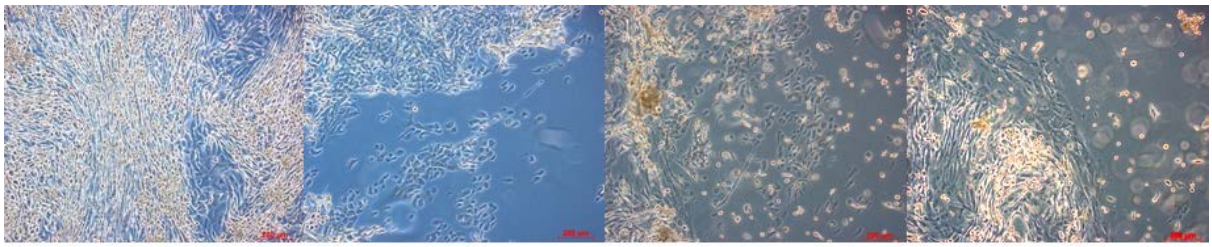

Pre-wound | Day 1: Wounded culture | Day 2: Cell migration and proliferation | Day 3: Increased proliferative cells

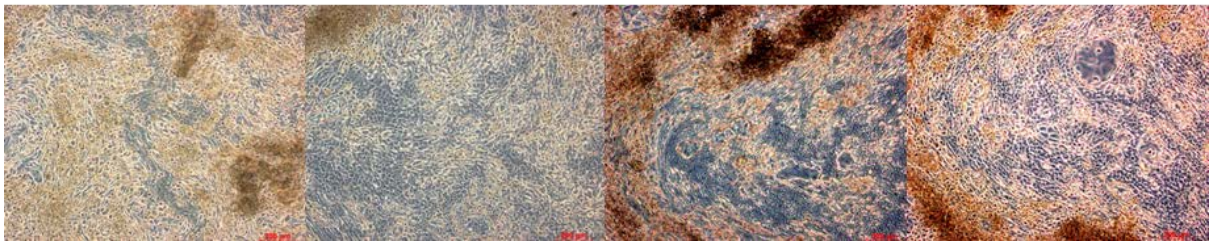

Day 4: wound closure | Day 5 | Day 6 | Day 7: thickening of the cell layer covering the wound.

Figure 13: 20% mechanical wounding

Images taken with the phase contrast microscope ZEISS Axio Cam HRC Axiovert. Scale bars: 200µm.

It was important to compare chemical and mechanical wounding because LSCD is mostly caused by chemical and thermal burns to the eye and an *in vitro* comparison of a physical injury compared to a chemical one was achieved in order to observe any wound healing differences between the two. However, chemical and mechanical wounding both took four days to heal and therefore chemical and mechanical wounding did not have a significant impact on the healing mode and outcome of the wounds.

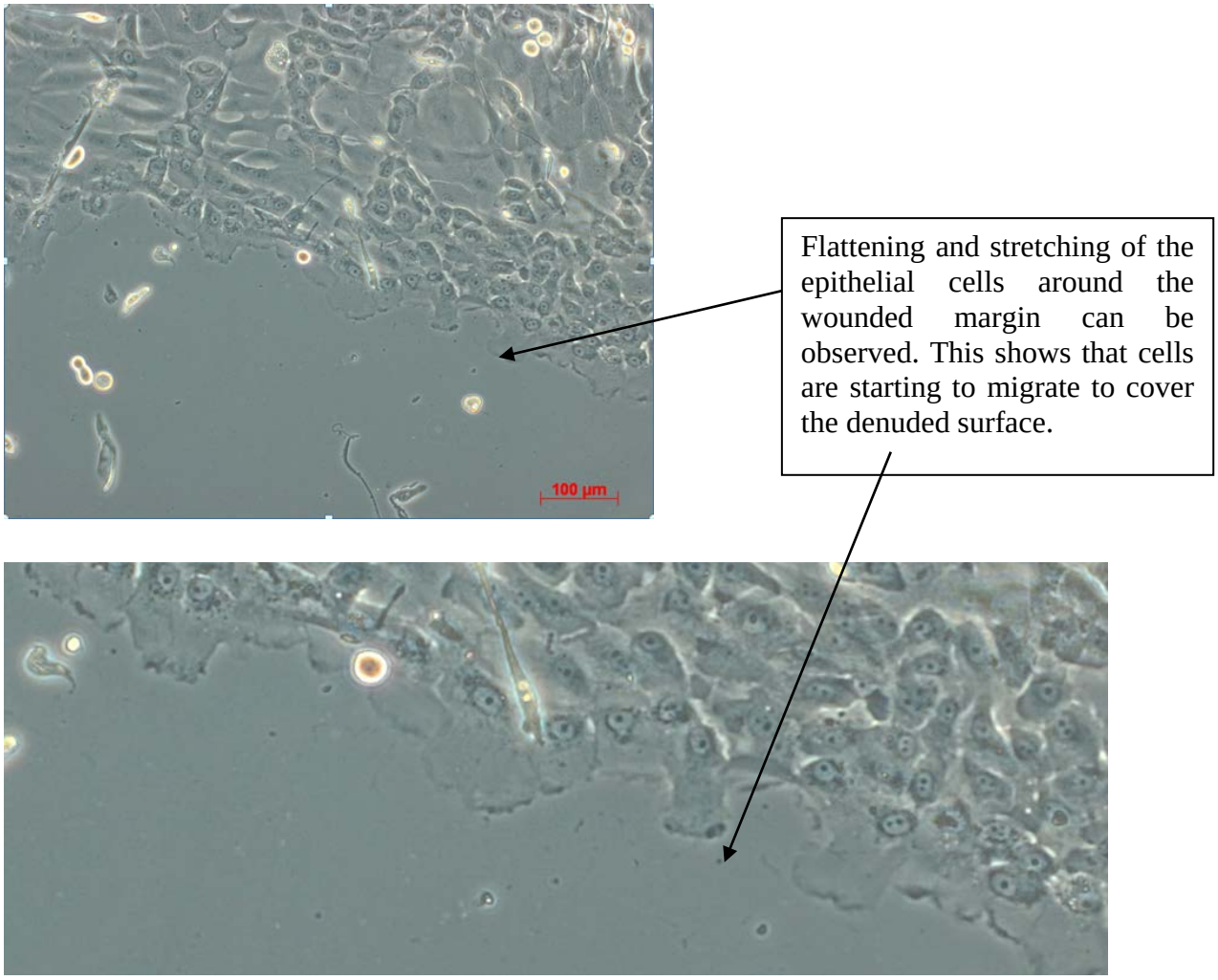

Figure 14: The wound margin

A picture of a wounded corneal epithelial culture and a zoomed version of the same picture to show the wounded margin and the cell morphology. The picture was taken with the phase contrast microscope ZEISS Axio Cam HRC Axiovert. Scale bar: 100µm.

2.3.2.2 Experiment 2: Mechanical wounding; increasing the wound size by 50%

Experiment 2 was performed mechanically and the size of the wound was increased to approximately 50%. Wound closure took place at day 9.

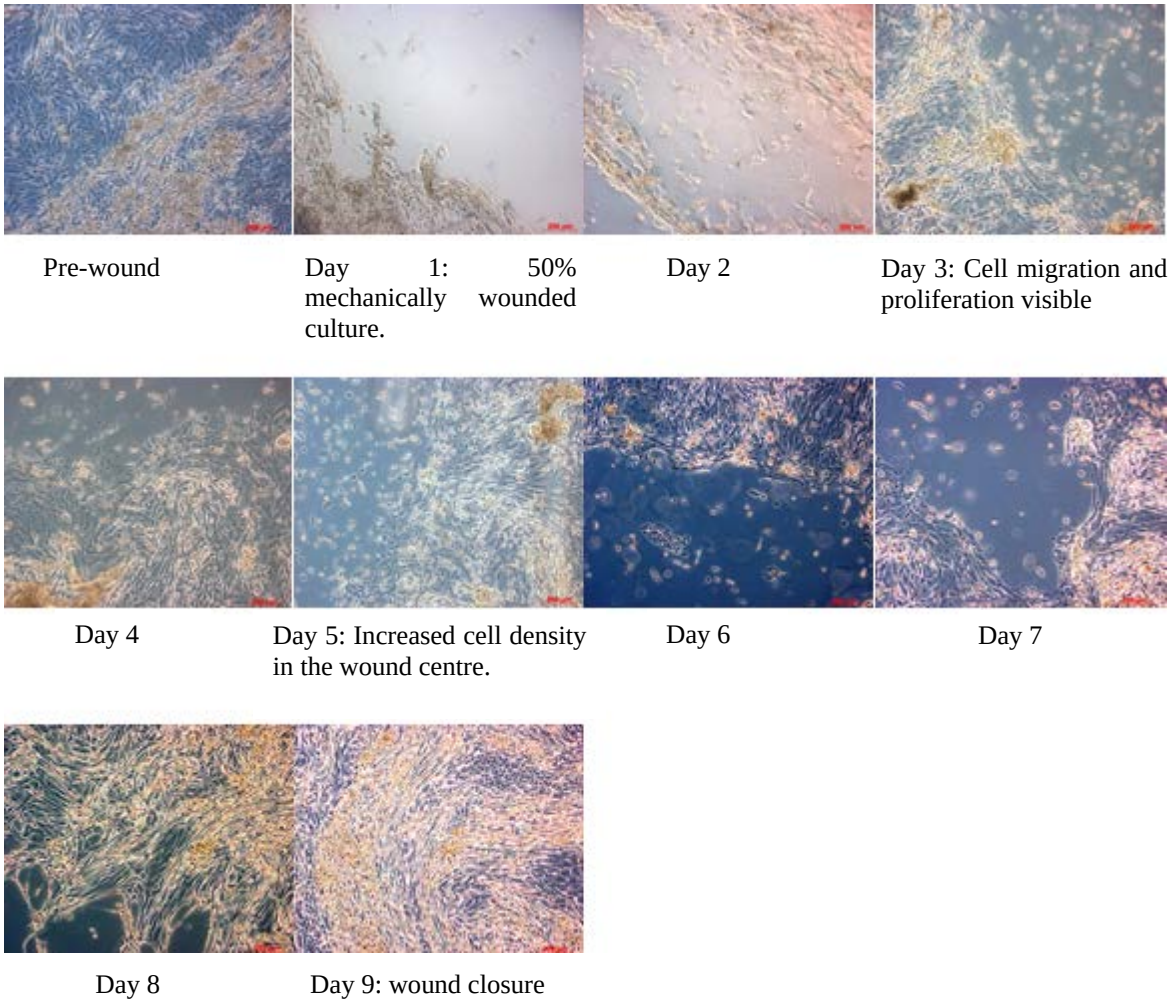

Figure 15: 50% mechanical wounding

Pictures taken with the phase contrast microscope ZEISS Axio Cam HRC Axiovert. Scale bars: 200µm.

Mechanical wounding by 50% surface area gave a good time span to observe the wound healing stages. Therefore this type of wounding system was chosen as the most preferable one to test gene expression by using quantitative real-time pcr.

2.3.3 Investigating wound healing by qRT-PCR

In order to identify and quantify the expression of the limbal stem cell expression markers *ΔNp63, ABCG2, C/EBPΔ, p63α, p63β* as well as the putative negative markers *Ck12* and $p27^{KIP1}$ and *BimS* expression, real-time pcr was performed. The measured DNA sequences of interest were compared to a standard reference gene (*GAPDH*). Results were analysed using the Comparative Ct Method, as described in the Methods section 2.2.2.2. This analysis method calculates a relative normalised quantification of gene expression.

Results are shown for two corneas belonging to two different donors. These were dissected and the corneal epithelial cells extracted from the corneal tissue were cultured separately following the culture techniques previously described in the Methods section 2.2.2.1. When the cultures were confluent, these were wounded and cell samples were taken at different time points of wound healing for RNA extraction. Therefore, “w0” shows the primary culture that is unwounded and therefore acts as a negative control. The “wound” sample shows gene expression immediately after wounding the culture. The “half healed” sample shows gene expression when the corneal epithelial cell culture is half healed and the “confluent” sample is when the wound has completely healed and is fully confluent.

2.3.3.1 Limbal stem cell markers: ΔNp63, p63γ, p63α, ABCG2 and C/EBPΔ

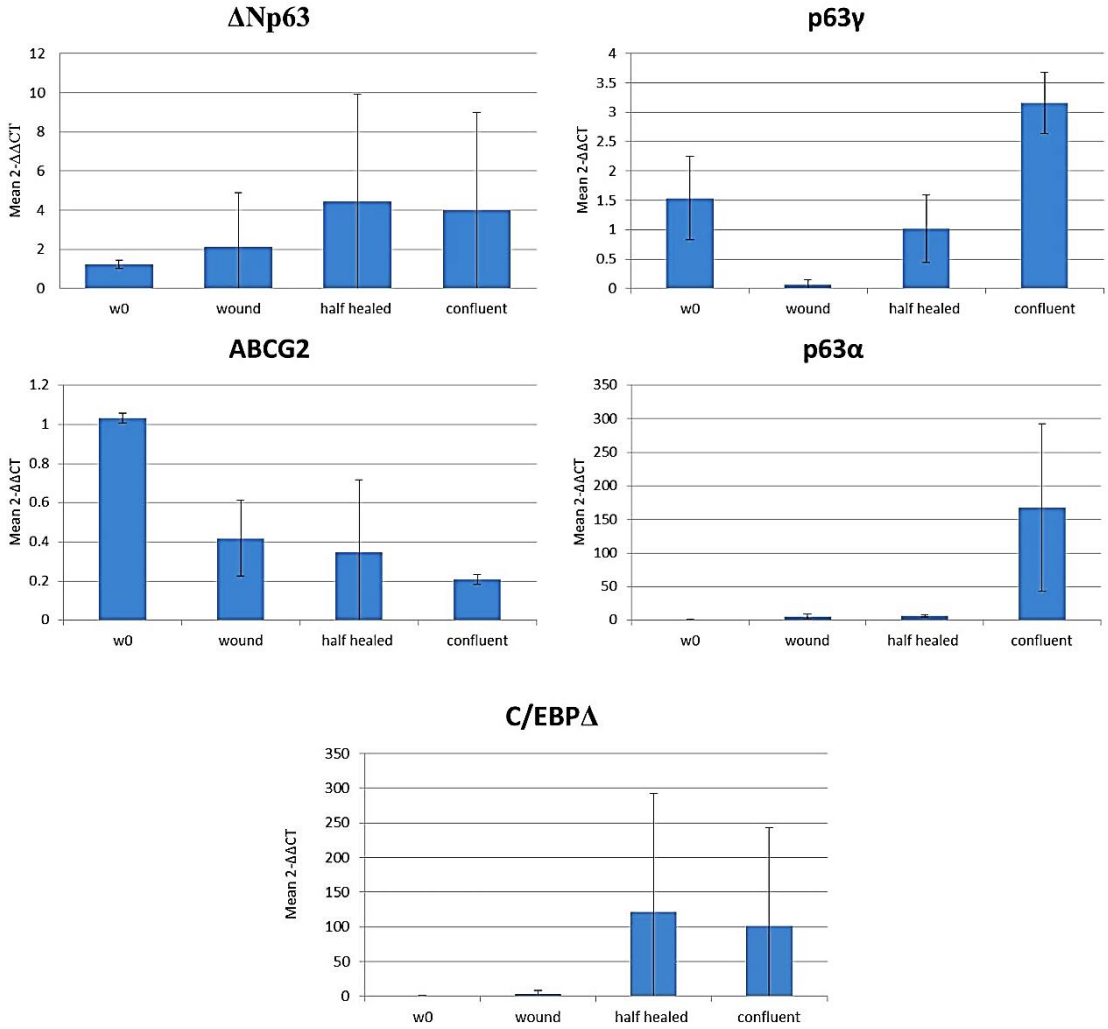

Figure 16: Relative normalised ΔNp63, p63γ, p63α, ABCG2 and C/EBPΔ expression during wound healing, n = 2.

The x-axis represents the wound healing stage. The y-axis represents the result of the formula $2^{-\Delta\Delta Ct}$ which is expressed in terms of fold changes.

Quantitative real-time pcr results for both donors showed an extensive variation for the majority of the markers shown in Figure 16, such as ΔNp63, ABCG2 (half healed data), p63α and C/EBPΔ (half healed and confluent data). Given the very high error bars for most of the results shown in Figure 16, it is difficult to interpret the above represented data. *P63γ* expression shown above in Figure 16 is the most accurate data between the

two donors. *P63γ* expression decreased after wounding of the cultures and later during wound healing its expression increased and was expressed twice as much in the fully healed/confluent cultures when compared to the positive unwounded control. *P63γ* is thought to be involved in epithelial differentiation, hence during corneal regeneration (Di Iorio *et al.*, 2006). The fact that the two fully healed and confluent cultures expressed double the amount of *P63γ* compared to the positive control could reflect the fact that an increasing amount of corneal epithelial differentiation was taking place as a result of the re-establishment of an epithelial layer.

P63α expression increasedwhen wound healing was fully completed, i.e. when the culture was fully confluent. . However,*ABCG2* expression was seen to be very low during wound healing and did not restore its full expression (as seen in the positive control) when the cultures were fully healed. This possibly reflects a decrease in LSCs.

Results for *C/EBPΔ* expression showed very different expression levels and trends between the two donors, hence the very large error bars shown for the half healed and confluent data. However, *in vivo* studies have shown that *C/EBPΔ* identifies quiescent limbal stem cells (Barbaro *et al.*, 2007).

2.3.3.2 LSC negative markers: Ck12 and p27^{KIP1}

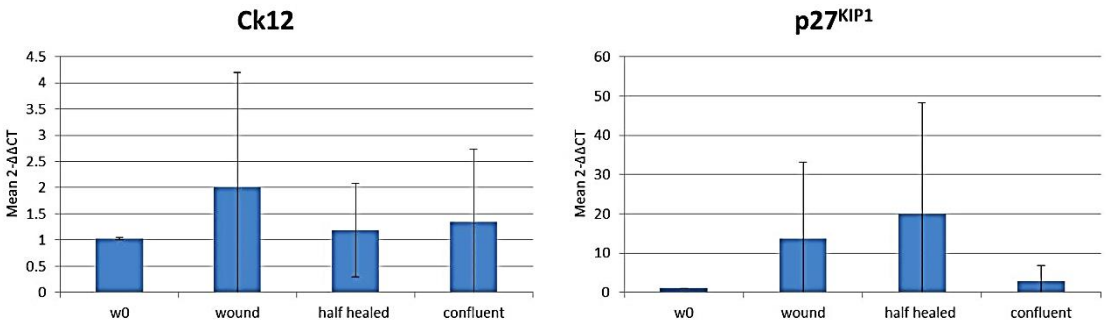

Figure 17: Relative normalised Ck12 and p27^{KIP1} expression during wound healing, n = 2.

The x-axis represents the wound healing stage. The y-axis represents the result of the formula $2^{-\Delta\Delta Ct}$ which is expressed in terms of fold changes.

Ck12 expression during wound healing was not seen to be consistent between the two donors, hence the very large error bars in all of the data. $P27^{KIP1}$ expression also seemed to variate extensively between the two donors and therefore it is difficult to make consistent conclusions. However, it is known that $p27^{KIP1}$ levels decrease after wounding and during wound repair, thus showing that $p27^{KIP1}$ decreased in cells that were stimulated to proliferate (Zieske *et al.*, 2004).

2.3.3.3 Pro-apoptotic marker BimS

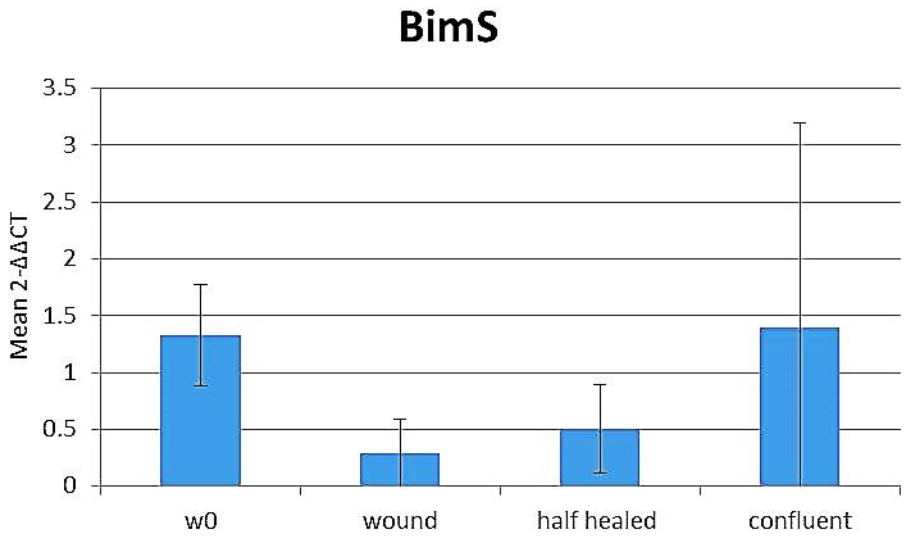

Figure 18: Relative normalised BimS expression during wound healing, n = 2.

The x-axis represents the wound healing stage. The y-axis represents the result of the formula $2^{-\Delta\Delta Ct}$ which is expressed in terms of fold changes. *BimS* induces apoptosis.

Results shown in Figure 18 showed decreased levels of *BimS* after wounding in both donors. However, upon confluency, the two donors show very different expression and for this reason the error bar is very high for the “confluent” data.

2.4 Discussion & Conclusion

Overall gene expression profiles in both of the cultured corneo-scleral rings tested did not show many similarities during wound healing. This could be due to the fact that the approach used (the scratch assay) is very limited because of how the scratch differently affects the migrating cells that are nearby the wound as well as cells that are located more far away from the wound and measuring the whole cell population at the RNA level may have been causing the very inconsistent data and may therefore not allow correct interpretation of the results. The limitations of this study are not only the fact that the stroma, mainly involved in corneal wound healing, is absent in this study, but also that this wound healing model is developed in a 2D culture environment. Recent studies (Espana *et al*., 2003; Bray *et al*., 2012) have highlighted the importance of the presence of the stroma in contact with the epithelium in healthy cornea *in vitro* models as well as those studying corneal wound healing *in vitro*, not only to better elucidate the interactions taking place between the corneal epithelium and its underlying stroma, but also to better understand the factors involved in controlling homeostasis and transparency in the cornea and how such factors can be controlled in culture. In addition, recent work by Huang *et al*., 2015, has described that not only the limbal stroma acts as structural basis for the LSC niche, but also the importance of the limbal microvascular net microenvironment in supporting the limbal stem cell niche. Furthermore, assays such as the sphere-forming assay described by Yoon *et al*., 2013 and Huang *et al*., 2015, can measure the wound healing ability of specific cell population in culture. Huang and co-workers demonstrated that sphere-forming cells isolated from the peripheral cornea were reacting as whole units when injured through direct compression or remote scratch injury experiments and that they could possibly be used as transplantable units for regenerating the corneal epithelium.

3 Environmental reprogramming of skin epidermal cells in a 2D corneal epithelial culture environment

3.1 Introduction & Aims

The unmet need of corneal epithelial cells for treating eye diseases, in particular in cases of bilateral LSCD, has led to the extensive search of alternative stem cell sources that can be used to regenerate the corneal epithelium. Recently, attention has been drawn to the use of adult stem cells derived from the hair follicle. These are stored within the bulge region of the outer root sheath (ORS), are of epithelial origin most importantly are easily accessible.

Recent studies have shown that hair follicle derived stem cells have the potential to express corneal epithelial markers when placed under specific culture conditions (Blazejewska *et al*., 2009) thus proving they possess a high degree of plasticity and can be pushed to the extremes of lineage boundaries by simply modifying their microenvironment. However, this work did not show a long-term establishment of corneal epithelial markers.

The main aim of this study was to reprogram human hair follicle cells and tran-differentiate these into corneal epithelial cells using an *in vitro* 2D culture system approach. This goal was attempted by modifying the environment, i.e. by utilising the corneal epithelial culture method.

The study described in this Chapter investigated the following questions:

- Can we transdifferentiate on the long term hair follicle stem cells (ORS) into corneal epithelial cells?
- What are the parameters of the limbal cell microenvironment that decide the behaviour of cells placed in culture?
- Can we re-create this microenvironment in order to induce trans-differentiation of hair follicle stem cells (ORS) into corneal epithelial cells?

Markers	Characteristics
Keratins	
Ck3	Detected in the cornea only, marker for differentiated corneal epithelium
Ck4	Conjunctiva marker
Ck5	Expressed in ORS (mainly expressed in the basal layer of stratified epithelia)
Ck10	Epidermal differentiation marker
Ck12	Marker for differentiated corneal epithelial cells
Ck15	Marker for corneal epithelial progenitor cells + Hair follicle stem cell and progenitor marker (ORS)
Ck17	Expressed in ORS (mainly expressed in stratified epithelia)
Ck19	Expressed in ORS + marker for conjunctival cells (mainly expressed in the basal layer of stratified epithelia)
Integrins	
Integrinα6	Bulge-specific cell surface marker (ORS), expressed also in the cornea
Others	
Pax6	Marker of transcription factor important in the development of the eye, expressed in the differentiated corneal epithelium.
p63	Expressed in corneal epithelial stem and progenitor cells
CD200	Bulge-specific cell surface marker

Table 5: Putative positive and negative markers for LSC, corneal epithelial progenitor cells and ORS stem and progenitor cells

Aims of this study

- Establishing human ORS cultures using corneal limbal stem cell culture parameters such as feeder layer and medium. In parallel, corneal limbal stem cell cultures will be established.
- External observations as well as Colony Forming Efficiency (CFE), qRTpcr and Immunofluorescence will be used to identify any phenotypic change and LSC as well as ORS markers expression within ORS cultures. This will be compared to LSC cultures.

3.2 Materials & Methods

All the experimental procedures carried out in Chapter 1 were conducted in compliance with Newcastle University Health & Safety Policy according to the Control of Substances Hazardous to Health (COSHH) regulations. All tissue culture work was undertaken at Containment Level 2 using standard aseptic techniques.

3.2.1 Materials

All reagents used in this chapter were directly derived from the relevant suppliers and COSHH regulations were respected throughout their usage.

3.2.1.1 Cells

Human limbal corneal epithelial cells were cultured from corneas obtained from human limbal tissue donated for research, obtained from the UK Eye Banks.

Human outer root sheath cells (ORS) were extracted from two different living donors.

Both corneal epithelial cells as well as outer root sheath cells were co-cultured with mitotically inactivated 3T3 J2 mouse fibroblasts using an established protocol described in the Chapter 2 Methods section 2.2.2.1.

3.2.1.2 Culture media & tissue culture components

3T3 J2 mouse fibroblast and Limbal Epithelial Medium components were described in the previous Material & Methods section in Chapter 2. Both corneal epithelial and ORS cultures were cultured in Limbal Epithelial Medium. Further tissue culture components are listed below in Table 6.

Reagent	Supplier
Mitomycin C from *Streptomyces caespitosus*	Sigma-Aldrich
DPBS for tissue culture	Gibco
0.02% EDTA	Sigma-Aldrich
0.05% Trypsin-EDTA	Sigma-Aldrich
0.25% Trypsin-EDTA	Sigma-Aldrich
DMEM supplemented with 1% Penycillin/Streptomycin (100IU/ml and 100µg/ml) and 0.5% Fungizone (2.25µg/ml)	DMEM – Gibco P/S – Sigma-Aldrich Fungizone - Gibco

Table 6: Tissue culture components

3.2.1.3 Antibodies & Immunohistochemistry solutions

Primary and Secondary antibodies used in Chapter 3 are all listed in Table 7 and 8 below.

Target	Raised in:	Dilution used	Supplier
Ck3	Mouse	1:100	Abcam
Ck4	Mouse	1:100	Abcam
Ck5	Mouse	1:100	Abcam
Ck10	Mouse	1:100	Abcam
Ck12	Goat	1:100	Santa Cruz Biotechnology
Ck15	Mouse	1:100	Abcam
Ck17	Rabbit	1:100	Abcam
Ck19	Mouse	1:100	Dako
Pax6	Rabbit	1:100	Abcam
CD200	Mouse	1:100	Abcam
Integrinα6	Mouse	1:50	Abcam
CD34	Rabbit	1:100	Abcam

Table 7: Primary Antibodies

Secondary Antibodies	Raised in:	Dilution used	Supplier
IgG-FITC (sc-2024)	Donkey anti goat	1:400	Santa Cruz Biotechnology
IgG1 FITC (43C-CB1521)	Rabbit anti mouse	1:500	Fitzgerald

Table 8: Secondary Antibodies

Primary and Secondary antibodies were diluted in the Diluting buffer listed in Table 9 below.

Reagent	Composition	Supplier
Permeabilisation Buffer	1% Triton X-100 (in 1x PBS)	Sigma-Aldrich
Quenching buffer	100mM Glycine (in H_2O)	Sigma-Aldrich
Diluting buffer	0.5% Tween 20 (in 1x PBS)	Sigma-Aldrich
Blocking Solution	5% Goat Serum or 5% Donkey Serum in Diluting buffer	Sigma-Aldrich
Mowoil	n/a	Calbiochem
DAPI	DAPI (diluted 1:1000 in Diluting Buffer)	
4% PFA	(in 1x PBS)	Sigma-Aldrich
1x PBS (pH 7.4)	n/a	n/a

Table 9: Materials and solutions for Immunohistochemical analysis

3.2.1.4 Molecular Biology materials

RNA extraction

The same RNA extraction components were used as those described in section 2.2.1.3 of Chapter 2.

Reverse Transcription

Reverse Transcription was performed using the same components used in section 2.2.1.3 of Chapter 2.

Primers

Primers were manually designed as described in the Methods section 2.2.2.2 of Chapter 2 and ordered from Sigma-Aldrich. The primers were diluted with RNase free dH_2O to 100umole to keep as a primer stock solution frozen at -20°C. For quantitative real-time pcr, primers were diluted 1:10 (to a final concentration of 10µm) in RNase free dH_2O from the primer stock solution. The primer sequences are listed below in Table 10.

Gene	Primer	Sequence
CD200	Forward	CTGGGGACTGTGACCGACTT
	Reverse	TCGGTCCTGATTCCGGTGAC
CD34	Forward	CAACGGTACTGCTACCCCAG
	Reverse	ACACAGGGTGCAGGCTGGTA
Ck4	Forward	ATGCAGAGCAGCGAGGTGAG
	Reverse	CCAAGGCCAGCTTCACACTC
Ck17	Forward	GGCCTTGGAGATAGAGCTGC
	Reverse	GTTGCCCTCCAGGGATGCTT
Ck15	Forward	GGATGTCGAGGCCTGGTTCT
	Reverse	ACTGCAGCTCGATCTCCAGC
Ck5	Forward	TGGAGCTGGAGGCCAAGGTT
	Reverse	CATGCGTCTGCATCTGGGAC
Ck10	Forward	TGGCAACTCACATCAGGGGG
	Reverse	GCCTGAAGTCATCAGCTGCC
Ck19	Forward	ACACGACCATCCAGGACCTG
	Reverse	CTCATGCGCAGAGCCTGTTC
Integrinα6	Forward	GCCAATCACAGTGGAGCCGT
	Reverse	ACCACCGCCACATCATAGCC
Pax6	Forward	CTCGGTGGTGTCTTTGTCAAC
	Reverse	ACTTTTGCATCTGCATGGGTC
Ck3	Forward	GGATGTGGACAGTGCCTATATG
	Reverse	AGATAGCTCAGCGTCGTAGAG
Ck12	Forward	GAAGAAGAACCACGAGGATG
	Reverse	TCTGCTCAGCGATGGTTTCA
ΔNp63	Forward	GAAACGTACAGGCAACAGCA
	Reverse	GCTGCTGAGGGTTGATAAGC

Table 10: Primers and their sequences

Quantitative real-time pcr

Quantitative real-time pcr was performed using the LightCycler Real Time PCR machine [Roche] and by using the GoTaq qPCR Master Mix kit from Promega.

3.2.2 Methods

3.2.2.1 Tissue culture

Derivation and establishment of outer root sheath keratinocytes from human plucked hair follicles

At least 20 hair follicles were plucked in anagen phase (when hairs have a white sheath around it of approximately 0.5 – 1 cm) using sterile forceps and these were washed twice in DMEM supplemented with antibiotic/antimycotic and antimycoplasma. The extremities of the hair containing the outer root sheath (ORS) were placed in wash medium in a petri dish and the rest of the hair was cut and disposed appropriately. The hair containing the ORS was cut and transferred into a small petri dish with 5ml of pre-warmed 0.25% trypsin/EDTA and this was incubated for 15 minutes at 37°C. After 15 minutes incubation and using a 1ml pipette the trypsin suspension was aspirated and released a couple of times in order to release cells from the hair shaft. The trypsin suspension was aspirated and deactivated by the addition of an equal volume (5ml) of culture medium high glucose DMEM. The suspension was subsequently centrifuged at 1300 rpm for 3 minutes, the supernatant removed and the pellet was re-suspended in a couple of ml of culture medium. At the same time fresh 5ml of 0.25% trypsin/EDTA was added to the ORS and a further cycle of 15 minutes incubation at 37°C was performed. This was repeated three times. The ORS cell pellets were all combined and cells were counted using a haematocytometer. ORS were then plated onto previously mitotically inactivated 3T3 mouse fibroblasts in corneal epithelial specific medium (LEM) and incubated at 37°C for three days.

In parallel corneal epithelial cells were also cultured (as described in the Methods section 2.2.2.1 in Chapter 2) onto mitotically inactivated 3T3 mouse fibroblasts in corneal epithelial medium (LEM).

The diagram below in Figure 19 summarises the techniques used in this study.

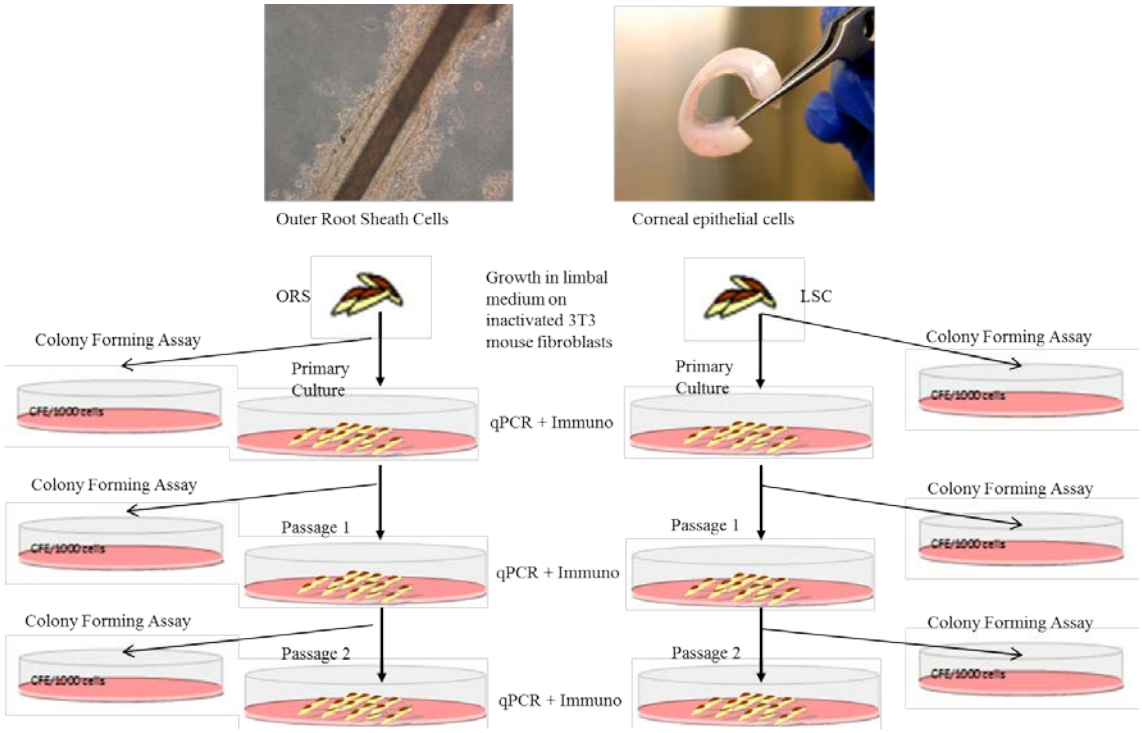

Figure 19: Diagram of the techniques used to monitor ORS reprogramming

The corneal epithelial (LSC) and outer root sheath (ORS) cells that needed to be examined by immunohistochemistry were plated on to coverslips that had been placed into tissue culture wells. For immunohistochemistry purposes, 12,000 ORS and CEC were separately plated into 24 well plates in which mitotically inactivated 3T3 mouse fibroblasts had been previously plated onto coverslips. For passaging purposes both ORS and CEC were plated (48,000 cells per well) into 6 well plates that contained previously mitotically inactivated 3T3 mouse fibroblasts.

3.2.2.2 Colony Forming Efficiency

Colony Forming Efficiency (CFE) was performed in order to determine the efficiency/ability of the corneal epithelial and outer root sheath cells to form new colonies and therefore this assay gives an indication of the number of stem cells and progenitors present in the culture. The CFE assay was carried out in the following way: mitotically inactivated 3T3 cells in 3T3 medium were plated in a 9.6cm² tissue culture well at a density of 230,400 cells and placed into a tissue culture incubator overnight at 37°C. This allowed the 3T3 cells to settle down and create a feeder layer. The following

day the 3T3 medium was removed and 1000 ORS/corneal epithelial cells were plated onto the prepared 3T3 cells together with 2ml of limbal medium. The 1000 cells culture was then placed into the 37°C incubator and the culture was left in the incubator for 3 days. On the third day the limbal medium was exchanged with 2ml of fresh limbal medium. Then the medium was changed every other day. After 12 days of culture the limbal medium was removed and the culture was washed with 1ml of DPBS (Gibco). DPBS was removed and the culture was fixed with 1.5ml of 3.8% formaldehyde for 10 min. The formaldehyde solution was then removed and appropriately disposed and the culture was stained through the addition of 1ml of 1% Rhodamine B in methanol for 10 minutes. Rhodamine B was then removed and the culture was left to air dry for 1h. Colonies were then easily counted and CFE was calculated through the formula: number of colonies formed/ number of cells plated x 100.

3.2.2.3 Immunofluorescent analysis

The tissue culture wells were washed in 1x PBS for 5 minutes, fixed in 4% Paraformaldehyde (PFA) for 30 minutes, washed in 1x PBS for 5 minutes, quenched with 100mM glycine for 30 minutes, washed in 1x PBS for 5 minutes, permeabilized with 0.1% Triton X-100 for 30 minutes (for nuclear antibodies), 20 minutes for all the others. Wells stained for Integrinα6, CD200 and CD34 were not permeabilized at all. The wells were then washed in 1x PBS for 5 minutes, blocked in 5% Goat serum or 5% Donkey serum (Blocking solution) for 1 hour. Everything was performed at room temperature. Samples were then incubated with primary antibodies at the appropriate dilutions in Diluting Buffer and placed in a humidified chamber at 4°C overnight. The following day, the wells were rinsed three times for 5 minutes in 1x PBS and incubated for 1-1.5 hours with appropriate secondary antibodies, diluted with the appropriate dilutions in Diluting Buffer. This step was kept at room temperature and in the dark. Wells were then washed three times 5 minutes each in 1x PBS and incubated with DAPI, diluted 1:1000 in Diluting Buffer, for 10 minutes at room temperature and in the dark. Coverslips were then removed from the wells and mounted onto slides with Mowoil, sealed with nail varnish and let to dry at room temperature and protected by light before visualising them using a Zeiss microscope [Carl Zeiss]. Slides could then be stored in appropriate slide boxes protected from the light in the fridge at 4°C.

3.2.2.4 Molecular Biology

RNA extraction & isolation

The same RNA extraction and isolation method was used as described in the Methods section 2.2.2.2 of Chapter 2.

Reverse Transcription

Reverse transcription was performed using the same method as described in section 2.2.2.2 of Chapter 2.

Quantitative real-time pcr

Real-time PCR was performed in order to detect and quantify gene expression by measuring the DNA sequences of interest compared with a standard reference gene. In this case the reference gene was glyceraldehyde-3-phopshate dehydrogenase (GAPDH). The sequences of the primers tested and the relevant annealing temperatures are described in the Materials section 3.2.1.4.

Real-time PCR was performed using the LightCycler Real Time PCR machine [Roche] and using the GoTaq qPCR Master Mix kit [Promega] in which all primers could be run together regardless from variation in annealing temperatures between all the primers.

The reaction mix was composed of 5µl of GoTaq qPCR Master Mix, 0.1µl Rox, 0.5µl Forward Primer, 0.5µl Reverse Primer, 2.9µl dH_2O and 1µl cDNA or dH_2O for the negative control. 10µl of the mixture was used to fill each capillary tube to be amplified. Each sample was measured in triplicate with GAPDH as the endogenous control and using dH_2O as the negative control.

The tubes were capped and centrifuged at low speed for a couple of minutes to ensure the mix moved to the base of the tube. The capillary tubes were then placed into the LightCycler. The reaction parameters are described in Table 11.

Steps	Cycles	Standard Cycling Program
Hot-Start Activation	1	95°C for 2 minutes
Denaturation, Annealing and extension	40	95°C for 15 seconds, 60°C for 60 seconds
Dissociation	1	60 - 96°C

Table 11: Reaction Paramters used for qRT-PCR

Data was collected during the annealing step of each cycle. Results were analysed using the Comparative Ct Method based on 3 steps: step 1: normalization to endogenous control, step 2: normalization to reference sample and step 3: uses the formula $2^{-\Delta\Delta Ct}$ to calculate fold changes. This analysis method calculates a relative quantification of gene expression.

3.3 Results

The following questions were raised in order to test ORS when cultured in LSC culture conditions. These were:

- Do ORS cells grow in limbal media conditions?
- How does the morphology and rate of growth of ORS cells compare with the limbal cells?
- How does the colony forming efficiency of ORS compare with the one of the limbal cells?
- Do ORS cells grown in limbal medium express any limbal cell markers and limbal cells in limbal medium express any ORS markers?

3.3.1 Culturing human ORS & corneal epithelial cells

The selection of hair roots containing cells in a high proliferative phase was important in order to successfully establish the ORS primary culture. Hairs that had a white sheath of approximately 0.5-1cm around the hair shaft (as seen in Fig. 20) were known to be in the anagen phase. The anagen phase in the hair cycle is the phase of the end of the follicle development and, therefore contains a fully grown outer root sheath. At the end of this phase cells in the lower part of the hair follicle undergo apoptosis. This is known as the catagen phase.

Early growth of LSC and ORS colonies showed stem cell appearance, such as homogenous looking cells with large nuclei and a little cytoplasm.

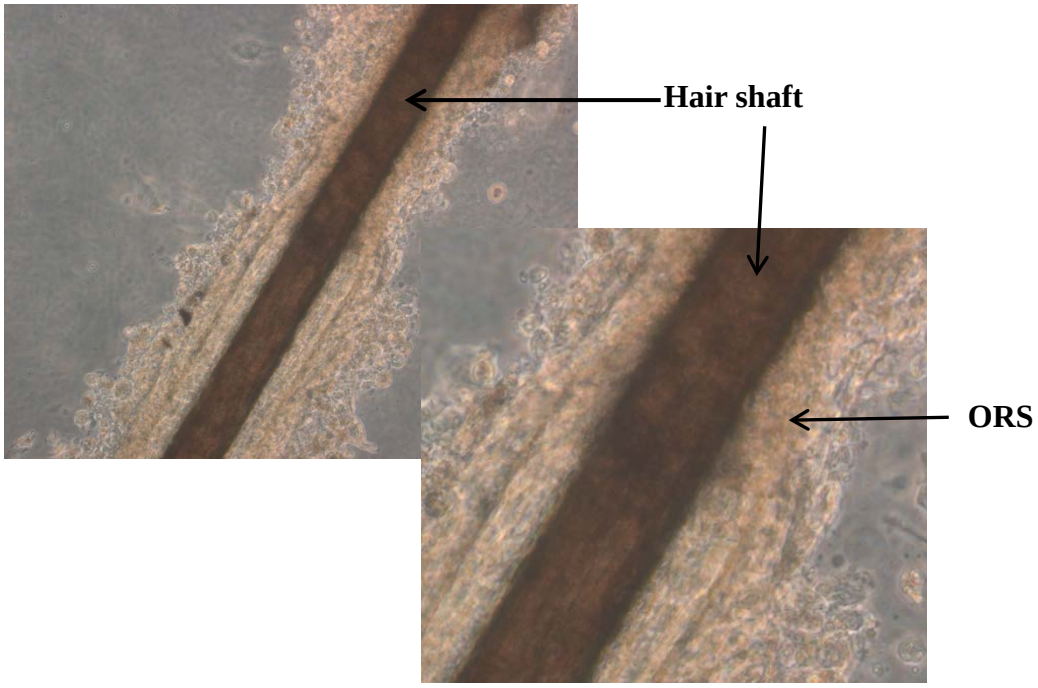

Figure 20: Image of a single hair root after plucking, showing the hair shaft and its surrounding outer root sheath cells

Typically, corneal epithelial colonies were noted after 3-4 days (see Fig. 21 below) of culture and reached confluence after one week. On the other hand, ORS cultures showed the presence of colonies after 7-8 days and reached confluence after 18-20 days.

Corneal epithelial and ORS Primary Cultures

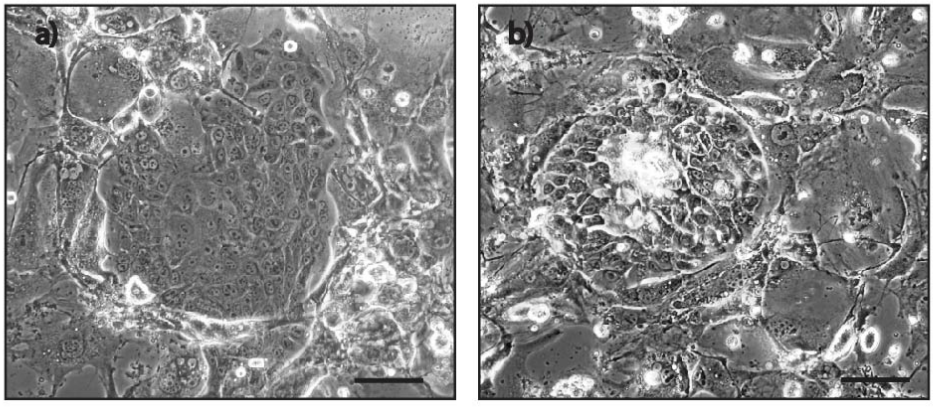

Figure 21: Corneal epithelial (LSC) & Outer root sheath (ORS) cultured on 3T3's

Image a) corneal epithelial cells at culture day 4 and b) Outer root sheath cells at culture day 7 of, both co-cultured on inactivated 3T3 mouse fibroblasts. Phase contrast micrograph. Scale bars: 100µm.

The corneal epithelial and ORS cell cultures were both cultured and fed in the same environmental conditions, i.e. the same feeder layer on which they were cultured (inactivated 3T3 mouse fibroblasts) and the same medium (corneal epithelial stem cell specific medium). However, they showed to take a longer time than corneal epithelial cultures to develop early colonies (as seen in Fig. 21) and to reach full confluence, thus demonstrating a more slow-cycling behaviour compared to corneal epithelial stem cells. Morphologically speaking, early colonies of both cell cultures types showed no difference (see Fig. 21) and from one sub-culture to the next the two cell cultures showed little morphological difference (as seen in Fig. 23 – 25 compared to Figure 22).

Corneal epithelial cells at different stages of culture

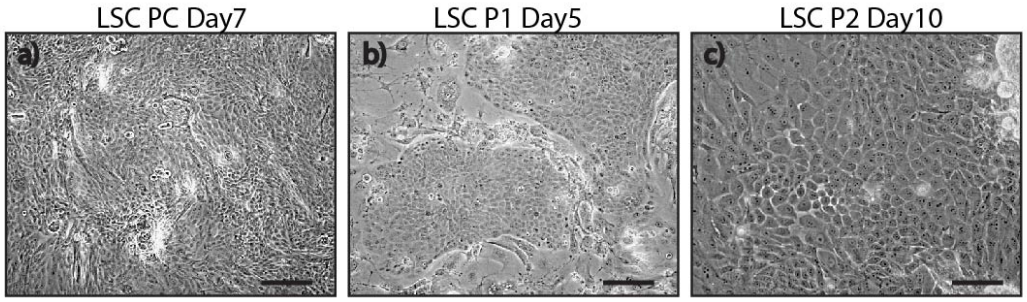

Figure 22: Corneal epithelial cells at primary culture, P1 and P2

Corneal epithelial Primary Culture (PC) at day 7 (a), Passage 1(P1) at day 5 (b) and Passage 2 (P2) at day 10 (c). Phase contrast micrograph of a corneal epithelial culture at different stages of culture. Scale bars: 200µm for a) and b), 100µm for c).

The corneal epithelial culture was sub-cultured until Passage 3 (image not shown) after which it started to show terminal differentiation and fibroblastic cell morphology. The culture was therefore terminated at that stage.

ORS cells Primary Culture

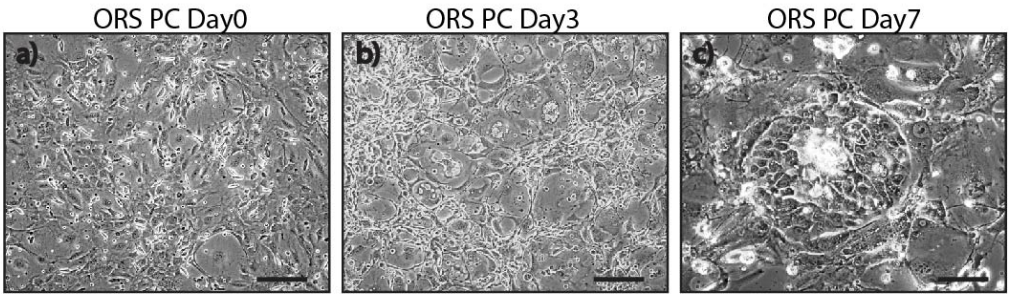

Figure 23: ORS Primary Culture (PC) at culture days 0, 3 and 7

Phase contrast micrograph of an ORS culture at different days of growth during primary culture. This is a representative example of 3 experiments as ORS cultures have been grown with different donors. Scale bars: 200µm for a) and b), 100µm for c).

ORS cells at Passage 1

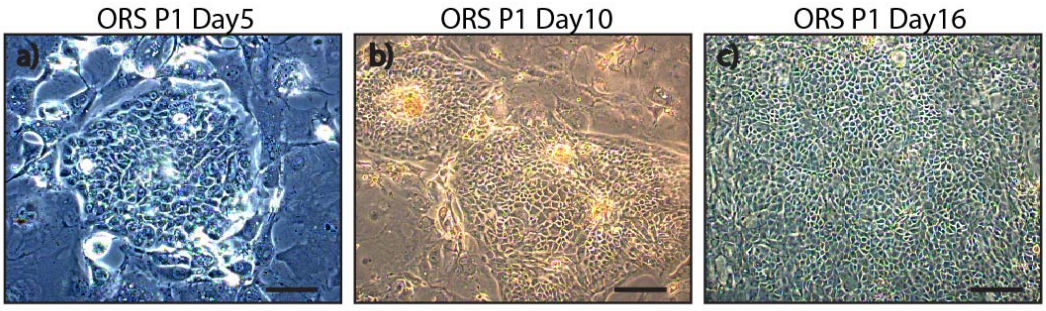

Figure 24: ORS at Passage 1 (P1) at culture days 5, 10 and 16

Phase contrast micrograph of an ORS culture at different days of growth during passage 1. This is a representative example of 3 experiments as ORS cultures have been grown with different donors. Scale bars: 100µm for a), 200µm for b) and c).

ORS cells at Passage 2

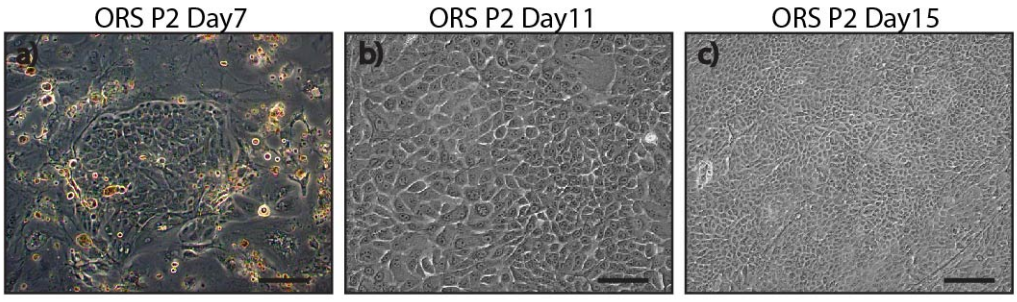

Figure 25: ORS at Passage 2 (P2) at culture days 7, 11 and 15

Phase contrast micrograph of an ORS culture at different days of growth during passage 2. This is a representative example of 3 experiments as ORS cultures have been grown with different donors. Scale bars: 200µm for a) and c), 100µm for b).

Conclusion

ORS cells grow in "limbal" culture conditions are morphologically similar to corneal epithelial cells. However, ORS cells grow at a slower rate than the limbal cells and on several occasions could not be passaged beyond P2 without dying, therefore for the subsequent experiments comparisons were performed with Primary Culture, P1 and P2 cells.

3.3.2 Colony Forming Efficiency (CFE)

To investigate the potential of self-renewal and therefore the potential of both corneal epithelial and ORS stem cells to give rise to colonies, Colony Forming Efficiency (CFE) was performed at every stage of subculture as well as with freshly extracted uncultured cells. The CFE assay is performed using specific culture conditions within a specific time period. CFE is expressed as a percentage and calculated using the following formula: number of colonies formed / number of cells plated x 1000 (as described and explained in the Methods section 3.2.2.2 of this chapter).

Because CFE measures the ability of cells to give rise to colonies, it not only gives an indication of corneal/ORS stem cell colony forming potential but also of progenitor cell potential of colony forming activity as also these cells grow in colonies. Therefore, the colony forming efficiency assay is not stem cell specific.

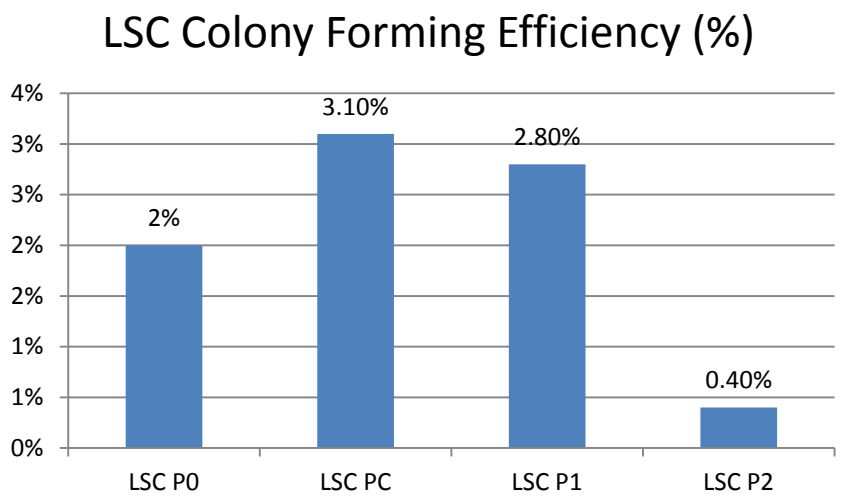

Figure 26: Colony Forming Efficiency of corneal epithelial stem cells at every stage of culture

The x axis represents the stages of subculture, the y-axis the LSC potential of forming colonies expressed in %.

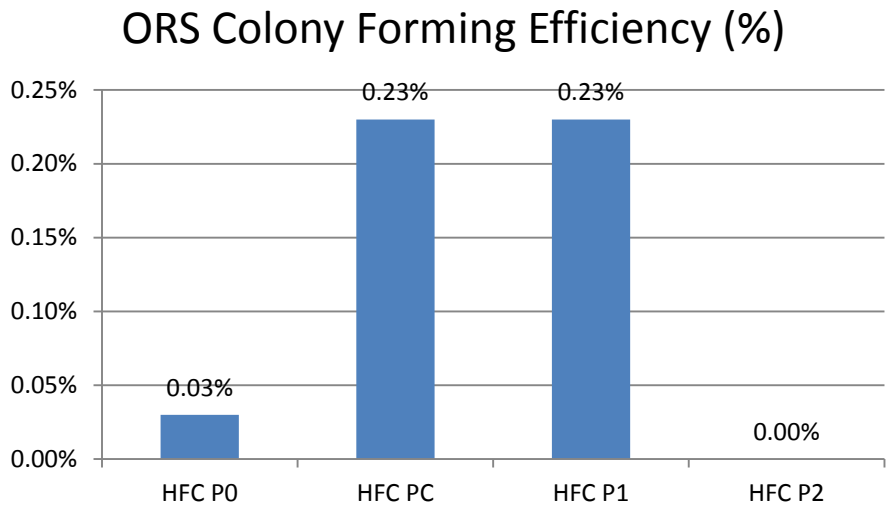

Figure 27: Colony Forming Efficiency of outer root sheath cells at every stage of culture

The x axis represents the stages of subculture, the y-axis the ORS potential of forming colonies expressed in %.

The colony forming efficiency of outer root sheath cells was a lot lower than that of LSC cultures, however they both showed a similar trend of increasing colony forming

efficiency in the primary culture and passage 1 (P1) and an abrupt decline in passage 2 for LSC but a total absence of colony formation of ORS in passage 2.

Conclusion

To sum up, other than the difference in cell doubling potential between the ORS and LSC cultures, no particular observations were made concerning the morphology of cells, as both looked very similar. CFE showed a lower colony forming efficiency of ORS in culture and this could reflect a lower amount of progenitor cells extracted and plated compared to the LSC cultures as well as a slower cycling phenotype.

3.3.3 Quantitative real-time pcr for relative gene expression

In order to monitor the *in vitro* trans-differentiation of ORS cells over time when cultured in the same *in vitro* conditions as LSC, further tests were performed that looked into the expression of the RNA of specific markers through the use of quantitative real-time pcr. The expression of putative positive limbal stem cell markers (ΔNp63, Cytokeratin 15), corneal developmental markers (Pax6), specific corneal epithelial differentiation markers (negative markers for limbal stem cells: Cytokeratin 3, Cytokeratin 12, Cytokeratin 19) was assessed. Cytokeratin 3 and Cytokeratin 19 have been demonstrated to discriminate between corneal and conjunctival epithelia respectively.

Markers expressed in ORS cells comprise a large variety of Keratins such as: Ck5, Ck15, Ck17 and Ck19. Ck15 has been reported to be a specific stem cell and progenitor cell marker, however it is expressed in limbal stem cells as well and therefore in this study it was used to assess the presence and capacity of stem cells and their self-renewal in both LSC and ORS cultures over time. Ck19 has also been found to be expressed in ORS cells. Other markers that have been used in the past to isolate and purify stem cells from the hair follicle bulge region are the cell surface markers integrin α6 and CD200. Similarly to Ck15, integrin α6 also has been generally used as a putative stem cell marker and it is expressed in both corneal epithelial cells and ORS cells. Cytokeratin 10 was used as an epidermal differentiation marker to assess the direction of ORS cell

differentiation in culture. A list of all the markers and their characteristics was shown in the introduction of this chapter.

The measured DNA sequences of interest were compared to a standard reference gene (GAPDH). Results were analysed using the Comparative CT Method which calculates a relative normalised quantification of gene expression.

Results are shown for one human cornea and ORS extracted from one living donor (n = 1) and results are shown in triplicate. When the cultures were confluent, the cultures were sub-cultured and a portion of these cells were used to sub-culture, for CFE's, Immunohistochemistry (as shown later in the Results section 3.3.4) and the remaining cells were used for RNA extraction and consequently transcription into cDNA.

3.3.3.1 Markers expressed in corneal epithelial stem cells (LSC) and progenitor cells

p63 expression in LSC and ORS cell cultures

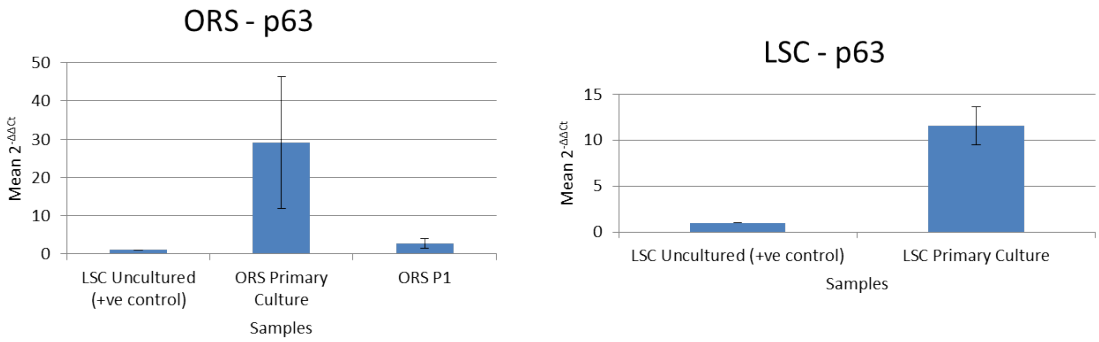

Figure 28: Relative normalised p63 expression in ORS and LSC cultures, n=1

The x-axis represents the culture stage. The y-axis represents the results of the formula $2^{-\Delta\Delta Ct}$ which is expressed in terms of fold changes. Relative p63 expression in ORS is compared to relative p63 expression in uncultured LSC.

Results show that the levels of p63 expression in ORS Primary Culture and LSC Primary Culture are both significantly higher than that of LSC uncultured cells (positive control). From the values obtained p63 expression in ORS Primary Culture also seems to be higher than in LSC Primary Culture, however the large standard error bar means that p63 gene expression in the former could in reality be similar to that in LSC. At P1 the levels of p63 expression in the ORS culture appeared to drop sharply. Given the

growth rates of ORS compared to the LSC growth rates, one would not expect ORS cells to have more p63 expression. On the other hand, the decline in p63 expression in ORS P1 is interesting and may reflect the limited proliferative capacity of these cells.

3.3.3.2 Markers expressed in differentiated corneal epithelial stem cells

<u>Pax6, Ck3 and Ck12 expression in ORS and LSC cultures</u>

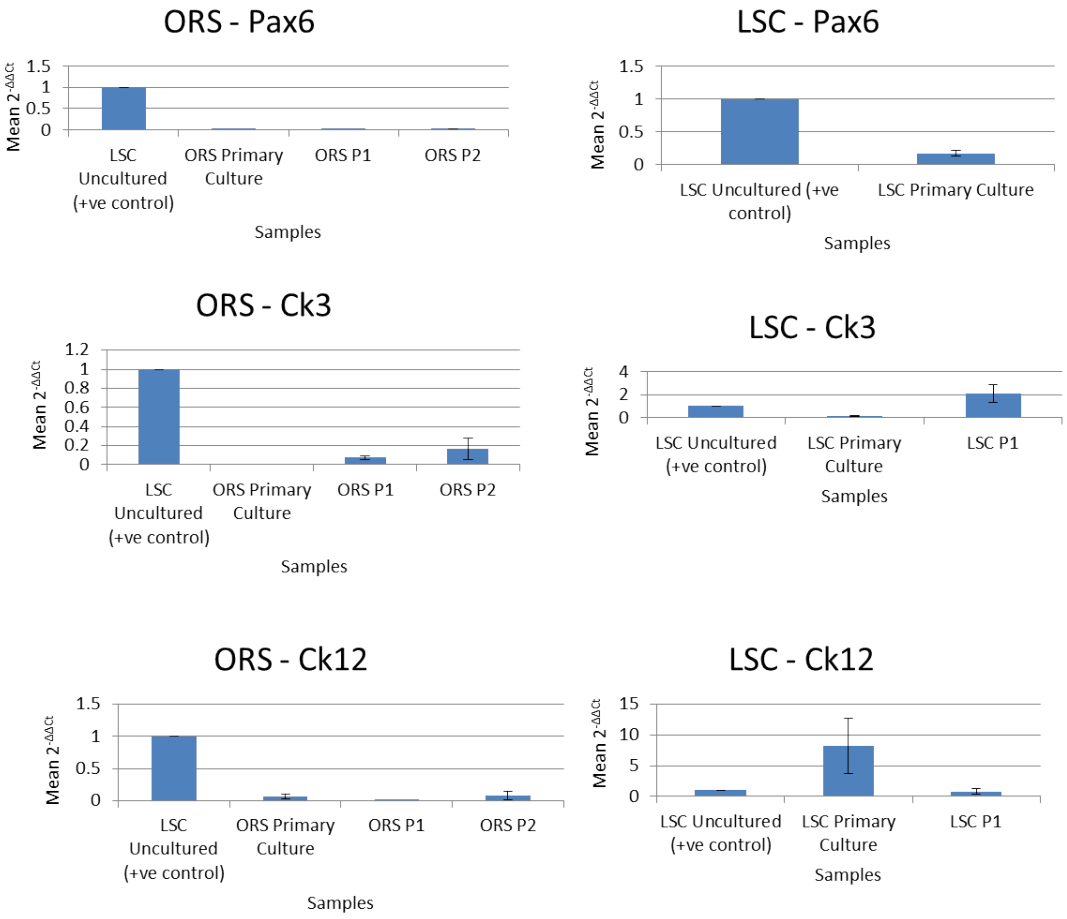

Figure 29: Relative normalised Pax6, Ck3 and Ck12 expression in ORS and LSC cultures, n=1

The x-axis represents the culture stage. The y-axis represents the results of the formula $2^{-\Delta\Delta Ct}$ which is expressed in terms of fold changes. Relative Pax6, Ck3 and Ck12 expression in ORS is compared their relative expression in uncultured LSC.

The markers Ck3 and Ck12 associated with corneal epithelial differentiation generally showed little expression in the ORS cultures although Ck3 expression was seen to

increase slightly from Primary Culture to Passage 2. The relative levels of Ck3 gene expression were still significantly lower than in the uncultured LSC (positive control). Levels of Ck12 expression in ORS cultures were very low and in Passage 1 samples Ck12 expression was nearly absent. Pax6 expression in ORS cultures was basically absent. To sum up, ORS cultures grown under the same environmental conditions as LSC cultures, generally express very low amounts of LSC differentiation markers although there was an indication that they could be switched on. Interestingly as might be anticipated the LSC cells showed increases in differentiation makers in culture.

3.3.3.3 Negative markers of corneal epithelial cells

Ck4 and Ck19 expression in LSC and ORS cultures

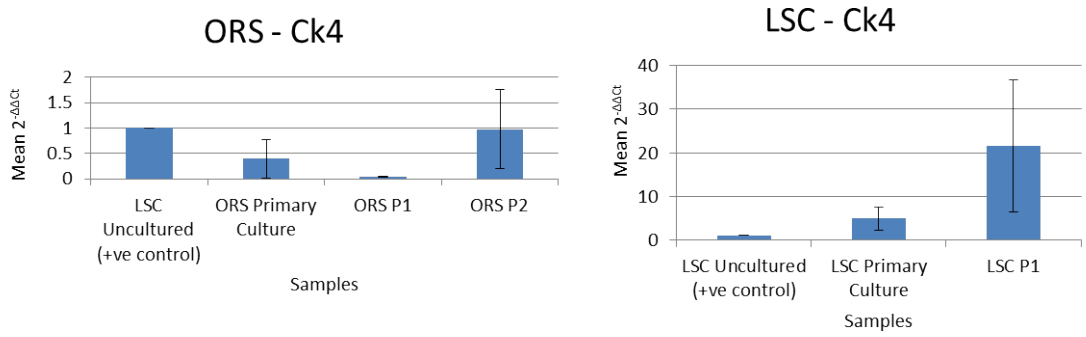

Figure 30: Relative normalised Ck4 expression in ORS and LSC cultures, n=1

The x-axis represents the culture stage. The y-axis represents the results of the formula $2^{-\Delta\Delta Ct}$ which is expressed in terms of fold changes. Relative Ck4 expression in ORS is compared to relative Ck4 expression in uncultured LSC.

Ck4 expression in ORS is present in Primary Culture and passage 2, however, the standard error bars suggest that Ck4 expression could be a lot lower. Ck4 is a conjunctiva cell marker and its expression in LSC cultures suggests the culture contains a mixed population of cells.

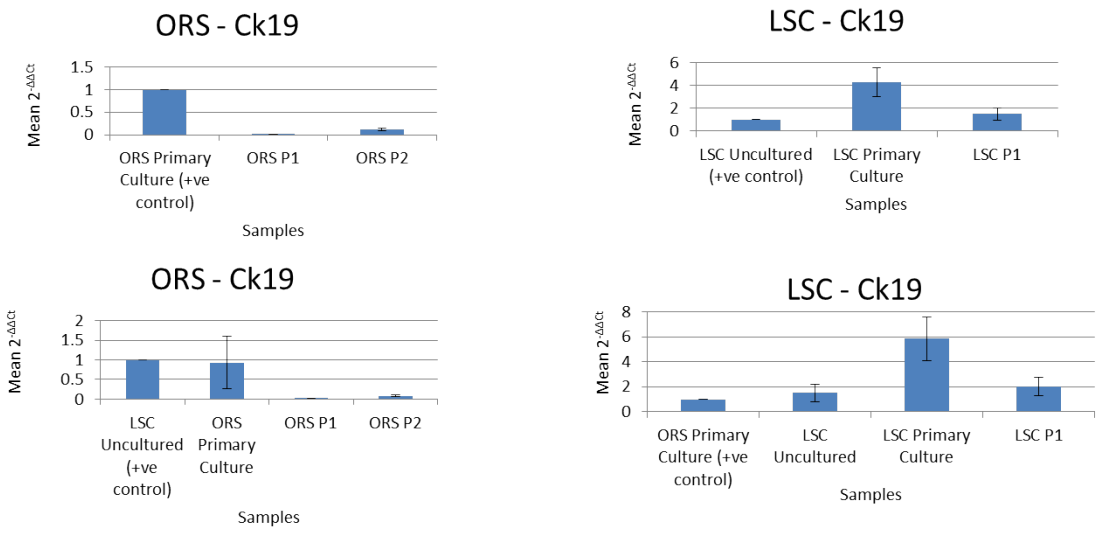

Figure 31: Relative normalised Ck19 expression in ORS and LSC cultures, n=1

The x-axis represents the culture stage. The y-axis represents the results of the formula $2^{-\Delta\Delta Ct}$ which is expressed in terms of fold changes. Relative Ck19 expression in ORS and LSC is compared to relative Ck19 expression in ORS Primary Culture as well as uncultured LSC as it is expressed in both types of cells.

Ck19 is a conjunctiva marker as well as an ORS marker, therefore its presence in ORS cultures suggests ORS cell presence in culture. In LSC cultures it is a marker for conjunctiva cells, showing there are some conjunctiva cells in the LSC cultures.

3.3.3.4 ORS markers

Expression of CD200, Ck5, Ck17, Integrinα6, Ck15 in ORS and LSC cultures

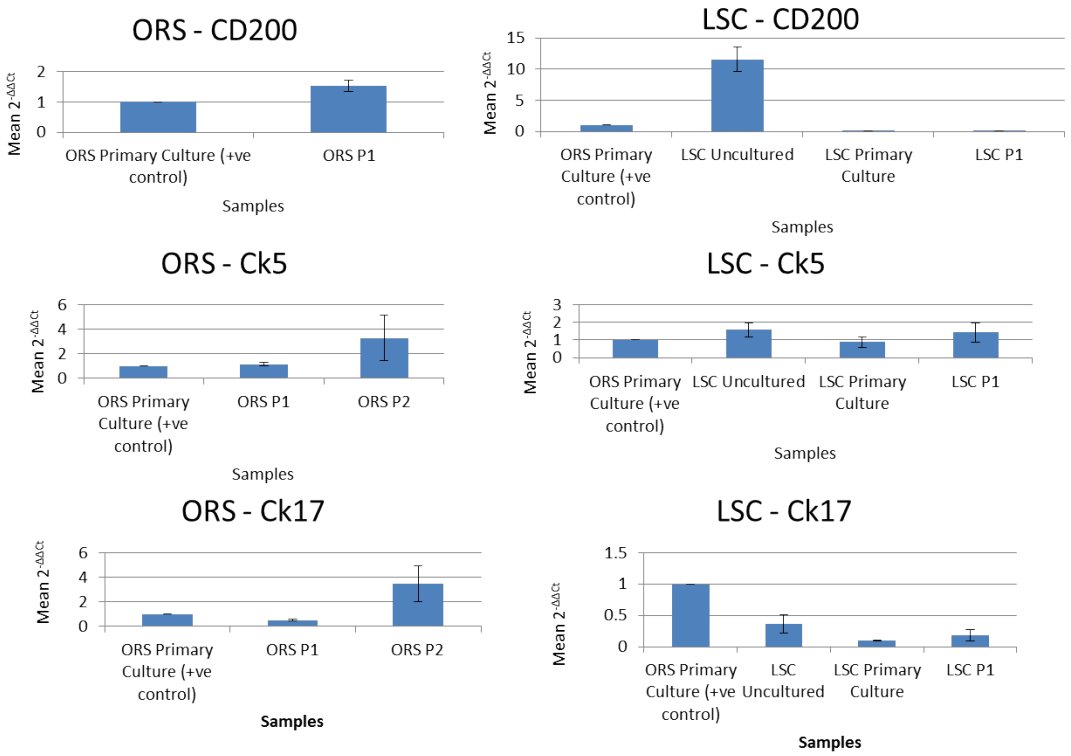

Figure 32: Relative normalised CD200, Ck5 and Ck17 expression in ORS and LSC cultures, n=1

The x-axis represents the culture stage. The y-axis represents the results of the formula $2^{-\Delta\Delta Ct}$ which is expressed in terms of fold changes. Relative CD200, Ck5 and Ck17 expressions in ORS and LSC are compared to their relative expression in ORS Primary Culture.

ORS markers CD200, Ck5 and Ck17 are all present and do not decrease in outer root sheath cell cultures, thus showing that ORS have retained their cell identity and not changed into corneal epithelial cells. However, some ORS markers were unexpectedly expressed in the corneal epithelial cultures. In particular Ck5 and Ck17 were expressed throughout all sub-cultures.

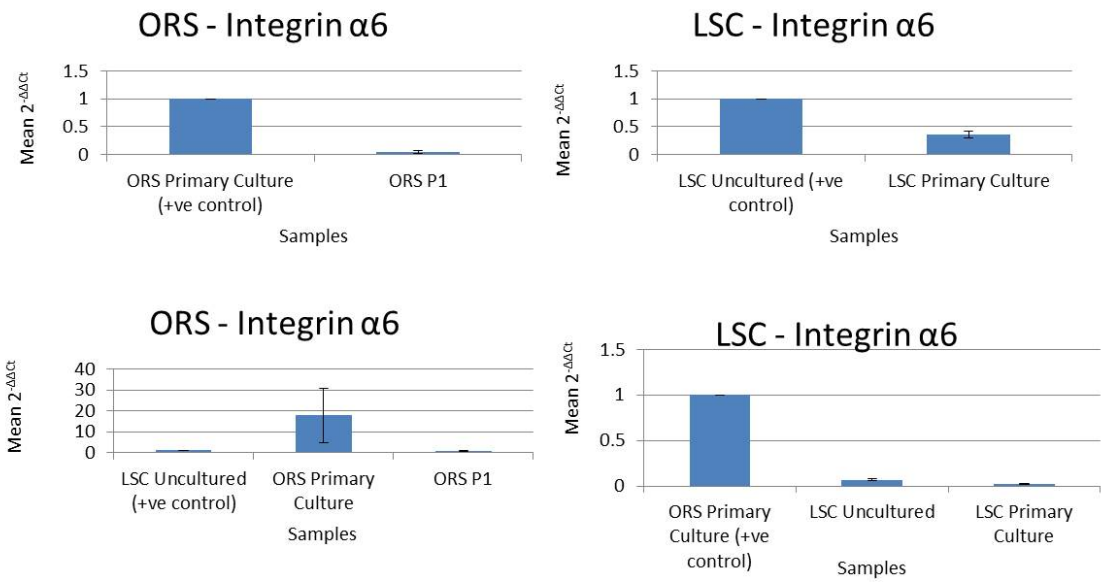

Figure 33: Relative normalised Integrinα6 expression in ORS and LSC cultures, n=1

The x-axis represents the culture stage. The y-axis represents the results of the formula $2^{-\Delta\Delta Ct}$ which is expressed in terms of fold changes. Relative Integrinα6 expression in ORS and LSC is compared to relative Integrinα6 expression in ORS Primary Culture as well as uncultured LSC as it is expressed in both types of cells.

Integrinα6, a marker of ORS as well as a gene expressed in the cornea was shown to be expressed in ORS cultures and LSC cultures at RNA levels.

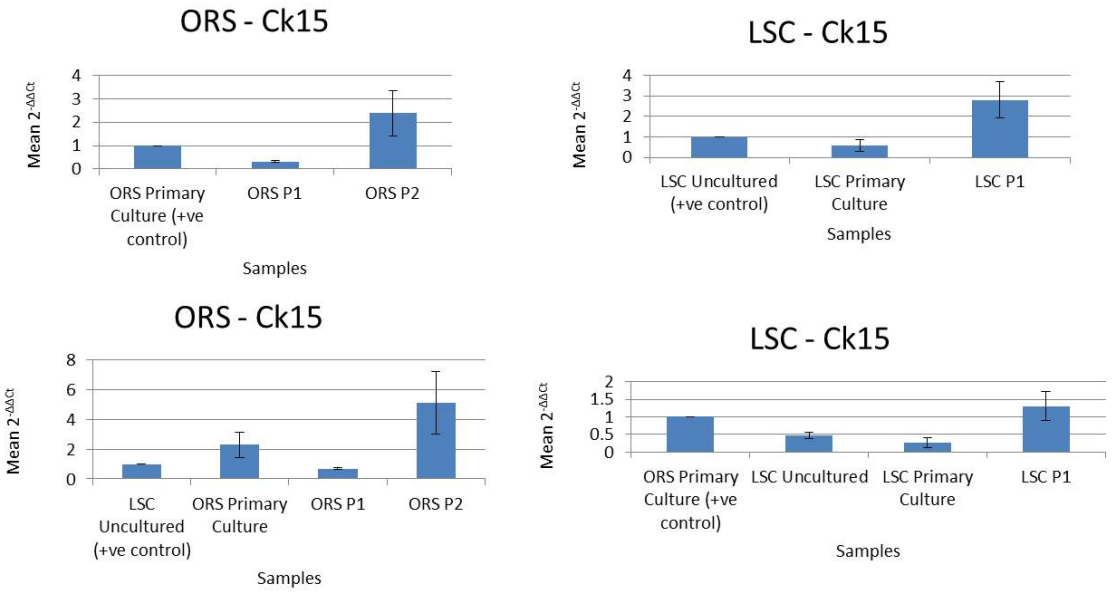

Figure 34: Relative normalised Ck15 expression in ORS and LSC cultures, n=1

The x-axis represents the culture stage. The y-axis represents the results of the formula $2^{-\Delta\Delta Ct}$ which is expressed in terms of fold changes. Relative Ck15 expression in ORS and LSC is compared to relative Ck15 expression in ORS Primary Culture as well as uncultured LSC as it is expressed in both types of cells.

Ck15, a stem cell marker of self-renewal was found to be well expressed in ORS culture therefore demonstrating that these cells in culture are stem-cell-like.

3.3.3.5 ORS differentiation markers

Ck10 expression in ORS and LSC cultures

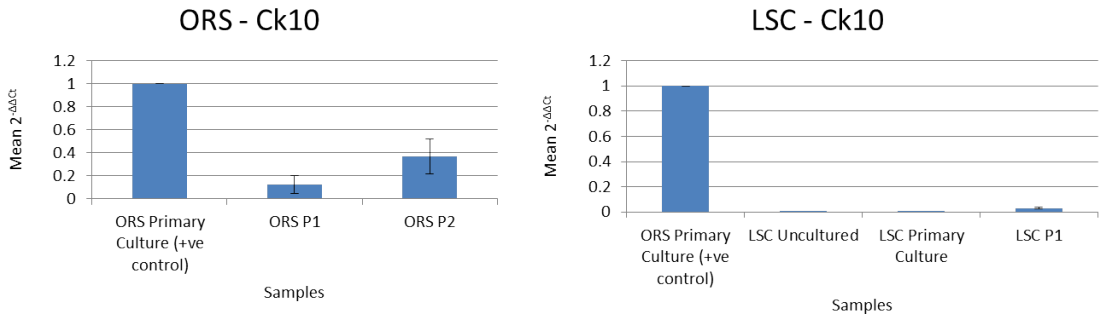

Figure 35: Relative normalised Ck10 expression in ORS and LSC cultures, n=1

The x-axis represents the culture stage. The y-axis represents the results of the formula $2^{-\Delta\Delta Ct}$ which is expressed in terms of fold changes. Relative Ck10 expression in ORS and LSC are compared to the relative Ck10 expression in ORS Primary Culture.

Ck10, a marker of differentiated ORS cells, showed there was a low level of differentiated cells in culture. This marker was absent in culture LSC's, although LSC's at passage 1 expressed very low amounts of Ck10.

3.3.4 Immunohistochemical analysis

Some of the results obtained from the quantitative real-time pcr data shown in the previous section 3.3.3 were confirmed through immunohistochemical analysis. These were Ck19, Ck17 and Integrinα6.

Immunofluorescence: Ck19 expression in ORS and LSC cultures

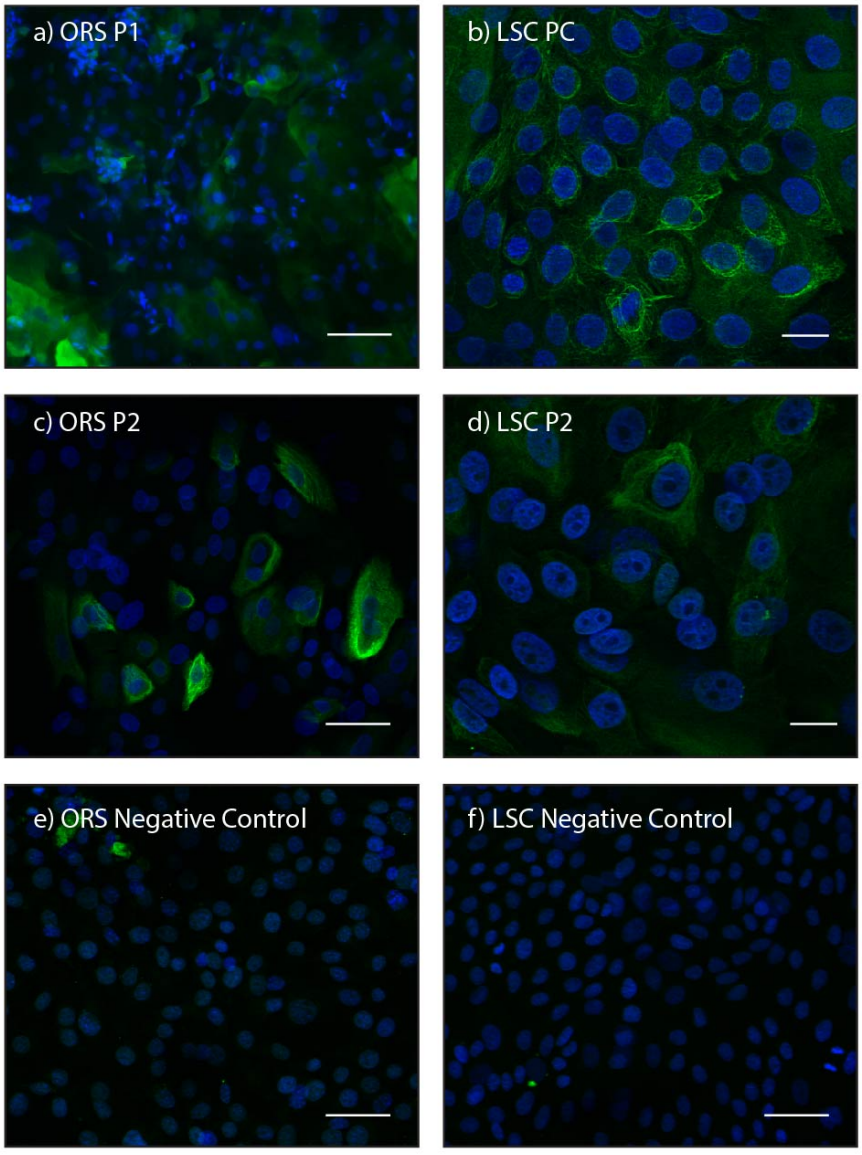

Figure 36: Immuno-fluorescence of Ck19 in ORS and LSC cultures and their respective negative controls

Negative controls were stained with the Secondary Antibody Donkey-anti-mouse only. Images were taken with an Axiovert Zeiss microscope. Scale bars: 100µm for a), 50µm for c), e) and f), 20µm for b) and d).

The conjunctiva marker as well as ORS marker, Ck19 was present at RNA levels (as shown in the qRT-pcr data in Fig. 31 of section 3.3.3) in both ORS and LSC cultures as well as at protein level as shown by immunohistochemical analysis shown in Figure 36. Ck19 presence in LSC cultures (Figure 36 b,d) reflects the presence of conjunctiva cells within the LSC cultures.

Immunofluorescence: Ck17 expression in ORS and LSC cultures

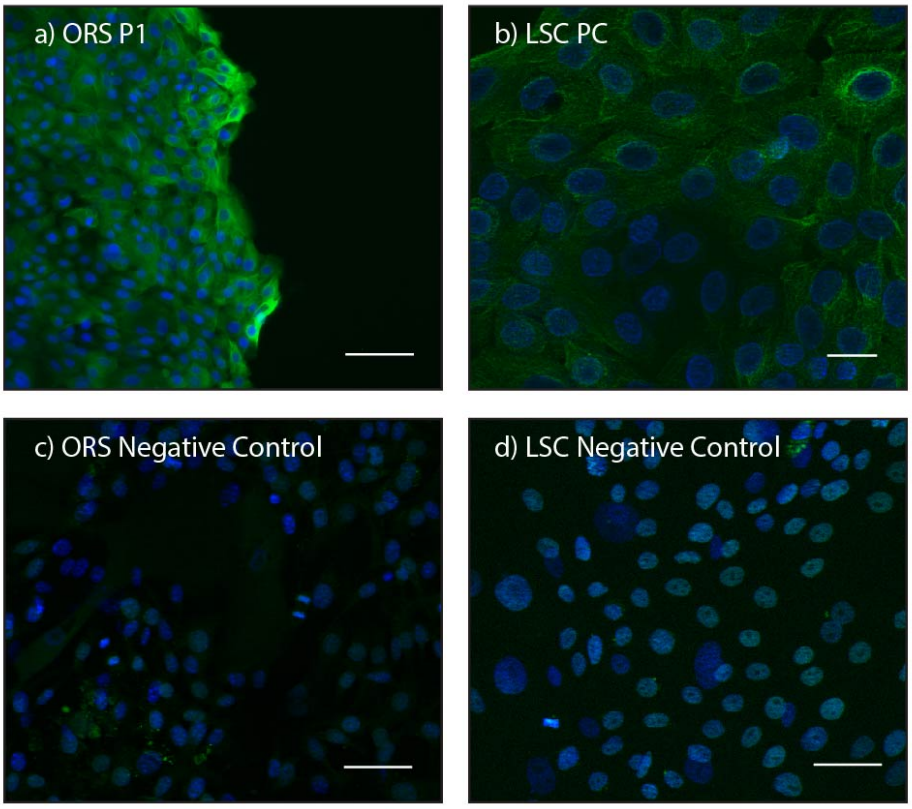

Figure 37: Immunofluorescence of Ck17 protein level in ORS and LSC cultures and their respective negative controls

Negative controls were stained with the Secondary Antibody Goat-anti-rabbit only. Images were taken with an Axiovert Zeiss microscope. Scale bars: 100µm for a), 20µm for b) and 50µm for c) and d).

The ORS marker Ck17 did not decrease in the ORS culture at RNA level in the qRT-pcr data shown in Figure 32 of section 3.3.3. This was also shown at protein level in the immunohistochemical analysis of ORS at Passage 1 (Figure 37 a). Ck17 expression in LSC cultures at RNA level was also confirmed by immunohistochemistry in Figure 37 b).

Immunofluorescence: Integrinα6 expression in ORS and LSC cultures

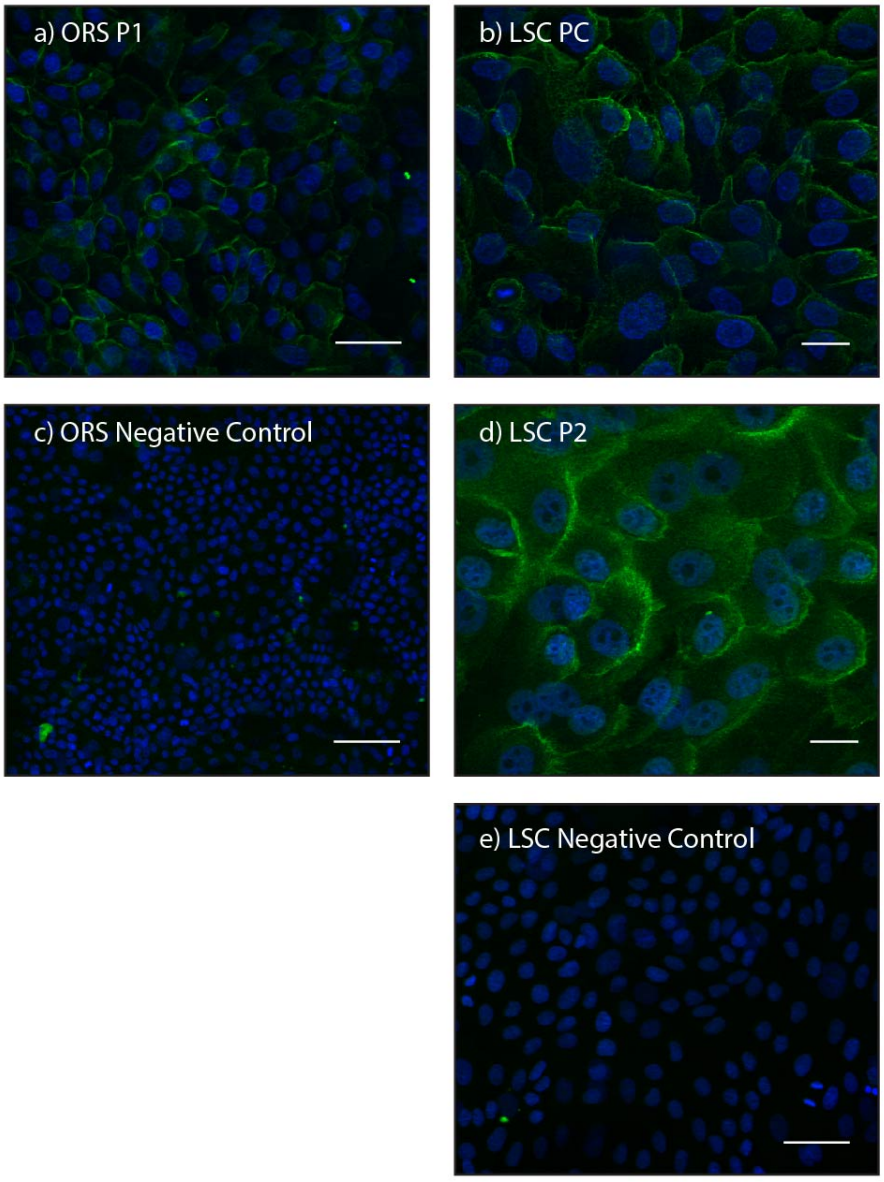

Figure 38: Immunofluorescence of Integrinα6 protein level in ORS and LSC cultures and their respective negative controls

Negative controls were stained with the Secondary Antibody Donkey-anti-mouse only. Images were taken with an Axiovert Zeiss microscope. Scale bars: 50µm for a) and e), 20µm for b) and d), 100µm for c).

The ORS marker integrinα6, also expressed in the cornea, was expressed in both ORS and LSC cultures at protein levels (as shown in Figure 38 a,b,c), thus confirming the qRT-pcr data shown Figure 33 of section 3.3.3.

3.4 Discussion & Conclusion

In summary these observation suggest that hair follicle, ORS cells cultured under the same conditions of culture as corneal epithelial cells do not change marker expression even with serial passaging. Specific corneal epithelial markers, although occasionally detectable at low levels are not decisively expressed. ORS markers are retained during culture and no decline in expression was noted. A limitation of this study is the fact that some of the ORS markers such as Ck17 are also expressed in LSC cultures. This was not expected. However, this also indicates that LSC and ORS cultures may actually be quite similar in the described 2D culture system. In conclusion, this study would need to be repeated, in order to confirm these conclusions. However, it seems that the LSC culture conditions, on their own are not sufficient in order to trans-differentiate ORS cells. Other studies have shown that co-culture (Karaoz *et al*., 2011) or direct cell interactions (Hu, *et al*., 2013) are required to provide the necessary signals. This has led on to the next chapter where a 3D cornea model was developed in order to study the epithelial-mesenchymal interactions taking place between the stroma and the corneal epithelium. This study would also give a better insight into corneal epithelial-mesenchymal interactions *in vivo*, which is a limitation of the 2D culture system.

4 Establishing an *in vitro* cornea 3D model

4.1 Introduction & Aims

Cornea 3D models are being created for a variety of purposes including but not exclusively for a) replacement and transplantation after injury or loss of the cornea, b) as research models to study the underlying biology and c) for replacing animal models, such as the Draize Eye Irritation Test that is performed on living rabbits, for testing drugs, toxins, treatments and cosmetics. From growing epithelial cells in 2D for transplantation purpose (described in the main Introduction), to the establishment of more complex models, there is an extensive number of varying cornea 3D models. Two strategies that are commonly used to engineer biocompatible, optically transparent and mechanically stable 3D cornea models are cell-based strategies, where cells are manipulated in order to create their own extracellular matrix and scaffold-based strategies, where the use of matrices that are strong and transparent are used to grow cells.

The two major challenges in developing a cornea 3D model, have been to re-create optical transparency, a corneal characteristic that depends on both tissue structure and cellular protein expression, and tissue strength. In order to address these challenges, studies on the corneal stroma have been performed. The quiescent nature of stromal keratocytes and of their progenitor cells, makes them difficult to culture *in vitro* as these cells lose most of their *in vivo* characteristics when cultured in 2D monolayers by becoming fibroblastic. The fibroblastic and activated myofibroblastic phenotype is associated with reduced corneal transparency due to the down-regulation of the corneal crystalline and transparency marker Aldh3a1 (in the human, known as Aldh1a1 in the rabbit), therefore re-creating the *in vivo* phenotype of stromal keratocytes as well as their ECM structure and organization has been a major aim in cornea tissue engineering. Moreover, recent work has highlighted the importance of the corneal stroma containing a mesenchymal stem cell population located below and in close contact to the corneal limbus (Branch *et al*., 2012). Studies have shown that interaction between the stromal stem cell niche and LSC niche is taking place and that both rely on each other for optimal maintenance and stem cell plasticity (Espana *et al*., 2003; Du *et al*., 2009).

Cell-based strategies

Various cell-based approaches have been developed that can induce stromal keratocytes to produce their native ECM *in vitro*. While epithelial cell sheets have been created from autologous cells from biopsies taken from the cornea (as explained in the main Introduction), other methods have been developed such as using a novel technique that uses temperature-responsive culture dishes (also used to create endothelial cell sheets) and biodegradable fibrin layers. Additionally, studies have attempted at engineering a complete cornea by co-culturing more corneal cell types together.

Creating stromal tissue. Studies have shown that one way of stimulating stromal cells to produce their ECM in culture and to interact with it, has been to use ascorbic acid. This has shown to increase their proliferation and also collagen secretion (Saika *et al*., 1992; Pasonen-Seppanen *et al*., 2001). Human keratocytes have shown to produce a 3D matrix made of parallel collagen fibers when cultured in ascorbic acid. These have been found to be similar to the ones find in the *in vivo* human cornea (Guo *et al*., 2007). Further studies are needed to assess the mechanical and optical properties of these self-assembled matrix structures. Collagen matrices with different stiffness have also been used to study cell morphology and collagen production of stromal fibroblasts (Karamichos *et al*., 2007). This resulted in stromal fibroblasts aligned and produced more collagen along the ECM stiffness axis, which suggested that mechanical signalling was could potentially re-produce collagen matrix structure similar to that of the native cornea. A study by (Orwin *et al*., 2007) discussed the various existing materials that can be used in a bioreactor to apply mechanical signals to create corneal tissue.

Creating epithelial tissue. A novel technique has been to create epithelial cell sheets that can be transplanted straight onto the patient's eye without using sutures, by using temperature-responsive culture dishes. These are based on the temperature-responsive polymer that is hydrophobic at 37°C, therefore promoting cell attachment, however by reducing the temperature to 20°C, the polymer become hydrophilic, therefore resulting in cell detachment (Shah *et al*., 2008). This enables the growth of cell sheets that can be readily detached without breaking the established ECM and without the polymer as this remains attached to the dish (Yang *et al*., 2006). Epithelial sheets created using this method have been shown to resemble the compact and stratified native epithelial structure (Yang *et al*., 2006). In a study by Hayashida *et al*., 2006, rabbit cultured

epithelial cells grown on temperature-responsive dishes stratified into a thick sheet composed of three to five differentiated cell layers. These were transplanted into rabbit eyes that were wounded with laser ablation, restoring the epithelial defect.

Creating endothelial tissue. Endothelial cell sheets have been created in a similar way to the epithelial sheets, using temperature-responsive culture dishes. Studies by (Lai *et al*., 2006; Sumide *et al*., 2006) have shown that endothelial cell sheets grown using this technique are similar to the natural endothelium. Sumide *et al*., 2006 demonstrated that corneas with an endothelial cell sheet had an increased corneal transparency, by using the slit lam microscope. Another study by Lai *et al*., 2006 showed that endothelial cell sheets engineered through the temperature-responsive technique had intact barriers and pump functions. This demonstrated that there was no need for cell carriers to obtain these functions when culturing endothelial cells.

Co-cultures. In addition, co-culture techniques have been developed were two types of corneal cells were cultured together. This was performed in order to investigate the cell-cell interactions taking place with the aim to re-create cellular behaviour as that found *in vivo*. Epithelial cells and fibroblasts have been cultured together on collagen gels in a study by (Nakamura *et al*., 2002), where it was demonstrated that secretion of a soluble factor by injured epithelial cells, caused collagen gel contractions by stromal fibroblasts, their proliferation and differentiation to myofibroblasts (Nakamura *et al*., 2002). In a study by Zieske *et al*., 1994 epithelial cell differentiation and the assembly of the basement membrane were assessed by culturing all three corneal cell types together, in order to assess the influence of endothelial cell interaction and the culture condition (Zieske *et al*., 1994). In this three-dimensional construct endothelial cells were layered on the bottom, covered with a layer of stromal fibroblasts that were placed in a collagen gel matrix. This was then covered by a layer of epithelial cells (Zieske *et al*., 1994). This study showed that by including the endothelial layer in the model, the basal layer was formed that displayed stratification and a columnar morphology. Moreover, structural proteins such as collagen type VII and laminin were found at the junction between the epithelium and matrix. In addition, other groups used the same technique to study collagen biosynthesis and scarring using the three major corneal cell types (epithelial, fibroblasts and endothelial cells) (Dreier *et al*., 2013; Yanez-Soto *et al*., 2013).

Scaffold-based strategies

Biomaterials have been widely studied to be used in corneal tissue engineering. The main requirements for these biomaterials is that they have to be transparent, mechanically stable, biocompatible and allow cells to adhere, proliferate and migrate (Shah *et al*., 2008). In order to mimic the native corneal tissue composition, many groups have used scaffolds made of collagen type I, whereas the mechanical properties that are found in the cornea were studied by using synthetic polymers.

Collagen: Many studies have used type I collagen gels and some data indicated by Kato *et al*., 2007, that there is a potential in producing stromal equivalents using this method, however it has been reported that they degrade rapidly *in vivo* and have poor mechanical properties. For this reason studies have attempted to improve collagen gels by testing different ways to crosslinking the collagen gel (Doillon *et al*., 2003; Duan and Sheardown, 2006). However, such constructs have been used to grow immortalized human epithelial cells and have not been used to grow stromal fibroblasts.

Collagen sponges: In a study by Orwin *et al*., 2003, collagen sponges were used to grow stromal cells and were found to be superior to collagen gels in terms of transparency and from a mechanical point of view. (Borene *et al*., 2004)This study found that fibronectin, decorin sulfate, collagenase and gelatinase were expressed therefore indicating that stromal cells were expressing the repair fibroblast phenotype.

Synthetic polymers: Some of the limitations of collagen gels are that they shrink when in presence with cells. Synthetic polymers have been found to be more stable and have been used in different studies. Natural biodegradable and biocompatible polyesters have beed described by Zorlutuna *et al*., 2006 to use as foams for stromal and films epithelial cells. However, fibroblast maintenance was compromised due to the decreased porosity of the foam. Other variations have been described such as modifying polymers with EGF (Klenkler *et al*., 2005), this improved growth and adhesion of epithelial cells (Klenkler *et al*., 2005) and TGFβ2 to stimulate stromal proliferation (Merrett *et al*., 2003).

Modified hydrogels with different factors such as with type I collagen (Myung *et al*., 2007), which supported epithelial and stromal cell growth, and amniotic membrane (Uchino *et al*., 2007), which showed to support epithelial cell differentiation, were

investigated. However, when the latter was transplanted into the rabbit stroma, epithelial defects were formed. In addition, studies have been performed to assess the *in vivo* behaviour of poly-glycolic acid (PGA) scaffolds by placing these, containing stromal cells, into a rabbit cornea stroma (Hu *et al*., 2005). Results showed that stromal tissue was formed by the implants and not by stromal cells located in the rabbit cornea.

Other corneal equivalents have been explored. In 1999, Griffith *et al*., produced three main corneal layers *in vitro* by using a collagen-based scaffold and immortalized cell lines. This work showed that these constructs were very similar to the native cornea. In addition, Griffith's work has also concentrated on the innervation of tissue-engineered corneas, an essential function for corneal wound healing and fully functional epithelial cells (Suuronen *et al*., 2004). Griffith's group also developed recombinant human collagen-phosphorylcholine hydrogels to use as corneal substitutes. This work has had success in Phase 1 clinical trials by showing robust signs of corneal regrowth and also partial vision recovery (Fagerholm *et al*., 2010).

However, in the current literature no cornea model has been developed that lies between the very simple 2D culture model of epithelial cell sheets and the more complex 3D models that usually involve biomaterials, larger number of cells, are time consuming to make and cannot be used for high-throughput screening studies. In addition, no tissue engineered model has yet shown to re-create the stromal native architecture *in vitro* (Torbet *et al*., 2007).

One form of 3D model, the 3D spheroid, is now valuable not only for studying basic cell biology and physiology, but also in biotechnology, drug discovery, and toxicitiy testing (Achilli *et al*., 2012). Spheroids have been created by several methods including, centrifugation and seeding cells into non-adhesive moulds, but classically they have been produced using hanging drop culture (Fennema *et al*., 2013).

In the Durham laboratory a skin 3D spheroid model using the hanging drop culture technique has been developed. This model involved two cell types, the mesenchymal dermal skin component and the skin keratinocytes to create a two-layered sphere in suspension culture (see Fig. 39 below).

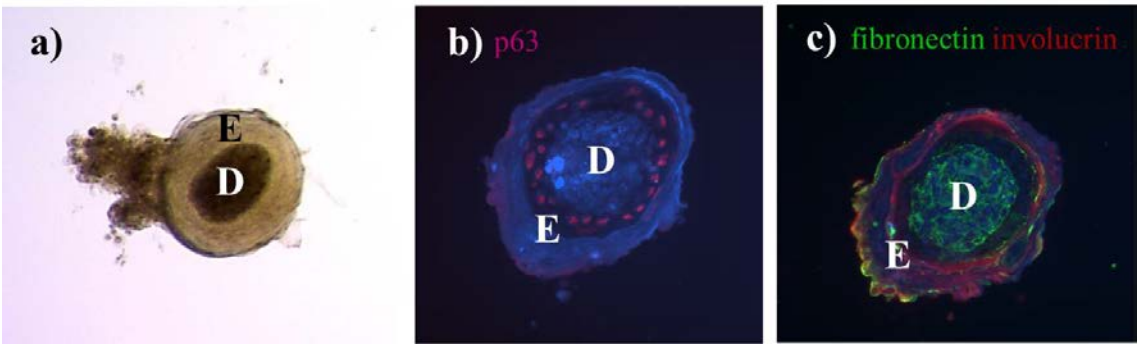

Figure 39: Human 3D skin model in a hanging drop culture & immunohistochemical analysis

a) Shows a macroscopic image of a skin 3D model in a hanging drop culture, with (D) indicating the dermis and (E) the epithelium.
b) and c) show p63, fibronectin and involucrin immuno-staining.

The skin 3D model using the hanging drop technique showed to be successful in re-creating the epithelial stratification process *in vitro*, as indicated by p63 expression in the epithelial layer (E) in image b), fibronectin expression in the dermal component (D), indicating an active ECM forming proteins such as collagen, and involucrin expression.

Recent work by Higgins *et al*., 2013, showed that by placing human dermal papilla cells in the above mentioned 3D spheroid structures, induced de novo human hair-follicle growth in human skin, a feature that is lost when these cells are placed in 2D monolayers.

The focus of this chapter has therefore been to adapt the three-dimensional spheroid technique to corneal stromal and epithelial cells. This has not been previously done. Because of human corneal tissue limitation, rabbit corneal tissue was used initially to establish and study the 3D spheroid method.

Initially, a comparison was made between stromal keratocytes extracted from below the limbal region and keratocytes extracted from the entire stroma, placed in 3D spheroid cultures and compared to their 2D counterparts. The hypothesis was that 3D culture would cause the stromal cells to revert to becoming more like their counterparts *in vivo*.

Analysis was performed using quantitative real-time pcr and immunohistochemistry on a range of stromal markers. The next step involved the establishment and refinement of a rabbit cornea 3D bilayered spheroid model, using corneal epithelial cells around a stromal keratocyte core. The model was monitored using macroscopic images, and histological and immunofluorescent analysis of corneal epithelial and stromal *in vivo* markers were used to determine model quality and function. The same technology was then applied to human cells, in order to extend the technique between species, and to make it more clinically relevant.

Aims of this study

The aims in this chapter were:

- Initially, to study corneal stromal keratocytes in 3D cultures by forming stromal spheres and establishing a working protocol.
- Assess corneal stromal 3D spheres vs. 2D stromal keratocytes using a range of markers tested by immunofluorescent and quantitative real-time pcr analysis, in order to elucidate whether the 3D culture environment was indeed a better culture system compared to 2D cultures. The hypothesis was that 3D environments replicate the *in vivo* cellular conditions to a better extent than 2D.
- Studying corneal stromal and corneal epithelial interactions using the 3D culture environment. This required the development of a working protocol to establish a successful 3D cornea model, as this had never been previously done.

4.2 Materials & Methods

All the experimental procedures carried out in Chapter 4 were conducted in compliance with Durham University Health & Safety Policy according to the Control of Substances Hazardous to Health (COSHH) regulations. All tissue culture work was undertaken at Containment Level 2 using standard aseptic techniques.

4.2.1 Materials

All reagents used in this chapter were directly derived from the relevant suppliers and COSHH regulations were respected throughout their usage.

4.2.1.1 Rabbit & Human cornea cells & tissue

All rabbit corneal epithelial cells and stromal keratocytes used were extracted straight after post mortem from rabbit (New Zealand Whites) eyes from the Life Sciences Support Unit (LSSU) at Durham University in the Biological and Biomedical department. Cells were extracted using established protocols described in the methods section 4.2.2.1.

Human corneas, donated for research, were obtained from the UK Eye Banks. Cells extracted from these corneas were used to establish corneal epithelial cell cultures. These were co-cultured with mitotically inactivated 3T3 J2 mouse fibroblasts using an established protocol.

Rabbit and Human corneal tissue and 3D single spheres and 3D models were all placed in O.C.T embedding matrix (Fisher) in small disposable base moulds (Fisher) before snap freezing these in liquid nitrogen for immunohistochemistry/fluorescence or histology.

Stromal keratocytes were extracted from one freshly donated pair of eyes obtained from the Newcastle Royal Victoria Infirmary in conjunction with Newcastle University. The second human stromal keratocyte sample used (ID: 9173) was kindly sent by Prof. Julie Daniel from UCL in London. These stromal keratocytes were obtained as a frozen vial

after a Material Transfer Agreement was made between UCL and Durham University and according to the Human Tissue Act 2004.

4.2.1.2 Culture media & tissue culture components

3T3 J2 mouse fibroblast and Limbal Epithelial Medium components were described in the Material & Methods section 2.2.1.2 in Chapter 2.

The media used to culture stromal keratocytes was the same one used to culture 3T3 J2 mouse fibroblasts and was composed of DMEM, 10% FBS (instead of Adult Bovine Serum) and 1% Penycillin/Streptomycin. This media was used for both rabbit and human stromal keratocyte primary cultures and is designated "Standard stromal media" in this thesis.

Rabbit eyes that were extracted post-mortem were washed multiple times in MEM with triple strength antibiotics, designated "Triple Strength MEM" to ensure that no contaminating agents would affect stromal and epithelial cultures. The components of this medium are summarised in Table 12.

Prior to creation of 3D cultures, stromal cells were placed in medium in which FBS was replaced by serum from the same origin and as the cells – so adult rabbit serum was used for rabbit stromal keratocytes and adult human serum for human stromal keratocytes. This medium was designated "Species specific medium" and its components are listed below in Table 13.

Reagent	Composition	Supplier
MEM (1x) + GlutaMAX Minimal Essential Medium	95%	Gibco Life Technologies
PenStrep (10,000 units Penicillin and 10mg/ml Streptomycin)	5%	Gibco Life Technologies
Fungizone (Antimycotic)	0.6%	Gibco Life Technologies

Table 12: Composition of Triple Strength MEM

Reagent	Composition	Supplier
MEM (1x) + GlutaMAX Minimal Essential Medium	90%	Gibco Life Technologies
Rabbit or Human Serum	10%	Both from Sigma-Aldrich

Table 13: Composition of Species Specific Medium for rabbit and human stromal keratocytes

The aqueous humor used to culture some of the rabbit cornea 3D models was freshly extracted from the rabbit eyes before dissecting these for cell extraction. It was kept in the fridge at 4°C and used within a couple of days from the extraction date.

Other materials used for cell extraction and tissue processing are listed below in Table 14.

Reagent	Supplier
Dispase II 2.4U/ml (diluted 2mg/ml in MEM + 20% FBS)	Sigma-Aldrich
Disposable Biopsy Punch 4mm diameter	Stiefel
0.02% EDTA	Sigma-Aldrich
Mitomycin C from *Streptomyces caespitosus*	Sigma-Aldrich
Sterile 1x PBS for tissue culture	n/a
0.05% Trypsin-EDTA	Sigma-Aldrich
Fetal Bovine Serum	Sigma-Aldrich

Table 14: Materials for tissue processing and cell culture

4.2.1.3 Histology solutions

Rabbit corneal tissue and 3D models were cut on the animal cryostation, a Leica CM3050S. Human corneal tissue and 3D models were cut on the human cryostation, a Leica CM1900UV. Sections were left to dry at room temperature on Colourfrost Plus Yellow slides (Fisher). For H&E staining the materials used are listed in the Appendix section 8.3.

4.2.1.4 Antibodies & Immunohistochemistry

Primary and Secondary antibodies used in Chapter 4 are all listed in Table 15 and 16 below.

Target	Raised in:	Dilution used	Supplier
Pax6	Rabbit	1:100	Sigma
Ck3	Mouse	1:200	Abcam
Ck3Ck12	Mouse	1:50	Abcam
Ck10	Mouse	1:100	Millipore
Aldh1a1	Chicken	1:100	Vasiliou Lab*
Vimentin	Mouse	1:100	Amersham
αSMA	Mouse	1:100	Abcam

Table 15: Primary Antibodies

*The Aldh1a1 antibody was kindly donated by the Vasiliou Lab, Pharmacy & Pharm Sci Bldg V20-C238, Aurora, CO 80045, United States.

Secondary Antibodies	Raised in:	Dilution used	Supplier
Alexa Fluor 488	Goat anti rabbit	1:500	Invitrogen
Alexa Fluor 488	Goat anti mouse	1:500	Invitrogen
Alexa Fluor 594	Goat anti chicken	1:500	Invitrogen

Table 16: Secondary Antibodies

Primary and Secondary antibodies were diluted in the dilution buffer listed in Table 17 below.

Reagent	Composition	Supplier
Permeabilisation Buffer	1% Triton X-100 (in 1x PBS)	Sigma-Aldrich
Quenching buffer	100mM Glycine (in H_2O)	Sigma-Aldrich
Diluting buffer	0.5% Tween 20 (in 1x PBS)	Sigma-Aldrich
Blocking Solution	5% Goat Serum in Diluting buffer	Sigma-Aldrich
Mowoil	n/a	Sigma-Aldrich
DAPI	DAPI (diluted 1:1000 in Diluting Buffer)	Invitrogen
4% PFA	(in 1x PBS)	Sigma-Aldrich
1x PBS (pH 7.4)	n/a	n/a

Table 17: Materials and solutions for Immunohistochemical analysis

4.2.1.5 Molecular Biology materials

RNA extraction

RNA extraction from rabbit cells and rabbit 3D spheres was achieved using the RNeasy Mini Kit (50) from Qiagen (Cat No. 74104). RNA extraction from whole corneal tissue was done by using the Trizol Method. Materials for the latter are listed below:

- TRIzol (Invitrogen)
- Chloroform (BDH)
- Isopropyl alcohol (BDH)
- 75% ethanol in RNase free DEPC treated dH_2O
- RNase free dH_2O

Once RNA was extracted its concentration was measured using a NanoDrop Spectrophotometer (ND-1000).

Reverse Transcription

Reverse transcription was performed following a standard protocol using the reagents listed in Table 18 and using a Thermocycler (Biometra Tpersonal) with a specific program (described in the Methods section 4.2.2.4 Table 21).

Name	**Supplier**	**Catalogue#**
RNAse free PCR tubes	n/a	n/a
Oligo-dT	Ambion	5730G
dNTP	Bioline	DA-10513
RNAse free H_2O	Invitrogen	n/a
5x first strand buffer	Invitrogen	Y02321
SuperScript III RT	Invitrogen	56575
0.1 M DTT	Invitrogen	X00147
RNAse Out	Invitrogen	100000840

Table 18: Reagents and materials used for Reverse Transcription

Primers

Primer sequences were taken from the paper Jester *et al*., 2012 and had been specifically designed to work in the rabbit. The primers were all supplied by Invitrogen and were diluted with RNase free dH_2O to 100umole to keep as a primer stock solution frozen at -20°C. For quantitative real-time pcr, primers were diluted 1:10 in RNase free dH_2O from the primer stock solution. The primer sequences are listed below in Table 19.

Gene	Primer	Sequence (5'-3')	Ta (°C)
Lumican	Forward	TGCAGCTTACCCACAACAAG	50.7°C
	Reverse	AGGCAGTTTGCTCATCTGGT	51.9°C
Keratocan	Forward	GTCTCACAATCGCCTCACAA	50.1°C
	Reverse	GGTCCATGGATGAACGAATC	48.4°C
Aldh1a1	Forward	ACTCCCCTCACTGCTCTTCA	52.9°C
	Reverse	AACACTGGCCCTGATGGTAG	51.9°C
αSMA	Forward	TGCTGTCCCTCTATGCCTCT	52.7°C
	Reverse	GAAGGAATAGCCACGCTCAG	50.6°C
GAPDH	Forward	GAGCTGAACGGGAAACTCAC	50.9°C
	Reverse	CCCTGTTGCTGTAGCCAAAT	50.6°C
β-actin	Forward	ATCGTGATGGACTCCGGCGAC	63°C
	Reverse	AGCGCCACGTAGCACAGC	55°C

Table 19: Primers, their sequences and annealing temperatures (Ta)

Quantitative real-time pcr

qRTpcr was performed by using the Corbett Research Rotor-gene Q Series machine with the 72 well Rotor, by using the Power SYBR Green PCR Master Mix (Cat.No.4367659) from Applied Biosystems (Life Technology) and the Qiagen Strip tubes and caps. The program was a 3-step one and was repeated for 40 cycles and the steps involved in the program are described in the Methods section of this chapter.

Summary of primers & antibodies tested

Marker	Description
Aldh1a1 (qRTPCR and Immuno) specific only for the rabbit	Crystallin protein expressed in the corneal stroma and epithelium.
Lumican (qRTPCR)	Crystallin protein
Keratocan (qRTPCR)	Marker for stromal keratocytes
GAPDH (qRTPCR)	Crystallin protein
α-smooth muscle actin (αSMA) (qRTPCR and Immuno)	Marker for myofibroblasts "activated" keratocytes
Pax6 (Immunohistochemistry)	Eye development marker
Ck3 (Immunohistochemistry)	Corneal epithelial differentiation marker only expressed in the corneal epithelium
Ck12 (Immunohistochemistry)	Corneal epithelial differentiation marker only expressed in the corneal epithelium
Vimentin (Immunohistochemistry)	Marker for mesenchymal cells
Ck10 (Immunohistochemistry)	Expressed in the rabbit limbal epithelium, therefore specifically associated with more stem like (limbal) corneal epithelial cells in the rabbit.

Table 20: Description of markers used in this study

4.2.2 Methods

4.2.2.1 Tissue culture

Dissection of human and rabbit eyes

One pair of fresh human eyes was received within 24 hours post-mortem from the Royal Victoria Infirmary in Newcastle. Under a laminar and sterile flowhood, the eyes were placed in a petri dish and kept moist in 1x PBS. With a pair of sterile forceps and scissors the cornea was cut out from the rest of the eye and placed in clean 1x PBS for a quick wash. This work was carried out at the Centre for Life in Newcastle.

Fresh rabbit eyes were cut out from the rabbit post-mortem in the Life Sciences Support Unit (LSSU) at Durham University and placed in a 50ml falcon tube containing Triple Strength MEM washing media in order to keep the eyes moist as well as to disinfect the eyes from fungi and bacteria. The eyes were taken to a laminar flowhood, placed in a petri dish filled with fresh Triple Strength MEM and the cornea was cut out by using sterile forceps and scissors.

Dissociation Protocol for stromal cell extraction

For human and rabbit stromal keratocyte cell extraction, the corneas were cut in small 2mm squares and placed in Dispase II solution (diluted 2mg/ml in MEM and 20% FBS). The FBS was a crucial ingredient as without it the stromal keratocytes did not survive. The corneal tissue pieces were incubated for 18 hours in the fridge at 4°C. After 18 hours incubation the corneal tissue pieces were removed from the Dispase solution and the epithelial and endothelial layers were peeled off from the stroma.

For the rabbit upper stromal keratocyte extraction, once the epithelial and endothelial layers had been peeled off, approximately 1cm of the superior layer of the stroma, close to the epithelial layer, was cut off with a pair of scissors. This superior part of the stroma was named “upper” and cultured. In order to be able to distinguish which way up the corneal pieces were sitting in the Dispase solution, the endothelial layer was a shiny layer, whereas the epithelial layer was thin and opaque and had a tendency to break while peeling off.

For the rabbit limbal stromal keratocyte extraction, 4mm in diameter punch biopsies were made in the limbal region of the rabbit cornea, before placing these in the diluted Dispase solution for 18 hours.

Once endothelial and epithelial layers had been removed, human and rabbit stromal pieces were washed in Triple Strength MEM (only for the rabbit stroma), placed in a T25 flask with Standard stromal medium and the stromal tissue pieces were allowed to stick at the bottom of the flask in an incubator at 37°C with a humidified gas mixture containing 5% CO_2.

A week later, stromal keratocyte growth could be observed and when these were 80-90% confluent they were passaged. First, the remaining stromal tissue had to be carefully removed before trypsinising the stromal keratocytes. This was done by using sterile forceps. The remaining stromal tissue was disposed appropriately. Stromal keratocytes were trypsinised for 5 minutes with 0.05% warmed up Trypsin, the Trypsin was inactivated with Standard stromal medium, stromal keratocyte suspension was transferred into a 15ml falcon tube and centrifuged at 1000rpm for 5 minutes. The supernatant was disposed and the pellet was re-suspended with 2ml of Standard stromal medium. The re-suspended stromal keratocytes were plated in two new T25 flasks and allowed to reach semi-confluence. One of the two T25 flasks was frozen down at -80°C to be kept as a stock.

Human & rabbit limbal corneal epithelial cells

Human limbal corneal epithelial cell extraction protocol is described in the Methods section 2.2.2.1 in Chapter 1. The same protocol was used for rabbit limbal corneal epithelial cell extraction. In short, cells were released from the tissue by serial trypsinisation to release free epithelial cells in suspension. The culture of human and rabbit limbal corneal epithelial cells is achieved by plating these on a layer of mitotically inactivated 3T3 J2 mouse fibroblasts (as has been previously described in the Methods Section in Chapter 1, section 2.2.2.1) and cultured in Limbal Epithelial Medium (LEM). All cell cultures discussed in this chapter were maintained at a temperature of 37°C with a humidified gas mixture containing 5% CO_2.

4.2.2.2 Cornea 3D model

Single stromal 3D spheres

Human and rabbit stromal keratocytes were passaged into new T25 flasks containing Species specific medium. After 2 or 3 days, the keratocytes were 70% confluent. At this stage they were trypsinised, spun down, re-suspended in Species specific medium and counted with a Haemocytometer. 3000 stromal keratocytes were placed per 10µl drop in the lid of a plastic petri dish. Approximately 20 to 25 drops were pipetted per dish lid.

20ml of sterile dH_2O were put in the main dish base. The lid containing the stromal keratocyte drops was turned over quickly and placed onto the petri dish base. The plastic petri dishes were then placed into an incubator at 37°C and were not moved for three days. After three days, stromal keratocytes had aggregated into tight 3D spheres and these were now either embedded in OCT matrix for cryosectioning for H&E and immuno-staining, processed for RNA extraction or it was proceeded in establishing a cornea 3D model.

Creating a cornea 3D model

Coating of single stromal spheres to produce a cornea 3D model was achieved by having limbal corneal epithelial cells cultured onto a 3T3 feeder layer at around 30-40% confluency. What was found was that the best conditions for making a 3D model was when the corneal epithelial cultures had formed many small sized colonies that were not in physical contact with one another. LEM was removed from the tissue culture wells and replaced with 2ml of EDTA. This was necessary to first remove any remaining 3T3 feeder layer cells. This did not remove the corneal epithelial colonies. The EDTA solution was disposed and replaced with 2ml of pre-warmed 0.05% Trypsin to detach the corneal epithelial colonies from the wells of the tissue culture plate. After 5 minutes Trypsin incubation, the Trypsin was neutralised with LEM, pipetted into a 15ml falcon tube and centrifuged at 1000rpm for 3 minutes. The supernatant was removed and the pellet re-suspended in 2ml of LEM. The cells were counted with a Haemocytometer and 6000 corneal epithelial cells were pipetted into each single stromal 10µl drop previously made, as described above. The plastic petri dish was returned to the incubator at 37°C and left untouched for three days.

At culture day 3, corneal epithelial cells had aggregated around the stromal spheres and created compact double-layered spheres. These were visualised under a dissecting microscope, macroscopic images were taken and the media was changed. To change the media, each 3D model was pipetted into a fresh 20µl drop (in a fresh petri dish with fresh sterile dH_2O in the base of the dish) containing 50% Species specific media and 50% LEM. The 3D cornea models were placed back in the incubator at 37°C, the media was changed every other day, macroscopic images were taken and at several different time intervals 15 to 20 double-layered spheres were snap frozen in O.C.T embedding

matrix as described below. Figure 40 below summarises the techniques used to create a cornea 3D model.

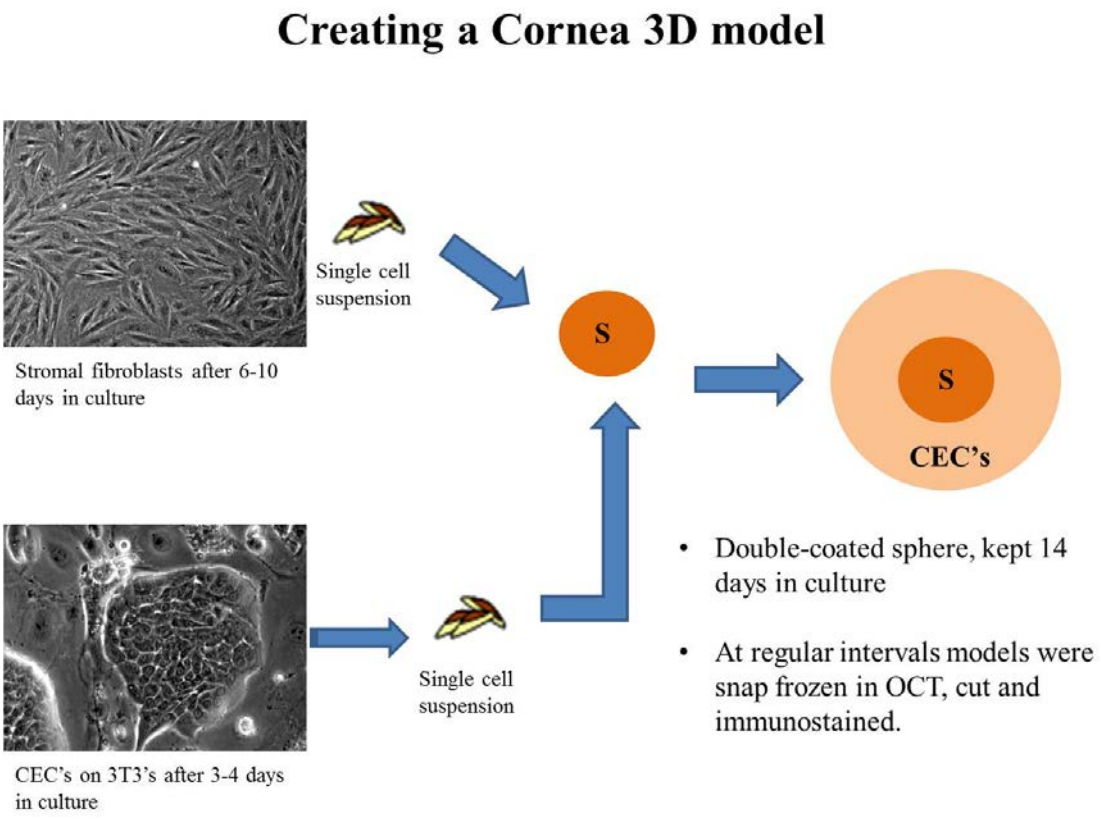

Figure 40: Representative summary of the steps involved in creating a cornea 3D model

4.2.2.3 H&E & Immunofluorescent analysis

Embedding and sectioning

Rabbit and human corneal tissue and single/double-coated spheres were embedded in a disposable mould in OCT embedding matrix and snap frozen in liquid nitrogen for 5 minutes. The embedded and frozen blocks could then be kept in the freezer at -80°C until needed. 7µm sections of the embedded samples were cut using a Cryostat (Leica) with disposable blades. The sections were mounted on slides and were left to air dry for at least one hour at room temperature.

Haematoxylin and eosin staining

The slides were immersed in 1x PBS for 5 minutes, then placed in haematoxylin for 10 minutes and then carefully rinsed under a light stream of tap water without damaging the sections. The slides were washed further in distilled water for 5 minutes, following 8-12 dips in acidic ethanol and then two additional washes in distilled water of one minute each. The slides were then immersed in eosin for 30 seconds, 75% ethanol in distilled water three times 5 minutes each, 100% ethanol three times 5 minutes each and finally Histoclear three times 5 minutes each. The slides were mounted in distyrene/plasticiser/xylene (DPX) with a coverslip, under a laminar flowhood and let to dry at room temperature. The dry slides were visualised using a Zeiss microscope (Carl Zeiss) and images were taken using the Axiovert software (Carl Zeiss).

Immunohistochemistry

The slides were washed in 1x PBS for 5 minutes, fixed in 4% Paraformaldehyde (PFA) for 30 minutes, washed in 1x PBS for 5 minutes, quenched with 100mM glycine for 30 minutes, washed in 1x PBS for 5 minutes, permeabilized with 0.1% Triton X-100 for 30 minutes (for nuclear antibodies), 20 minutes for all the others. The slides were then washed in 1x PBS for 5 minutes, blocked in 5% Goat serum (Blocking solution) for 1 hour. Everything was performed at room temperature. Samples were then incubated with primary antibodies at the appropriate dilutions in Diluting Buffer and placed in a humidified chamber at 4°C overnight. The following day, the slides were rinsed three times for 5 minutes in 1x PBS and incubated for 1-1.5 hours with appropriate secondary antibodies, diluted at 1:500 in Diluting Buffer. This step was kept at room temperature and in the dark. Slides were then washed three times 5 minutes each in 1x PBS and incubated with DAPI, diluted 1:1000 in Diluting Buffer, for 10 minutes at room temperature and in the dark. Slides were mounted in Mowoil with a coverslip and let to dry at room temperature and protected by light before visualising them using a Zeiss microscope (Carl Zeiss) and/or acquiring images on a confocal microscope (SP5). Slides could then be stored in appropriate slide boxes protected from the light at 4°C.

4.2.2.4 Molecular Biology

RNA extraction & Isolation from rabbit stromal 3D & 2D keratocytes

RNA from rabbit single 3D spheres and rabbit 2D stromal cultures was extracted using the RNeasy Mini Kit (50) (Qiagen) and following the protocol described in the RNeasy Mini Handbook. Before starting to extract RNA, the spheres and 2D cultured cells were washed in 1x PBS to ensure that the majority of culture medium was disposed of. In short, 3D spheres and 2D cultured stromal keratocytes were lysed using β-mercaptoethanol (β-ME) in Buffer RLT (10µl β-ME per 1ml Buffer RLT) and by pipetting this up and down until cells and spheres had dissolved completely. One volume of 70% ethanol was then added to the homogenized lysate, this was mixed well by pipetting and up to 700µl of the sample was added to an RNeasy spin column placed in a 2ml collection tube. The sample was centrifuged for 15 seconds at 10,000rpm and the flow-through at the bottom of the tube was discarded. 700µl Buffer RW1 was added to the RNeasy spin column and the sample was centrifuged for 15 seconds at 10,000rpm, the flow-through was discarded. Next, 500µl Buffer RPE was added to the spin column and centrifuged for 15 seconds at 10,000rpm to wash the spin column membrane. The flow-through was discarded. Another 500µl Buffer RPE was added to the spin column and centrifuged for 2 minutes at 10,000 rpm to dry the spin column membrane, ensuring that no ethanol was carried over during RNA elution. This was important because residues of ethanol in the sample may interfere with downstream reactions. The Rneasy spin column was then placed into a new 1.5ml collection tube and 20µl RNase-free water was directly added to the spin column membrane and centrifuged at 10.000rpm for 1 minute to elute the RNA. The eluted RNA was kept on ice and its concentration measured using a NanoDrop Spectrophotometer. The RNA samples were either immediately reverse transcribed into cDNA or stored at -80°C until needed.

RNA extraction & Isolation from rabbit whole corneal tissue

RNA isolation from rabbit corneal tissue required an alternative method to the RNeasy Mini Kit due to the large amount of collagenous structure in the cornea that would clog up the RNeasy spin columns.

The method used was therefore the very basic TRIzol RNA extraction method that is used to isolate total RNA from cells and tissues and it maintains the integrity of RNA while disrupting cells and dissolving cell components. The following procedures were followed: 0.2ml of chloroform was added per 1ml TRIzol reagent to the tested samples. The reaction tube was shaken vigorously for 15 seconds and then centrifuged at 12,000 rpm for 15 minutes at 4°C. The aqueous supernatant was pipetted off and transferred into a fresh RNase free eppendorf tube. 0.5ml of isopropyl alcohol was added to the sample containing the aqueous supernatant and was left to incubate at room temperature for 10 minutes. The reaction tube was then centrifuged at 12,000 rpm for 10 minutes at 4°C, the supernatant was removed from the resulting RNA pellet and 1ml of 75% ethanol was added and the reaction tube was vortexed, centrifuged at 7,500 rpm for 5 minutes at 4°C. The supernatant was removed and the pellet was allowed to dry for 10 minutes. The dried pellet was then dissolved in 11µl of dH_2O and the reaction tube incubated for 10 minutes at 60°C. The RNA mixture was kept on ice and its concentration measured using a NanoDrop Spectrophotometer. The RNA samples were either immediately reverse transcribed into cDNA or stored at -80°C until needed.

Reverse Transcription

The quantity of RNA extracted was measured using a NanoDrop machine. The RNA values in ng/µl were converted into µg/µl and the volume in µl was made up to 11µl with RNase free dH_2O with a final RNA concentration of 1000ng (= 1µg).

To 11µl RNA in an RNase free PCR tube, 1µl of Oligo-dT and 1µl of Deoxyribonucleotide triphosphate (dNTP) were added. Oligo-dTs act as a primer for the reverse transcriptase allowing formation of a sense cDNA strand, specifically binding to the poly-A tail that is present on mRNAs but not to other RNA molecules. dNTPs provide the bases required for the formation of the complementary sense cDNA strand. The sample was placed in the thermal cycler (Biometra) and the specific reverse transcription program was selected. As soon as the program paused, the sample was removed and placed on ice for 1 minute. Then for each sample 4µl of 5x First strand buffer, 1µl of SuperScript III reverse transcriptase, 1µl Dithiothreitol (DTT) and 1µl of RNAse Out were added. The Reverse Transcriptase uses the Oligo-dT binding as a primer for encoding the cDNA, the DTT disrupts the structure of RNAses by breaking

di-sulphide bonds inhibiting their action in the cycler. RNAse Out performs the same as DTT.

The tube was then returned to the thermal cycler and the program was allowed to complete. The program settings are described in Table 21.

Temperature	Time
65°C	5 minutes
55°C	1hour
70°C	15 minutes
4°C	Hold

Table 21: Thermal Cycling Parameters for Reverse Transcription

The reverse transcribed cDNA was then either stored at -20°C in the freezer or immediately used for qRT-PCR.

Quantitative real-time PCR

Real-time PCR was performed in order to detect and quantify gene expression by measuring the DNA sequences of interest compared with a standard reference gene. In this case the reference gene was β-actin. The sequences of the primers tested are listed in the Materials section.

Quantitaive real-time PCR was performed using the Corbett Research Rotor-gene Q Series machine with the 72 well Rotor and by using the Power SYBR Green PCR Master Mix (Cat.No.4367659) from Applied Biosystems (Life Technology). The program used was a Three Step qRT-PCR procedure and was repeated for 40 cycles (see below Table 22 for program specification).

Each reaction was composed of 10µl Power SYBR Green PCR Master Mix, 1µl Forward Primer, 1µl Reverse Primer, 7µl dH_2O and either 1µl cDNA or 1µl dH_2O for the negative control. The cDNA used was diluted in dH_2O 1:10 from the original cDNA stock. 20µl of the mixture was used to fill each strip tube to be amplified. Each sample was measured in triplicate with β-actin as the endogenous control and using dH_2O as the negative control.

The strip tubes were capped and placed into the Rotor-gene Q machine. The reaction parameters are described in Table 22. Results were analysed using the Comparative Ct Method based on 3 steps: step 1: normalization to endogenous control (β-actin), step 2: normalization to reference sample (in this study the *in vivo* stroma) and step 3: uses the formula $2^{-\Delta\Delta Ct}$ to calculate fold changes. This analysis method calculates a relative quantification of gene expression.

Temperature	**Time**
95°C	10 minutes
95°C	10 seconds
51°C	15 seconds
72 °C	20 seconds

Table 22: Thermal Cycling Parameters for qRTpcr

Analysis

Data are presented as means and standard deviations. Comparisons between groups were done using ANOVA (Analysis of Variance) assuming a single factor analysis with a confidence level of 95%. $p < 0.05$ was considered significant.

ANOVA is a statistical test used to determine whether the variability between and within more than 2 sets of the tested samples are significantly different. The test is based on the Null Hypothesis.

4.3 Results

4.3.1 Upper stromal keratocyte culture and 3D sphere formation

Keratocytes from the upper part of the stroma were extracted from the rabbit cornea as described in the methods section 4.2.2.1 and cultured in Standard stromal medium on a standard 2D tissue culture plastic environment. In this medium they showed a fibroblastic phenotype (Fig. 42a). Prior to being turned into 3D spheres, keratocytes were passaged and placed in Species specific medium. This decreased the rate at which the stromal keratocytes grew as witnessed by the increased time between passages. Keratocytes placed in Species specific medium took approximately 4 days to reach full confluency, while keratocytes in normal condition took around 24-48 hours to reach 100% confluence.

3D spheres were created from stromal keratocytes 3 to 5 days after their switch to Species specific medium (Fig. 42 a,b). In general sphere production was reliable and reproducible. Spheres normally took between 3 to 4 days to form, the intermediate stages comprising smaller cell aggregates that subsequently coalesced (see Fig. 41).

Rabbit 3D stromal sphere formation over three days

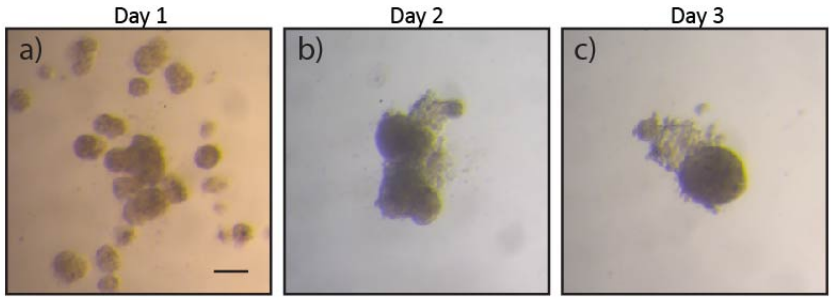

Figure 41: Rabbit 3D sphere formation steps over 3 days

a) Shows small cell aggregates at culture day 1
b) One single aggregation, but no sphere formation yet at culture day 2
c) Fully formed 3D sphere at culture day 3

Images were taken with a Zeiss Axiocam. Scale bar: 100µm.

Preliminary investigations showed that out of the 20 to 25 spheres per plastic dish, between 10 and 20% did not form at all or were of poor quality. The macroscopic quality of spheres was based on appearance; good spheres were round with compact outer borders while lower quality spheres presented a looser appearance with “fluffy” rounded cells on the outside, some of which were detached (see Fig. 2 in the Appendix, section 8.2.2).

Variation was also observed among stacks of petri dishes containing hanging drop spheres from the same origin and produced at the same time. The location of the petri dishes within the stack made an impact on the outcome of the sphere formation. Often petri dishes sitting on the extremities of the stack contained more badly formed spheres and therefore the success rate was lower than what could be found in petri dishes sitting in the middle of the stack.

It has to be noted that early stromal keratocyte passages did not produce 3D spheres at the beginning and this changed during the course of the experimental development. Still early passages such as P1 and P2 still did not produce 3D spheres. Sphere formation success is shown in Table 23 below where the number of experiments performed at creating single upper stromal spheres was attempted at various passage numbers.

2D stromal keratocytes vs. 3D stromal keratocytes

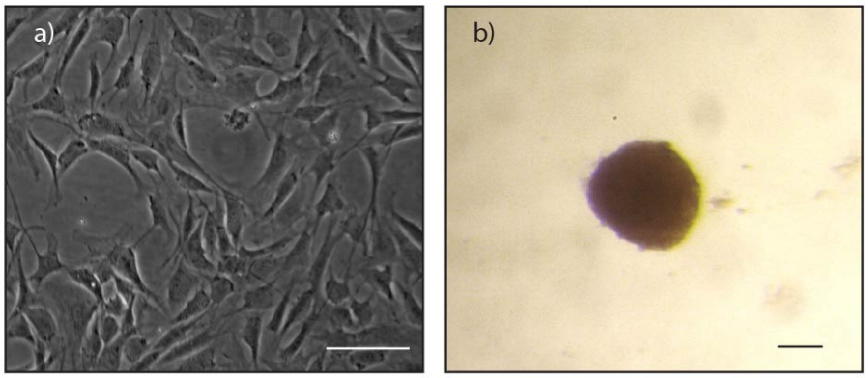

Figure 42: *2D stromal keratocytes and a 3D stromal sphere*

a) upper stromal keratocytes in 2D culture, Zeiss Axiocam. Scale bar: 200µm
b) single upper stromal 3D sphere at Day3 in culture, Zeiss Axiocam. Scale bar: 100µm

Passage number	**No. of experiments performed**	**No. of successful exp.**	**No. of unsuccessful exp.**
3	5	1	4
4	6	4	2
5	1	-	1
6	3	3	-
7	2	1	1
8	1	-	1
9	2	1	1
10	2	1	1
11	1	1	-

Table 23: Numbers of experiments performed to create upper single 3D spheres at different passages

Stromal expression in 3D

Based on what others in the host laboratory had found with skin cells (namely 3D expression of dermal fibroblasts much more closely resembles the dermis *in vivo*), the next step was to investigate the idea that stromal keratocytes placed in a 3D spherical culture might show more similarities to those in the corneal stroma *in vivo*, compared to those found in the standard 2D culture system. To do this, a number of markers known to be expressed in the corneal stroma were examined using immunohistochemistry and qPCR.

The first marker seen as crucial in determining whether the 3D culture approach was qualitatively superior to the 2D culture method was the smooth muscle specific alpha

isoform of actin (αSMA), a biomarker for myofibroblast differentiation or “activated” keratocytes (Jester *et al*., 1999).

αSMA and Vimentin in in Vivo, 2D and 3D stromal keratocytes

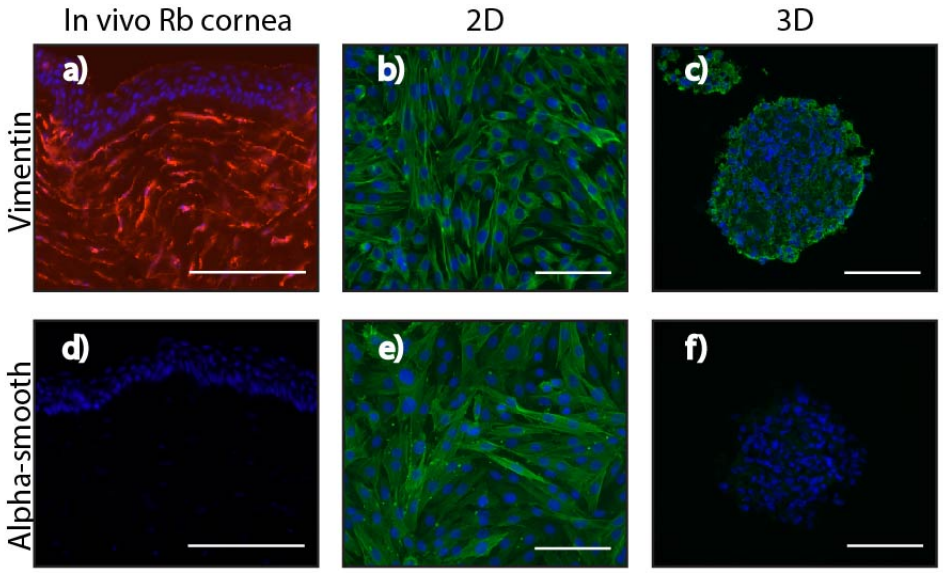

Figure 43: Immunofluorescent comparison of stromal cell expression in vivo and in vitro

Vimentin (Rhodamine for a) FITC for b and c and FITC staining of αSMA (d,e,f) expression in the stroma and in upper stromal keratocytes in 2D and 3D culture. Images were taken with an Axiovert Zeiss microscope. Scale bar: 100µm.

Upper stromal keratocytes in 2D and 3D cultures were stained with Vimentin to confirm that the cells used for the experiment were of mesenchymal origin (Fig. 43 b,c) and αSMA to identify whether the keratocytes were activated or quiescent (Fig. 43 e,f). The *in vivo* rabbit cornea was stained with Vimentin (Fig. 43a) while αSMA was not expressed in the *in vivo* stroma, (Fig. 43d), but was expressed in the 2D stromal culture (Fig. 43e) and turned off in upper stromal 3D spheres (Fig. 43f).

Immunocytochemistry and immunohistochemistry in Figure 43 showed that αSMA expression was turned off when rabbit upper stromal keratocytes were changed from a 2D to a 3D culture environment, restoring it to that seen with the *in vivo* stroma.

4.3.1.1 Quantitative Real-time PCR expression of crystalline protein markers

The next step was to establish whether keratocytes from the upper region of the stroma placed in 3D cultures expressed crystalline protein markers at a similar level to the *in vivo* stroma. Three biological samples of rabbit upper stromal keratocytes were cultured in the normal 2D culture conditions and then turned into 3D spheres (as explained in the Methods section 4.2.2.2). Additional stromal keratocytes in 2D cultures were kept in parallel to the 3D stromal spheres and both cultures were stopped at the same time for RNA extraction.

In order to identify and quantify the expression of the corneal crystalline markers ALDH1A1, GAPDH and Lumican as well as the marker for quiescent keratocytes, Keratocan, real-time pcr was performed. αSMA gene expression was also investigated to confirm the immunocytochemistry and immunohistochemistry results shown in Figure 56. The measured cDNA sequences of interest were compared to a standard reference gene (β-actin). Results were analysed using the Comparative Ct Method, as described in the Methods section 4.2.2.4. This analysis method calculates a relative normalised quantification of gene expression. Relative gene expression within the 2D and 3D samples was compared to that found in the *in vivo* stroma.

Stromal keratocyte markers tested by QRT-PCR

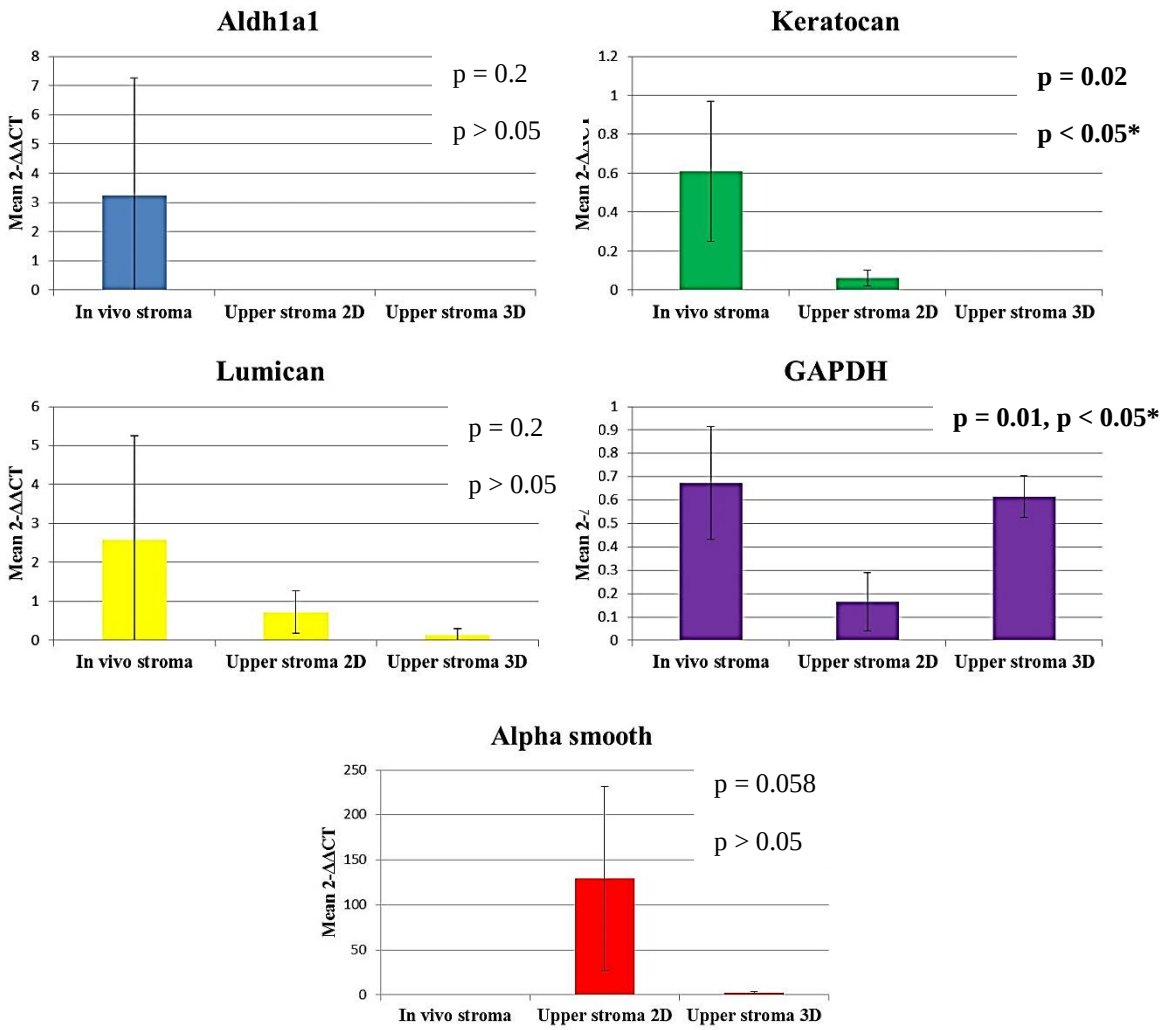

Figure 44: Relative normalised gene expression of crystalline, keratocan and αSMA markers in upper stromal 3D vs. 2D keratocytes, n=3

The x-axis represents the samples tested. The y-axis represents the mean result of the formula $2^{-\Delta\Delta Ct}$ which is expressed in terms of fold changes.

Quantitative real-time pcr of 2D and 3D stromal keratocytes vs. the *in vivo* stroma shown in Figure 44, revealed that expression of the corneal crystalline marker ALDH1A1 was almost non-existent both in 2D and 3D cultures when compared to the *in vivo* stroma and ANOVA results showed a p-value of 0.2 resulting to be non-significant. Keratocan, the marker for stromal keratocytes was not expressed at all in 3D cultures and only slightly expressed in 2D cultures, compared to the *in vivo* stroma. Statistical analysis showed that this result was significant as indicated by the p-value 0.02. Lumican gene expression was only partially restored in 3D cultures, and

expression was less than in 2D cultures. However, results were non-significant (p = 0.2). Gene expression of corneal crystalline marker GAPDH was closer to that of the stroma in 3D cultures compared with 2D cultures and this result was significant (p = 0.01). αSMA gene expression decreased in 3D stromal keratocytes when compared to the 2D stromal keratocytes, therefore confirming the previously shown result in Figure 43 (d - f). The high standard error bar in the αSMA gene expression 2D culture is due to the fact that the three individual donor cultures had very different levels of αSMA gene expression, however they were always higher than in the 3D cultures or the stroma. Due to the high variation in the 2D sample, this result was non-significant (p = 0.058).

By placing the stromal keratocytes in 3D cultures it was hypothesised that the markers tested through quantitative real time pcr would show more similar levels to those found in the *in vivo* stroma than to the 2D cultures. Although the results shown in Figure 44 show that two of the markers GAPDH and αSMA gene expressions are restored in 3D spheres to levels approaching those found in the *in vivo* stroma, only results for GAPDH and Keratocan are statistically significant, whereas the other results have many variations in gene expression between the three donors.

In the next section, the development of a 3D model was attempted, by double coating single stromal 3D spheres with corneal epithelial cells. This is described from section 4.3.2 onwards.

4.3.2 Double layered spheres – development of a spherical 3D bilayered model of the cornea

A cornea 3D model was established using the upper stromal 3D spheres and coating them with rabbit limbal corneal epithelial cells (as described in the method section 4.2.2.2). Sections 4.3.2.1 to 4.3.2.3 describe the initial production of the model and sections 4.3.2.3 to 4.3.3.3 subsequent work aimed at its further development, optimisation and refinement.

4.3.2.1 Rabbit cornea 3D model 1

The first established rabbit cornea 3D model was made with rabbit upper stromal keratocytes at passage 10. Rabbit upper stromal 3D spheres were established for 3 days and then double coated with passage 1 limbal corneal epithelial cells. The basic 3D model technique is explained in the Methods section 4.2.2.2. 98 examples were made in total, the media was changed every other day and bright field macroscopic images were taken. Three, seven, ten and fourteen days after the bilayered spheres were created, between 15 and 20 were snap frozen in OCT, cryo-sectioned and their histological features (Fig. 45) and the expression of key markers (Fig. 46) examined.

Rabbit cornea model 1: macroscopic & H&E images

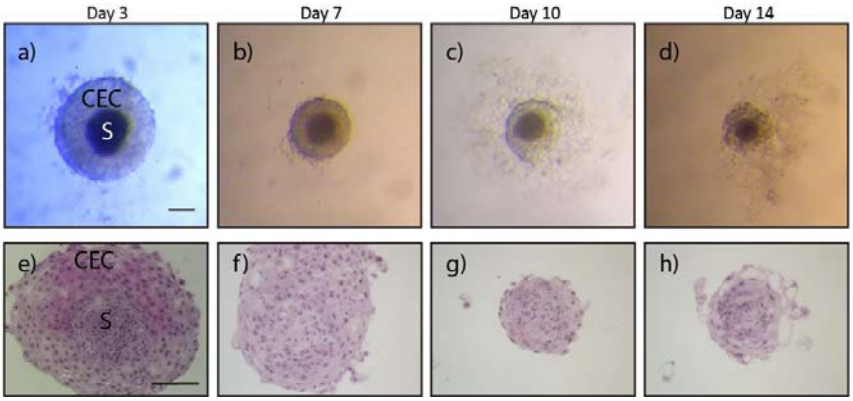

Figure 45: Rabbit cornea 3D model (1) in a hanging drop culture, bright field macroscopic images & H&E over the period of 14 days

a) – d) show macroscopic images of double spheres made of the stromal component (S) at the centre of the sphere and corneal epithelial cells (CEC) coated around the stromal core. Zeiss Axiocam. Scale bar: 100µm.

e) – h) H&E staining of the cornea 3D model at four given time points. Images were taken with an Axiovert Zeiss microscope. Scale bar: 100µm.

At 3 days a clearly defined bilayer structure was evident macroscopically in the vast majority of examples, and this was reflected histologically (Fig. 45 a,e). This configuration was maintained at 7 days (Fig. 45 b,f) however by 10 days there was an evident deterioration in the structures. Under the dissecting microscope they appeared

smaller with, in particular, loose cells visible around the outer epithelial stratum (Fig. 45 g). These features were accentuated by day 14 (Fig. 45 d) when the distinction between the stromal and epithelial layers became very difficult to see histologically (Fig. 45 h).

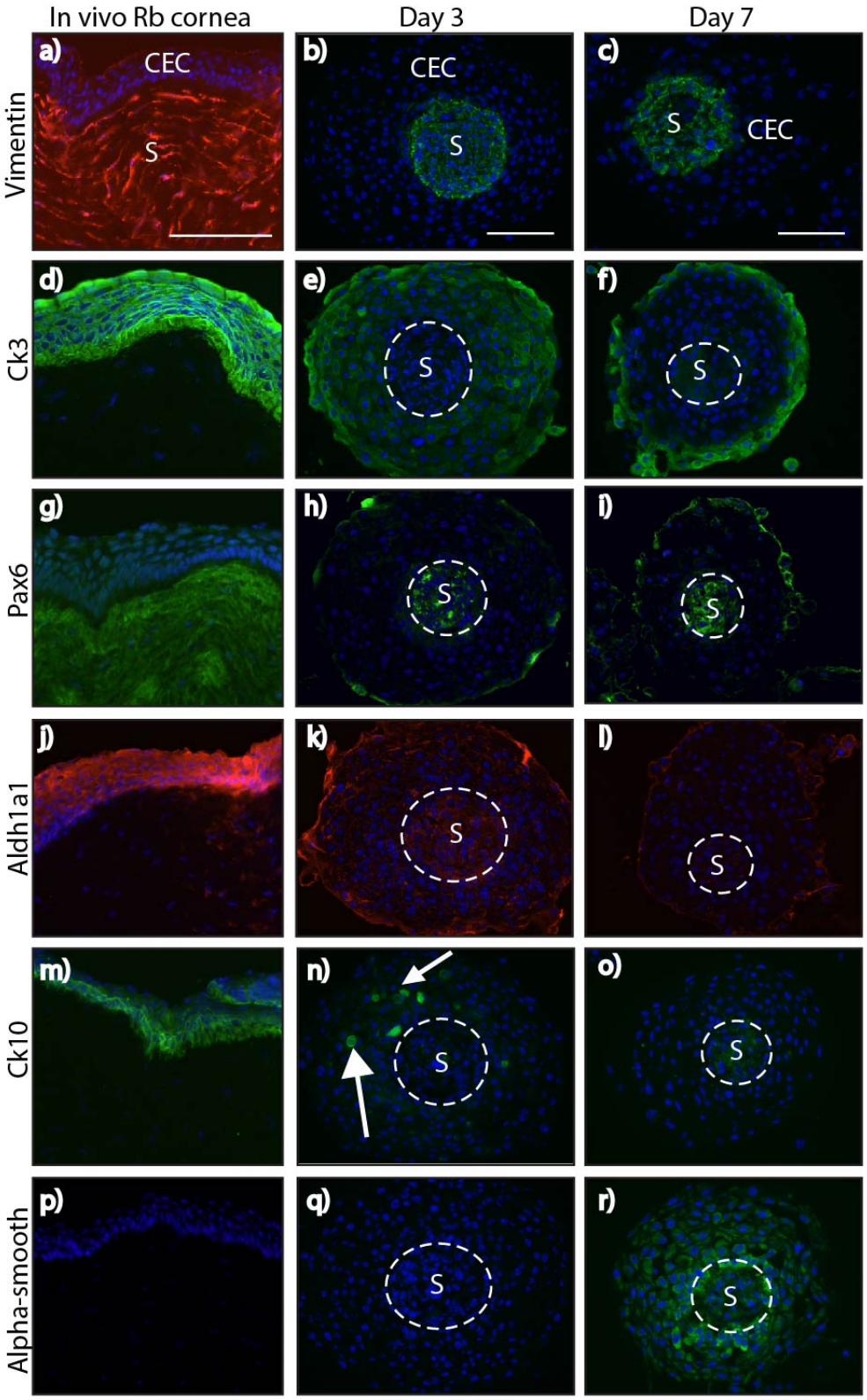

Figure 46: Immunohistochemistry of in vivo rabbit cornea and rabbit cornea 3D model (1) at time points Day3 and Day7

First column from the left: a,d,g,j,m,p show immunohistochemistry staining of the *in vivo* rabbit cornea with the mesenchymal marker vimentin (a), corneal epithelial differentiation marker Cytokeratin 3 (d), eye development marker Pax6 (g), corneal crystalline marker Aldh1a1 (j), Cytokeratin 10 (m) and biomarker for myofibroblasts αSMA (p). Second and third column show immunostaining of the rabbit cornea 3D model at days 3 and 7 with the respective markers. The stromal core is marked as (S) and the corneal epithelial cell coating as (CEC). All images were taken with an Axiovert Zeiss microscope. Scale bars: 100μm.

Immunohistochemistry performed on day 3 and day 7 models in Figure 46 revealed a decline in all markers from day 3 to day 7. At day 3 the model stained positively for vimentin (b) within the stromal compartment and this gave a clear boundary between the stroma and the corneal epithelial (CEC) layer. At day 7 (c) this boundary was less distinct. Immuno-staining for the corneal differentiation marker Ck3 was present at day 3 (e) but not as strongly expressed as in the *in vivo* cornea. At day 7 Ck3 expression declined and was only visible at the sphere marginal level (f). Pax6 staining resulted negative in the positive control (g) and Pax6 expression was cytoplasmic in the CEC layer at days 3 and 7 (h,i) and not nuclear as one would expect. This result was also confirmed in Figure 47 below, showing larger images of Pax6 staining without the DAPI staining (c,d). The fluorescence seen in the stromal compartments and outer CEC border is auto-fluorescence as it was also seen in the negative control below in Figure 48 (e).

Aldh1a1 expression, present at low levels, in both the stroma and the CEC of the structures at day 3 (k), was down-regulated at day 7 (l). Ck10 stained some positive cells in the CEC layer at day 3 (n) as indicated by the arrows, but this expression disappeared at day 7 (o). αSMA expression on the other hand was not present at day 3 (q) but was switched on in both stromal and CEC compartments at day 7 (r).

Time points days 10 and 14 are not shown as the models were too degraded (as seen in Fig. 45). Immunohistochemistry was performed on the model at 10 days, however the staining was unsatisfactory due to the extremely thin and fragile corneal epithelial layer.

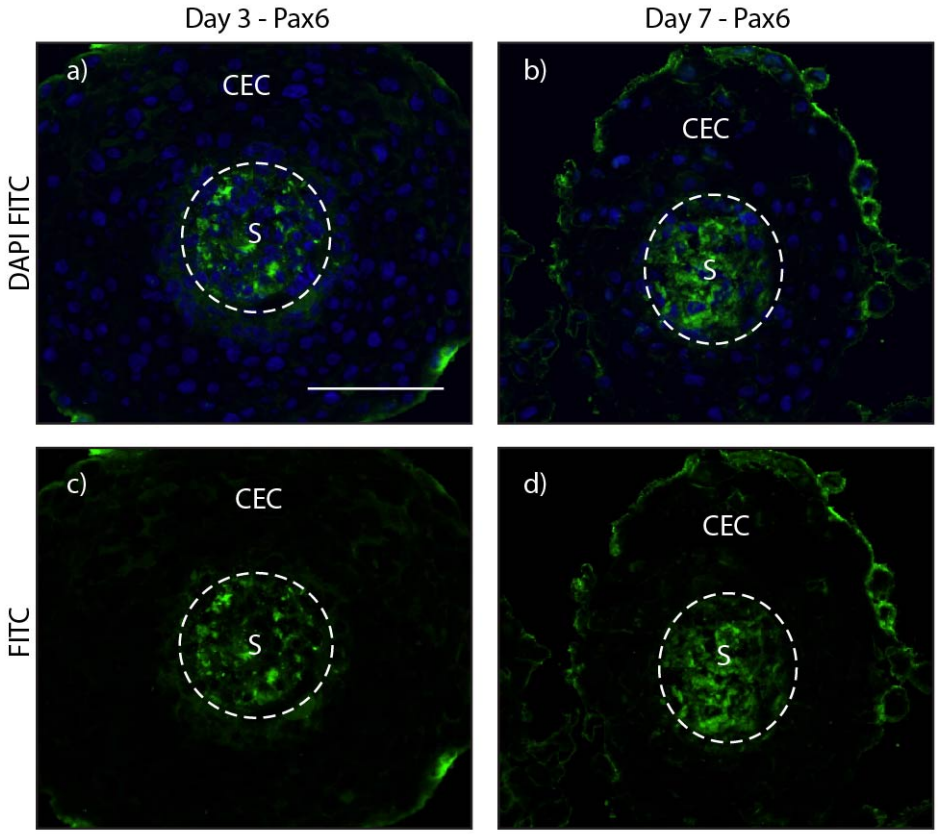

Figure 47: Pax6 immunostaining of rabbit cornea 3D model (1) at time points Day3 and Day7

Images were taken with an Axiovert Zeiss microscope. Scale bars: 100µm.

<u>Negative controls:</u>

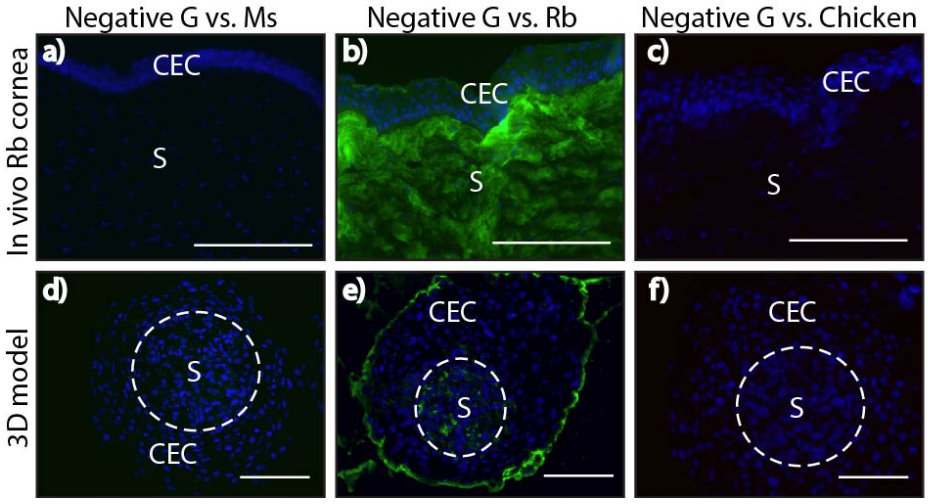

Figure 48: Negative controls for immunohistochemistry results in Figure 46 & 47

Images a) – f) represent the negative controls for the experiment shown in Figure 46 & 47. Images b) and e) show auto-fluorescence in the stroma and outer CEC borders e). Images were taken with an Axiovert Zeiss microscope. Scale bars: 100µm.

These initial results showed a relatively well established model at day 3, with the expression of the crystalline marker Aldh1a1 in both the stromal and CEC compartments suggesting that stromal Aldh1a1 expression could be dependent on its close interaction with the corneal epithelium.

However, the model declined with time as reflected by observations at day 7 in Figure 46. These showed a loss of the epithelial phenotype within the CEC layer, as represented by increased αSMA expression (r), marginalisation of Ck3 expression (f), no Pax6 expression and general decline of Aldh1a1 and Ck10 expression.

One explanation for the decline in the quality of the model was the age/late passage (P10) of the stromal keratocytes used to establish it.

4.3.2.2 Rabbit cornea model 2

A second rabbit cornea 3D model was established using stromal cells from a different biological sample. These cells made good 3D spheres at passage 3, earlier than those used in the first rabbit cornea model, leading to the hope that these younger cells would support epithelial cells better and thus improve the quality of the model. However, they took longer to form, so were coated after 7 days with rabbit limbal CEC at passage 1. 152 examples were made in total, the medium was changed every other day and dark field macroscopic images were taken. The bilayered spheres were maintained for 10 days and at days 5, 7 and 10, between 15 and 20 were snap frozen in OCT, cryo-sectioned and their histological features (Fig. 49) and the expression of key markers (Fig. 50) were examined.

Rabbit cornea model 2: macroscopic & H&E images

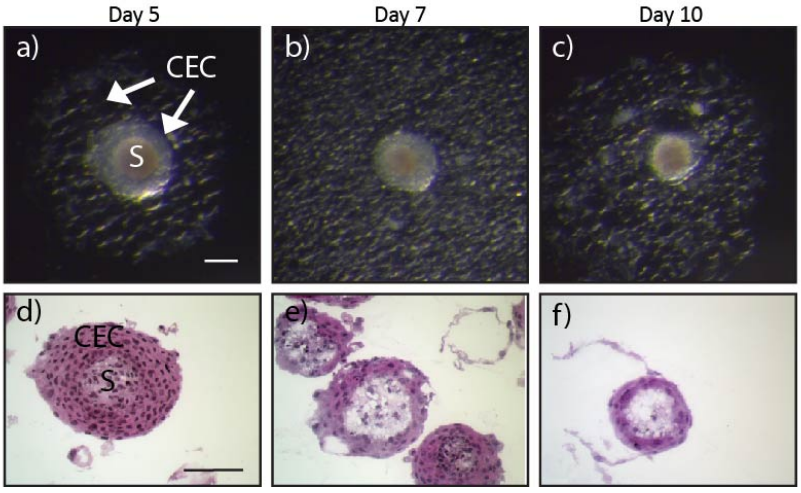

Figure 49: Rabbit cornea 3D model (2) in a hanging drop culture, dark field macroscopic images & H&E over the period of 10 days

a) – c) show dark field macroscopic images of double spheres made of the stromal component (S) at the centre of the sphere and corneal epithelial cells (CEC) coated around the stromal core. Zeiss Axiocam. Scale bar: 100µm.

d) – f) H&E staining of the cornea 3D model. Images were taken with an Axiovert Zeiss microscope. Scale bar: 100µm.

Dark field macroscopic images revealed a transparent corneal epithelial layer around the stromal core. A vast amount of CEC was detached from the model and spread around it in a circular manner. These cells had a bubble appearance and seemed air. Macroscopic images (Fig. 49 a - c) show that throughout the 10 day timescale the model increasingly lost its corneal epithelial coating resulting in a decreasing size over time. The increasingly marked degradation of the model was also reflected by H&E staining (Fig. 49 d - f), where an intact cornea 3D model with tight outer borders (d), loses compactness and corneal epithelial cells (e,f) over time.

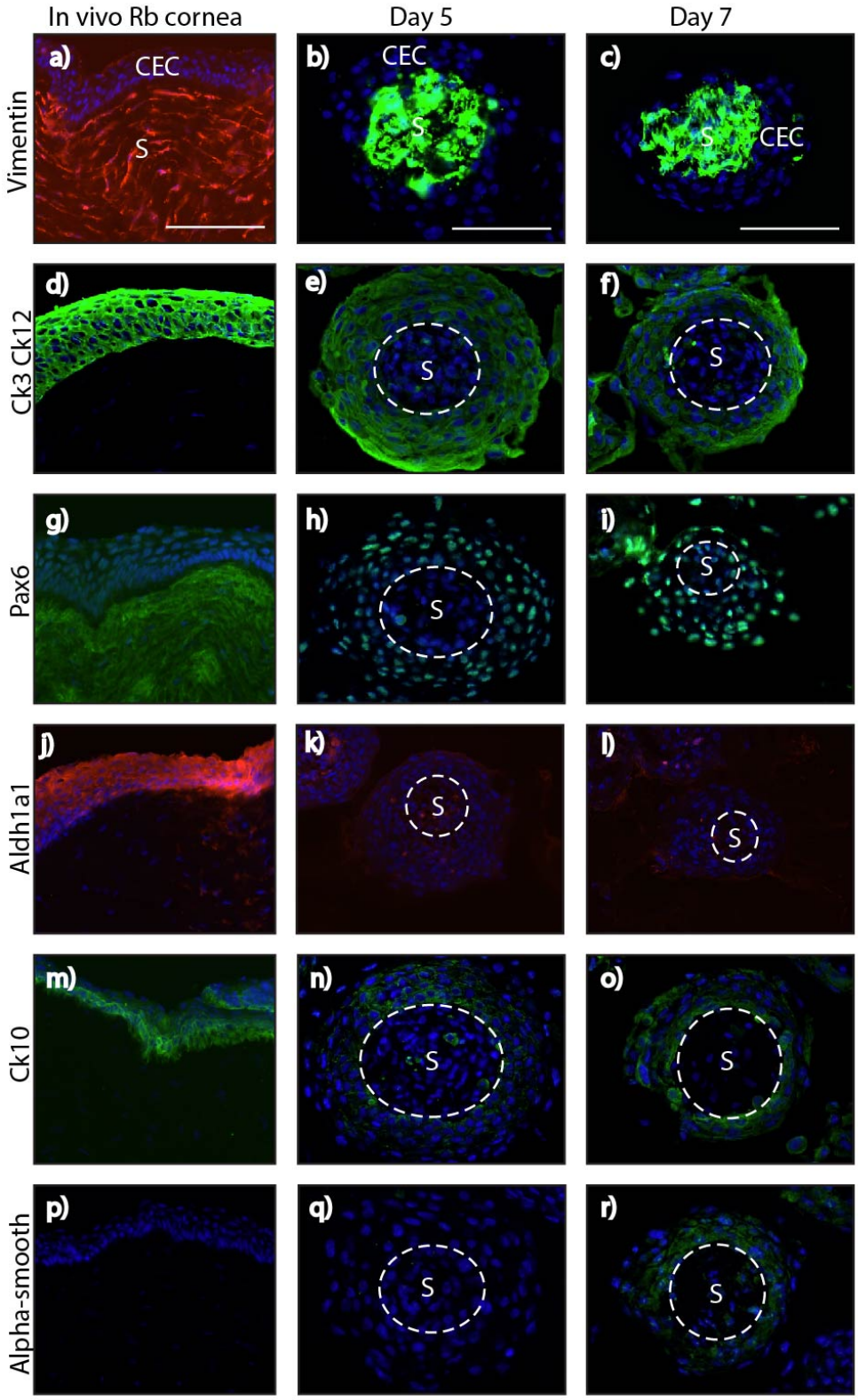

Figure 50: Immunohistochemistry of in vivo rabbit cornea and rabbit cornea 3D model (2) at time points Day5 and Day7

First column from the left: a,d,g,j,m,p shows immunohistochemistry of the *in vivo* rabbit cornea stained with vimentin (a), Cytokeratin 3/12 (d), Pax6 (g), Aldh1a1 (j), Cytokeratin 10 (m) and αSMA (p). Second and third columns show immunohistochemistry of the rabbit cornea 3D model at days 5 and 7 with the respective markers. The stromal core is marked as (S) and the corneal epithelial cell coating as (CEC). All images were taken with an Axiovert Zeiss microscope. Scale bars: 100µm.

Figure 50 represents immunohistochemical analysis of the 3D model at days 5 and 7. Day 10 was not immunostained because it was degraded and had lost most of its corneal epithelial layer, as seen in the macroscopic images and H&E staining in Figure 49. Day 5 revealed a good quality model when looking at the macroscopic images and H&E staining. By this time there was a loss of CEC but H&E staining revealed a compact layer of these cells, whereas at day 7 air bubbles and holes appeared in the CEC layer and it was evident that this layer was increasingly being lost over time. Immunohistochemical analysis resulted in very strong staining of vimentin in the stroma (b,c), Ck3Ck12 (e,f) and Pax6 (h,i) in the CEC layer at days 5 and 7. The antibody Ck3 used in the first model experiment was substituted by the antibody Ck3Ck12 which stained both important corneal differentiation markers. Strong expression of Ck3Ck12 and Pax6 were maintained in the CEC layer, even when cells were detaching from the model at day 7 (f,i). The crystalline marker Aldh1a1 was expressed at a very low level at both time points (k,l). Ck10 expression was present in some CECs in the model at day 5 (n) and up-regulated at day 7 (o), especially within the surrounding area of the stromal core. αSMA was not expressed at day 5 (q) but was up-regulated at day 7 (r) within the CEC layer, especially in the area around the stromal core.

The model described in this section indicated some improvements such as strong Pax6, Ck10 and Ck3Ck12 expression, all reflecting a more *in vivo* like limbal CEC layer and indicating that the stromal 3D core was acting as a good support layer for the corneal epithelial cells.

4.3.2.3 Rabbit cornea 3D model 3

In an attempt to prolong the culture life and integrity of the rabbit cornea 3D model, it was decided to culture the latter in different media. This experiment used rabbit upper stromal 3D spheres made from P4 stromal keratinocytes from a third biological sample, double coated at day 7 with rabbit limbal CEC at P1. At first all the bilayered spheres were maintained in standard culture medium, (50% Species specific medium and 50% LEM) but at culture day 5, between 15 and 20 were switched to aqueous humour while another 15 to 20 were placed in 50% rabbit serum and 50% Species specific medium. The remainder were kept in the standard medium for comparison, and the whole experiment lasted until culture day 7. Spheres were snap frozen in OCT at day 5 and at the end of the experiment at day 7, for histological (Fig. 51) and immunohistochemical (Fig. 52) analysis. The models were switched to different media at day 5 because that was the latest time point when they were in an optimum state for experiments 1 (Fig. 51) and 2 (Fig. 52) after which they declined.

Rabbit cornea model 3: macroscopic & H&E images

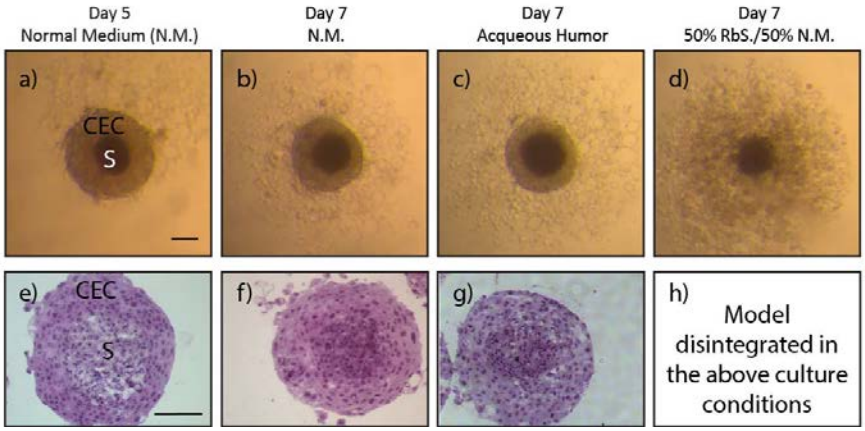

Figure 51: Rabbit cornea 3D model (3) in a hanging drop culture, bright field macroscopic images & H&E over the period of 7 days

a) – d) show bright field macroscopic images of double spheres made of the stromal component (S) at the centre of the sphere and corneal epithelial cells (CEC) coated around the stromal core. Images were taken with a Zeiss Axiocam. Scale bar: 100µm.

e) – g) H&E staining of the cornea 3D model. Images were taken with an Axiovert Zeiss microscope. Scale bar: 100µm.

When cultured in the Species specific/LEM medium mix or in aqueous humour no external change in the quality or size of the spheres was seen between day 5 and day 7 (Fig. 51). However when the model was cultured in the media containing a higher percentage of rabbit serum the model completely disintegrated (Fig. 51 d). H&E staining also confirmed good quality double layered spheres and no aesthetic difference could be noted between models that were placed in the different media (Fig. 51 e - g) apart from the one with rabbit serum that could not be analysed as it had completely degraded.

Immunohistochemical analysis revealed strong vimentin expression at day 5 (b) that stained the stromal core and clearly delineated the boundaries between stroma and CECs. This staining appears to be uniform and compact, however at day 7 in the Species specific/LEM medium mix as well as in the aqueous humour (c,d), the staining was less uniform and the boundary between stroma and CEC's was also less evident. Ck3Ck12 immunostaining revealed positive staining of the CEC layer at day 5 (f) and day 7 in both mediums (g,h), however very compact CEC layer at day 5 was lost at day 7 in both culture mediums. Pax6 staining resulted to be cytoplasmic in the corneal epithelium (j – l). Interestingly, Ck10 was switched on only at day 7 in the Species specific/LEM medium mix and the aqueous humour (s,t), possibly reflecting increasing gain of function towards a limbal CEC phenotype. The crystalline marker Aldh1a1 was expressed in all of the time points and was particularly strong at day 7 in the spheroid models maintained in the Species specific/LEM medium mix (o). Positive Aldh1a1 expression was visible within the stromal compartment and the CEC layer (Fig. 52 n - p).

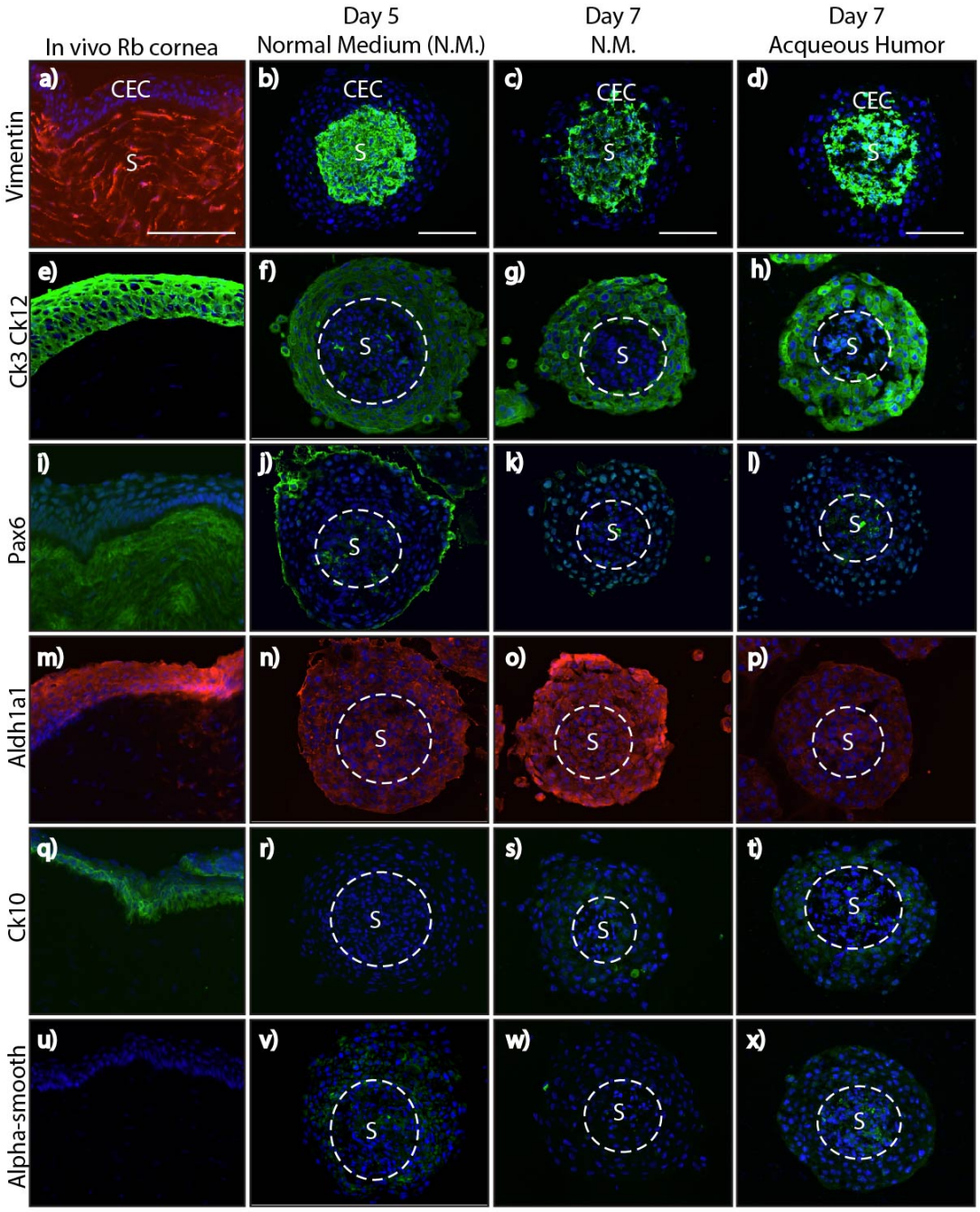

Figure 52: Immuno-histochemistry of in vivo rabbit cornea and rabbit cornea 3D model (3) at time points Day5 and Day7 Species specific/LEM medium mix and Day7 in aqueous humour

First column from the left: a,e,i,m,q,u shows immunohistochemistry of the *in vivo* rabbit cornea stained with vimentin (a), Cytokeratin 3/12 (e), Pax6 (i), Aldh1a1 (m), Cytokeratin 10 (q) and αSMA (u). Column 2 & 3 shows immunohistochemistry of the rabbit cornea 3D model at days 5 and 7 in Species specific/LEM (N.M.) medium mix with the respective markers. Column 4 shows models at day 7 in aqueous humour. The stromal core is marked as (S) and the corneal epithelial cell coating as

(CEC). All images were taken with an Axiovert Zeiss microscope. Scale bars: 100µm.

In this experiment there was an improvement in the expression pattern of most of the markers at day 7, however this did not seem to be due to the change in culture conditions. Aldh1a1 for instance was expressed at a stronger level in the models placed in the Species specific/LEM medium mix compared to those in aqueous humour. Therefore, the idea of using aqueous humour to culture the models was excluded in future procedures.

4.3.2.4 Rabbit cornea 3D model 4

The next experiment established to test alternative culture conditions used rabbit upper stromal 3D spheres made from P4 stromal keratocytes from a fourth biological sample, double coated at day 4 with rabbit limbal CEC at P1. The model was kept in the Species specific/LEM medium mix (N.M.) for five days after coating and then switched to limbal (epithelial) medium or Species specific (stromal) media alone. Some models were maintained in the mixed medium as a control and the bilayered spheres kept in culture for 10 days. Up 20 models were snap frozen in OCT, cryo-sectioned and their histological features (Fig. 53) and the expression of key markers (Fig. 54) examined at day 5 and at the end of the experiment at day 10.

Rabbit cornea model 4: macroscopic & H&E images

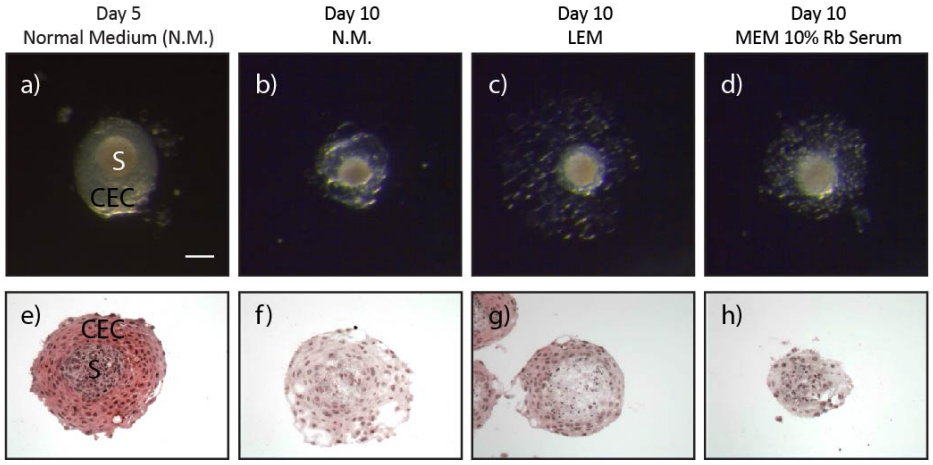

Figure 53: Rabbit cornea 3D model (4) in a hanging drop culture, dark field macroscopic images & H&E over the period of 10 days

a) – d) show macroscopic images of double spheres made of the stromal component (S) at the centre of the sphere and corneal epithelial cells (CEC) coated around the stromal core. Images were taken with a Zeiss Axiocam. Scale bar: 100µm.

e) – h) H&E staining of the cornea 3D model at days 5 and 10. Images were taken with an Axiovert Zeiss microscope. Scale bar: 100µm.

In the Species specific stromal medium (MEM 10% rabbit serum) the models lost the CEC layer completely, meaning that this medium could not successfully sustain the corneal epithelial layer. These specimens could therefore not be cut and stained and are therefore not represented in Figure 54. On the other hand, the limbal medium alone sustained the model in a similar way to those in the Species specific/LEM medium mix until day 10 (Fig. 53 b,c,f,g). However, a general degradation of the model in the latter could be observed over time, where the outer CEC layer seemed to be degrading and spaces formed within the stromal stratum (Fig. 53 g). H&E staining revealed that the CEC layer in specimens placed in limbal medium at day 10 was in good condition but having visibly decreased in size compared to day 5. Although macroscopic images of the models in N.M at day 10 (b) seemed larger in size with a transparent CEC layer compared to those in LEM only, H&E staining ruptured the CEC layer as seen in image f). However, immunohistological examination of the model at day 10 in N.M (Fig. 54) revealed a healthy looking CEC layer.

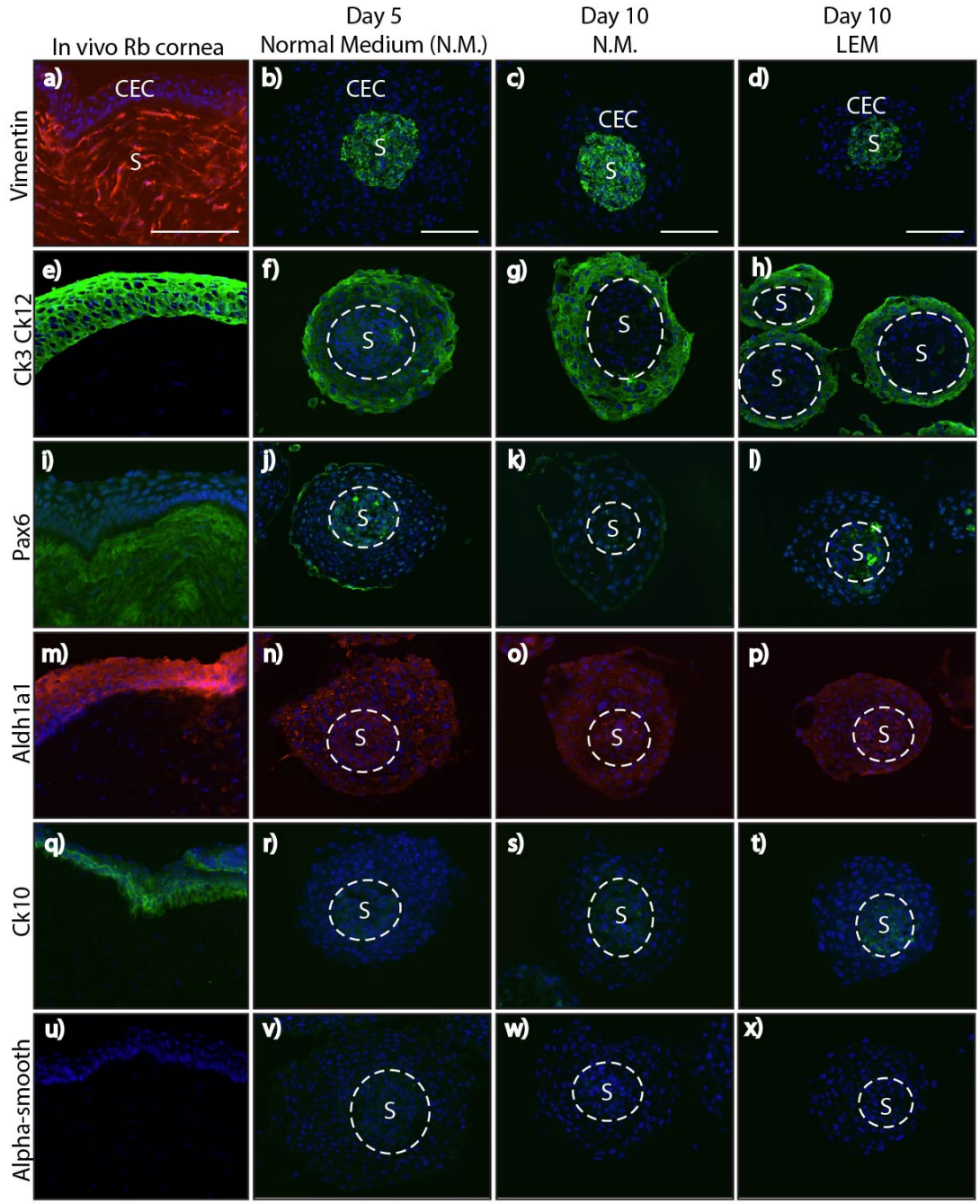

Figure 54: Immuno-histochemistry of in vivo rabbit cornea and rabbit cornea 3D model (4) at time points Day5 and Day10 in standard normal medium and Day10 in only LEM

First column: a,e,i,m,q,u show immunohistochemistry of the *in vivo* rabbit cornea stained with vimentin (a), Cytokeratin 3/12 (e), Pax6 (i), Aldh1a1 (m), Cytokeratin 10 (q) and αSMA (u). Columns 2 & 3 show immunohistochemistry of the rabbit cornea 3D model at Day 5 in N.M. and Day 10 in N.M., and column 4 in LEM stained with the respective markers. The stromal core is marked as (S) and the corneal epithelial cell coating as (CEC). All images were taken with an Axiovert Zeiss microscope. Scale bars: 100µm.

Vimentin stained the models shown in Figure 54 b - d identifying the mesenchymal stromal core within the model. From these pictures the decreasing size of the models from day 5 to day 10 in both culture media conditions became very clear. Strong Ck3Ck12 staining in the CEC in all of the models (f - h) was shown, indicating a much thinner CEC layer in LEM at day 10, compared to the models found in the standard medium (N.M). Pax6 staining was expressed at cytoplasmic level in the CEC layer at all three time points (j – l) . Aldh1a1 was expressed in the stroma and CEC in all of the models from day 5 to day 10 in both culture media conditions (n,o,p). Ck10 and αSMA were not expressed at all in any of the models (r - t and v - x).

Antibody staining did not reveal any particular difference between the models in the culture medium variations, but rather highlighted the decreasing size of the models over time, in particular from day 5 to day 10. The models placed in LEM resulted in being the smallest in size, reflecting a greater loss of CECs, therefore indicating that the better culture medium was the Standard (N.M) medium (Species specific/LEM medium mix).

4.3.2.5 Rabbit cornea 3D model 5 - using limbal stromal keratocytes

The idea of using stromal keratocytes from the upper region of the cornea in the 3D models (as shown in the above experiments) arose from presumption that stromal keratocytes underneath the corneal epithelium would be more efficient at sustaining the corneal epithelium because of their constant close contact with the latter *in vivo*. However, stromal keratocytes from the limbal region of the cornea, also known as limbal stromal keratocytes, have been shown in a rabbit model of recombined tissue (Espana *et al*., 2003) to favour the stem cell-like phenotype of the corneal epithelium, by dictating its plasticity. Recent work by Branch *et al* 2012 found that the human corneal limbal stroma harboured mesenchymal stem cells and Nakatsu *et al*., 2014 more recently reported that limbal stromal mesenchymal cells could substitute the traditionally used 3T3 feeder layer when expanding LSCs in a 3D culture method.

In the next refinement of the model, rabbit limbal stromal keratocytes at P7 were used to create 3D single spheres (Fig. 55) and after 3 days these were coated with rabbit limbal CEC at P2. These spheres were cultured in the Species specific/LEM medium mix for 7 days, the media was changed every other day and at 3, 5 and 7 days up to 20

specimens were snap frozen in OCT for cryosectioning and histological (Fig. 56) or immunohistochemical (Fig. 57) analysis.

2D limbal stromal keratocytes & 3D stromal keratocytes

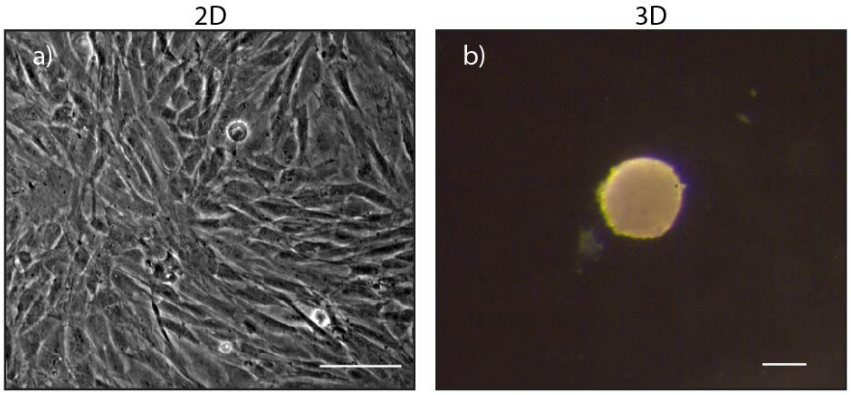

Figure 55: *2D stromal keratocytes and a 3D stromal sphere*

a) limbal stromal keratocytes in 2D culture Image taken with a Zeiss Axiocam. Scale bar: 200µm
b) single limbal stromal 3D sphere at Day3 in culture. Image taken with a Zeiss Axiocam. Scale bar: 100µm

Rabbit cornea model 5: macroscopic & H&E images

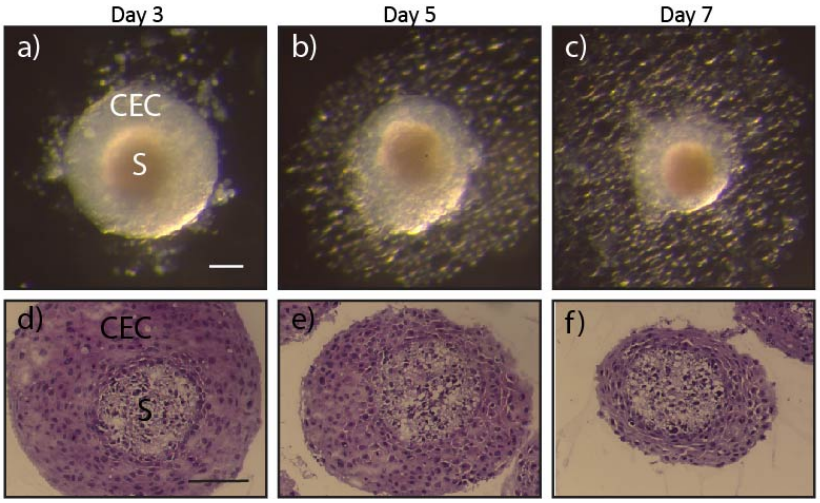

Figure 56: Rabbit cornea 3D model (5) in a hanging drop culture, dark field macroscopic images & H&E over the period of 7 days

a) – c) show macroscopic dark field images of double spheres made of the stromal component (S) at the centre of the sphere and corneal epithelial cells (CEC) coated around the stromal core. Images taken with a Zeiss Axiocam. Scale bar: 100µm.

d) – f) H&E staining of the cornea 3D model at three given time points. Images were taken with an Axiovert Zeiss microscope. Scale bar: 100µm.

Dark field macroscopic images of the bilayered structures revealed very well formed and fairly transparent CEC coatings around the stromal cores (Fig. 56 a), with the epithelial layer shrinking in size over the 7 day timespan in most specimens. H&E staining confirmed this observation, and also showed that even though the corneal layer was decreasing in thickness over time, its compactness and tightness remained stable (Fig. 56 d - f).

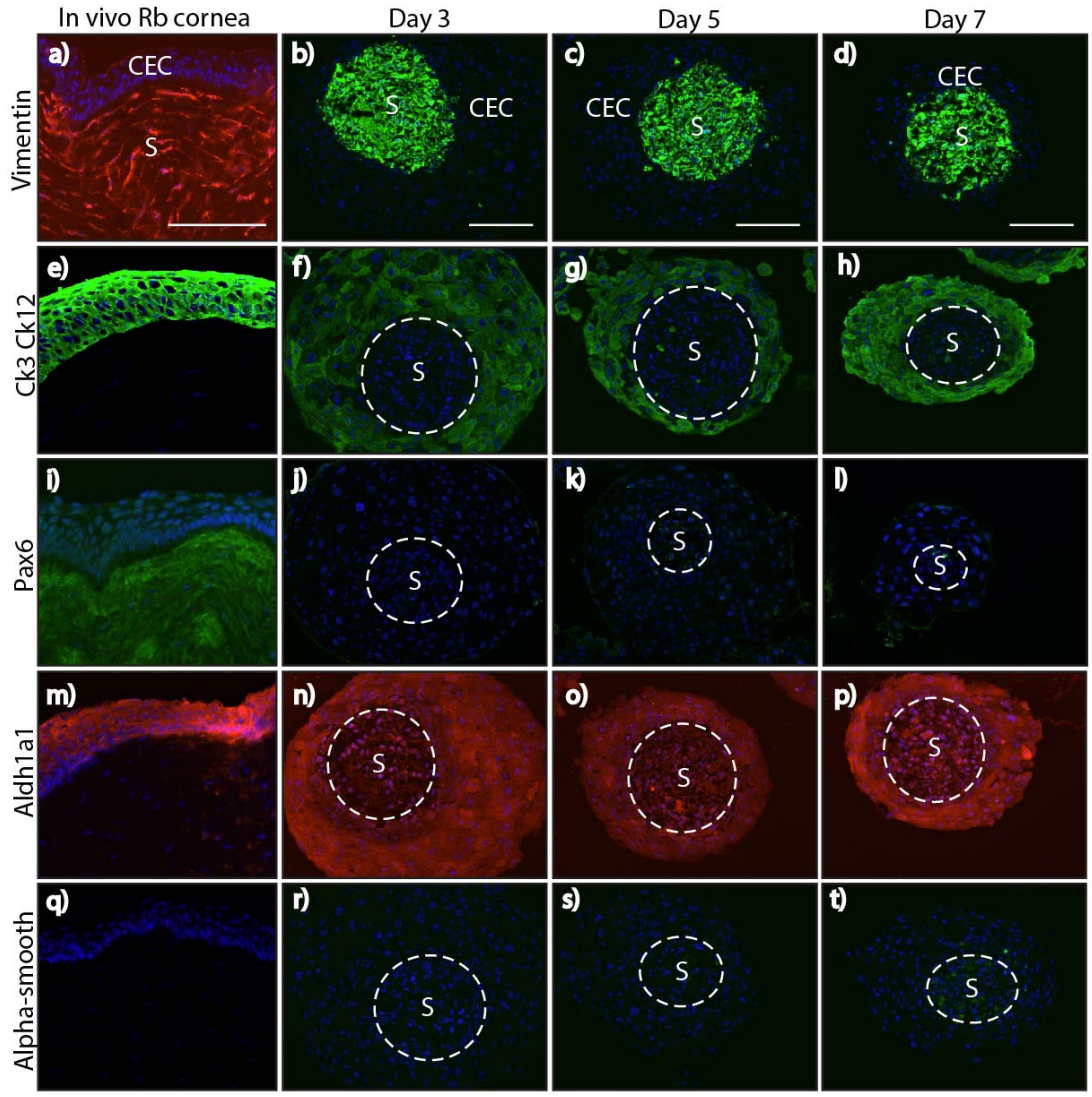

Figure 57: Immuno-histochemistry of in vivo rabbit cornea and rabbit cornea 3D model (5) at time points Day3, 5 and Day7 in Species specific/LEM medium mix

First column from left: a,e,i,m,q shows immunohistochemistry of the *in vivo* rabbit cornea stained with vimentin (a), Cytokeratin 3/12 (e), Pax6 (i), Aldh1a1 (m) and αSMA (q). Columns 2, 3 and 4 show immunohistochemistry of the rabbit cornea 3D model at Days 3, 5 and 7 with the respective markers. The stromal core is marked as (S) and the corneal epithelial cell coating as (CEC). All images were taken with an Axiovert Zeiss microscope. Scale bars: 100µm.

Vimentin stained the models shown in Figure 57 b - d identifying the mesenchymal stromal core within the model. Ck3Ck12 staining was seen in the CEC in all of the models (f - h). Pax6 nuclear staining was not present in the CEC layer of the models (j - l). Aldh1a1 was very strongly expressed in the stroma and CEC in all of the models

throughout all of the time points (n - p). αSMA was not expressed at all in any of the models (r - t). By using limbal stromal keratocytes it was expected to obtain a strong Pax6 expression, as these are believed to sustain the more stem-cell like phenotype of limbal CEC at a greater level than stromal keratocytes from the central or peripheral cornea. Unfortunately, cytokeratin 10 which is only expressed in the limbal corneal epithelium was not tested in this experiment due to the missing antibody at that particular time.

4.3.3 Single whole stromal spheres

At the beginning of this chapter, the aim had been to compare upper stromal keratocytes to stromal keratocytes extracted from the whole stroma in 2D, 3D and within a bi-layered 3D model. However, first attempts at making stromal keratocytes from the whole stroma did not produce good 3D single spheres, so the 3D bilayered models were made with upper stromal keratocytes only. Later experiments using whole stromal keratocytes to make single spheres as well as using them within a bi-layered 3D model was repeated and successfully achieved. These experiments are described in the following section below.

4.3.3.1 Whole single spheres 2D vs. 3D

Rabbit whole stromal keratocytes in 2D culture (a) and as a 3D fully formed single sphere at culture day 3 (b) are shown in Figure 58.

Whole 2D vs. 3D stromal keratocytes

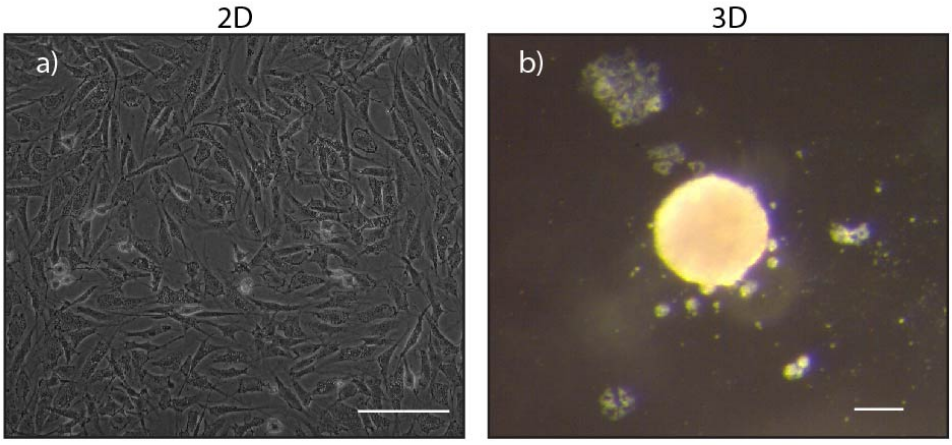

Figure 58: *2D stromal keratocytes and a 3D stromal sphere*

a) whole stromal keratocytes in 2D culture. Image was taken with a Zeiss Axiocam. Scale bar: 200µm
b) single whole stromal 3D sphere at day 3 in culture. Image was taken with a Zeiss Axiocam. Scale bar: 100µm

RNA was extracted from 150 to 200 of the whole stromal keratocyte 3D spheres and from the equivalent cells in 2D culture, and converted to cDNA and quantitative real-time PCR was used to determine the relative gene expression of stromal crystalline protein markers (as described in section 4.3.1.1). This experiment is described further in the next section below.

4.3.3.2 Quantitative Real-time PCR expression of crystalline protein markers

Three biological samples of rabbit whole stromal keratocytes were cultured in the normal 2D culture conditions and then turned into 3D spheres (as explained in the Methods section 4.2.2.2). In order to identify and quantify the expression of the corneal crystalline markers Aldh1a1, GAPDH and Lumican as well as the marker for quiescent keratocytes, Keratocan and marker for myofibroblasts αSMA was investigated. The

measured cDNA sequences of interest were compared to a standard reference gene (β-actin). Results were analysed using the Comparative Ct Method, as described in the Methods section 4.2.2.4. This analysis method calculates a relative normalised quantification of gene expression. Relative gene expression within the 2D and 3D samples was compared to the relative gene expression found in the *in vivo* stroma.

Stromal keratocyte markers tested by QRT-PCR

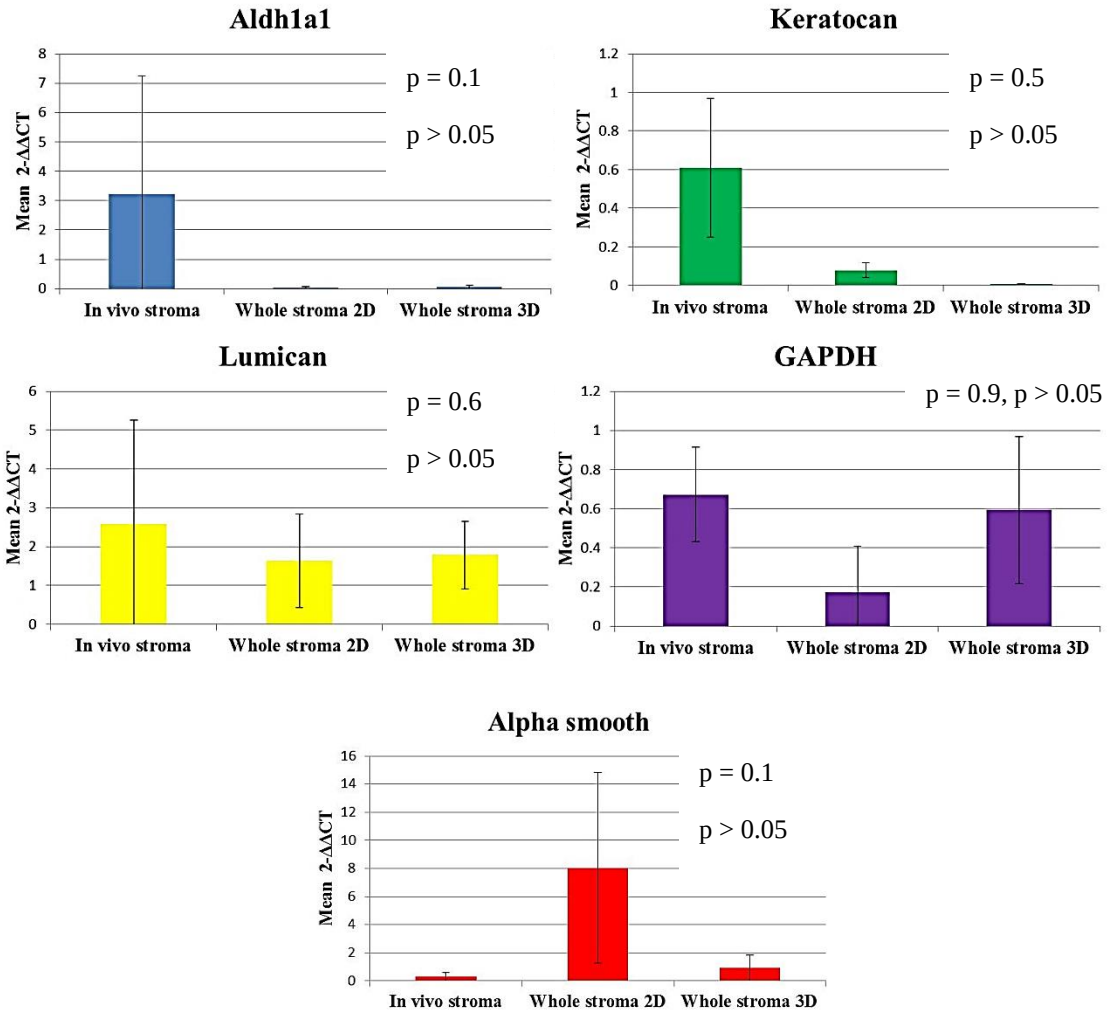

Figure 59: Relative normalised gene expression of crystalline, keratocan and αSMA markers in whole stromal 3D vs. 2D keratocytes, n=3

The x-axis represents the samples tested. The y-axis represents the result of the formula $2^{-\Delta\Delta Ct}$ which is expressed in terms of fold changes.

Quantitative real-time pcr of 2D and 3D whole stromal keratocytes vs. the *in vivo* stroma revealed no relative Aldh1a1 gene expression in 3D whole stromal keratocytes compared to the *in vivo* stroma and also none in 2D stromal keratocytes. However, results were non-significant due to the very high variation between samples. Keratocan relative gene expression in 3D whole stromal keratocytes was no restored to *in vivo* stromal levels and was also lower than in 2D cultures. Lumican on the other hand showed a high expression both in 2D and 3D, with relative gene expression levels more closely to the ones found in the *in vivo* stroma. However the error bars were very high due to a strong variation occurring between the three biological samples and ANOVA statistical results showed these were non-significant results ($p = 0.6$). GAPDH relative gene expression was found to be high in 3D, with levels almost reaching to those found in the *in vivo* stroma. GAPDH levels were lower in 2D cultures. The ANOVA test resulted being non-significant due to the high variation between biological samples. αSMA gene expression was extremely high in 2D, although the error bar was extremely high due to strong data variations in the biological samples tested. Similarly to the upper 3D stromal keratocytes, whole 3D keratocytes did not show any significant αSMA expression, with levels trending towards those found in the *in vivo* stroma. However, results were non-significant due to the very high variation between biological samples.

4.3.3.3 Double layered spheres – development of a spherical 3D bilayered model of the cornea using whole stromal keratocytes

Rabbit whole stromal keratocytes at P6 were placed in 3D cultures and at day 4 were coated with rabbit limbal CEC at P2. The models were cultured in Species specific/LEM medium mix 10 days and the medium changed every other day. At time points 3, 5, 7 and 10, up to 20 models were snap frozen in OCT, cryosectioned and their histological features (Fig. 60) and the expression of key markers (Fig. 61) were examined.

Dark field macroscopic images and H&E staining (Fig. 60) at various time points, revealed that the model was in very good conditions throughout all time points, however detachment and loss of cells from the CEC layer (c,d) resulted in a smaller sized model at culture day 10 (Fig. 60 d, h).

3D cornea model using whole stromal keratocytes: macroscopic & H&E images

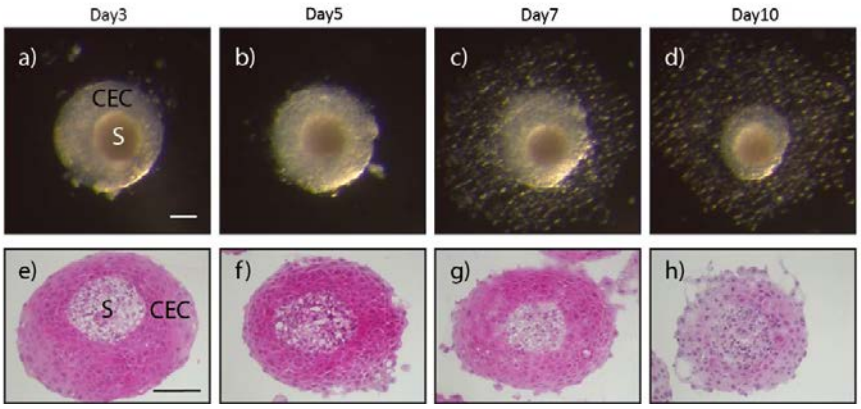

Figure 60: Rabbit cornea 3D model (6) in a hanging drop culture, dark field macroscopic images & H&E over the period of 10 days

a) – d) show macroscopic dark field images of double spheres made of the stromal component (S) at the centre of the sphere and corneal epithelial cells (CEC) coated around the stromal core. Images were taken with a Zeiss Axiocam. Scale bar: 100µm.

e) – h) H&E staining of the cornea 3D model. Images were taken with an Axiovert Zeiss microscope. Scale bar: 100µm.

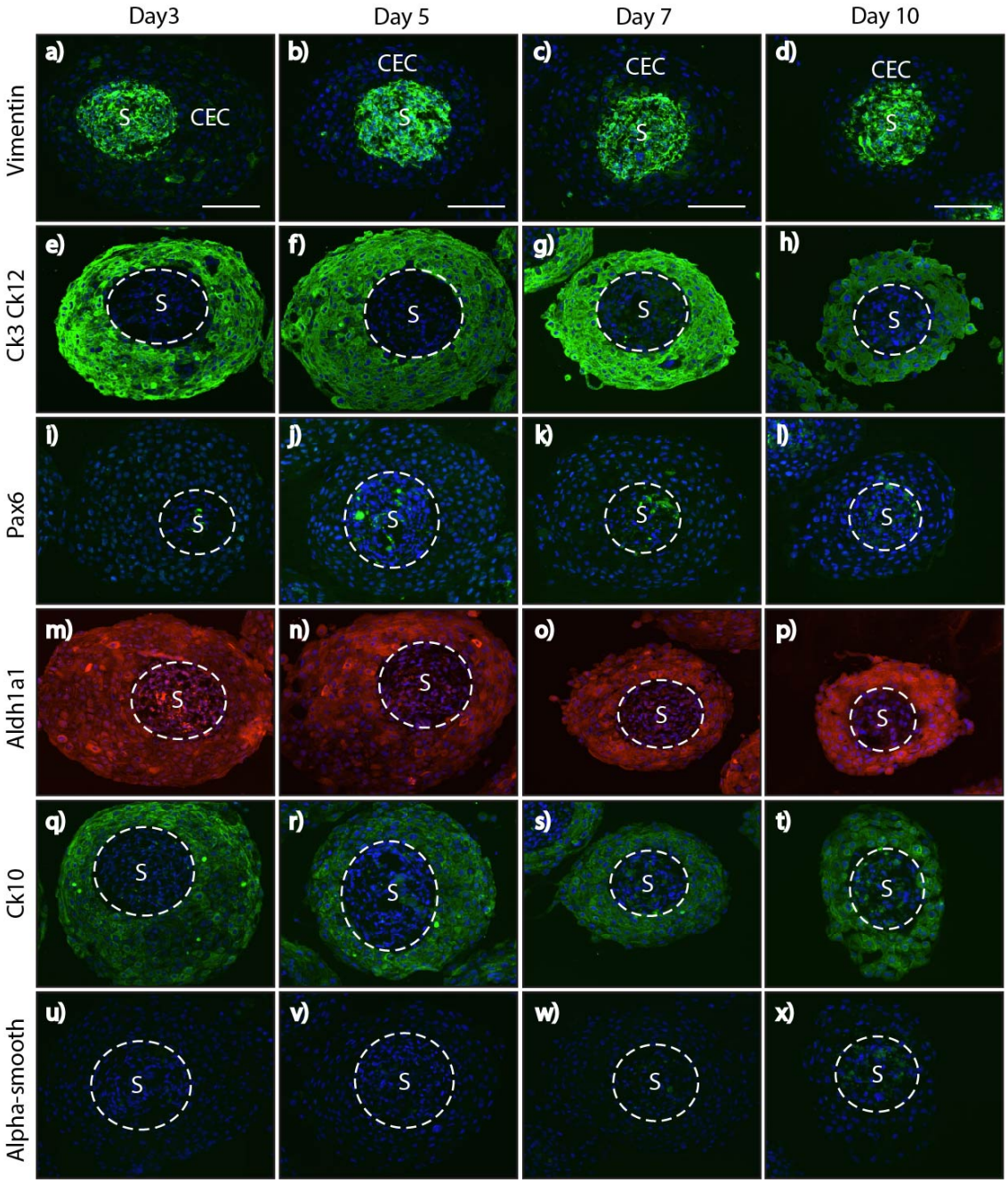

Figure 61: Immunohistochemistry of rabbit cornea 3D model (6) at time points Day3, 5, 7 and Day10 in Species specific/LEM medium mix

Immunohistochemistry of the *in vivo* rabbit cornea is not shown due to space constrictions; however the same *in vivo* images apply as shown in the previous experiments. Immunohistochemistry of the rabbit cornea 3D model at Day 3, 5, 7 and 10 with the respective markers is shown. The stromal core is marked as (S) and the corneal epithelial cell coating as (CEC). All images were taken with an Axiovert Zeiss microscope. Scale bars: 100µm.

Immunohistochemistry (Fig. 61) of the models at the above given time points exhibited very strong and consistent labelling of most of the tested markers. Vimentin, Ck3Ck12,

Aldh1a1 and Ck10 were very positively expressed at all the time points, mirroring an *in vivo* CEC layer, lasting throughout the experiment. Pax6 expression was present at all the time points (see Fig. 62 below for enlarged images). αSMA was not expressed at all during the early time points (u - w) and at day 10 weakly stained the stromal core (x).

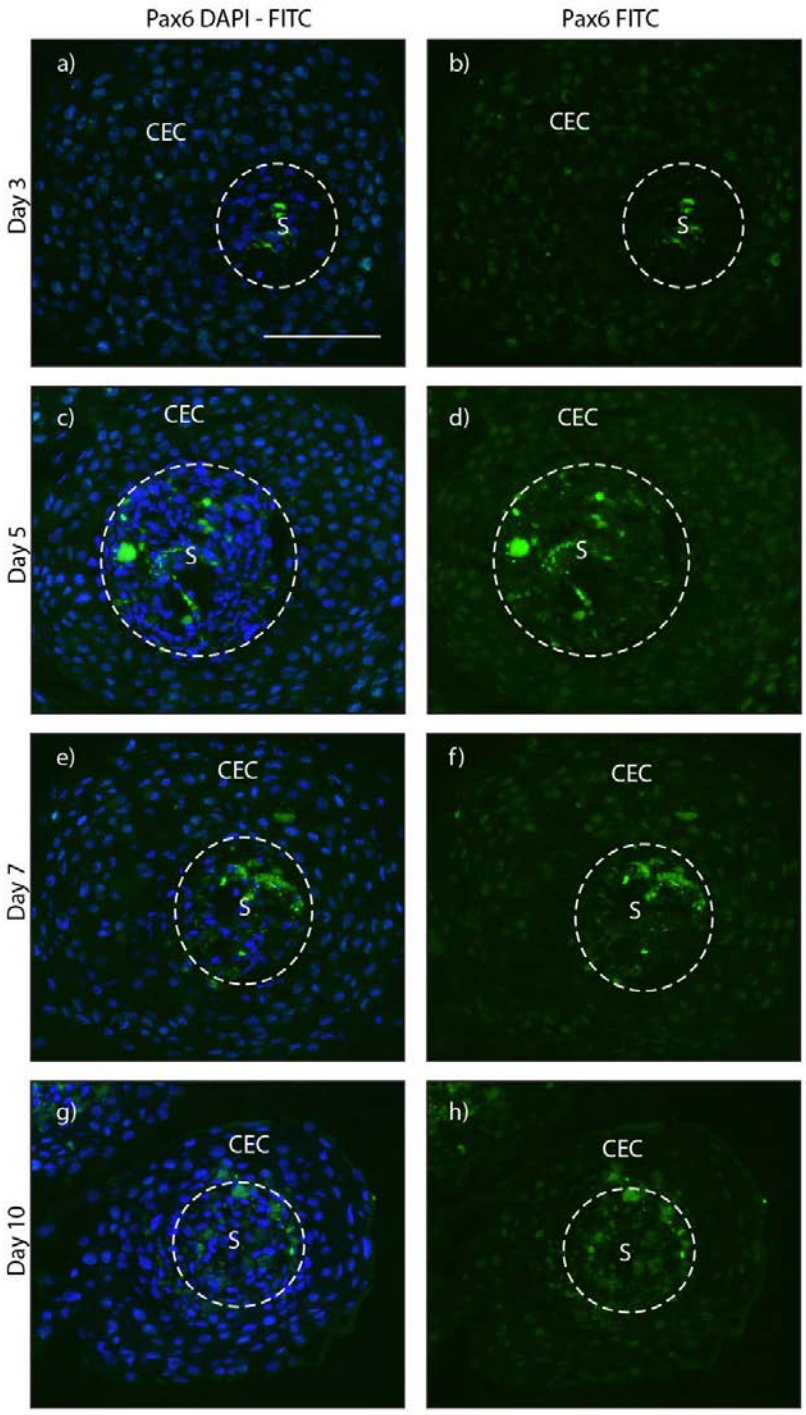

Figure 62: Pax6 immunostaining of rabbit cornea 3D model (6) at time points Day3, 5, 7 and 10

Images were taken with an Axiovert Zeiss microscope. Scale bar: 100µm.

4.3.4 Evidence of epithelial-mesenchymal interactions within the 3D models

Throughout the previously established and described rabbit 3D models, proof of epithelial-mesenchymal interactions taking place within these models became evident when examining the crystalline marker Aldh1a1. Upper and whole single stromal 3D spheres were cryo-sectioned and immuno-stained with Aldh1a1 for which they both stained positive to (Fig. 63 a, b). However, when the 3D upper and whole single stromal spheres were double-coated with CEC, the Aldh1a1 staining became stronger (Fig. 63 c, d), raising the possibility that increased Aldh1a1 expression within both epithelial and mesenchymal layers is a result of their interactions within the 3D model.

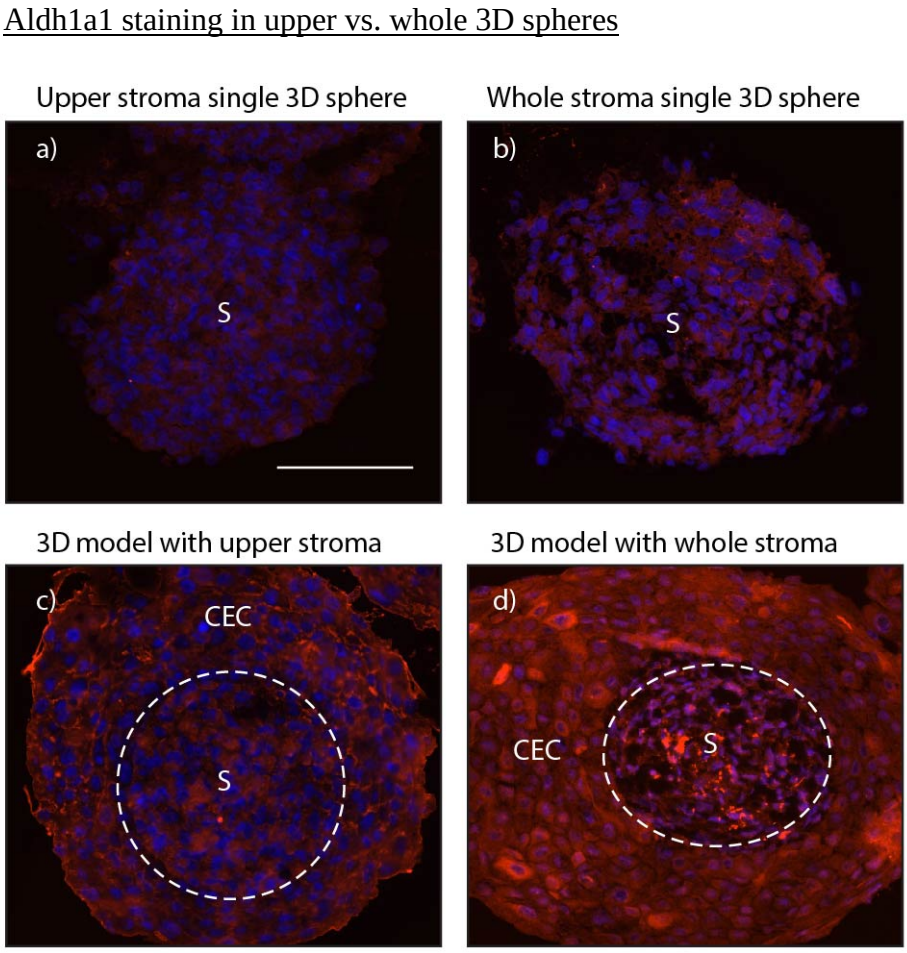

Figure 63: Aldh1a1 antibody staining of upper and whole single stromal 3D spheres and of 3D models made with upper and whole stromal spheres

a) and b) show immunohistochemistry of 3D upper and whole stromal spheres stained with Aldh1a1. c) represents a 3D model made with upper stromal 3D spheres

and d) represents a 3D model made with whole stromal 3D spheres. Both are stained with Aldh1a1. The stromal core is marked as (S) and the corneal epithelial cell coating as (CEC). All images were taken with an Axiovert Zeiss microscope. Scale bar: 100µm.

This effect was also evident when single 3D spheres were made from rabbit limbal CEC (without the stromal core), cultured for 7 days in LEM, in parallel with double spheres created with the same limbal CEC cells, coated onto 3D spheres made from limbal stromal keratocytes. Immuno analysis with Aldh1a1, Ck3Ck12, Pax6 and Ck10 further implied that interactions between the stromal and epithelial layers of the models were important (Fig. 64). No Aldh1a1 expression was observed within the corneal epithelial single 3D spheres (Fig. 64 a), however when the CEC were added to the stromal compartment (Fig. 64 b), Aldh1a1 expression in the CEC layer was strong. Likewise, Ck10 expression was present in the CEC layer only when the stromal compartment was in direct proximity to the CEC layer (Fig. 64 e,f). On the other hand, Pax6 and Ck3Ck12 were both expressed in single CEC 3D spheres as well as within the 3D models (Fig. 64 c,d,g,h).

Aldh1a1, Ck3Ck12, Ck10 & Pax6 expression in single 3D CEC vs. CEC in a bilayered 3D model

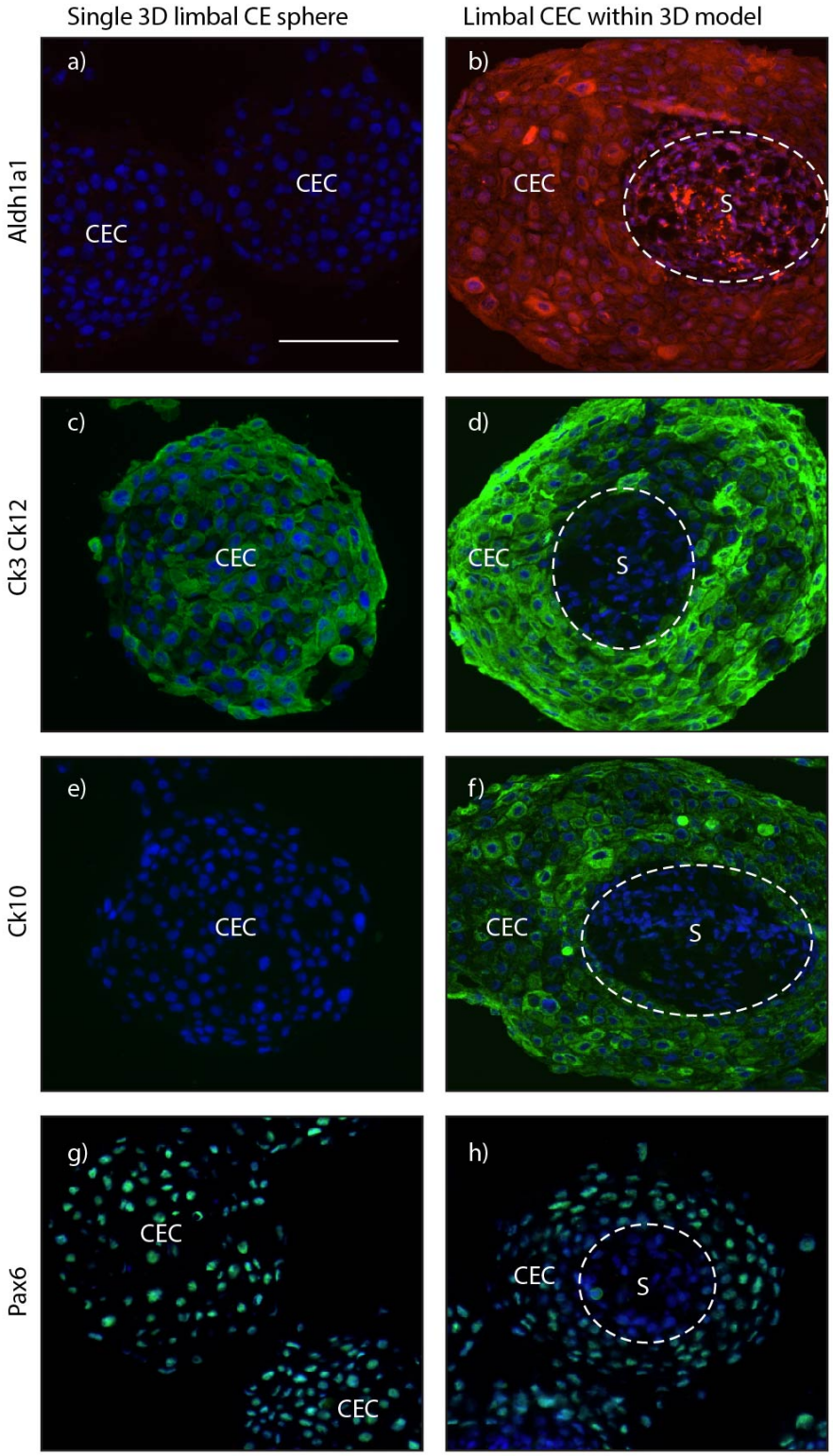

Figure 64: Immuno-histochemistry of single limbal CEC 3D spheres compared to 3D models

a) – g) show limbal CEC 3D spheres, b) - h) show 3D models. All were stained with immunohistochemistry with Aldh1a1, Ck3Ck12, Ck10 and Pax6. The stromal core is marked as (S) and the corneal epithelial cell coating as (CEC). All images were taken with an Axiovert Zeiss microscope. Scale bar: 100µm.

4.3.5 A human cornea 3D model

After having developed and mastered the 3D cornea model technique using rabbit corneal epithelial and stromal keratocytes, it was important to develop a human cornea model. At first, it was difficult to obtain human tissue material, as the model required both fresh stromal and corneal epithelial tissue for optimal results and the human corneas available for research were always a few months old and cell extraction became very difficult due to hardening of the corneal tissue over time.

The three human cornea 3D models described in the next few sections were developed using fresh stromal keratocytes and corneal epithelial cells extracted from non-fresh corneas that were discarded due to their transplantation unsuitability (as explained in the Methods section 4.2.2.1).

The first step was to establish human stromal single 3D spheres and this is shown below in Figure 65. The method is described in the Methods section 4.2.2.2 whereby human stromal keratocytes were placed in Species specific medium for 2 to 3 days prior plating these as single 3D spheres. After three days in culture, round and compact spheres had formed (Fig. 65 b) and these were snap frozen in OCT, cryosectioned and immuno-stained (Fig. 66 c,f).

No distinction between upper and whole stromal keratocytes could be made because the very first stromal tissue sample was received at a time when the project had not been developed yet, whereas the second stromal sample was kindly given as a cell stock sample by Prof. Julie Daniel. All of the stromal keratocytes used below were extracted from the limbal region of the cornea.

Human limbal stromal keratocytes 2D vs. 3D

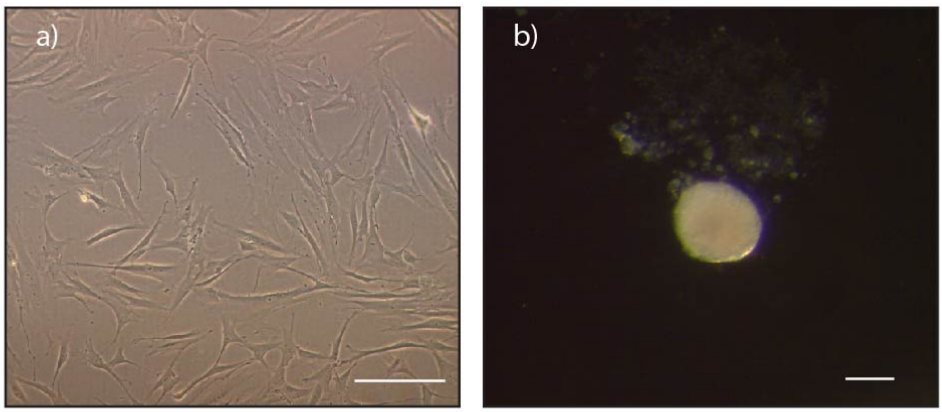

Figure 65: 2D human limbal stromal keratocytes and a human 3D stromal sphere

a) Human limbal stromal keratocytes in 2D culture. Image was taken with a Zeiss Axiocam. Scale bar: 200µm
b) Human single stromal 3D sphere at Day3 in culture. Image was taken with a Zeiss Axiocam. Scale bar: 100µm

The human stromal 3D spheres were tested for the presence or absence of αSMA (biomarker of "activated" keratocytes) to determine whether the 3D culture approach was qualitatively superior to the 2D culture method and whether it mirrored the *in vivo* human stroma. Figure 66 below showed that αSMA was not expressed in the *in vivo* stroma (d). αSMA was expressed in the human 2D stromal cultures (e) and was switched off in the 3D culture environment (f). Vimentin was used to show that the keratocytes were of mesenchymal origin (a - c).

Vimentin & αSMA expression in in vivo, 2D and 3D human stromal keratocytes

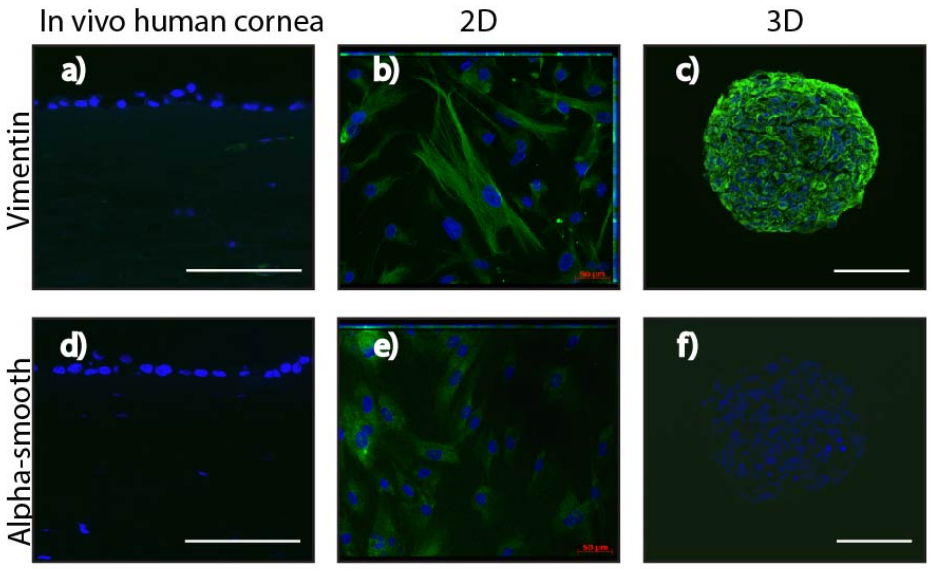

Figure 66: Immunofluorescent comparison of human stromal cell expression in vivo and in vitro

Vimentin (a - c) and αSMA (d - f) expression in the human stroma and in human stromal keratocytes in 2D and 3D culture. Images were taken with an Axiovert Zeiss microscope. Scale bars: 100µm and 50 µm (in red).

In the next sections 4.3.5.1 to 4.3.4.3 three human cornea 3D models are described. These were replicated with different human stromal and epithelial donors. In the human experiments, not all markers that were used for immunofluorescent analysis in the rabbit cornea 3D models could be used for the human model as well due to species specificity. The Aldh1a1 marker was rabbit specific and could not be used for the human 3D models.

4.3.5.1 Human cornea 3D model 1

The first human cornea model was developed by using human limbal stromal keratocytes at P12. The stromal keratocytes were cultured in Species specific media for 2 to 3 days, placed in 3D culture, as previously described in the Methods section 4.2.2.2 and allowed to form for 3 days. At culture day 3, the fully formed stromal single

spheres were coated with primary cultures of human limbal CEC. The models were cultured in 50% Species specific media and 50% LEM, the media was changed every other day and dark field macroscopic images were taken. At time points 3, 5 and 7 after the bilayered spheres were created, up to 20 models were snap frozen in OCT, cryosectioned and their histological features (Fig. 67) and the expression of key markers (Fig. 68) were examined.

Human cornea model 1: macroscopic & H&E images

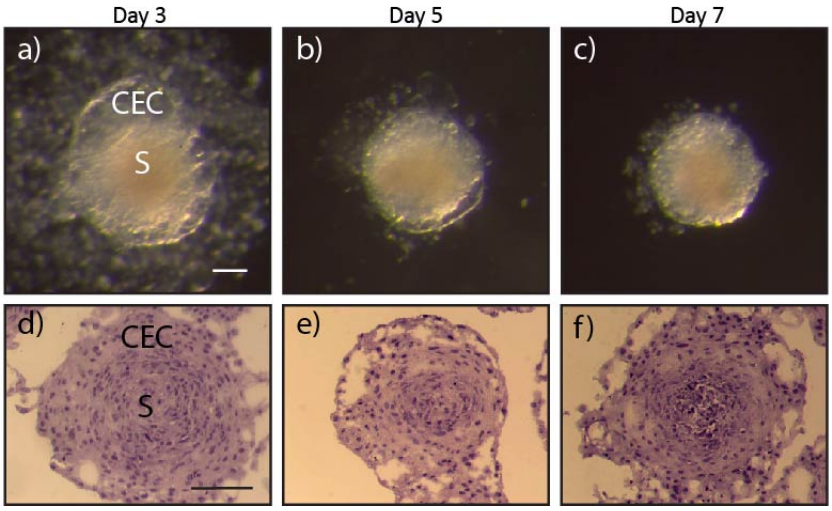

Figure 67: Human cornea 3D model (1), dark field macroscopic images & H&E over the period of 7 days

a) – c) macroscopic dark field images of double spheres made of the stromal component (S) at the centre of the sphere and corneal epithelial cells (CEC) coated around the stromal core. Image was taken with a Zeiss Axiocam. Scale bar: 100µm.

d) – f) H&E staining of the cornea 3D model. Images were taken with an Axiovert Zeiss microscope. Scale bar: 100µm.

During the 7 culture days, the models size decreased as shown in Figure 67 in the dark field macroscopic images (a – c). H&E staining showed increasingly disrupted CEC layer borders from day 3 to day 7 (e,f). Already at culture day 3 (d) the outer borders of the CEC layer lacked compactness and an increasing number of gaps formed towards later stages of the culture at days 5 and 7 (e,f). However, some of the CEC remained in a compact layer around the stromal compartment.

Human cornea 3D model 1: Immunohistochemistry

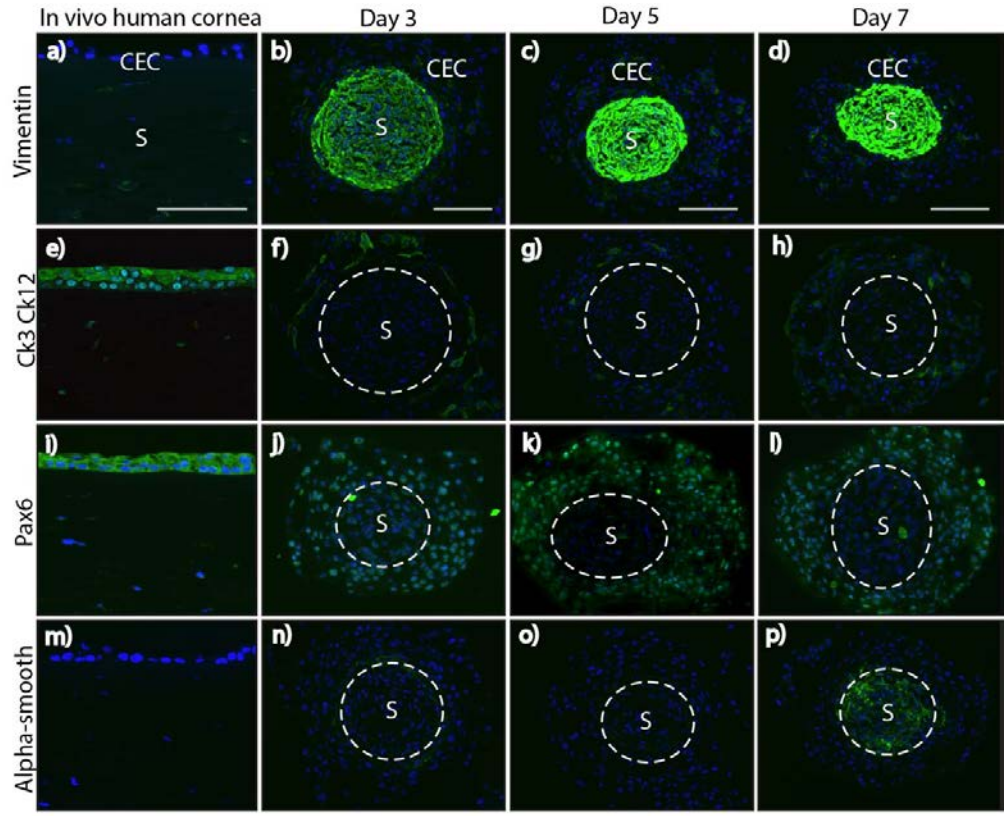

Figure 68: Immunohistochemistry of in vivo human cornea and human cornea 3D model (1) at Day 3, 5 and 7

First column: a,e,i,m shows immunohistochemistry of the *in vivo* human cornea stained with Vimentin (a), Cytokeratin 3/12 (e), Pax6 (i) and αSMA (m). Columns 2, 3 and 4 show immunohistochemistry of the human cornea 3D model at days 3, 5 and 7 with the respective markers. The stromal core is marked as (S) and the corneal epithelial cell coating as (CEC). All images were taken with an Axiovert Zeiss microscope. Scale bars: 100µm.

Immunohistochemical analysis of the model in Figure 68 showed vimentin expression in the stromal compartment throughout all time points, Ck3Ck12 was expressed in a small part of the CEC layer at culture day 3 (f) and was almost completely switched off in the later culture days (g,h). CytoplasmicPax6 staining was shown in the positive control (i) but was expressed at nuclear level throughout all time intervals within the CEC layer (j - l). αSMA staining was absent at culture days 3 and 5 (n,o) but was present within the stromal compartment at day 7 (p). Immunohistochemical analysis

showed that Pax6 expression was maintained throughout all time points and the low Ck3Ck12 expression indicated less corneal epithelial differentiated cells in the model.

4.3.5.2 Human cornea 3D model 2

A second human cornea 3D model was made using passage 5 human limbal fibroblasts from a second biological. Stromal spheres were created and after three days in culture these were coated with primary cultured human limbal CEC. The model was cultured in 50% Species specific media and 50% LEM and this media was changed every other day. Dark field macroscopic images were taken and at culture days 3 and 5 after the bilayered spheres were created up to 20 models were snap frozen in OCT, cryosectioned and their histological features (Fig. 69) and the expression of key markers (Fig. 70) were examined. The model did not show a spherical and compact formation (Fig. 69 a,b). The CEC layer had expanded and created transparent bubbles (a,b). H&E staining (c,d) indicated that the CEC layer had mostly torn apart, possibly due to the transparent bubbles within the CEC layer.

Human cornea model 2: macroscopic & H&E images

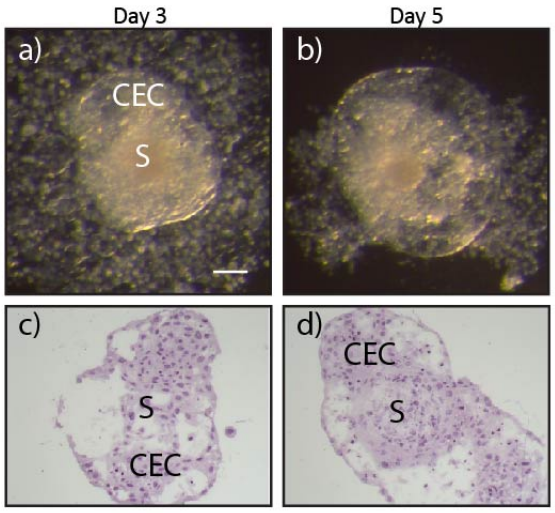

Figure 69: Human cornea 3D model (2), dark field macroscopic images & H&E over the period of 5 days

a) and b) show macroscopic dark field images of double spheres made of the stromal component (S) at the centre of the sphere and corneal epithelial cells

(CEC) coated around the stromal core. Images were taken with a Zeiss Axiocam. Scale bar: 100µm.

c) and d) show H&E staining of the cornea 3D model. Images were taken with an Axiovert Zeiss microscope. Scale bar: 100µm.

Human cornea 3D model 2: Immunohistochemistry

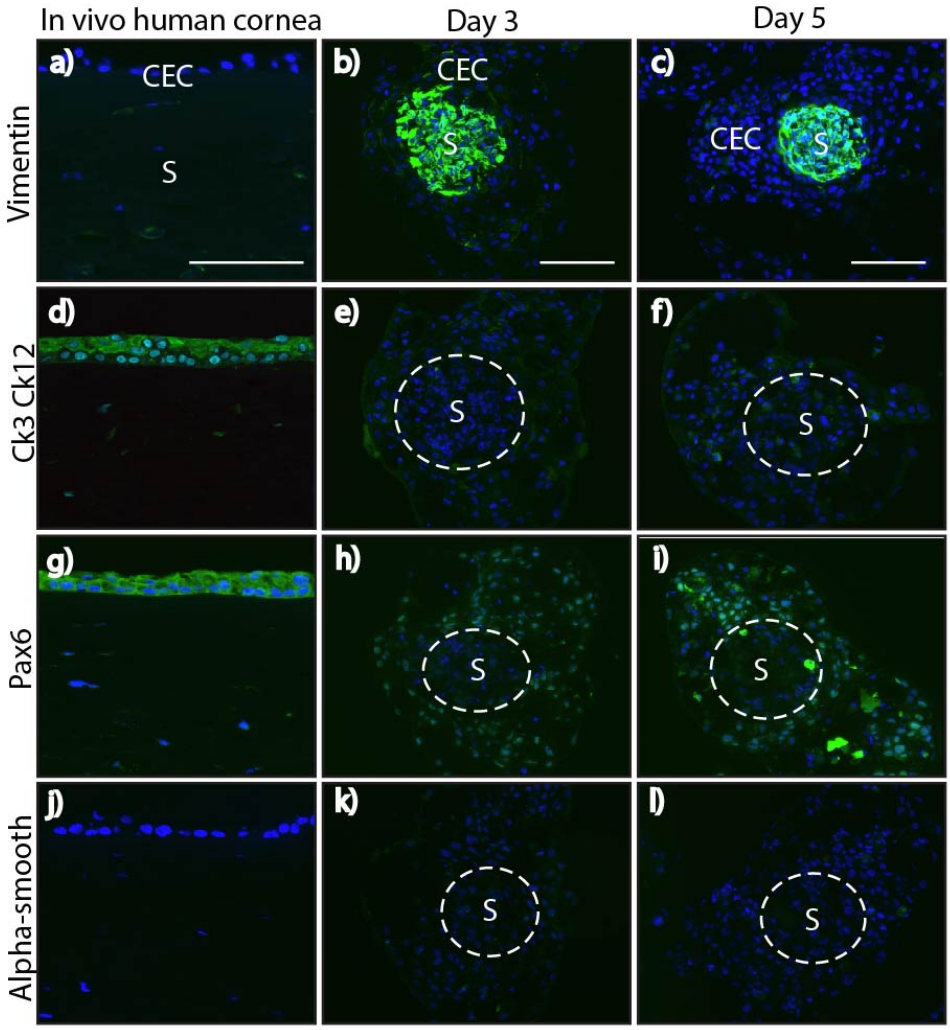

Figure 70: Immunohistochemistry of in vivo human cornea and human cornea 3D model (2) at time points Day3 and 5

Column 1: a,d,g,j shows immunohistochemistry of the *in vivo* human cornea stained with vimentin (a), Cytokeratin 3/12 (d), Pax6 (g) and αSMA (j). Columns 2 & 3 show immunohistochemistry of the human cornea 3D model at days 3 and 5 with the respective markers. The stromal core is marked as (S) and the corneal epithelial cell

coating as (CEC). All images were taken with an Axiovert Zeiss microscope. Scale bars: 100μm.

Immunofluorescent analysis in Figure 70 showed vimentin expression in the stromal compartment (b,c) and nuclear Pax6 staining in the CEC layer of the models (h,i) at culture days 3 and 5. No Ck3Ck12 expression was seen indicating no differentiated CECs. Also αSMA was not expressed in any of the models.

4.3.5.3 Human cornea 3D model 3

This human cornea 3D model was made using the same stromal keratocytes used in the previous model 2 at passage 6. Stromal spheres were coated at culture day 3 with passage 1 human limbal CEC and cultured in 50% Species specific media and 50% LEM. The media was changed every other day and dark field macroscopic images were taken. At 3, 5 and 7 culture days after the bilayered spheres were created up to 20 models were snap frozen in OCT, cryosectioned and their histological features (Fig. 71) and the expression of key markers (Fig. 72) were examined. Macroscopic images at days 3 and 5 (a,b) showed a round model with tight outer CEC borders. However, at day 7 (c) the CEC borders had a transparent bubble appearance. H&E staining showed gaps in the CEC outer layer at all the time points (d – f) and was almost completely degraded at day 7 (f).

Human cornea 3D model 3: macroscopic & H&E images

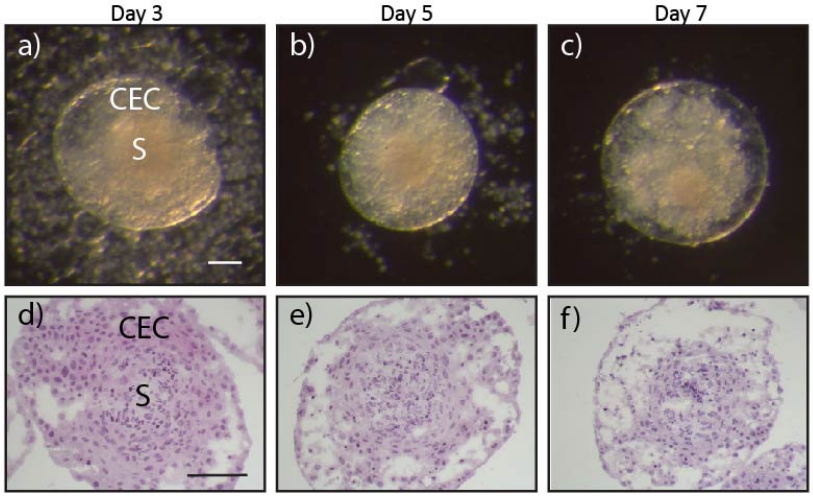

Figure 71: Human cornea 3D model (3), dark field macroscopic images & H&E over the period of 7 days

a) – c) show macroscopic dark field images of double spheres made of the stromal component (S) at the centre of the sphere and corneal epithelial cells (CEC) coated around the stromal core. Images were taken with a Zeiss Axiocam. Scale bar: 100µm.

d) – f) H&E staining of the cornea 3D model. Images were taken with an Axiovert Zeiss microscope. Scale bar: 100µm.

Human cornea 3D model 3: Immunohistochemistry

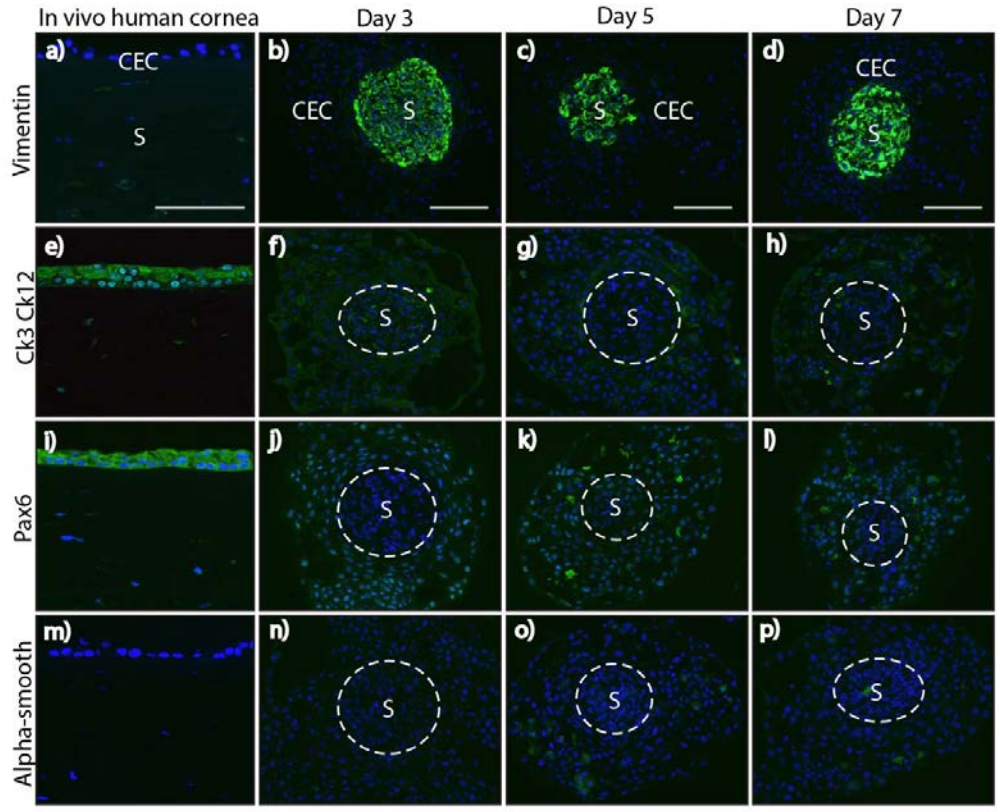

Figure 72: Immunohistochemistry of in vivo human cornea and human cornea 3D model (3) at time points Day3, 5, and 7

Column 1: a,e,i,m show immunohistochemistry of the *in vivo* human cornea stained with vimentin (a), Cytokeratin 3/12 (e), Pax6 (i) and αSMA (m). Columns 2, 3 and 4 show immunohistochemistry of the human cornea 3D model at Day 3, 5 and 7 with the respective markers. The stromal core is marked as (S) and the corneal epithelial cell coating as (CEC). All images were taken with an Axiovert Zeiss microscope. Scale bars: 100µm.

Immunohistochemical analysis in Figure 72 showed strong vimentin expression in the stromal compartment (b – d) and nuclear Pax6 expression in the CEC layer (j – l) at all the time points. Ck3Ck12 and αSMA were not expressed in any of the models (f – h and n – p).

In the described three human models Ck3Ck12 expression was very scarce in model 1 and not present at all in the second and third models. The experiment described in section 4.3.5.4 was performed with the aim to investigate the low or lack of Ck3Ck12

expression within the human CEC layer throughout the models. To do this a human and rabbit hybrid model was created.

4.3.5.4 A Cornea 3D human-rabbit hybrid model

The hybrid cornea model was composed of rabbit upper (P4) stromal spheres coated with passage 1 human limbal CEC. The model was cultured in 50% Species specific media and 50% LEM, this was changed every other day and dark field macroscopic images were taken (Fig. 73 a - c). Up to 15 models were snap frozen in OCT at culture day 5, cryosectioned and expression of key marker (Fig. 74) was examined. No histological featured could be examined due to the small number of available spheres. No models were obtained from culture day 7 as these were too degraded (c). Macroscopic images (a - c) showed a strong model deterioration over time.

Macroscopic images of a human and rabbit hybrid cornea 3D model

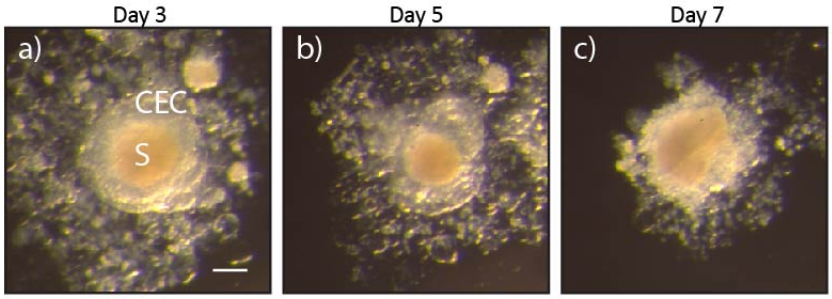

Figure 73: Macroscopic dark field images of a hybrid human and rabbit model at days 3, 5 and 7

a) – c) show macroscopic images of double spheres made of the rabbit stromal component (S) at the centre of the sphere and human corneal epithelial cells (CEC) coated around the rabbit stromal core. Images were taken with a Zeiss Axiocam. Scale bar: 100µm.

Immunohistochemistry of human/rabbit hybrid cornea 3D model

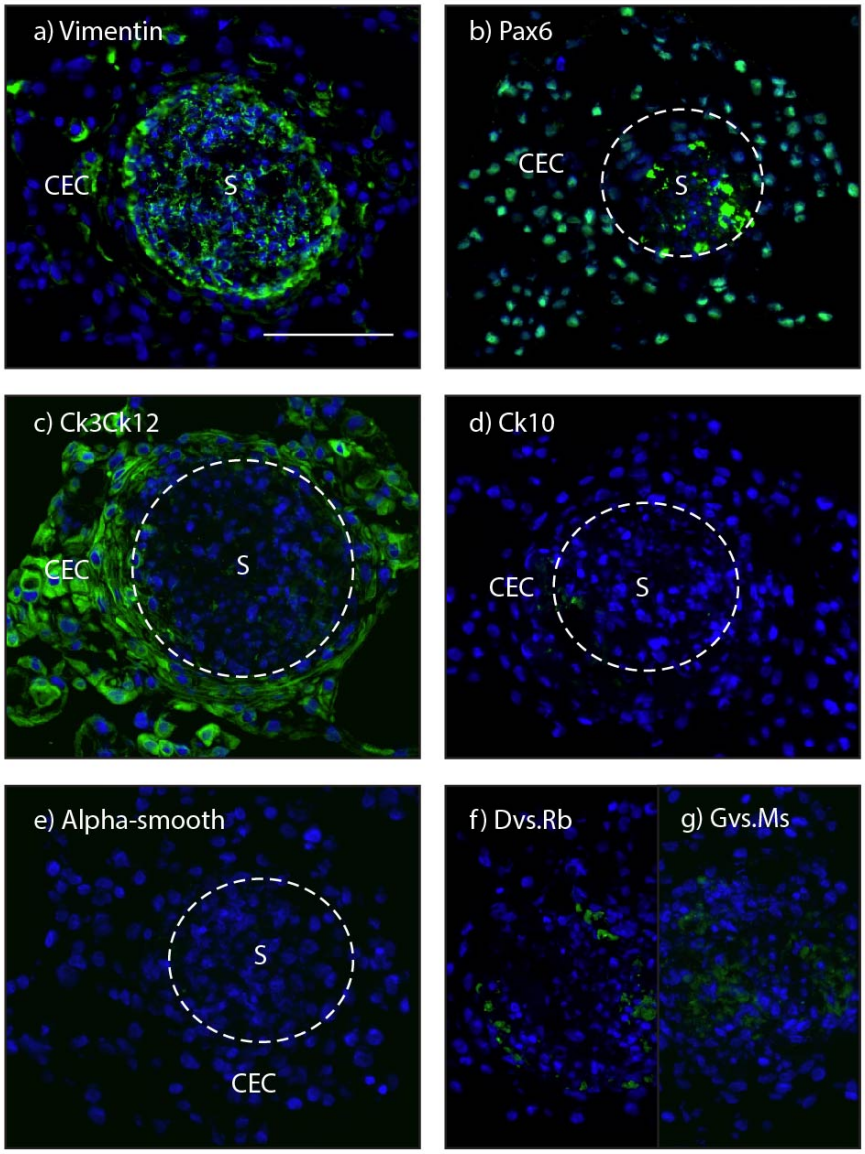

Figure 74: Immunohistochemistry of the human and rabbit hybrid 3D model at day 5

a) – e) show immunohistochemistry of the human and rabbit hybrid model at day 5 stained with the respective markers. f) represents two negative controls overlapping. The rabbit stromal core is marked as (S) and the human corneal epithelial cell coating as (CEC). All images were taken with an Axiovert Zeiss microscope. Scale bar: 100µm.

Immunohistochemical analysis in Figure 74 showed vimentin expression within the stromal compartment (a) as well as in some of the CEC cells around the stromal core. Nuclear Pax6 (b) and cytoplasmic Ck3Ck12 (c) staining were seen to be both strongly expressed in the CEC layer. No αSMA expression was observed in the models (e).

The hybrid model showed very strong Pax6 and Ck3Ck12 staining in the human CEC layer when combined with the rabbit stroma in 3D.

4.4 Discussion

In the work described in this chapter I created a refined bilayered model of the cornea, using a modified hanging drop culture technique – initially using cells form the rabbit cornea, then subsequently with human cells. Stromal and epithelial cells in the model displayed many characteristics of their counterparts *in vivo*, and analysis suggested that active epithelial-mesenchymal interactions were driving changes in gene expression.

The first part of this study, involving the establishment of stromal 3D spheres using rabbit stromal keratocytes from the upper or whole region of the stroma, proved to be more challenging than anticipated. Some inconsistency and variation was observed between different plates of spheres in the same run, possibly due to microclimate and humidity issues within the incubators. Currently this issue is being investigated and alternative ways of controlling moisture within petri dishes are being tested.

Successful sphere formation was also found to be influenced by passage number. Lower passages did not form spheres at all, but at later passage number the same cells successfully made spheres. Superficially this might appear surprising as it is would be expected that stromal keratocytes and mesenhcymal cells would overall lose their cell identity with time in culture, making them less likely to reverse to an *in vivo* phenotype (Branch *et al*., 2012; Banfi *et al*., 2000; Baxter *et al*., 2004). However in our laboratory the same phenomenon has also been observed with skin dermal fibroblasts. Therefore this suggests that the cells are losing some feature which, in early passage, is more evident and that might inhibit adhesion. One possibility is some extracellular element, for example it has long been recognised that some cultured cells possess a pericellular coat of hyaluronan (Clariss and Fraser, 1968) and now known to be scaffolded by cell projections (Kultti *et al*., 2006). Perhaps loss of this coat, or something equivalent over time allows spheroid formation.

When comparing rabbit upper vs. whole stromal 3D spheres to their 2D counterparts and *in vivo* stroma through qRTPCR, the amount of RNA extracted from 3D spheres was very low, something not seen for skin dermal 3D spheres. In order to test the viability of stromal spheres, these were put back into 2D culture, where fibroblasts adhered and grew out of the spheres (data not shown).

It has been shown that fibroblastic activation of native stromal keratocytes caused by injury or when placed in 2D cultures, modulates their crystalline protein expression, by down-regulating ALDH1a1, lumican and keratocan and to significantly up-regulate αSMA (Jester *et al*., 2012). It has also been shown that placing stromal activated fibroblasts in three-dimensional cultures, partially restores the quiescent and native keratocyte phenotype by expressing ALDH1a1 and drastically down-regulating αSMA (Thompson *et al*., 2013).

Analysing the single upper and whole 3D stromal spheres compared to their counterparts indicated that stromal keratocytes had potentially assumed a quiescent phenotype when placed in 3D cultures. This was indicated by the absence of αSMA expression in stromal 3D spheres as was also the case in the *in vivo* stroma. Stromal keratocytes in 2D monolayers on the other hand exhibited strong αSMA expression, indicating a mitotically active fibroblastic phenotype. This showed that the utilized 3D spheroid environment was suppressing αSMA which is associated with activated fibroblasts. This result was also shown by qRTPCR in both upper and whole stromal single spheres, indicating αSMA was down-regulated at both at a protein and gene expression level.

Analysis of stromal keratocyte *in vivo* markers by qRTpcr for both upper and whole stromal spheres, using different donors showed partial recovery of some of the markers, such as GAPDH where relative gene expression levels in 3D upper and whole stromal spheres almost reached the same level found in the *in vivo* stroma. qRTPCR GAPDH results for upper stromal 3D spheres was found to be significantly up-regulated compared to the 2D cultures. However, Lumican was only partially expressed in 3D spheres and the characteristic phenotype marker keratocan as well as the crucial crystalline marker Aldh1a1 were not found. This result indicated that a) αSMA expression in 3D spheroid cultures was not key in regulating presence or absence of Aldh1a1 and keratocan within these 3D sphere cultures. It also suggested that possibly the cellular organization of stromal keratocytes within the 3D spheres was not optimal and did not replicate the keratocyte cell organization found in the *in vivo* stroma, where their orientation is horizontal, with gaps between one keratocyte cell and the next (Pinnamaneni and Funderburgh., 2012). The tight and compact nature of the model, together with its spherical shape confers a very different keratocyte orientation. Another factor potentially contributing to the absence of crucial stromal markers when testing

3D stromal spheres is time. RNA was extracted from 3D spheres after 3-4 days in culture, possibly not long enough for some proteins to be expressed or for rRNA expression to reflect the changed environment. In a study by Thompson et al., 2013, that used a 3D collagen film to culture rabbit stromal keratocytes *in vitro*, found that ALDH1a1 was partially recovered in the stromal keratocytes. Down-regulation of αSMA at almost undetectable levels analysed by immunofluorescence and significant up-regulation of ALDH1a1 that was assessed with quantitative real-time pcr were observed. This study also investigated the cell density of stromal keratocytes placed into the collagen gels and αSMA was seen to be down-regulated in both instances. The possibility exists that stromal keratocytes placed in the 3D spheroids were in an extremely compact environment, therefore unable to produce native stromal extracellular matrix. This could potentially explain the absence of keratocan and Aldh1a1 in 3D stromal spheres.

Various studies have attempted to reverse the stromal fibroblast phenotype with serum free cultures and also by blocking TGF-β signalling, known to be crucial for myofibroblast differentiation (Jester *et al*., 2002; Watsky *et al*., 2010; Kawakita *et al*., 2006). Furthermore, stromal keratocytes were found to express characteristic markers found in *in vivo*, such as keratocan, lumican and decorin, as well as collagen tupe-I, when cultured in serum free conditions containing retinoic acid (Gouveia & Connon, 2013). It is known that the growth factor TGFβ, largely involved in wound healing in the cornea, induces αSMA expression and also causes the phenotypic change of the stromal keratocytes into myofibroblasts and fibroblasts (Hogan *et al*., 1971). During keratocyte phenotypic change to activated fibroblasts, crucial functionalities are lost such as the ability to express corneal crystalline proteins, known to be involved in maintaining transparency in the cornea.

Therefore, the absence of αSMA expression in stromal 3D cultures does not necessarily mean that stromal keratocytes have returned to their native phenotype, instead it indicates down-regulation of TGF-β, which is known to activate αSMA.

The next part of this study involved the establishment of rabbit cornea models using the spheroid hanging drop culture method, investigating the use of upper, whole and limbal stromal keratocytes as mesenchymal compartment in the model.

The first four models established using upper stromal keratocytes were all made with different biological samples and also showed very variable expression of corneal and stromal markers. Passage number of the stromal keratocytes used to make the inner compartment of the model seemed to influence the model outcome; a higher stromal passage was not able to sustain the corneal epithelial phenotype. This was seen in model 1, where Pax6 expression in the CECs resulted cytoplasmic andstrong αSMA expression was found to be activated both in stromal and epithelial cells at culture day 7, therefore indicating transformation of both cell types into fibroblastic phenotypes.

On the other hand, a lower passage number such as P3 stromal cells used in model 2, created spheres after 7 days. This model showed an improved Pax6 and Ck10 expression, however Ck3Ck12 decreased over time and no Aldh1a1 was found to be expressed. Absence/low expression of Aldh1a1 indicated that cells had no light scattering properties. αSMA expression was switched on at day 7 indicating stromal keratocytes lost quiescence.

The effect of different culture media was investigated to improve the models markers expression and lifespan in culture. Aqueous humour, LEM and higher percentages of rabbit serum were investigated in models 3 and 4, however no particular improvement was noted in the models placed in the media alternatives, therefore the best culture medium remained the same.

The 5th model established using limbal stromal keratocytes at a relatively higher passage (P7) than those used in the previous three models (models 2, 3 and 4) showed great improvement especially in Aldh1a1 and Ck3Ck12, however Pax6 expression remained very low.

The 6th rabbit model established with whole stromal keratocytes resulted to be the best among them all, kept in culture for 10 days, which was the longest observed, and expressing as well as maintaining expression of all markers at high levels until day 10. Possibly the last models have generally shown some improvement due to personal technical improvement in establishing the models. Unfortunately models utilising whole and limbal stromal keratocytes have only been produced once, therefore it is not clear yet whether the whole stromal model has some advantages compared to the models made with upper stromal keratocytes.

The epithelial-mesenchymal interaction study investigating Aldh1a1, Pax6, Ck3Ck12 and Ck10 immunofluorescent staining in rabbit single corneal epithelial 3D spheres, as well as combined to the stromal 3D layer, indicated that the corneal stroma plays an essential part within the *in vitro* 3D model, conferring important signals to the CEC layer. This was shown by the fact that single CEC 3D spheres retain their cell identity even when un-coupled from the underlying mesenchymal layer (as seen for Pax6 and Ck3Ck12 expression), however, they do not retain stem cell identity or corneal epithelial functionality, as seen by the lack of Ck10 and Aldh1a1 expression respectively, when not in contact with the stromal compartment. This short experiment therefore raises the question whether keratocan expression could also be activated in the stromal compartment in 3D when in contact with the epithelial layer. This could not been investigated due to the lack of the antibody at the time.

To assess cell viability within the models, once fully formed, some were placed back into culture, either directly on plastic culture dishes or on inactivated 3T3 mouse fibroblasts. Cells within the models proliferated when placed back into culture. More epithelial-like cells were seen on 3T3's feeders, while more fibroblastic cells were observed when plated on plastic. Data is shown in the Appendix, Figure 3, section 8.1.3.

The last three models were made with human limbal CEC and stromal cells from the limbus. The general outcome of these three models was the lack or almost absent Ck3Ck12 expression, however all expressed Pax6. The corneal epithelium was shown to be degrading from the very beginning of the cultures, possibly reflecting the low quality human corneal epithelial tissue used. Human corneas received for research were a couple of months old and often no primary cultures could be established at all. For optimal results fresh corneal tissue is required for both stromal and CEC extraction and culture. Also, the three described models could not be immuno-stained with Aldh1a1 or Ck10 being markers specific for the rabbit only. This limited the interpretation of the model's results.

In order to investigate whether stroma or CEC were responsible for low markers (Ck3Ck12 mainly) expression, a hybrid model made with rabbit stromal keratocytes and human CEC was established. Although the CEC layer still seemed to look fragile and degraded, Ck3Ck12 and Pax6 were strongly expressed, indicating that the human

stromal keratocytes in the previous human models could be responsible for the previously described results.

The established novel cornea 3D models have shown a positive improvement when using rabbit corneal cells. Aldh1a1 expression was found to be present when the stroma and the epithelium were in contact with each other within the 3D culture sphere environment, thus indicating that epithelial-mesenchymal interactions were taking place and were necessary within the models to activate this transparency marker in both cell types. This has not been previously shown in a 3D cornea model.

The corneal epithelial layer within the 3D models expressed corneal specific markers Pax6 and Ck3 Ck12 and often, but not always, Ck10 (Limbal epithelial marker in the rabbit), Aldh1a1 after 3 days of culture. Aldh1a1, Ck10 markers expression in the rabbit models were highly dependent on epithelial-mesenchymal interactions, whereas Ck3Ck12 and Pax6 expressions were up-regulated in the human model when combined with rabbit stromal keratocytes in a 3D spheroid model. Epithelial-mesenchymal interactions have been studied in organotypic rabbit and human cornea 3D cultures, where epithelial stratification was only present when combined with the stromal fibroblasts (Kobayashi et al., 2015). In addition, the study described Ck3 and Ck12 expression only at day 9 of culture. Pax6 expression was often found in the cytoplasm rather than in the nucleus in the corneal epithelial layer of the rabbit and human 3D models. This could probably be due to the quality of the cells or/and of the sections cut.

This cornea 3D model has major advantages over other models as it does not require any additional biomaterials or scaffolds, it can be reproducible in a large number and it does not require large numbers of cells.

Although the model is not perfect as it lacks a basement membrane, it has shown to express the main corneal markers, including Aldh1a1 indicating transparency within the model. The model is a great tool to study epithelial-mesenchymal interactions as it can be modified very quickly, adding or changing cell types to use on it. In addition, the spheroids created more possibly resemble an embryonic/foetal cornea due to the high number of cells in each layer, while adult corneas have fewer cells in the stroma and more extracellular matrix. Moreover, an embryonic-like stroma is potentially more effective to use for reprogramming, than an adult stroma, as the former will contain more early corneal developmental signals.

This still has to be refined by using human cells from freshly extracted corneas. A limitation of this study is the organization of the stromal keratocytes within the model, possibly making this only available to a limited number of applications, such as using it for high throughput screening to evaluate toxicity testing. Most importantly, it is a good model to study epithelial-mesenchymal interactions in the cornea as well as potentially use it to perform reprogramming studies as it quickly can be formed using different cell types. In the next Chapter, the spheroid model was used in a short attempt at reprogramming skin keratinocytes.

5 Reprogramming hDS and skin epithelial cells into corneal epithelial cells

5.1 Introduction & Aims

In this final chapter two reprogramming studies that involved the use of the 3D sphere culture system technique, developed in the previous Chapter 4, were explored. The final aim of both studies was to ultimately reprogram skin keratinocytes and human dermal sheath cells into corneal epithelial cells. It is known that the opposite, cornea to skin, is possible as demonstrated in a study by Pearton *et al*., 2005 where rabbit corneal epithelial trans-differentiation into epidermis was achieved by placing the corneal epithelium in close contact with mouse embryonic dermis. This study also underlined the reprogramming potential of the mesenchymal layer of the skin (dermis).

As discussed in the main Introduction in Chapter 1, various studies have attempted using different cell sources to be reprogrammed into corneal epithelial cells, such as oral mucosal epithelial cells (Nakamura *et al*., 2003), mesenchymal stem cells (Ma *et al*., 2006), embryonic stem cells (Ahmad *et al*. 2007), neural crest derived stem cell-like cells (Brandl *et al*., 2009) and immature dental pulp stem cells (Gomes *et al*., 2010). However none of these alternative cell sources resulted to be successful candidates. The study by Blazejewska *et al*., 2009, showed that hair follicle derived stem cells expressed corneal epithelial markers when placed under specific culture conditions. This showed the high degree of plasticity of these cells by simply modifying their microenvironment. However, the work carried out by Blazejewska *et al*., 2009, did not show a long-term establishment of corneal epithelial markers expression. In a study by Hayashi *et al*., 2012, corneal epithelial cells were generated from induced pluripotent stem cells that were derived from human dermal fibroblasts and corneal limbal epithelial cells.

The main focus in this study was to reprogram cells by using environmental modifications (3D spherical culture) as well as utilising the natural reprogramming ability of the mesenchymal layer of the cornea (stroma).

The study previously described in Chapter 3, used hair follicle keratinocytes with the aim to reprogram these using the corneal epithelial cell culture conditions in 2D. This study was quickly abandoned due to results showing that there were no changes in hair follicle keratinocytes cell identity. For this reason a cornea 3D model was created in

Chapter 4 that would re-create the environmental conditions found in the *in vivo* cornea and also by focusing on the mesenchymal corneal stromal keratocytes. Using mesenchymal stem cells in three-dimensional spheroid cultures has been reported to enhance their ability to differentiate as well as microarray analysis indicating a greater expression in genes involved in cellular architecture and extracellular matrix in these cells when placed in 3D (Genever 2010; Frith *et al*., 2010), thus underlining the idea that 3D culture methods re-create a cellular environment that is more similar to that found *in vivo*.

As mentioned earlier in the main Introduction in Chapter 1, there is a strong need in finding alternative cell sources that can be reprogrammed to corneal epithelial cells for transplantation purposes in cases of bilateral corneal disease. The potential of being able to use a patient's own cells to reprogram into corneal epithelial stem cells for transplantation would mark a successful new therapeutic strategy to treat many corneal diseases. In this study skin epithelial cells have been used in an attempt to reprogram these into corneal epithelial cells due to the many similarities shared with the latter: corneal and skin epithelium both are characterised by their stratified epithelial morphology and by their stem cell maintenance marked by p63 expression in the basal cell layer staining positive for Cytokeratin 5 and 14 (Pellegrini *et al*., 2001; Koster *et al*., 2004). Recent work by Ouyang *et al*., 2014 described a novel role for WNT7A and Pax6 acting together in determining skin epithelial stem cell trans-differentiation into corneal-like epithelium. This was shown by a series of knockdown experiments as well as by transducing Pax6 in skin epithelial stem cells. The work by Ouyang *et al* was published during the course of the first part of this study described in section 5.3.1, in which transfection of human dermal sheath cells with the transcription factor Glis1 was performed. This was a pilot experiment that had been previously tested by a colleague and first results had indicated positive Pax6 expression in the Glis1 transfected hDS 3D spheres. Although the initial idea had been to transfect human skin cells with Pax6, this could not be performed at the time due to problems concerning the plasmid vector. For this reason, the transcription factor Glis1 was utilised instead to transfect hDS cells in order to activate Pax6 expression in these cells. Glis1 had been chosen by a colleague as this had shown to promote direct reprogramming in somatic cells (Maekawa *et al*., 2011). In the study described by Maekawa *et al*., DNA microarray analysis showed that Glis1 was promoting a number of pro-reprogramming pathways such as Myc, Nanog,

among others, including Wnt and the epithelial-to-mesenchymal transition. For this reason Glis1 transcription factor seemed interesting to test in human skin cells.

The second part of this study described in section 5.3.2 aimed at reprogramming skin epithelial cells into corneal epithelial cells using the 3D sphere culture system previously described in Chapter 4. In this study human skin epithelial cells (keratinocytes) were used to double-coat human corneal stromal 3D spheres. The aim was to utilise environmental and epithelial-mesenchymal interactions taking place between the two cell types, hoping that stromal mesenchymal cells in 3D cultures had acquired *in vivo* functionality and were able to reprogram skin keratinocytes into corneal epithelial cells. In the previous Chapter 4, results shown in section 4.3.4 Figure 76 and Figure 77, indicated that the 3D rabbit stroma had the potential to activate and/or increase expression of corneal epithelial markers within the corneal epithelial cell layer, such as the crystalline transparency marker Aldh1a1, Ck10 (in the rabbit found to be only expressed in the limbus) and corneal epithelial differentiation markers Ck3 and Ck12. This clearly indicated epithelial-mesenchymal interactions and the corneal stroma sending corneal specific signals to the epithelium. For this reason it was believed that placing skin keratinocytes on the corneal stroma in 3D could potentially push these to become more like corneal epithelial cells.

To summarise, the aims in this chapter are:

- Reprogramming hDS cells into corneal cells by transfecting these with Glis1 and placing these in 3D culture. This was believed to activate Pax6 expression within these cells. 3D spherical cultures were stained and compared to un-transfected 3D as well as the same transfected and un-transfected cells in 2D cultures.
- Reprogramming skin epithelial into corneal epithelial cells in a 3D culture system (bilayered spheres), using the mesenchymal corneal stromal keratocytes as the core within the double spheres onto which skin epithelial cells are in direct contact with. This was a short pilot study and bilayered spheres were stained with Pax6, Ck3Ck12 and Vimentin antibodies only.

5.2 Materials & Methods

All the experimental procedures carried out in Chapter 5 were conducted in compliance with Durham University Health & Safety Policy according to the Control of Substances Hazardous to Health (COSHH) regulations. All tissue culture work was undertaken at Containment Level 2 using standard aseptic techniques.

5.2.1 Materials

All reagents used in this chapter were directly derived from the relevant suppliers and COSHH regulations were respected throughout their usage.

5.2.1.1 Cells

Human stromal fibroblasts used in this chapter were the same ones used in Chapter 4. At the time of this experiment only the very first stromal fibroblast sample was available at P14. The stromal cell extraction method is described in Chapter 4 in the Methods section 4.2.2.1.

Human dermal sheath cells and human skin keratinocytes were extracted from human skin that was donated for research by the Durham hospital. The tissue processing and cell extraction method as well as the growth of these cells was performed by a member of the group under standardised methods and protocols.

5.2.1.2 Media & tissue culture components

Human stromal fibroblasts were first grown in standard medium as previously mentioned in Chapter 4 in the Materials section 4.2.1.2. Human dermal sheath cells were grown in Standard medium (described in the Materials section 4.2.1.2) and human skin keratinocytes were cultured in Epilife^{TM} growth medium (Invitrogen).

5.2.1.3 Cell Transfection

Cell transfection was performed using the Amaxa Human Dermal Fibroblast Nucleofactor Kit (Lonza). The kit was composed of the Human Dermal Fibroblast Nucleofactor Solution, the pmaxGFP Vector (0.5µg/µl in 10mM Tris pH 8.0), certified cuvettes and plastic pipettes. The cell transfection was achieved by using the Nucleofector Device.

The cells were all transfected with the Glis1 gene. The genetic sequence was chosen and ordered by a member of the lab, Dr. Aaron Gardner as this was also part of his own project. The Glis1 gene construct sequence was ordered from Invitrogen Life Technologies and is listed in the Appendix. The construct was optimized for being Homo sapiens specific. The Glis1 gene construct was recombined into a vector by Dr. Aaron Gardner who used the Invitrogen Vivid Colors pcDNA 6.2/EmGFP-Bsd/V5-DEST Mammalian Expression Vector Kit.

5.2.1.4 Histology

Transfected and un-transfected 3D spheres were embedded in O.C.T matrix (Fisher) in small (7x7x5mm) disposable base molds (Fisher) before snap freezing these in liquid nitrogen. The samples were then cryo-sectioned using the human cryostat (Leica CM1900UV). Sections were placed onto Colourfrost Plus Yellow slides (Fisher) and left to dry at room temperature before performing Immunohistochemistry.

H&E staining was performed on the stromal-keratinocyte double spheres only and components are listed in the Appendix section 8.2.

5.2.1.5 Antibodies & Immunohistochemistry

Primary and Secondary antibodies used in Chapter 5 are all listed in Table 24 and 25 below.

Target	Raised in:	Dilution used	Supplier
Pax6	Rabbit	1:100	Sigma
Glis1	Rabbit	1:100	Sigma
Ck3Ck12	Mouse	1:50	Abcam
Vimentin	Mouse	1:100	Amersham

Table 24: Primary Antibodies

Secondary Antibodies	Raised in:	Dilution used	Supplier
Alexa Fluor 488	Goat anti rabbit	1:500	Invitrogen
Alexa Fluor 488	Goat anti mouse	1:500	Invitrogen

Table 25: Secondary Antibodies

Primary and Secondary antibodies were diluted in the dilution buffer listed in Table 26 below.

Reagent	Composition	Supplier
Permeabilisation Buffer	1% Triton X-100 (in 1x PBS)	Sigma-Aldrich
Quenching buffer	100mM Glycine (in H_2O)	Sigma-Aldrich
Diluting buffer	0.5% Tween 20 (in 1x PBS)	Sigma-Aldrich
Blocking Solution	5% Goat Serum in Diluting buffer	Sigma-Aldrich
Mowoil	n/a	Sigma-Aldrich
DAPI	DAPI (diluted 1:1000 in Diluting Buffer)	Invitrogen
4% PFA	(in 1x PBS)	Sigma-Aldrich
1x PBS (pH 7.4)	n/a	n/a

Table 26: Materials and solutions for Immunohistochemical analysis

5.2.2 Methods

5.2.2.1 Tissue Culture

Human stromal fibroblast extraction and culture has already been explained in the Methods section 4.2.2.1 in Chapter 4. Human stromal fibroblasts were cultured in Standard medium and switched to Species specific medium prior to using them for making single 3D spheres.

Primary human skin keratinocytes were established from fresh skin samples that were cut to 2x2mm^2 small pieces and were plated to the bottom of a 35mm diameter culture dish and cultured with MEM containing 20% foetal bovine serum and 1% antibiotics/antimycotics. After 3 to 4 days the cultures were passaged using Tryple Express (Gibco) and cultured in Epilife^{TM} (Invitrogen).

Human dermal sheath cell cultures were established from human scalp samples. Briefly, skin samples were dissected and under a dissecting microscope each follicle was removed and micro-dissected to isolate the surrounding dermal sheath. At least 10 dermal sheaths were placed in one 35mm diameter culture well and cultured in MEM 10% FBS supplemented with 1% PenStrep. Dermal sheath cells were passaged in Species specific medium prior to transfecting them with Glis1.

3D single and bilayered spheres were established using the same techniques explained in the Methods section 4.2.2.2 in Chapter 4.

5.2.2.2 Glis1 Transfection

Glis1 transfection of cells was performed using the Amaxa Human Dermal Fibroblast Nucleofector kit [Lonza]. Prior transfection, cells were passaged in Species specific medium until 80% confluent. This took up to two days. Cells were then trypsinised with 0.25% Trypsin-EDTA for 5 minutes, the Trypsin was neutralised with the same amount of Species specific medium, cells were spun down at 1000rpm for 5 minutes, the supernatant removed and the sample was re-suspended in one ml of Species specific medium. Cells were counted using a Haemocytometer. 200,000 cells were needed for transfection, the remaining cells were plated back down in a T25 flask in Species specific medium. The 200,000 cells were placed in a 2ml tube and spun down again at 1000rpm for 5 minutes to remove any remaining trace of medium. The supernatant was carefully removed without disturbing the pellet. The pellet was re-suspended in 100µl of Human Dermal Fibroblast Nucleofector Solution. Consequently, 2µl of the plasmid encoding the Glis1 gene were added to the sample and it was important that the plasmid was added to all samples (if multiple cell samples were transfected at the same time) at the same time. The sample was then vortexed quickly; the sample solution was pipetted into the cuvettes supplied by the kit making sure that no air bubbles were created within

the cuvettes that could interfere with an optimal transfection. The cuvettes were placed into the Nucleofector machine and the program specifically designed for human dermal fibroblasts called NHDF human, adult, high viability P-022 was selected. Once the program had finished, the cuvettes were removed from the machine and carefully transported back under the cell culture hood. 500µl of Species specific medium was added per cuvette and using the kit supplied plastic pipettes the sample was removed from the cuvette and plated into a tissue culture well of a 6-well plate. 2ml of Species specific medium was added to the well. The sample was incubated at 37°C and the medium was changed the following day. The 2ml of old medium was kept and dead cells were counted using a Haemocytometer. This gave an indication of cell viability after transfection. 48 hours post transfection, the transfected cells within the wells were visualised under UV light and a rough percentage of GFP positive cells (Glis1 transfected cells) was made. Cells were washed in 1xPBS, trypsinised with 0.25% Trypsin-EDTA, spun down and re-suspended in Species specific medium.

Around 20 single spheres were made using the transfected cells using the technique explained in the Methods section 4.2.2.2 in Chapter 4. The remaining cells were plated in 2D cultures in a 12 well plate onto coverslips and in Species specific medium.

In parallel, acting as a negative control, untransfected cells that had been plated back in T25 flasks at the beginning of the Glis1 transfection procedure were also placed in 3D and 2D culture systems using the same medium and technique used for the transfected cells.

Transfected and untransfected 3D single spheres were incubated for three days, on the third culture day macroscopic images were taken and spheres were consequently embedded in O.C.T matrix and snap frozen in liquid nitrogen for cryosectioning and immunofluorescent analysis.

Transfected and untransfected 2D cells were incubated for up to 5 days and they were washed in 1xPBS and fixed in 4% PFA overnight in the fridge at 4°C.

5.2.2.3 H&E & Immunofluorescent analysis

Embedding, sectioning and H&E staining of single and double-coated 3D spheres were performed using the techniques described in the Methods section 4.2.2.3 in Chapter 4.

Immunohistological analysis of single, double-coated 3D spheres and cells in 2D cultures was performed using the protocol described in the Methods section 4.2.2.3 in Chapter 4.

Immunofluorescent visualisation was achieved using the Axiovert Zeiss microscope and using the SP5 confocal microscope.

5.3 Results

5.3.1 Glis1 Transfection

The transcription factor Glis1 has been reported to promote direct reprogramming of somatic cells (Momoko *et al*., 2011). A previously short pilot study performed by a post-doc in the Durham laboratory had indicated that following Glis1 transfection of human dermal sheath cells placed in 3D cultures, positive expression of the eye developmental marker Pax6 could be observed in these cells. The following short experimental study described in this section was performed in order to repeat the previously reported findings with the same hDS donor cells as well as with a different hDS cell donor. In addition, transfected and untransfected hDS cells were kept in 2D culture and immunostained. This acted as a comparison to the transfected and untransfected hDS cells in 3D in order to investigate any potential morphological as well as immunofluorescent markers expression differences between transfected cells in 2D and 3D cultures systems.

5.3.1.1 Glis1 Transfection in human dermal sheath cells

The human dermal sheath cells (hDS) were used in this experiment were at P5. These were cultured in standard medium and passaged in Species specific medium before being transfected with the Glis1 transcription factor according to the described protocol in the Methods section 5.2.2.2. 24 hours post-transfection, detached cells were counted to assess cell viability. This resulted in 95% cell viability. 48 hours post-transfection the cells were visualised under the UV lamp (Fig. 75a) to assess the number of Glis1 transfected cells. Roughly 65% GFP positive cells were counted. hDS were placed into 3D culture as decribed in the Methods Section 4.2.2.2 in Chapter 4 and 3D spheres were left to form for three days. At culture day 3, dark field macroscopic images were taken (Fig. 75b) and the spheres were embedded in O.C.T, snap frozen, cryosectioned and the expression of Pax6 was investigated by immunofluorescence (Fig. 76). In parallel, transfected hDS in 2D culture were cultured on coverslips, as well as untransfected 3D and 2D hDS as a control. Untransfected 3D hDS spheres were also snap frozen in O.C.T

embedding matrix and cryosectioned. Transfected and untransfected hDS in 2D cultures were fixed and stained as described in the Methods section 4.2.2.3 of Chapter 4.

Glis1 transfected hDS cells in 2D & 3D culture

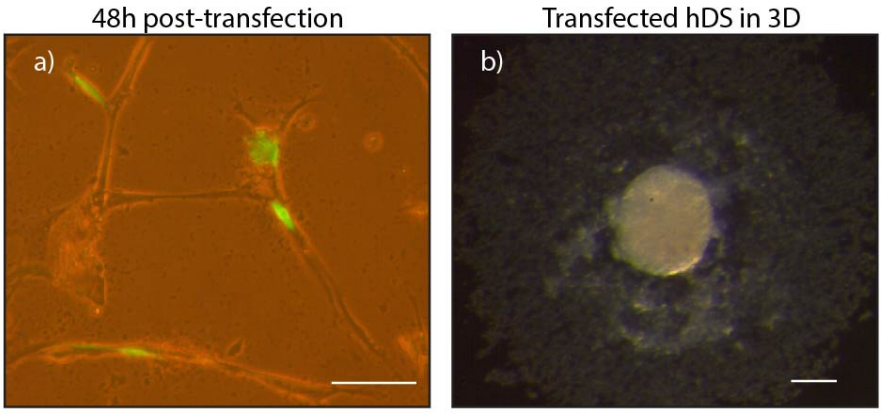

Figure 75:Glis1 transfected human DS 48 hours post transfection (a) and in 3D culture (b)

Human DS Cells visualised under UV (a) to assess GFP positive cells and Glis1 transfection rate. Transfected DS 3D spheres (b) at day3. Images were taken with an Axiocamera Zeiss microscope. Scale bars: 100µm.

Pax6 immunofluorescent staining of 3D & 2D hDS cells

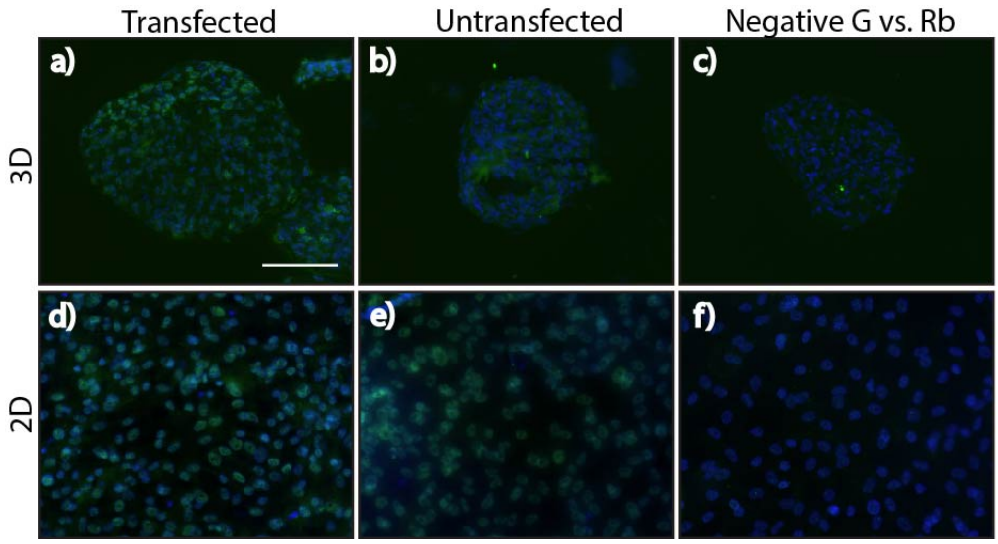

Figure 76: Immunofluorescent Pax6 staining of Glis1 transfected vs. untransfected human DS cells in 3D and 2D culture systems

Pax6 staining of Glis1 transfected human DS cells in 3D (a) and 2D (d) culture systems. Same untransfected hDS cells were stained with Pax6 in 3D (b) and 2D (e). Negative controls are displayed in c) and f). Images were taken with an Axiovert Zeiss microscope. Scale bar: 100µm.

Pax6 positive staining was seen in transfected hDS cells in 3D and 2D (Fig. 76 a,d). Pax6 expression within the transfected 3D hDS cells was particularly concentrated in the upper region of the sphere (a). No Pax6 positive staining was found in untransfected 3D and 2D hDS (b,e), although in untransfected 2D hDS cells green fluorescent staining is shown and this was due to a problem with the coverslip (as shown by the foggy appearance in image e).

5.3.1.2 Glis1 Transfection of hDS cells repeated with new donor

A new hDS cell donor was used to repeat the experiment performed in the previous section. The exact same procedures and methods were used as described previously. Human DS cells in this experiment were used at Passage 3.

The percentage of Glis1 transfected positive cells was similar as in the previous experiment having 50% (Fig. 77 a) GFP positive cells and cell viability was 85% high. hDS transfected and untransfected 3D spheres were similar in size (Fig. 77 b,c), however transfected hDS 3D spheres had a large amount of detached cellular debris floating around the sphere (b) compared to the very small amount of cell debris found in the untransfected 3D spheres (c).

Glis 1 transfected hDS cells in 2D & 3D culture vs. untransfected hDS in 3D

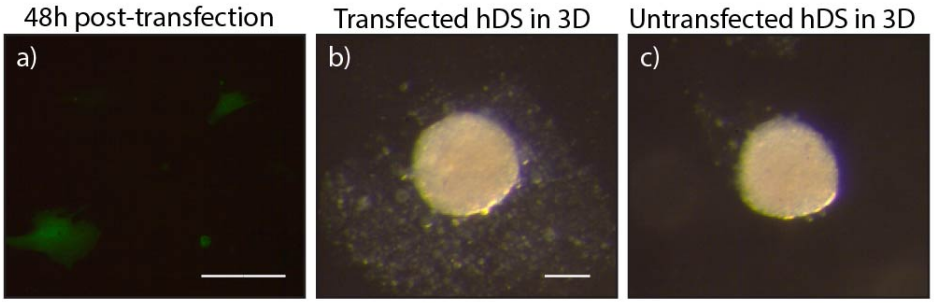

Figure 77: Glis1 transfected hDS 3D spheres vs. untransfected hDS 3D spheres repeated with a new donor

Human DS Cells visualised under UV (a) to assess GFP positive cells/Glis1 transfection rate. Transfected DS 3D (b) and untransfected DS 3D spheres at culture day 3 (c). Images were taken with an Axiocamera Zeiss microscope. Scale bars: 100µm.

3D and 2D transfected and untransfected hDS cells were analysed with immunofluorescent Pax6 and Glis1 staining. Glis1 immunostaining was introduced in this experiment to investigate the correlation between Glis1 expression within Glis1 transfected hDS cells and the amount of Pax6 expression. Furthermore, the question arose whether the amount of Glis1 expression was positively or negatively affected by the 3D and 2D cell culture systems.

Pax6 immunofluorescent staining of transfected and untransfected 3D hDS

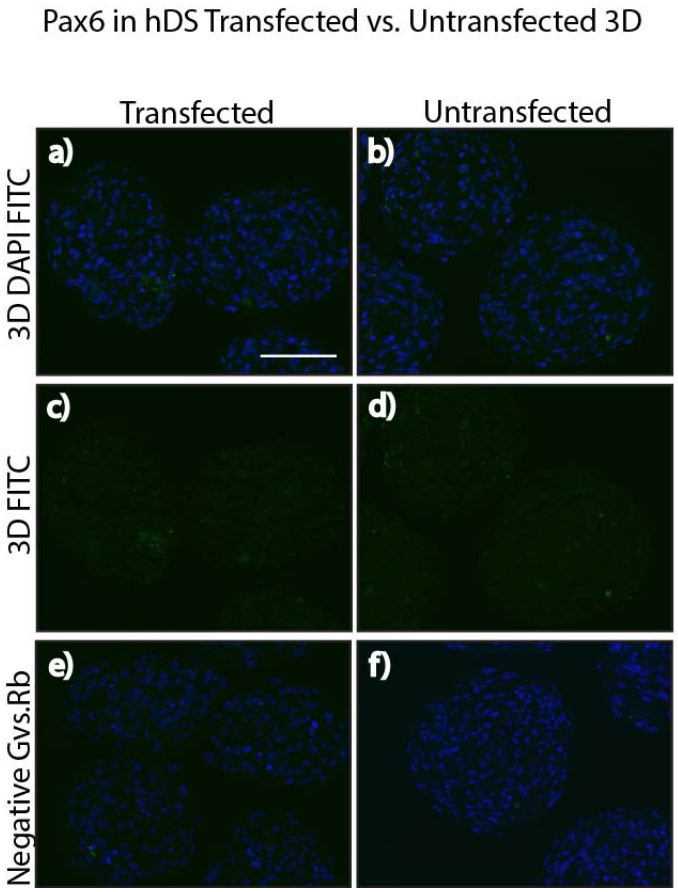

Figure 78: Immunofluorescent Pax6 staining of Glis1 transfected vs. untransfected human DS 3D spheres

Pax6 staining of Glis1 transfected human DS cells in 3D (a). Same untransfected hDS cells were stained with Pax6 in 3D (b). FITC only images shown in c,d. Negative controls are displayed in e,f. Images were taken with an Axiovert Zeiss microscope. Scale bar: 100µm.

Pax6 immunofluorescent results shown in Figure 79 indicated no Pax6 expression in transfected (a,c) and untransfected hDS 3D spheres (b,c). Also, there was no Pax6 expression in transfected and untransfected hDS 2D cells as seen in images g) and h) in Figure 79 below.

Pax6 immunofluorescent staining of transfected and untransfected 2D hDS

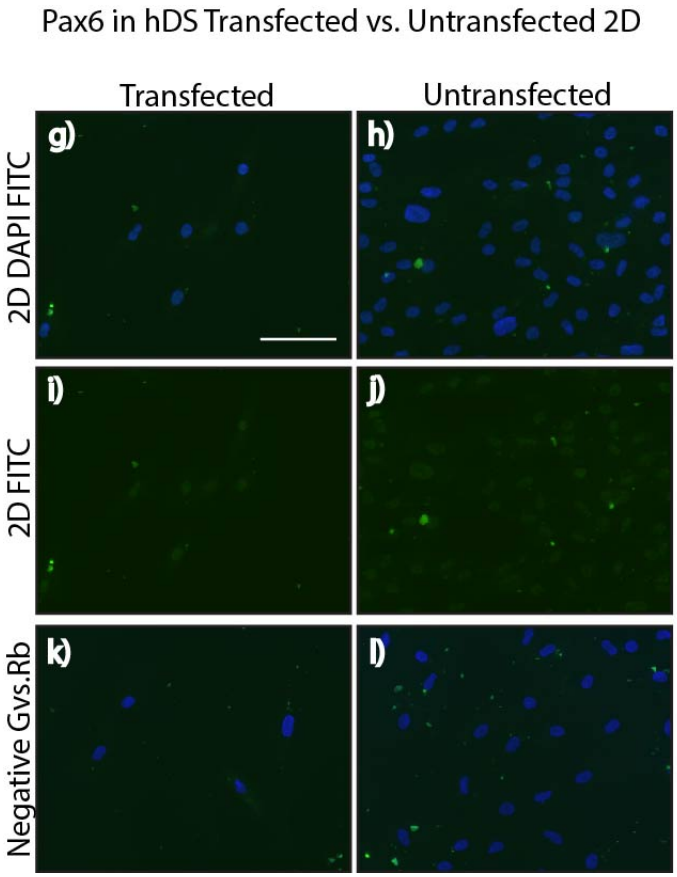

Figure 79: Immunofluorescent Pax6 staining of Glis1 transfected vs. untransfected human DS cells in 2D culture

Pax6 staining of Glis1 transfected (g,i) and untransfected (h,j) human DS cells in 2D cultures. Negative controls are displayed in k,l. Images were taken with an Axiovert Zeiss microscope. Scale bar: 100µm.

Glis1 immunofluorescent staining of transfected and untransfected 3D & 2D hDS

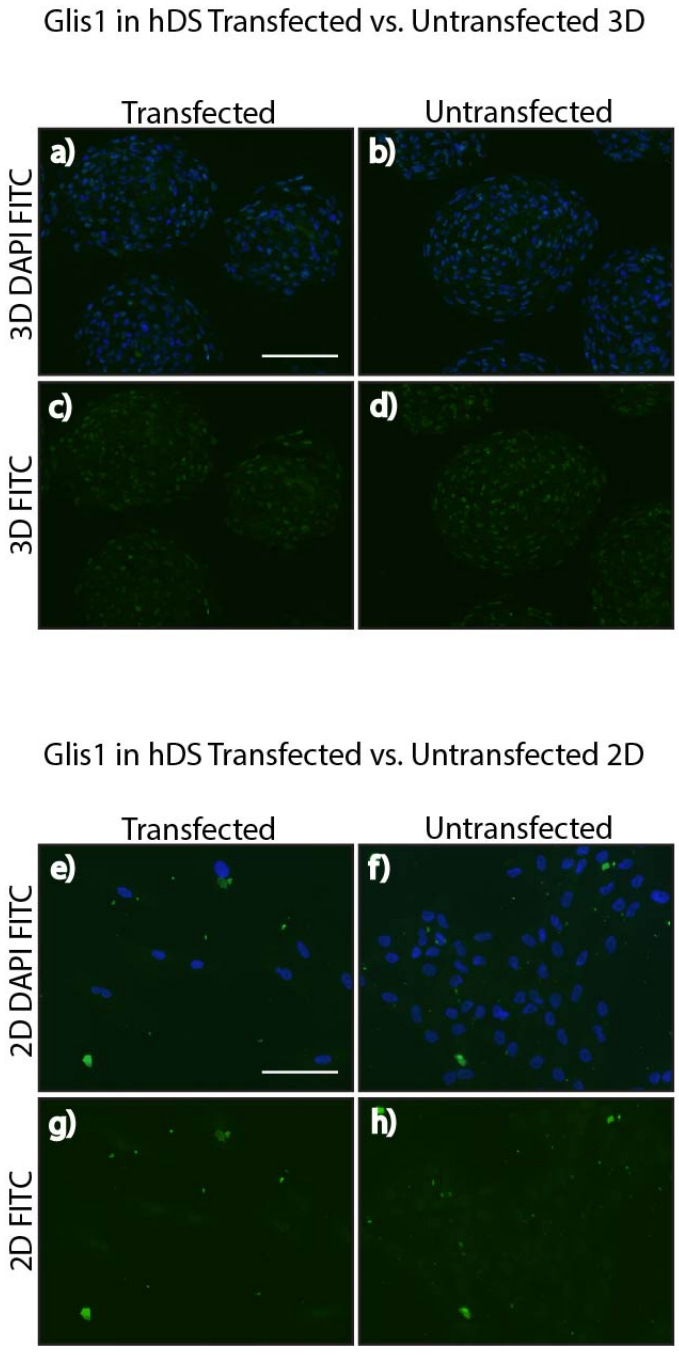

Figure 80: Immunofluorescent Glis1 staining of Glis1 transfected vs. untransfected human DS cells in 3D and 2D culture systems

Glis1 staining of Glis1 transfected human DS cells in 3D (a) and 2D (e) culture systems. Same untransfected hDS cells were stained with Glis1 in 3D (b) and 2D (f). Only FITC images were shown in c,d,g,h. Negative controls are the same as in Figure 91 and 92. Images were taken with an Axiovert Zeiss microscope. Scale bars: 100µm.

On the other hand, Glis1 expression was found in both transfected and untransfected hDS 3D spheres (Fig. 80, a - d) and not in the hDS 2D cultured cell equivalents (e - h).

The whole experiment was repeated again with a third hDS cell donor and results were inconclusive (data not shown), therefore excluding any correlation between Glis1 and Pax6 expression. In addition, Glis1 transfection was also performed on human dermal fibroblasts and human abdominal fibroblasts and results also showed no Pax6 activation. Human stromal keratocytes were also transfected with Glis1 in order to test whether Pax6 could be enhanced in these cells, however these cells did not survive the transfection protocol.

Originally it had been planned to transfect skin keratinocytes with Pax6, however as mentioned in the introduction, the Pax6 vector was not functioning and it had to be postponed. Due to time restrictions at the end of the PhD project this experiment could not be performed in the end.

The very last study described in the next section investigated human skin keratinocyte reprograming through corneal stromal interactions using the 3D bilayered sphere culture environment, thus focusing on epithelial-mesenchymal interactions and the three-dimensional culture environment as reprogramming tool.

5.3.2 Human corneal stromal – skin keratinocyte double 3D spheres

Human skin keratinocytes at Passage 2 were cultured in Epilife^{TM} under standard culture conditions. Human stromal keratocytes were first cultured in standard medium and then passaged and cultured in Species specific medium before being placed into 3D culture as previously described in the Methods section 4.2.2.2 of Chapter 4. 3D stromal spheres were allowed to form over three days. At culture day 3, the fully formed stromal single spheres were double coated with the human skin keratinocytes. The stromal-skin keratinocyte double coated spheres were cultured in 50% Species specific medium and 50% Limbal epithelial medium and the media was changed every other day. At intervals after the bilayered spheres were created (days 3, 5, 8 and 11), dark field macroscopic images were taken (Fig. 81 a - d) and around 10 bilayered spheres were snap frozen in

O.C.T embedding matrix, cryosectioned and their histological features (Fig. 81 e - g) and the expression of key markers (Fig. 82) were examined.

Human stroma & skin keratinocyte bilayered spheres – macroscopic & H&E images

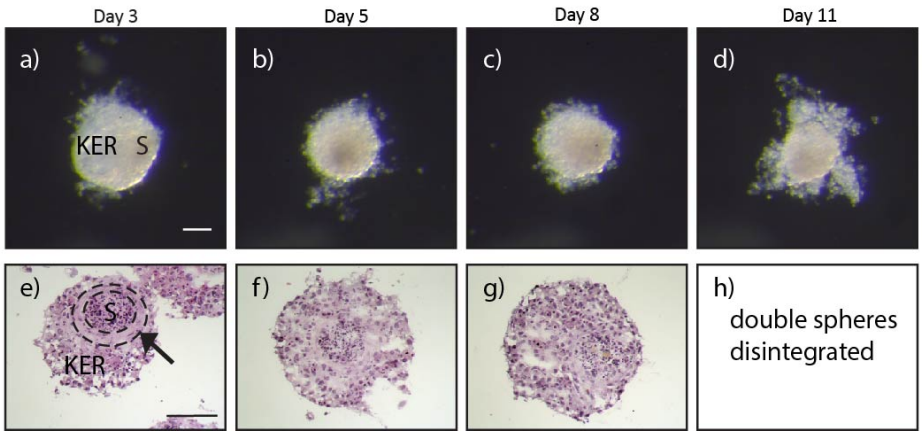

Figure 81: Human stroma – keratinocyte double spheres in a hanging drop culture, bright field macroscopic images & H&E over the period of 11 days

a) – d) show macroscopic images of double spheres made of the stromal component (S) at the centre of the sphere and skin keratinocytes (KER) coated around the stromal core. Images were taken with a Zeiss Axiocam. Scale bar: 100µm.

e) – g) H&E staining of the human stroma – keratinocyte double spheres at three given time points. Images were taken with an Axiovert Zeiss microscope. Scale bar: 100µm.

Small sized bilayered spheres with no tight outer borders were observed under the microscope (Fig. 81 a-d). The bilayered spheres were completely degraded at day 11 and no histological examination could be performed for that interval. The stromal core was almost not visible in the macroscopic images, especially at culture day 3 (a) and this was possibly due to the non-transparent nature of skin keratinocyte cells. Interestingly, histological examination of the bilayered spheres revealed a layered structure around the stromal core as indicated by the arrow in Figure 81 e. This three – layer effect is also a typical characteristic of the skin 3D model indicating the formation of a skin equivalent structure within the double-coated sphere. This observation had never been made in the rabbit or human cornea 3D models discussed in Chapter 4.

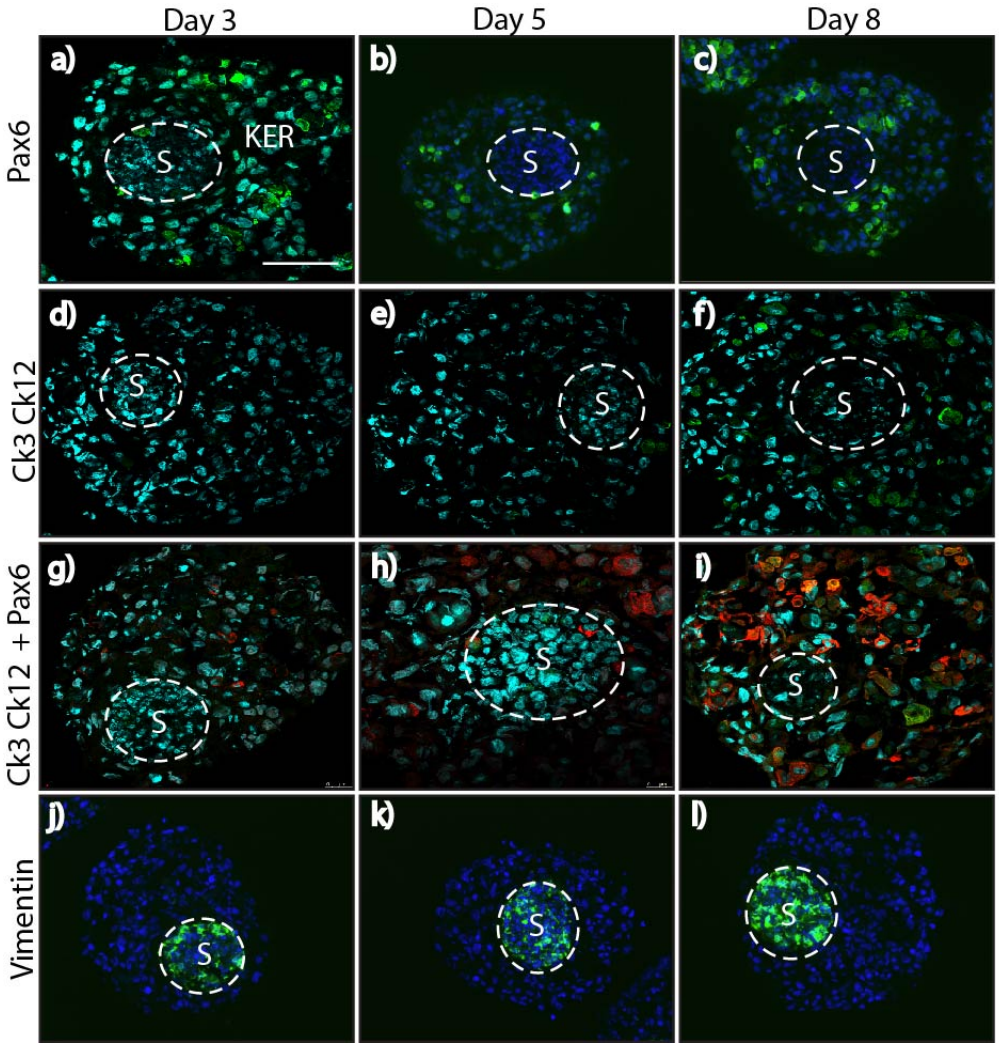

Figure 82: Immunohistochemistry of stromal – keratinocyte double spheres

a) – c) immuno stained with Pax6, d) – f) Ck3Ck12, g) – i) Ck3Ck12 (FITC) and Pax6 (Rhodamine) co-staining and j) – l) Vimentin. The stromal core is marked as (S) and the skin keratinocyte coating as (KER). Images were taken with a Confocal SP5 and an Axiovert Zeiss microscope. Scale bars: 50µm for a),d) – f) and 100µm for b), c), j) – l).

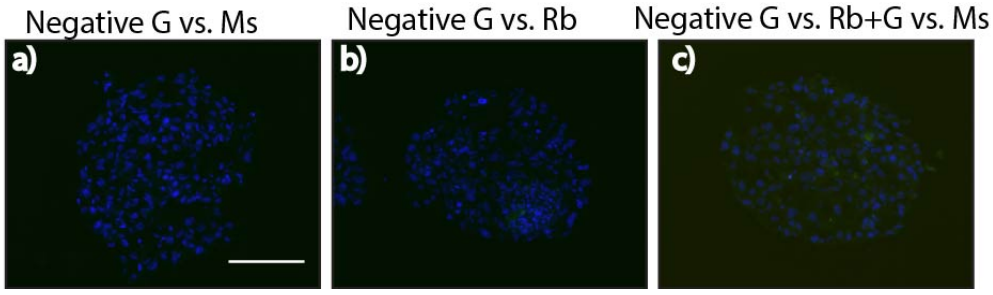

Figure 83: Negative controls for immunohistochemistry results in Figure 83

Images were taken with an Axiovert Zeiss microscope. Scale bar: 100µm.

Immunofluorescent analysis of the bilayered spheres in Figure 82 at culture days 3, 5 and 8 revealed an increasing positive Pax6 expression in skin keratinocyte cells from culture day 3 to day 8 (Fig. 82, a – c). Pax6 expression was not present in all of the skin keratinocyte cells, but rather present in several clustered areas. The corneal epithelial differentiation marker antibody Ck3Ck12 was not expressed at day 3. At day 5 only a few cells were Ck3Ck12 positive and at day 8 this was expressed strongly in skin keratinocyte cells (f). Pax6 and Ck3Ck12 immunofluorescent co-staining (Fig. 82, g – i) revealed that there was an increasing expression of both of the corneal epithelial markers together over time, with Pax6 being expressed at an earlier stage and more strongly and Ck3Ck12 expression following at a later stage. Furthermore, the majority of skin keratinocytes expressing Pax6 also expressed Ck3Ck12 at day 8 as seen by the orange coloured overlay effect (i). The mesenchymal marker Vimentin was used to routinely stain the mesenchymal stromal core as shown in images j – l. Negative controls for this experiment are shown in Figure 83.

This short pilot study was a first attempt at reprogramming skin keratinocytes into corneal epithelial cells using the 3D sphere culture environment and the corneal stroma as mesenchymal layer interacting with the skin keratinocytes. Results indicate that skin keratinocytes have gained some crucial corneal epithelial cell characteristics as shown by Pax6 and Ck3Ck12 positive staining and that their expression increases over time, thus reflecting a continuous evolvement of the cell identity change taking place in skin keratinocytes cells. Skin keratinocyte specific markers, such as Ck1 and Ck10 for instance, could not be tested at the time due to the very small number of double-layered spheres available and it is therefore not clear yet whether skin keratinocytes have completely lost their original cell identity. This would have to be further tested in additional experiments repeating this study. However, as previous published work has stated, the presence of Pax6 and Ck3Ck12 corneal specific markers is sufficient to indicate that the epithelial cells in question are of corneal identity and that as a result skin specific markers are down-regulated (Ouyang *et al*., 2014). In fact Pax6, Ck3 and Ck12 expression has shown to be absent in areas of diseased corneal epithelium (such as metaplasia) where transparency of the cornea is affected, whereas skin specific

markers such as Ck10 was found to be present in these diseased areas of the corneal epithelium, suggesting that corneal epithelial cells were turning into non-transparent skin-like epithelial cells (Ouyang *et al*., 2014).

5.3 Discussion

In the first results section 5.3.1 a short pilot study was described that aimed to use the transcription factor Glis1, indicated by a previous study by Maekawa *et al*., 2011 to have reprograming properties, to transfect human dermal sheath cells. Glis1 transfected hDS were found to express Pax6 in one of the hDS cell donors, as shown in Figure 76. This was observed first only in 3D hDS spheres by a colleague (data not shown), confirmed in Figure 76 and Pax6 was additionally found to be expressed in 2D hDS Glis1 transfected cells (Fig. 76). On the other hand, Pax6 was not found to be expressed in untransfected hDS 3D and 2D cells, thus indicating potential novel signalling mechanisms between Glis1 and Pax6 transcription factors. In order to confirm initial results, the same experiment was repeated twice with different hDS cell donors and results did not show any Pax6 expression upon Glis1 transfection indicating no correlation between Glis1 and Pax6. Pax6 activation with Glis1 transfection was therefore donor specific and due to time constraints and inconclusive results this study was abandoned. In addition to hDS cells, when human stromal keratocytes, human abdominal fibroblasts and dermal fibroblasts were transfected with Glis1 (data not shown) and these cell types tested did not survive the transfection protocol and/or showed inconclusive results any Pax6 including role of Glis1 was excluded.

The second and last part of this chapter described in section 5.3.2 outlined a short experiment aiming at reprogramming human skin keratinocytes into corneal epithelial cells by placing these in a 3D culture environment and in direct physical contact with human stromal mesenchymal keratocytes in 3D. Results showed Pax6 and Ck3Ck12 expression in skin keratinocytes, thus indicating a switch of the latter towards corneal epithelial-like cells. Work by Pearton *et al*., 2005, described corneal epithelial trans-differentiation into epidermis that was triggered by dermal developmental signals, by down-regulation of Pax6 and the consequent loss of expression of Ck3 and Ck12 markers.

It is therefore clear that the skin to cornea and vice versa trans-differentiation/reprogramming relies on Pax6 activation or down-regulation. This can be influenced by embryonic mesenchymal signals, such as in the study described by Pearton *et al*., 2005. The work carried out by Ouyang *et al*., 2014 showed that transduction of Pax6 in rabbit skin epithelial stem cells was sufficient in converting

these to corneal limbal stem cell-like cells. Because the spheroid created in the previous 3D cornea model study resembled much more to embryonic/foetal cornea, it indicates the possibility that corneal stroma in 3D spheroid structures are of an embryonic or of a less differentiated nature therefore holding strong reprogramming cornea mesenchymal signals that are able to reprogram skin keratinocytes to corneal epithelial-like cells. Further studies would need to be performed to assess these first results, however this study described a novel way to possibly induce the transition of skin to cornea via a 3D spheroid model. In contrast to the artificial ways of reprogramming cells into corneal epithelial cells, the method utilised in this chapter to reprogram skin keratinocytes through the 3D sphere culture environment solely relied on the 3D environment and the mesenchymal stromal keratocytes of the cornea both acting as reprogramming tools. Previous work by Espana *et al*., 2003 has shown that the limbal stroma controls the plasticity of the corneal epithelium, modulating corneal epithelial differentiation, proliferation and apoptosis towards a stem cell-like phenotype. In the study performed in Chapter 4 section 4.3.4 shown in Fig.58, it was observed that the 3D rabbit stroma had the potential to activate and/or increase expression of corneal epithelial markers within the corneal epithelial cell layer, such as the crystalline transparency marker Aldh1a1, Ck10 and corneal epithelial differentiation markers Ck3 and Ck12, as well as increase Pax6 and Ck3Ck12 expression, as shown in the human and rabbit hybrid model. This clearly indicated epithelial-mesenchymal interactions and the corneal stroma sending corneal specific signals to the epithelium when placed in a three-dimensional culture environment. Microenvironmental reprogramming has been shown to be a powerful tool even to reprogram cells of different embryological origins, as described by a study by Bonfanti *et al*., 2010, where thymic epithelial cells were reprogrammed to skin (endodermal and ectodermal origins respectively) through a an inductive skin microenvironment. This strengthens the idea that the corneal stroma could produce a strong inductive cornea microenvironment when placed in a 3D spheroid culture system. The study by Ouyang *et al*., 2014 described the role of Pax6 in determining LSC and CEC cell fate and differentiation and that the lack of Pax6 expression decreased Ck3 and Ck12 expression in the corneal epithelium and increasing expression of skin epithelial specific markers such as Ck1 and Ck10 was observed.

Further work investigating the expression of skin specific markers and other corneal epithelial markers would be necessary to strengthen and confirm these first results.

Once confirmed, this could become a novel way to reprogram skin keratinocytes into corneal epithelial cells solely by epithelial-mesenchymal interactions.

6 General Discussion & Conclusion

A scratch wound healing model was established in Chapter 2, where corneal epithelial cells were co-cultured onto 3T3 feeder cells, mechanically scratched and the expression of a set of markers were investigated using qRTPCR. This basic 2D scratch wound healing model was aimed at assessing the regeneration potential of LSC's *in vitro*. Results indicated variation between cultured donor's corneoscleral rings and expression of LSC's positive and negative markers was not conclusive. More recent work by Yoon *et al*., 2013 and Huang *et al*., 2015 have investigated a new way to measure the wound healing ability of specific corneal epithelial cell populations. The work carried out by Yoon and Huang showed that sphere-forming cells isolated from the peripheral cornea were good candidates for future transplantation use to regenerate the corneal epithelium. If the corneal wound healing topic would have been investigated further during the course of this PhD project, it could have been interesting to connect the 3D sphere work established in the later chapters of this thesis with the development of a novel and more efficient wound healing assay than the one described in Chapter 2.Environmental reprogramming of hair follicle keratinocytes (ORS) into corneal epithelial cells was investigated in Chapter 3. This was studied by growing ORS in CEC's culture conditions, on a 3T3 feeder layer and with corneal specific media. Results showed no gain of cornea specific markers expression, rather a similarity in ORS and CEC expression of markers, therefore suggesting that corneal epithelial cells and outer root sheath cells share similarities when cultured using the 3T3 co-culture and LEM conditions. Further work in reprogramming ORS into corneal epithelial cells could be to use these in the spheroid model established in Chapter 4. Placing these in contact with functional 3D stromal keratocytes could potentially lead to microenvironmental reprogramming.

An *in vitro* cornea 3D model was established in Chapter 4 through the use of a novel spheroid hanging drop culture technique. Important results were the epithelial-mesenchymal interactions observed in the rabbit model and expression of corneal markers such as Pax6, Ck3, Ck12 and Aldh1a1, indicating transparency of the cornea and quiescent keratocytes that were maintaining the corneal epithelium. Work by Davis *et al*., 2008 in the mouse cornea showed that the Aldh3a1 gene (Aldh1a1 in the rabbit cornea) is activated by Pax6, Oct1 and p300. However, the study did not take the stroma

into account when studying the transcriptional activation of the Aldh3a1 gene expression. The results shown in Chapter 4 indicate that Pax6 expression alone is not enough to activate Aldh1a1 expression in the rabbit corneal epithelial cells within the 3D model, therefore indicating that the stroma plays a fundamental part in the transcriptional activation of Aldh1a1 in the corneal epithelial layer.

Other work by Yoshida *et al*., 2005 for example has investigated serum-free mouse corneal keratocyte cultures indicating that serum-free cultures can maintain the phenotype of mouse keratocytes *in vitro* and express Aldh, Keratocan and CD34 throughout 12 passages. The effects of a serum-free culture environment on maintaining a keratocyte phenotype was also investigated by Foster *et al*., 2015 where it was found that low glucose and serum-free culture medium enhanced the keratocyte phenotype including the important phenotypic markers Aldh1a1, Aldh3a1, Keratocan and Lumican as well as CD34. It is therefore evident that serum-free and low glucose culture medium can maintain a keratocyte phenotype *in vitro* and this was not investigated during the course of this PhD project. When analysing single stromal 3D spheres, markers such as Aldh1a1, Keratocan and Lumican were not expressed at high levels when compared to the positive control (*in vivo* stroma). This could indicate that three-dimensional culture solely is not enough to activate keratocyte markers. Future work could test the three-dimensional method together with serum-free culture medium as well as low-glucose medium. It would be interesting to construct a bilayered model using stromal spheres that express the representative keratocyte phenotype markers at high levels. This could possibly result in a longer lasting model over time *in vitro*.

Further results showed that a human cornea model could be established, however this has to be improved in the future. The establishment of the cornea 3D spheroid model is novel and because it does not utilise any biomaterial/scaffold and indicates some of the corneal functional markers and epithelial-mesenchymal interactions, it is highly cost-effective, it can be easily used for high throughput assays and can be easily modified according to cell type. In fact, the ultimate aim of this study was to assess stromal functionality in the 3D spheroid model in order to then use the stromal spheres for reprogramming studies. This was attempted in Chapter 5. Future work lies in refining the human cornea 3D model by using higher quality primary corneal epithelial cells and by testing a variety of markers, including Aldh1a1. Structural characteristics in the model have not been investigated yet and may be necessary to assess, such as the

basement membrane. However, the 3D model simplicity can be used for performing quick tests, such as toxicity testing as it can be set up quickly and is highly reproducible. Furthermore, a spheroid model can be used to study cell-cell cohesion and cell-ECM adhesion and this is important when studying for example embryonic development, wound healing and can also be applied to tissue engineering.

Chapter 5 described two pilot studies, the first assessing Glis1 transfection in human dermal sheath cells with the aim to express Pax6. The second study used the technology developed in Chapter 4, to reprogram skin keratinocytes by placing these in contact with human stromal keratocytes in a 3D spheroid. Preliminary results showed that Pax6 together with Ck3 and Ck12 were expressed in skin keratinocytes, indicating corneal epithelial-like cells. Further studies need to be performed to confirm these results. In conclusion, this study highlighted a potential novel method to reprogram skin keratinocytes into corneal epithelial cells by using the environmental reprogramming ability of the 3D spheroid culture as well as the corneal stromal keratocyte spheroids. The work described, will first need to be confirmed and other markers such as skin specific markers (Ck1/Ck10) and skin structural markers (Involucrin), as well as corneal markers such as Aldh1a1 could assess and help characterise the reprogrammed skin keratinocytes. Further work could also use outer root sheath cells to be reprogrammed using this technique. Because they are widely accessible they make a good therapeutic target. Investigating the signals by which stromal keratocytes in the 3D spheroids act as reprogramming agents could also help to identify new insights and a potential new strategy to reprogram skin derived keratinocytes *in vitro* for transplantation purpose. New research discoveries have identified that Pax6 transduced rabbit skin epithelial cells can be reprogrammed to corneal epithelial-like cells and that Pax6 controls Ck3 and Ck12 expression in CECs, while a lack of Pax6 down-regulated the latter and increased skin epithelial markers Ck1 and Ck10 expression (Ouyang *et al*., 2014). Another interesting and novel discovery has identified a new marker that specifically identifies limbal stem cells in the cornea, ABCB5 (Ksander *et al*., 2014) and that is also expressed in skin, therefore indicating that enriched ABCB5 skin epithelial cells could be potentially targeted to be environmentally reprogrammed using for instance the 3D spheroid model without having to use transduction methods.

7 References

ACHILLI, T. M., MEYER, J. & MORGAN, J. R. 2012. Advances in the formation, use and understanding of multi-cellular spheroids. *Expert Opin Biol Ther,* 12**,** 1347-60.

AHMAD, S., STEWART, R., YUNG, S., KOLLI, S., ARMSTRONG, L., STOJKOVIC, M., FIGUEIREDO, F. & LAKO, M. 2007. Differentiation of human embryonic stem cells into corneal epithelial-like cells by in vitro replication of the corneal epithelial stem cell niche. *Stem Cells,* 25**,** 1145-55.

ALLEN-HOFFMANN, B. L. & RHEINWALD, J. G. 1984. Polycyclic aromatic hydrocarbon mutagenesis of human epidermal keratinocytes in culture. *Proc Natl Acad Sci U S A,* 81**,** 7802-6.

AMBATI, B. K., NOZAKI, M., SINGH, N., TAKEDA, A., JANI, P. D., SUTHAR, T., ALBUQUERQUE, R. J., RICHTER, E., SAKURAI, E., NEWCOMB, M. T., KLEINMAN, M. E., CALDWELL, R. B., LIN, Q., OGURA, Y., ORECCHIA, A., SAMUELSON, D. A., AGNEW, D. W., ST LEGER, J., GREEN, W. R., MAHASRESHTI, P. J., CURIEL, D. T., KWAN, D., MARSH, H., IKEDA, S., LEIPER, L. J., COLLINSON, J. M., BOGDANOVICH, S., KHURANA, T. S., SHIBUYA, M., BALDWIN, M. E., FERRARA, N., GERBER, H. P., DE FALCO, S., WITTA, J., BAFFI, J. Z., RAISLER, B. J. & AMBATI, J. 2006. Corneal avascularity is due to soluble VEGF receptor-1. *Nature,* 443**,** 993-7.

AMBATI, B. K., PATTERSON, E., JANI, P., JENKINS, C., HIGGINS, E., SINGH, N., SUTHAR, T., VIRA, N., SMITH, K. & CALDWELL, R. 2007. Soluble vascular endothelial growth factor receptor-1 contributes to the corneal antiangiogenic barrier. *Br J Ophthalmol,* 91**,** 505-8.

AMESCUA, G., COLLINGS, F., SIDANI, A., BONFIELD, T. L., RODRIGUEZ, J. P., GALOR, A., MEDINA, C., YANG, X. & PEREZ, V. L. 2008. Effect of CXCL-1/KC production in high risk vascularized corneal allografts on T cell recruitment and graft rejection. *Transplantation,* 85**,** 615-25.

AMITAI-LANGE, A., ALTSHULER, A., BUBLEY, J., DBAYAT, N., TIOSANO, B. & SHALOM-FEUERSTEIN, R. 2015. Lineage tracing of stem and progenitor cells of the murine corneal epithelium. *Stem Cells,* 33**,** 230-9.

ANG, L. P., NAKAMURA, T., INATOMI, T., SOTOZONO, C., KOIZUMI, N., YOKOI, N. & KINOSHITA, S. 2006. Autologous serum-derived cultivated oral epithelial transplants for severe ocular surface disease. *Arch Ophthalmol,* 124**,** 1543-51.

ANGUNAWELA, R. I., MEHTA, J. S. & DANIELS, J. T. 2013. Ex-vivo ocular surface stem cell therapies: current techniques, applications, hurdles and future directions. *Expert Rev Mol Med,* 15**,** e4.

ARAKI-SASAKI, K., OHASHI, Y., SASABE, T., HAYASHI, K., WATANABE, H., TANO, Y. & HANDA, H. 1995. An SV40-immortalized human corneal epithelial cell line and its characterization. *Invest Ophthalmol Vis Sci,* 36**,** 614-21.

BAHARVAND, H., HEIDARI, M., EBRAHIMI, M., VALADBEIGI, T. & SALEKDEH, G. H. 2007. Proteomic analysis of epithelium-denuded human amniotic membrane as a limbal stem cell niche. *Mol Vis,* 13**,** 1711-21.

BARBARO, V., TESTA, A., DI IORIO, E., MAVILIO, F., PELLEGRINI, G. & DE LUCA, M. 2007. C/EBPdelta regulates cell cycle and self-renewal of human limbal stem cells. *J Cell Biol,* 177**,** 1037-49.

BARRERO, M. J. & IZPISUA BELMONTE, J. C. 2011. Regenerating the epigenome. *EMBO Rep,* 12**,** 208-15.

BEALES, M. P., FUNDERBURGH, J. L., JESTER, J. V. & HASSELL, J. R. 1999. Proteoglycan synthesis by bovine keratocytes and corneal fibroblasts: maintenance of the keratocyte phenotype in culture. *Invest Ophthalmol Vis Sci,* 40**,** 1658-63.

BERNSTEIN, A. M., TWINING, S. S., WAREJCKA, D. J., TALL, E. & MASUR, S. K. 2007. Urokinase receptor cleavage: a crucial step in fibroblast-to-myofibroblast differentiation. *Mol Biol Cell,* 18**,** 2716-27.

BLANCO-MEZQUITA, J. T., HUTCHEON, A. E., STEPP, M. A. & ZIESKE, J. D. 2011. alphaVbeta6 integrin promotes corneal wound healing. *Invest Ophthalmol Vis Sci,* 52**,** 8505-13.

BLANPAIN, C. & FUCHS, E. 2009. Epidermal homeostasis: a balancing act of stem cells in the skin. *Nat Rev Mol Cell Biol,* 10**,** 207-17.

BLAZEJEWSKA, E. A., SCHLOTZER-SCHREHARDT, U., ZENKEL, M., BACHMANN, B., CHANKIEWITZ, E., JACOBI, C. & KRUSE, F. E. 2009. Corneal limbal microenvironment can induce transdifferentiation of hair follicle stem cells into corneal epithelial-like cells. *Stem Cells,* 27**,** 642-52.

BONFANTI, P., CLAUDINOT, S., AMICI, A. W., FARLEY, A., BLACKBURN, C. C. & BARRANDON, Y. 2010. Microenvironmental reprogramming of thymic epithelial cells to skin multipotent stem cells. *Nature,* 466**,** 978-82.

BORENE, M. L., BAROCAS, V. H. & HUBEL, A. 2004. Mechanical and cellular changes during compaction of a collagen-sponge-based corneal stromal equivalent. *Ann Biomed Eng,* 32**,** 274-83.

BRANCH, M. J., HASHMANI, K., DHILLON, P., JONES, D. R., DUA, H. S. & HOPKINSON, A. 2012. Mesenchymal stem cells in the human corneal limbal stroma. *Invest Ophthalmol Vis Sci,* 53**,** 5109-16.

BRANDL, C., FLORIAN, C., DRIEMEL, O., WEBER, B. H. & MORSCZECK, C. 2009. Identification of neural crest-derived stem cell-like cells from the corneal limbus of juvenile mice. *Exp Eye Res,* 89**,** 209-17.

BRAY, L. J., GEORGE, K. A., HUTMACHER, D. W., CHIRILA, T. V. & HARKIN, D. G. 2012. A dual-layer silk fibroin scaffold for reconstructing the human corneal limbus. *Biomaterials,* 33**,** 3529-38.

CALONGE, M., DIEBOLD, Y., SAEZ, V., ENRIQUEZ DE SALAMANCA, A., GARCIA-VAZQUEZ, C., CORRALES, R. M. & HERRERAS, J. M. 2004. Impression cytology of the ocular surface: a review. *Exp Eye Res,* 78**,** 457-72.

CANDI, E., CIPOLLONE, R., RIVETTI DI VAL CERVO, P., GONFLONI, S., MELINO, G. & KNIGHT, R. 2008. p63 in epithelial development. *Cell Mol Life Sci,* 65**,** 3126-33.

CHEN, H. C., CHEN, H. L., LAI, J. Y., CHEN, C. C., TSAI, Y. J., KUO, M. T., CHU, P. H., SUN, C. C., CHEN, J. K. & MA, D. H. 2009. Persistence of transplanted oral mucosal epithelial cells in human cornea. *Invest Ophthalmol Vis Sci,* 50**,** 4660-8.

CHEN, J. J. & TSENG, S. C. 1991. Abnormal corneal epithelial wound healing in partial-thickness removal of limbal epithelium. *Invest Ophthalmol Vis Sci,* 32**,** 2219-33.

CHEN, Z., LI, D. Q., TONG, L., STEWART, P., CHU, C. & PFLUGFELDER, S. C. 2006. Targeted inhibition of p57 and p15 blocks transforming growth factor beta-inhibited proliferation of primary cultured human limbal epithelial cells. *Mol Vis,* 12**,** 983-94.

CHINNERY, H. R., MCLENACHAN, S., BINZ, N., SUN, Y., FORRESTER, J. V., DEGLI-ESPOSTI, M. A., PEARLMAN, E. & MCMENAMIN, P. G. 2012. TLR9 ligand CpG-ODN applied to the injured mouse cornea elicits retinal inflammation. *Am J Pathol,* 180**,** 209-20.

CHIRILA, T., BARNARD, Z., ZAINUDDIN, HARKIN, D. G., SCHWAB, I. R. & HIRST, L. 2008. Bombyx mori silk fibroin membranes as potential substrata for epithelial constructs used in the management of ocular surface disorders. *Tissue Eng Part A,* 14**,** 1203-11.

CHISTOLINI, P., DE ANGELIS, G., DE LUCA, M., PELLEGRINI, G. & RUSPANTINI, I. 1999. Analysis of the mechanical properties of in vitro reconstructed epidermis: preliminary results. *Med Biol Eng Comput,* 37**,** 670-2.

CHUNG, E. H., HUTCHEON, A. E., JOYCE, N. C. & ZIESKE, J. D. 1999. Synchronization of the G1/S transition in response to corneal debridement. *Invest Ophthalmol Vis Sci,* 40**,** 1952-8.

CLARRIS, B. J. & FRASER, J. R. 1968. On the pericellular zone of some mammalian cells in vitro. *Exp Cell Res,* 49**,** 181-93.

COLLINS, C. A., KRETZSCHMAR, K. & WATT, F. M. 2011. Reprogramming adult dermis to a neonatal state through epidermal activation of beta-catenin. *Development,* 138**,** 5189-99.

COTSARELIS, G., CHENG, S. Z., DONG, G., SUN, T. T. & LAVKER, R. M. 1989. Existence of slow-cycling limbal epithelial basal cells that can be preferentially stimulated to proliferate: implications on epithelial stem cells. *Cell,* 57**,** 201-9.

DAVANGER, M. & EVENSEN, A. 1971. Role of the pericorneal papillary structure in renewal of corneal epithelium. *Nature,* 229**,** 560-1.

DAVIS, J., DAVIS, D., NORMAN, B. & PIATIGORSKY, J. 2008. Gene expression of the mouse corneal crystallin Aldh3a1: activation by Pax6, Oct1, and p300. *Invest Ophthalmol Vis Sci,* 49**,** 1814-26.

DE PAIVA, C. S., CHEN, Z., CORRALES, R. M., PFLUGFELDER, S. C. & LI, D. Q. 2005. ABCG2 transporter identifies a population of clonogenic human limbal epithelial cells. *Stem Cells,* 23**,** 63-73.

DI GIROLAMO, N., BOSCH, M., ZAMORA, K., CORONEO, M. T., WAKEFIELD, D. & WATSON, S. L. 2009. A contact lens-based technique for expansion and transplantation of autologous epithelial progenitors for ocular surface reconstruction. *Transplantation,* 87**,** 1571-8.

DI IORIO, E., BARBARO, V., FERRARI, S., ORTOLANI, C., DE LUCA, M. & PELLEGRINI, G. 2006. Q-FIHC: quantification of fluorescence immunohistochemistry to analyse p63 isoforms and cell cycle phases in human limbal stem cells. *Microsc Res Tech,* 69**,** 983-91.

DOILLON, C. J., WATSKY, M. A., HAKIM, M., WANG, J., MUNGER, R., LAYCOCK, N., OSBORNE, R. & GRIFFITH, M. 2003. A collagen-based scaffold for a tissue engineered human cornea: physical and physiological properties. *Int J Artif Organs,* 26**,** 764-73.

DREIER, B., THOMASY, S. M., MENDONSA, R., RAGHUNATHAN, V. K., RUSSELL, P. & MURPHY, C. J. 2013. Substratum compliance modulates corneal fibroblast to myofibroblast transformation. *Invest Ophthalmol Vis Sci,* 54**,** 5901-7.

DU, Y., CARLSON, E. C., FUNDERBURGH, M. L., BIRK, D. E., PEARLMAN, E., GUO, N., KAO, W. W. & FUNDERBURGH, J. L. 2009. Stem cell therapy restores transparency to defective murine corneas. *Stem Cells,* 27**,** 1635-42.

DU, Y., FUNDERBURGH, M. L., MANN, M. M., SUNDARRAJ, N. & FUNDERBURGH, J. L. 2005. Multipotent stem cells in human corneal stroma. *Stem Cells,* 23**,** 1266-75.

DUA, H. S., SAINI, J. S., AZUARA-BLANCO, A. & GUPTA, P. 2000. Limbal stem cell deficiency: concept, aetiology, clinical presentation, diagnosis and management. *Indian J Ophthalmol,* 48**,** 83-92.

DUA, H. S., SHANMUGANATHAN, V. A., POWELL-RICHARDS, A. O., TIGHE, P. J. & JOSEPH, A. 2005. Limbal epithelial crypts: a novel anatomical structure and a putative limbal stem cell niche. *Br J Ophthalmol,* 89**,** 529-32.

DUAN, X. & SHEARDOWN, H. 2006. Dendrimer crosslinked collagen as a corneal tissue engineering scaffold: mechanical properties and corneal epithelial cell interactions. *Biomaterials,* 27**,** 4608-17.

EBATO, B., FRIEND, J. & THOFT, R. A. 1988. Comparison of limbal and peripheral human corneal epithelium in tissue culture. *Invest Ophthalmol Vis Sci,* 29**,** 1533-7.

EDELHAUSER, H. F. U., J. L. 2003. The cornea and the sclera. *Adler's Physiology of the Eye.*

ESPANA, E. M., KAWAKITA, T., ROMANO, A., DI PASCUALE, M., SMIDDY, R., LIU, C. Y. & TSENG, S. C. 2003. Stromal niche controls the plasticity of limbal and corneal epithelial differentiation in a rabbit model of recombined tissue. *Invest Ophthalmol Vis Sci,* 44**,** 5130-5.

FAGERHOLM, P., LAGALI, N. S., MERRETT, K., JACKSON, W. B., MUNGER, R., LIU, Y., POLAREK, J. W., SODERQVIST, M. & GRIFFITH, M. 2010. A biosynthetic alternative to human donor tissue for inducing corneal regeneration: 24-month follow-up of a phase 1 clinical study. *Sci Transl Med,* 2**,** 46ra61.

FENNEMA, E., RIVRON, N., ROUWKEMA, J., VAN BLITTERSWIJK, C. & DE BOER, J. 2013. Spheroid culture as a tool for creating 3D complex tissues. *Trends Biotechnol,* 31**,** 108-15.

FERRARIS, C., CHEVALIER, G., FAVIER, B., JAHODA, C. A. & DHOUAILLY, D. 2000. Adult corneal epithelium basal cells possess the capacity to activate epidermal, pilosebaceous and sweat gland genetic programs in response to embryonic dermal stimuli. *Development,* 127**,** 5487-95.

FERRINGTON, D. A., ROEHRICH, H., CHANG, A. A., HUANG, C. W., MALDONADO, M., BRATTEN, W., RAGEH, A. A., HEUSS, N. D., GREGERSON, D. S., NELSON, E. F. & YUAN, C. 2013. Corneal wound healing is compromised by immunoproteasome deficiency. *PLoS One,* 8**,** e54347.

FINI, M. E. 1999. Keratocyte and fibroblast phenotypes in the repairing cornea. *Prog Retin Eye Res,* 18**,** 529-51.

FISH, R. & DAVIDSON, R. S. 2010. Management of ocular thermal and chemical injuries, including amniotic membrane therapy. *Curr Opin Ophthalmol,* 21**,** 317-21.

FOSTER, J. W., GOUVEIA, R. M. & CONNON, C. J. 2015. Low-glucose enhances keratocyte-characteristic phenotype from corneal stromal cells in serum-free conditions. *Sci Rep,* 5**,** 10839.

FRITH, J. E., THOMSON, B. & GENEVER, P. G. 2010. Dynamic three-dimensional culture methods enhance mesenchymal stem cell properties and increase therapeutic potential. *Tissue Eng Part C Methods,* 16**,** 735-49.

FUCHS, E. 2008. Skin stem cells: rising to the surface. *J Cell Biol,* 180**,** 273-84.

FUJIKAWA, L. S., FOSTER, C. S., GIPSON, I. K. & COLVIN, R. B. 1984. Basement membrane components in healing rabbit corneal epithelial wounds: immunofluorescence and ultrastructural studies. *J Cell Biol,* 98**,** 128-38.

FUKUDA, K., CHIKAMA, T., NAKAMURA, M. & NISHIDA, T. 1999. Differential distribution of subchains of the basement membrane components type IV collagen and laminin among the amniotic membrane, cornea, and conjunctiva. *Cornea,* 18**,** 73-9.

FUNDERBURGH, J. L., MANN, M. M. & FUNDERBURGH, M. L. 2003. Keratocyte phenotype mediates proteoglycan structure: a role for fibroblasts in corneal fibrosis. *J Biol Chem,* 278**,** 45629-37.

FUNDERBURGH, M. L., DU, Y., MANN, M. M., SUNDARRAJ, N. & FUNDERBURGH, J. L. 2005. PAX6 expression identifies progenitor cells for corneal keratocytes. *FASEB J,* 19**,** 1371-3.

GENEVER, P. G. 2010. The generation of three-dimensional tissue structures with mesenchymal stem cells. *Altern Lab Anim,* 38 Suppl 1**,** 31-4.

GIPSON, I. K. & KEEZER, L. 1982. Effects of cytochalasins and colchicine on the ultrastructure of migrating corneal epithelium. *Invest Ophthalmol Vis Sci,* 22**,** 643-50.

GIPSON, I. K. & KIORPES, T. C. 1982. Epithelial sheet movement: protein and glycoprotein synthesis. *Dev Biol,* 92**,** 259-62.

GIPSON, I. K., SPURR-MICHAUD, S., ARGUESO, P., TISDALE, A., NG, T. F. & RUSSO, C. L. 2003. Mucin gene expression in immortalized human corneal-limbal and conjunctival epithelial cell lines. *Invest Ophthalmol Vis Sci,* 44**,** 2496-506.

GIPSON, I. K., SPURR-MICHAUD, S. J. & TISDALE, A. S. 1987. Anchoring fibrils form a complex network in human and rabbit cornea. *Invest Ophthalmol Vis Sci,* 28**,** 212-20.

GOLDBERG, M. F. & BRON, A. J. 1982. Limbal palisades of Vogt. *Trans Am Ophthalmol Soc,* 80**,** 155-71.

GOMES, J. A., GERALDES MONTEIRO, B., MELO, G. B., SMITH, R. L., CAVENAGHI PEREIRA DA SILVA, M., LIZIER, N. F., KERKIS, A., CERRUTI, H. & KERKIS, I. 2010. Corneal reconstruction with tissue-engineered cell sheets composed of human immature dental pulp stem cells. *Invest Ophthalmol Vis Sci,* 51**,** 1408-14.

GOUVEIA, R. M. & CONNON, C. J. 2013. The effects of retinoic acid on human corneal stromal keratocytes cultured in vitro under serum-free conditions. *Invest Ophthalmol Vis Sci,* 54**,** 7483-91.

GREEN, H. 1978. Cyclic AMP in relation to proliferation of the epidermal cell: a new view. *Cell,* 15**,** 801-11.

GRIFFITH, M., OSBORNE, R., MUNGER, R., XIONG, X., DOILLON, C. J., LAYCOCK, N. L., HAKIM, M., SONG, Y. & WATSKY, M. A. 1999. Functional human corneal equivalents constructed from cell lines. *Science,* 286**,** 2169-72.

GUO, X., HUTCHEON, A. E., MELOTTI, S. A., ZIESKE, J. D., TRINKAUS-RANDALL, V. & RUBERTI, J. W. 2007. Morphologic characterization of organized extracellular matrix deposition by ascorbic acid-stimulated human corneal fibroblasts. *Invest Ophthalmol Vis Sci,* 48**,** 4050-60.

HANNON, G. J. & BEACH, D. 1994. p15INK4B is a potential effector of TGF-beta-induced cell cycle arrest. *Nature,* 371**,** 257-61.

HAYASHI, R., ISHIKAWA, Y., ITO, M., KAGEYAMA, T., TAKASHIBA, K., FUJIOKA, T., TSUJIKAWA, M., MIYOSHI, H., YAMATO, M., NAKAMURA, Y. & NISHIDA, K. 2012. Generation of corneal epithelial cells from induced pluripotent stem cells derived from human dermal fibroblast and corneal limbal epithelium. *PLoS One,* 7**,** e45435.

HAYASHIDA, Y., NISHIDA, K., YAMATO, M., YANG, J., SUGIYAMA, H., WATANABE, K., HORI, Y., MAEDA, N., KIKUCHI, A., OKANO, T. & TANO, Y. 2006. Transplantation of tissue-engineered epithelial cell sheets after excimer laser photoablation reduces postoperative corneal haze. *Invest Ophthalmol Vis Sci,* 47**,** 552-7.

HIGGINS, C. A., CHEN, J. C., CERISE, J. E., JAHODA, C. A. & CHRISTIANO, A. M. 2013. Microenvironmental reprogramming by three-dimensional culture enables dermal papilla cells to induce de novo human hair-follicle growth. *Proc Natl Acad Sci U S A,* 110**,** 19679-88.

HOGAN, M. J., ALVARADO, J. & WEDDELL, J. E. 1971. *Histology of the Human Eye*.

HU, S., WILSON, K. D., GHOSH, Z., HAN, L., WANG, Y., LAN, F., RANSOHOFF, K. J., BURRIDGE, P. & WU, J. C. 2013. MicroRNA-302 increases reprogramming efficiency via repression of NR2F2. *Stem Cells,* 31**,** 259-68.

HU, X., LUI, W., CUI, L., WANG, M. & CAO, Y. 2005. Tissue engineering of nearly transparent corneal stroma. *Tissue Eng,* 11**,** 1710-7.

HUANG, A. J. & TSENG, S. C. 1991. Corneal epithelial wound healing in the absence of limbal epithelium. *Invest Ophthalmol Vis Sci,* 32**,** 96-105.

HUANG, M., WANG, B., WAN, P., LIANG, X., WANG, X., LIU, Y., ZHOU, Q. & WANG, Z. 2015. Roles of limbal microvascular net and limbal stroma in regulating maintenance of limbal epithelial stem cells. *Cell Tissue Res,* 359**,** 547-63.

HUANG, S. U., YOON, J. J., ISMAIL, S., MCGHEE, J. J. & SHERWIN, T. 2015. Sphere-forming cells from peripheral cornea demonstrate a wound-healing response to injury. *Cell Biol Int,* 39**,** 1274-87.

IZUMI, K., FEINBERG, S. E., IIDA, A. & YOSHIZAWA, M. 2003. Intraoral grafting of an ex vivo produced oral mucosa equivalent: a preliminary report. *Int J Oral Maxillofac Surg,* 32**,** 188-97.

JAHODA, C. A., WHITEHOUSE, J., REYNOLDS, A. J. & HOLE, N. 2003. Hair follicle dermal cells differentiate into adipogenic and osteogenic lineages. *Exp Dermatol,* 12**,** 849-59.

JANIN-MANIFICAT, H., ROVERE, M. R., GALIACY, S. D., MALECAZE, F., HULMES, D. J., MOALI, C. & DAMOUR, O. 2012. Development of ex vivo organ culture models to mimic human corneal scarring. *Mol Vis,* 18**,** 2896-908.

JAVADI, M. A., YAZDANI, S., SAJJADI, H., JADIDI, K., KARIMIAN, F., EINOLLAHI, B., JA'FARINASAB, M. R. & ZARE, M. 2005. Chronic and delayed-onset mustard gas keratitis: report of 48 patients and review of literature. *Ophthalmology,* 112**,** 617-25.

JESTER, J. V., BARRY, P. A., LIND, G. J., PETROLL, W. M., GARANA, R. & CAVANAGH, H. D. 1994. Corneal keratocytes: in situ and in vitro organization of cytoskeletal contractile proteins. *Invest Ophthalmol Vis Sci,* 35**,** 730-43.

JESTER, J. V., BROWN, D., PAPPA, A. & VASILIOU, V. 2012. Myofibroblast differentiation modulates keratocyte crystallin protein expression, concentration, and cellular light scattering. *Invest Ophthalmol Vis Sci,* 53**,** 770-8.

JESTER, J. V. & HO-CHANG, J. 2003. Modulation of cultured corneal keratocyte phenotype by growth factors/cytokines control in vitro contractility and extracellular matrix contraction. *Exp Eye Res,* 77**,** 581-92.

JESTER, J. V., HUANG, J., PETROLL, W. M. & CAVANAGH, H. D. 2002. TGFbeta induced myofibroblast differentiation of rabbit keratocytes requires synergistic TGFbeta, PDGF and integrin signaling. *Exp Eye Res,* 75**,** 645-57.

JESTER, J. V., PETROLL, W. M., BARRY, P. A. & CAVANAGH, H. D. 1995. Expression of alpha-smooth muscle (alpha-SM) actin during corneal stromal wound healing. *Invest Ophthalmol Vis Sci,* 36**,** 809-19.

JESTER, J. V., PETROLL, W. M. & CAVANAGH, H. D. 1999. Corneal stromal wound healing in refractive surgery: the role of myofibroblasts. *Prog Retin Eye Res,* 18**,** 311-56.

JOHNSON, G. J. 1999. Vision 2020: The Right to Sight: Report on the Sixth General Assembly of the International Agency for the Prevention of Blindness (IAPB). *Community Eye Health,* 12**,** 59-60.

JOHNSON, P. F. 2005. Molecular stop signs: regulation of cell-cycle arrest by C/EBP transcription factors. *J Cell Sci,* 118**,** 2545-55.

JUMBLATT, M. M. & NEUFELD, A. H. 1981. Characterization of cyclic AMP-mediated wound closure of the rabbit corneal epithelium. *Curr Eye Res,* 1**,** 189-95.

KAO, W. W., LIU, C. Y., CONVERSE, R. L., SHIRAISHI, A., KAO, C. W., ISHIZAKI, M., DOETSCHMAN, T. & DUFFY, J. 1996. Keratin 12-deficient mice have fragile corneal epithelia. *Invest Ophthalmol Vis Sci,* 37**,** 2572-84.

KARAMICHOS, D., LAKSHMAN, N. & PETROLL, W. M. 2007. Regulation of corneal fibroblast morphology and collagen reorganization by extracellular matrix mechanical properties. *Invest Ophthalmol Vis Sci,* 48**,** 5030-7.

KARAOZ, E., AYHAN, S., OKCU, A., AKSOY, A., BAYAZIT, G., OSMAN GUROL, A. & DURUKSU, G. 2011. Bone marrow-derived mesenchymal stem cells co-cultured with pancreatic islets display beta cell plasticity. *J Tissue Eng Regen Med,* 5**,** 491-500.

KATO, J. Y., MATSUOKA, M., POLYAK, K., MASSAGUE, J. & SHERR, C. J. 1994. Cyclic AMP-induced G1 phase arrest mediated by an inhibitor (p27Kip1) of cyclin-dependent kinase 4 activation. *Cell,* 79**,** 487-96.

KATO, M., TAGUCHI, T. & KOBAYASHI, H. 2007. An attempt to construct the stroma of cornea using primary cultured corneal cells. *J Nanosci Nanotechnol,* 7**,** 748-51.

KAWAKITA, T., ESPANA, E. M., HE, H., HORNIA, A., YEH, L. K., OUYANG, J., LIU, C. Y. & TSENG, S. C. 2005. Keratocan expression of murine keratocytes is maintained on amniotic membrane by down-regulating transforming growth factor-beta signaling. *J Biol Chem,* 280**,** 27085-92.

KAWAKITA, T., ESPANA, E. M., HE, H., SMIDDY, R., PAREL, J. M., LIU, C. Y. & TSENG, S. C. 2006. Preservation and expansion of the primate keratocyte phenotype by downregulating TGF-beta signaling in a low-calcium, serum-free medium. *Invest Ophthalmol Vis Sci,* 47**,** 1918-27.

KENYON, K. R. 2005. Amniotic membrane: mother's own remedy for ocular surface disease. *Cornea,* 24**,** 639-42.

KENYON, K. R. & TSENG, S. C. 1989. Limbal autograft transplantation for ocular surface disorders. *Ophthalmology,* 96**,** 709-22; discussion 722-3.

KIM, A., LAKSHMAN, N., KARAMICHOS, D. & PETROLL, W. M. 2010. Growth factor regulation of corneal keratocyte differentiation and migration in compressed collagen matrices. *Invest Ophthalmol Vis Sci,* 51**,** 864-75.

KIM, J. S., KIM, J. C., NA, B. K., JEONG, J. M. & SONG, C. Y. 2000. Amniotic membrane patching promotes healing and inhibits proteinase activity on wound healing following acute corneal alkali burn. *Exp Eye Res,* 70**,** 329-37.

KIMURA, K., TERANISHI, S., ORITA, T., ZHOU, H. & NISHIDA, T. 2011. Role of beta-Pix in corneal epithelial cell migration on fibronectin. *Invest Ophthalmol Vis Sci,* 52**,** 3181-6.

KITAZAWA, T., KINOSHITA, S., FUJITA, K., ARAKI, K., WATANABE, H., OHASHI, Y. & MANABE, R. 1990. The mechanism of accelerated corneal epithelial healing by human epidermal growth factor. *Invest Ophthalmol Vis Sci,* 31**,** 1773-8.

KLENKLER, B. J., GRIFFITH, M., BECERRIL, C., WEST-MAYS, J. A. & SHEARDOWN, H. 2005. EGF-grafted PDMS surfaces in artificial cornea applications. *Biomaterials,* 26**,** 7286-96.

KOJIMA, T., CHANG, J. H. & AZAR, D. T. 2007. Proangiogenic role of ephrinB1/EphB1 in basic fibroblast growth factor-induced corneal angiogenesis. *Am J Pathol,* 170**,** 764-73.

KOSTER, M. I. & ROOP, D. R. 2004. Genetic pathways required for epidermal morphogenesis. *Eur J Cell Biol,* 83**,** 625-9.

KRUSE, F. E., CHEN, J. J., TSAI, R. J. & TSENG, S. C. 1990. Conjunctival transdifferentiation is due to the incomplete removal of limbal basal epithelium. *Invest Ophthalmol Vis Sci,* 31**,** 1903-13.

KRUSE, F. E., JOUSSEN, A. M., ROHRSCHNEIDER, K., YOU, L., SINN, B., BAUMANN, J. & VOLCKER, H. E. 2000. Cryopreserved human amniotic membrane for ocular surface reconstruction. *Graefes Arch Clin Exp Ophthalmol,* 238**,** 68-75.

KSANDER, B. R., KOLOVOU, P. E., WILSON, B. J., SAAB, K. R., GUO, Q., MA, J., MCGUIRE, S. P., GREGORY, M. S., VINCENT, W. J., PEREZ, V. L., CRUZ-GUILLOTY, F., KAO, W. W., CALL, M. K., TUCKER, B. A., ZHAN, Q., MURPHY, G. F., LATHROP, K. L., ALT, C., MORTENSEN, L. J., LIN, C. P., ZIESKE, J. D., FRANK, M. H. & FRANK, N. Y. 2014. ABCB5 is a limbal stem cell gene required for corneal development and repair. *Nature,* 511**,** 353-7.

KULKARNI, B. B., TIGHE, P. J., MOHAMMED, I., YEUNG, A. M., POWE, D. G., HOPKINSON, A., SHANMUGANATHAN, V. A. & DUA, H. S. 2010. Comparative transcriptional profiling of the limbal epithelial crypt demonstrates its putative stem cell niche characteristics. *BMC Genomics,* 11**,** 526.

KULTTI, A., RILLA, K., TIIHONEN, R., SPICER, A. P., TAMMI, R. H. & TAMMI, M. I. 2006. Hyaluronan synthesis induces microvillus-like cell surface protrusions. *J Biol Chem,* 281**,** 15821-8.

KURPAKUS, M. A., DANESHVAR, C., DAVENPORT, J. & KIM, A. 1999. Human corneal epithelial cell adhesion to laminins. *Curr Eye Res,* 19**,** 106-14.

LAI, J. Y., CHEN, K. H., HSU, W. M., HSIUE, G. H. & LEE, Y. H. 2006. Bioengineered human corneal endothelium for transplantation. *Arch Ophthalmol,* 124**,** 1441-8.

LAKO, M., ARMSTRONG, L., CAIRNS, P. M., HARRIS, S., HOLE, N. & JAHODA, C. A. 2002. Hair follicle dermal cells repopulate the mouse haematopoietic system. *J Cell Sci,* 115**,** 3967-74.

LAKSHMAN, N. & PETROLL, W. M. 2012. Growth factor regulation of corneal keratocyte mechanical phenotypes in 3-D collagen matrices. *Invest Ophthalmol Vis Sci,* 53**,** 1077-86.

LEE, S. B., LI, D. Q., TAN, D. T., MELLER, D. C. & TSENG, S. C. 2000. Suppression of TGF-beta signaling in both normal conjunctival fibroblasts and pterygial body fibroblasts by amniotic membrane. *Curr Eye Res,* 20**,** 325-34.

LEHRER, M. S., SUN, T. T. & LAVKER, R. M. 1998. Strategies of epithelial repair: modulation of stem cell and transit amplifying cell proliferation. *J Cell Sci,* 111 (Pt 19)**,** 2867-75.

LEVIS, H. J., BROWN, R. A. & DANIELS, J. T. 2010. Plastic compressed collagen as a biomimetic substrate for human limbal epithelial cell culture. *Biomaterials,* 31**,** 7726-37.

LI, W., HAYASHIDA, Y., CHEN, Y. T., HE, H., TSENG, D. Y., ALONSO, M., CHEN, S. Y., XI, X. & TSENG, S. C. 2008. Air exposure induced squamous metaplasia of human limbal epithelium. *Invest Ophthalmol Vis Sci,* 49**,** 154-62.

LI, W., HAYASHIDA, Y., HE, H., KUO, C. L. & TSENG, S. C. 2007. The fate of limbal epithelial progenitor cells during explant culture on intact amniotic membrane. *Invest Ophthalmol Vis Sci,* 48**,** 605-13.

LU, L., REINACH, P. S. & KAO, W. W. 2001. Corneal epithelial wound healing. *Exp Biol Med (Maywood),* 226**,** 653-64.

MA, A., ZHAO, B., BOULTON, M. & ALBON, J. 2011. A role for Notch signaling in corneal wound healing. *Wound Repair Regen,* 19**,** 98-106.

MA, Y., XU, Y., XIAO, Z., YANG, W., ZHANG, C., SONG, E., DU, Y. & LI, L. 2006. Reconstruction of chemically burned rat corneal surface by bone marrow-derived human mesenchymal stem cells. *Stem Cells,* 24**,** 315-21.

MAEKAWA, M. & YAMANAKA, S. 2011. Glis1, a unique pro-reprogramming factor, may facilitate clinical applications of iPSC technology. *Cell Cycle,* 10**,** 3613-4.

MAJO, F., ROCHAT, A., NICOLAS, M., JAOUDE, G. A. & BARRANDON, Y. 2008. Oligopotent stem cells are distributed throughout the mammalian ocular surface. *Nature,* 456**,** 250-4.

MARCACCI, M., BERRUTO, M., BROCCHETTA, D., DELCOGLIANO, A., GHINELLI, D., GOBBI, A., KON, E., PEDERZINI, L., ROSA, D., SACCHETTI, G. L., STEFANI, G. & ZANASI, S. 2005. Articular cartilage engineering with Hyalograft C: 3-year clinical results. *Clin Orthop Relat Res***,** 96-105.

MATSUDA, M., UBELS, J. L. & EDELHAUSER, H. F. 1985. A larger corneal epithelial wound closes at a faster rate. *Invest Ophthalmol Vis Sci,* 26**,** 897-900.

MELLER, D., PIRES, R. T., MACK, R. J., FIGUEIREDO, F., HEILIGENHAUS, A., PARK, W. C., PRABHASAWAT, P., JOHN, T., MCLEOD, S. D., STEUHL, K. P. & TSENG, S. C. 2000. Amniotic membrane transplantation for acute chemical or thermal burns. *Ophthalmology,* 107**,** 980-9; discussion 990.

MERRETT, K., GRIFFITH, C. M., DESLANDES, Y., PLEIZIER, G., DUBE, M. A. & SHEARDOWN, H. 2003. Interactions of corneal cells with transforming growth factor beta 2-modified poly dimethyl siloxane surfaces. *J Biomed Mater Res A,* 67**,** 981-93.

MEYER-BLAZEJEWSKA, E. A., KRUSE, F. E., BITTERER, K., MEYER, C., HOFMANN-RUMMELT, C., WUNSCH, P. H. & SCHLOTZER-SCHREHARDT, U. 2010. Preservation of the limbal stem cell phenotype by appropriate culture techniques. *Invest Ophthalmol Vis Sci,* 51**,** 765-74.

MILLAR, S. E. 2002. Molecular mechanisms regulating hair follicle development. *J Invest Dermatol,* 118**,** 216-25.

MOHAN, R. R., STAPLETON, W. M., SINHA, S., NETTO, M. V. & WILSON, S. E. 2008. A novel method for generating corneal haze in anterior stroma of the mouse eye with the excimer laser. *Exp Eye Res,* 86**,** 235-40.

MURAKAMI, J., NISHIDA, T. & OTORI, T. 1992. Coordinated appearance of beta 1 integrins and fibronectin during corneal wound healing. *J Lab Clin Med,* 120**,** 86-93.

MYUNG, D., KOH, W., BAKRI, A., ZHANG, F., MARSHALL, A., KO, J., NOOLANDI, J., CARRASCO, M., COCHRAN, J. R., FRANK, C. W. & TA, C. N. 2007. Design and fabrication of an artificial cornea based on a photolithographically patterned hydrogel construct. *Biomed Microdevices,* 9**,** 911-22.

NAKAMURA, K., KUROSAKA, D., YOSHINO, M., OSHIMA, T. & KUROSAKA, H. 2002. Injured corneal epithelial cells promote myodifferentiation of corneal fibroblasts. *Invest Ophthalmol Vis Sci,* 43**,** 2603-8.

NAKAMURA, T., ANG, L. P., RIGBY, H., SEKIYAMA, E., INATOMI, T., SOTOZONO, C., FULLWOOD, N. J. & KINOSHITA, S. 2006. The use of autologous serum in the development of corneal and oral epithelial equivalents in patients with Stevens-Johnson syndrome. *Invest Ophthalmol Vis Sci,* 47**,** 909-16.

NAKAMURA, Y., HIRANO, S., SUZUKI, K., SEKI, K., SAGARA, T. & NISHIDA, T. 2002. Signaling mechanism of TGF-beta1-induced collagen contraction mediated by bovine trabecular meshwork cells. *Invest Ophthalmol Vis Sci,* 43**,** 3465-72.

NAKATSU, M. N., GONZALEZ, S., MEI, H. & DENG, S. X. 2014. Human limbal mesenchymal cells support the growth of human corneal epithelial stem/progenitor cells. *Invest Ophthalmol Vis Sci,* 55**,** 6953-9.

NETTO, M. V., MOHAN, R. R., AMBROSIO, R., JR., HUTCHEON, A. E., ZIESKE, J. D. & WILSON, S. E. 2005. Wound healing in the cornea: a review of refractive surgery complications and new prospects for therapy. *Cornea,* 24**,** 509-22.

NISHIDA, K., YAMATO, M., HAYASHIDA, Y., WATANABE, K., YAMAMOTO, K., ADACHI, E., NAGAI, S., KIKUCHI, A., MAEDA, N., WATANABE, H., OKANO, T. & TANO, Y. 2004. Corneal reconstruction with tissue-engineered cell sheets composed of autologous oral mucosal epithelium. *N Engl J Med,* 351**,** 1187-96.

O'CONNOR, L., STRASSER, A., O'REILLY, L. A., HAUSMANN, G., ADAMS, J. M., CORY, S. & HUANG, D. C. 1998. Bim: a novel member of the Bcl-2 family that promotes apoptosis. *EMBO J,* 17**,** 384-95.

OKADA, Y., SAIKA, S., SHIRAI, K., HASHIZUME, N., YAMANAKA, O., OHNISHI, Y. & SENBA, E. 2001. Disappearance of desmosomal components in rat corneal epithelium during wound healing. *Ophthalmologica,* 215**,** 61-5.

ORWIN, E., SHAH, A., VOORHEES, A. & RAVI, V. 2007. Bioreactor design for cornea tissue engineering: Material-cell interactions. *Acta Biomater,* 3**,** 1041-9.

ORWIN, E. J., BORENE, M. L. & HUBEL, A. 2003. Biomechanical and optical characteristics of a corneal stromal equivalent. *J Biomech Eng,* 125**,** 439-44.

OSEI-BEMPONG, C., HENEIN, C. & AHMAD, S. 2009. Culture conditions for primary human limbal epithelial cells. *Regen Med,* 4**,** 461-70.

OUYANG, H., XUE, Y., LIN, Y., ZHANG, X., XI, L., PATEL, S., CAI, H., LUO, J., ZHANG, M., ZHANG, M., YANG, Y., LI, G., LI, H., JIANG, W., YEH, E., LIN, J., PEI, M., ZHU, J., CAO, G., ZHANG, L., YU, B., CHEN, S., FU, X. D., LIU, Y. & ZHANG, K. 2014. WNT7A and PAX6 define corneal epithelium homeostasis and pathogenesis. *Nature,* 511**,** 358-61.

PAL-GHOSH, S., BLANCO, T., TADVALKAR, G., PAJOOHESH-GANJI, A., PARTHASARATHY, A., ZIESKE, J. D. & STEPP, M. A. 2011. MMP9 cleavage of the beta4 integrin ectodomain leads to recurrent epithelial erosions in mice. *J Cell Sci,* 124**,** 2666-75.

PASONEN-SEPPANEN, S., SUHONEN, T. M., KIRJAVAINEN, M., SUIHKO, E., URTTI, A., MIETTINEN, M., HYTTINEN, M., TAMMI, M. & TAMMI, R. 2001. Vitamin C enhances differentiation of a continuous keratinocyte cell line (REK) into epidermis with normal stratum corneum ultrastructure and functional permeability barrier. *Histochem Cell Biol,* 116**,** 287-97.

PEARTON, D. J., YANG, Y. & DHOUAILLY, D. 2005. Transdifferentiation of corneal epithelium into epidermis occurs by means of a multistep process triggered by dermal developmental signals. *Proc Natl Acad Sci U S A,* 102**,** 3714-9.

PELLEGRINI, G., DELLAMBRA, E., GOLISANO, O., MARTINELLI, E., FANTOZZI, I., BONDANZA, S., PONZIN, D., MCKEON, F. & DE LUCA, M. 2001. p63 identifies keratinocyte stem cells. *Proc Natl Acad Sci U S A,* 98**,** 3156-61.

PELLEGRINI, G., RAMA, P., MAVILIO, F. & DE LUCA, M. 2009. Epithelial stem cells in corneal regeneration and epidermal gene therapy. *J Pathol,* 217**,** 217-28.

PELLEGRINI, G., TRAVERSO, C. E., FRANZI, A. T., ZINGIRIAN, M., CANCEDDA, R. & DE LUCA, M. 1997. Long-term restoration of damaged corneal surfaces with autologous cultivated corneal epithelium. *Lancet,* 349**,** 990-3.

PINNAMANENI, N. & FUNDERBURGH, J. L. 2012. Concise review: Stem cells in the corneal stroma. *Stem Cells,* 30**,** 1059-63.

PIPPARELLI, A., ARSENIJEVIC, Y., THURET, G., GAIN, P., NICOLAS, M. & MAJO, F. 2013. ROCK inhibitor enhances adhesion and wound healing of human corneal endothelial cells. *PLoS One,* 8**,** e62095.

POH, M., BOYER, M., SOLAN, A., DAHL, S. L., PEDROTTY, D., BANIK, S. S., MCKEE, J. A., KLINGER, R. Y., COUNTER, C. M. & NIKLASON, L. E. 2005. Blood vessels engineered from human cells. *Lancet,* 365**,** 2122-4.

POLISETTI, N., ISLAM, M. M. & GRIFFITH, M. 2013. The artificial cornea. *Methods Mol Biol,* 1014**,** 45-52.

POLISETTY, N., FATIMA, A., MADHIRA, S. L., SANGWAN, V. S. & VEMUGANTI, G. K. 2008. Mesenchymal cells from limbal stroma of human eye. *Mol Vis,* 14**,** 431-42.

PRUNIERAS, M., REGNIER, M. & WOODLEY, D. 1983. Methods for cultivation of keratinocytes with an air-liquid interface. *J Invest Dermatol,* 81**,** 28s-33s.

RAMA, P., BONINI, S., LAMBIASE, A., GOLISANO, O., PATERNA, P., DE LUCA, M. & PELLEGRINI, G. 2001. Autologous fibrin-cultured limbal stem cells permanently restore the corneal surface of patients with total limbal stem cell deficiency. *Transplantation,* 72**,** 1478-85.

RAMJI, D. P. & FOKA, P. 2002. CCAAT/enhancer-binding proteins: structure, function and regulation. *Biochem J,* 365**,** 561-75.

RASHID, S. T. & VALLIER, L. 2010. Induced pluripotent stem cells--alchemist's tale or clinical reality? *Expert Rev Mol Med,* 12**,** 25.

REN, R., HUTCHEON, A. E., GUO, X. Q., SAEIDI, N., MELOTTI, S. A., RUBERTI, J. W., ZIESKE, J. D. & TRINKAUS-RANDALL, V. 2008. Human primary corneal fibroblasts synthesize and deposit proteoglycans in long-term 3-D cultures. *Dev Dyn,* 237**,** 2705-15.

RHEINWALD, J. G. & GREEN, H. 1975. Serial cultivation of strains of human epidermal keratinocytes: the formation of keratinizing colonies from single cells. *Cell,* 6**,** 331-43.

RICHARDSON, G. D., ARNOTT, E. C., WHITEHOUSE, C. J., LAWRENCE, C. M., REYNOLDS, A. J., HOLE, N. & JAHODA, C. A. 2005. Plasticity of rodent and human hair follicle dermal cells: implications for cell therapy and tissue engineering. *J Investig Dermatol Symp Proc,* 10**,** 180-3.

ROBERTSON, D. M., LI, L., FISHER, S., PEARCE, V. P., SHAY, J. W., WRIGHT, W. E., CAVANAGH, H. D. & JESTER, J. V. 2005. Characterization of growth and differentiation in a telomerase-immortalized human corneal epithelial cell line. *Invest Ophthalmol Vis Sci,* 46**,** 470-8.

RUBERTI, J. W. & ZIESKE, J. D. 2008. Prelude to corneal tissue engineering - gaining control of collagen organization. *Prog Retin Eye Res,* 27**,** 549-77.

SAIKA, S. 2007. Yin and yang in cytokine regulation of corneal wound healing: roles of TNF-alpha. *Cornea,* 26**,** S70-4.

SAIKA, S., UENOYAMA, K., HIROI, K. & OOSHIMA, A. 1992. L-ascorbic acid 2-phosphate enhances the production of type I and type III collagen peptides in cultured rabbit keratocytes. *Ophthalmic Res,* 24**,** 68-72.

SCHERMER, A., GALVIN, S. & SUN, T. T. 1986. Differentiation-related expression of a major 64K corneal keratin in vivo and in culture suggests limbal location of corneal epithelial stem cells. *J Cell Biol,* 103**,** 49-62.

SCHLOTZER-SCHREHARDT, U., DIETRICH, T., SAITO, K., SOROKIN, L., SASAKI, T., PAULSSON, M. & KRUSE, F. E. 2007. Characterization of extracellular matrix components in the limbal epithelial stem cell compartment. *Exp Eye Res,* 85**,** 845-60.

SCHLOTZER-SCHREHARDT, U. & KRUSE, F. E. 2005. Identification and characterization of limbal stem cells. *Exp Eye Res,* 81**,** 247-64.

SCUDERI, N., ALFANO, C., PAOLINI, G., MARCHESE, C. & SCUDERI, G. 2002. Transplantation of autologous cultivated conjunctival epithelium for the restoration of defects in the ocular surface. *Scand J Plast Reconstr Surg Hand Surg,* 36**,** 340-8.

SECKER, G. A. & DANIELS, J. T. 2008. Limbal epithelial stem cells of the cornea. *StemBook.* Cambridge (MA).

SHAH, A., BRUGNANO, J., SUN, S., VASE, A. & ORWIN, E. 2008. The development of a tissue-engineered cornea: biomaterials and culture methods. *Pediatr Res,* 63**,** 535-44.

SHERR, C. J. & ROBERTS, J. M. 1995. Inhibitors of mammalian G1 cyclin-dependent kinases. *Genes Dev,* 9**,** 1149-63.

SHIN'OKA, T., IMAI, Y. & IKADA, Y. 2001. Transplantation of a tissue-engineered pulmonary artery. *N Engl J Med,* 344**,** 532-3.

SINGH, R., JOSEPH, A., UMAPATHY, T., TINT, N. L. & DUA, H. S. 2005. Impression cytology of the ocular surface. *Br J Ophthalmol,* 89**,** 1655-9.

SINGH, V., SANTHIAGO, M. R., BARBOSA, F. L., AGRAWAL, V., SINGH, N., AMBATI, B. K. & WILSON, S. E. 2011. Effect of TGFbeta and PDGF-B

blockade on corneal myofibroblast development in mice. *Exp Eye Res,* 93**,** 810-7.

SITALAKSHMI, G., SUDHA, B., MADHAVAN, H. N., VINAY, S., KRISHNAKUMAR, S., MORI, Y., YOSHIOKA, H. & ABRAHAM, S. 2009. Ex vivo cultivation of corneal limbal epithelial cells in a thermoreversible polymer (Mebiol Gel) and their transplantation in rabbits: an animal model. *Tissue Eng Part A,* 15**,** 407-15.

SNELL, R. S., LEMP, M.A. 1998. Clinical Anatomy of the Eye. *In:* SCIENCE, B. (ed.).

SOLOMON, A., ROSENBLATT, M., MONROY, D., JI, Z., PFLUGFELDER, S. C. & TSENG, S. C. 2001. Suppression of interleukin 1alpha and interleukin 1beta in human limbal epithelial cells cultured on the amniotic membrane stromal matrix. *Br J Ophthalmol,* 85**,** 444-9.

STA IGLESIA, D. D. & STEPP, M. A. 2000. Disruption of the basement membrane after corneal debridement. *Invest Ophthalmol Vis Sci,* 41**,** 1045-53.

STEPP, M. A., SPURR-MICHAUD, S. & GIPSON, I. K. 1993. Integrins in the wounded and unwounded stratified squamous epithelium of the cornea. *Invest Ophthalmol Vis Sci,* 34**,** 1829-44.

STEPP, M. A., ZIESKE, J. D., TRINKAUS-RANDALL, V., KYNE, B. M., PAL-GHOSH, S., TADVALKAR, G. & PAJOOHESH-GANJI, A. 2014. Wounding the cornea to learn how it heals. *Exp Eye Res,* 121**,** 178-93.

SUMIDE, T., NISHIDA, K., YAMATO, M., IDE, T., HAYASHIDA, Y., WATANABE, K., YANG, J., KOHNO, C., KIKUCHI, A., MAEDA, N., WATANABE, H., OKANO, T. & TANO, Y. 2006. Functional human corneal endothelial cell sheets harvested from temperature-responsive culture surfaces. *FASEB J,* 20**,** 392-4.

SUN, T. T. & GREEN, H. 1977. Cultured epithelial cells of cornea, conjunctiva and skin: absence of marked intrinsic divergence of their differentiated states. *Nature,* 269**,** 489-93.

SUURONEN, E. J., NAKAMURA, M., WATSKY, M. A., STYS, P. K., MULLER, L. J., MUNGER, R., SHINOZAKI, N. & GRIFFITH, M. 2004. Innervated human corneal equivalents as in vitro models for nerve-target cell interactions. *FASEB J,* 18**,** 170-2.

SUZUKI, K., SAITO, J., YANAI, R., YAMADA, N., CHIKAMA, T., SEKI, K. & NISHIDA, T. 2003. Cell-matrix and cell-cell interactions during corneal epithelial wound healing. *Prog Retin Eye Res,* 22**,** 113-33.

TAKAHASHI, K. & YAMANAKA, S. 2006. Induction of pluripotent stem cells from mouse embryonic and adult fibroblast cultures by defined factors. *Cell,* 126**,** 663-76.

TANIOKA, H., KAWASAKI, S., YAMASAKI, K., ANG, L. P., KOIZUMI, N., NAKAMURA, T., YOKOI, N., KOMURO, A., INATOMI, T. & KINOSHITA, S. 2006. Establishment of a cultivated human conjunctival epithelium as an alternative tissue source for autologous corneal epithelial transplantation. *Invest Ophthalmol Vis Sci,* 47**,** 3820-7.

THOFT, R. A. & FRIEND, J. 1983. The X, Y, Z hypothesis of corneal epithelial maintenance. *Invest Ophthalmol Vis Sci,* 24**,** 1442-3.

THOMPSON, R. E., BORAAS, L. C., SOWDER, M., BECHTEL, M. K. & ORWIN, E. J. 2013. Three-dimensional cell culture environment promotes partial recovery of the native corneal keratocyte phenotype from a subcultured population. *Tissue Eng Part A,* 19**,** 1564-72.

TODARO, G. J. & GREEN, H. 1963. Quantitative studies of the growth of mouse embryo cells in culture and their development into established lines. *J Cell Biol,* 17**,** 299-313.

TORBET, J., MALBOUYRES, M., BUILLES, N., JUSTIN, V., ROULET, M., DAMOUR, O., OLDBERG, A., RUGGIERO, F. & HULMES, D. J. 2007. Orthogonal scaffold of magnetically aligned collagen lamellae for corneal stroma reconstruction. *Biomaterials,* 28**,** 4268-76.

TOUHAMI, A., GRUETERICH, M. & TSENG, S. C. 2002. The role of NGF signaling in human limbal epithelium expanded by amniotic membrane culture. *Invest Ophthalmol Vis Sci,* 43**,** 987-94.

TOYOSHIMA, H. & HUNTER, T. 1994. p27, a novel inhibitor of G1 cyclin-Cdk protein kinase activity, is related to p21. *Cell,* 78**,** 67-74.

UCHINO, Y., SHIMMURA, S., MIYASHITA, H., TAGUCHI, T., KOBAYASHI, H., SHIMAZAKI, J., TANAKA, J. & TSUBOTA, K. 2007. Amniotic membrane immobilized poly(vinyl alcohol) hybrid polymer as an artificial cornea scaffold that supports a stratified and differentiated corneal epithelium. *J Biomed Mater Res B Appl Biomater,* 81**,** 201-6.

VACANTI, C. A., BONASSAR, L. J., VACANTI, M. P. & SHUFFLEBARGER, J. 2001. Replacement of an avulsed phalanx with tissue-engineered bone. *N Engl J Med,* 344**,** 1511-4.

VESELY, I. 2005. Heart valve tissue engineering. *Circ Res,* 97**,** 743-55.

WAGONER, M. D., KENYON, K. R., GIPSON, I. K., HANNINEN, L. A. & SENG, W. L. 1984. Polymorphonuclear neutrophils delay corneal epithelial wound healing in vitro. *Invest Ophthalmol Vis Sci,* 25**,** 1217-20.

WATSKY, M. A., WEBER, K. T., SUN, Y. & POSTLETHWAITE, A. 2010. New insights into the mechanism of fibroblast to myofibroblast transformation and associated pathologies. *Int Rev Cell Mol Biol,* 282**,** 165-92.

WILSON, S. E. 2002. Analysis of the keratocyte apoptosis, keratocyte proliferation, and myofibroblast transformation responses after photorefractive keratectomy and laser in situ keratomileusis. *Trans Am Ophthalmol Soc,* 100**,** 411-33.

XIE, H. T., CHEN, S. Y., LI, G. G. & TSENG, S. C. 2011. Limbal epithelial stem/progenitor cells attract stromal niche cells by SDF-1/CXCR4 signaling to prevent differentiation. *Stem Cells,* 29**,** 1874-85.

YAMADA, N., YANAI, R., NAKAMURA, M., INUI, M. & NISHIDA, T. 2004. Role of the C domain of IGFs in synergistic promotion, with a substance P-derived peptide, of rabbit corneal epithelial wound healing. *Invest Ophthalmol Vis Sci,* 45**,** 1125-31.

YAMAMOTO, K., LADAGE, P. M., REN, D. H., LI, L., PETROLL, W. M., JESTER, J. V. & CAVANAGH, H. D. 2001. Bcl-2 expression in the human cornea. *Exp Eye Res,* 73**,** 247-55.

YANEZ-SOTO, B., LILIENSIEK, S. J., MURPHY, C. J. & NEALEY, P. F. 2013. Biochemically and topographically engineered poly(ethylene glycol) diacrylate hydrogels with biomimetic characteristics as substrates for human corneal epithelial cells. *J Biomed Mater Res A,* 101**,** 1184-94.

YANG, A. & MCKEON, F. 2000. P63 and P73: P53 mimics, menaces and more. *Nat Rev Mol Cell Biol,* 1**,** 199-207.

YANG, A., SCHWEITZER, R., SUN, D., KAGHAD, M., WALKER, N., BRONSON, R. T., TABIN, C., SHARPE, A., CAPUT, D., CRUM, C. & MCKEON, F. 1999. p63 is essential for regenerative proliferation in limb, craniofacial and epithelial development. *Nature,* 398**,** 714-8.

YANG, C. C. & COTSARELIS, G. 2010. Review of hair follicle dermal cells. *J Dermatol Sci,* 57**,** 2-11.

YANG, J., YAMATO, M., NISHIDA, K., HAYASHIDA, Y., SHIMIZU, T., KIKUCHI, A., TANO, Y. & OKANO, T. 2006. Corneal epithelial stem cell delivery using cell sheet engineering: not lost in transplantation. *J Drug Target,* 14**,** 471-82.

YOON, J. J., WANG, E. F., ISMAIL, S., MCGHEE, J. J. & SHERWIN, T. 2013. Sphere-forming cells from peripheral cornea demonstrate polarity and directed cell migration. *Cell Biol Int,* 37**,** 949-60.

YOSHIDA, K., NAKAYAMA, K., NAGAHAMA, H., HARADA, T., HARADA, C., IMAKI, J., MATSUDA, A., YAMAMOTO, K., ITO, M., OHNO, S. & NAKAYAMA, K. 2002. Involvement of p27(KIP1) degradation by Skp2 in the regulation of proliferation in response to wounding of corneal epithelium. *Invest Ophthalmol Vis Sci,* 43**,** 364-70.

YOSHIDA, S., SHIMMURA, S., NAGOSHI, N., FUKUDA, K., MATSUZAKI, Y., OKANO, H. & TSUBOTA, K. 2006. Isolation of multipotent neural crest-derived stem cells from the adult mouse cornea. *Stem Cells,* 24**,** 2714-22.

YOSHIDA, S., SHIMMURA, S., SHIMAZAKI, J., SHINOZAKI, N. & TSUBOTA, K. 2005. Serum-free spheroid culture of mouse corneal keratocytes. *Invest Ophthalmol Vis Sci,* 46**,** 1653-8.

YUE, J. & MULDER, K. M. 2001. Transforming growth factor-beta signal transduction in epithelial cells. *Pharmacol Ther,* 91**,** 1-34.

ZIESKE, J. D. 2004. Corneal development associated with eyelid opening. *Int J Dev Biol,* 48**,** 903-11.

ZIESKE, J. D. & GIPSON, I. K. 1986. Protein synthesis during corneal epithelial wound healing. *Invest Ophthalmol Vis Sci,* 27**,** 1-7.

ZIESKE, J. D., GUIMARAES, S. R. & HUTCHEON, A. E. 2001. Kinetics of keratocyte proliferation in response to epithelial debridement. *Exp Eye Res,* 72**,** 33-9.

ZIESKE, J. D., MASON, V. S., WASSON, M. E., MEUNIER, S. F., NOLTE, C. J., FUKAI, N., OLSEN, B. R. & PARENTEAU, N. L. 1994. Basement membrane assembly and differentiation of cultured corneal cells: importance of culture environment and endothelial cell interaction. *Exp Cell Res,* 214**,** 621-33.

ZORLUTUNA, P., TEZCANER, A., KIYAT, I., AYDINLI, A. & HASIRCI, V. 2006. Cornea engineering on polyester carriers. *J Biomed Mater Res A,* 79**,** 104-13.

8 Appendices

8.1 3D Sphere work

8.1.1 Reproducibility of rabbit cornea 3D models

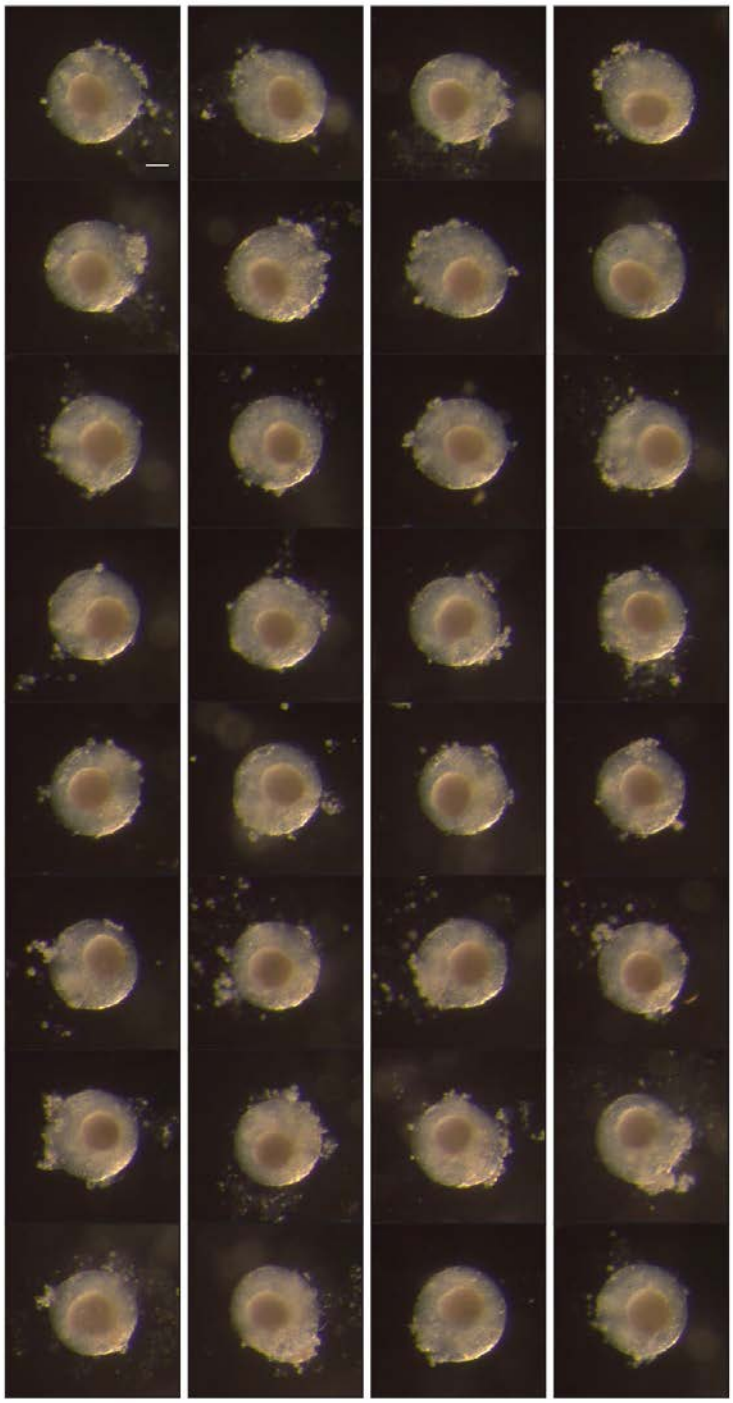

Figure 1: Rabbit cornea model reproducibility

Images were taken with a Zeiss Axiocam. Scale bar: 100µm.

8.1.2 Low quality single spheres

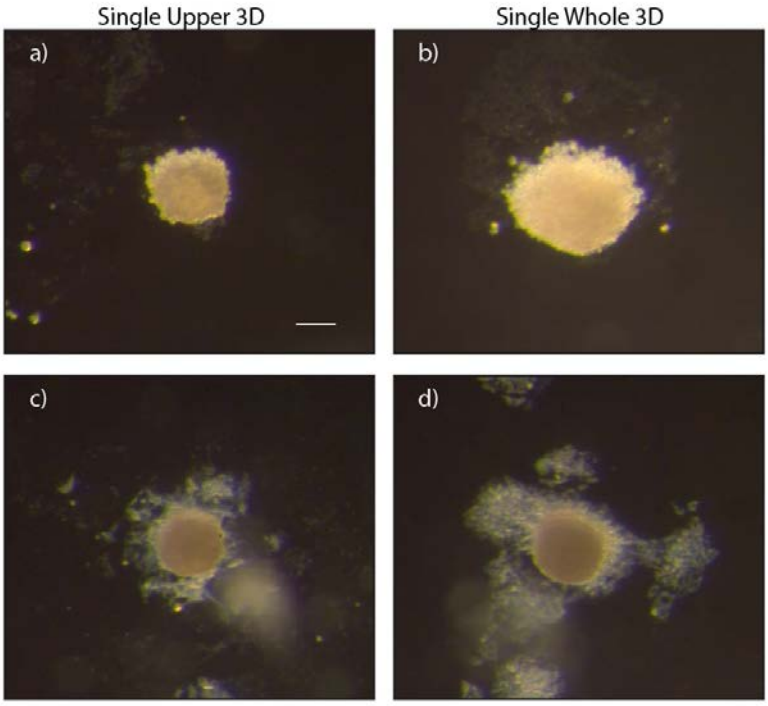

Figure 2: Low quality upper & whole single 3D spheres. Scale bar: 100µm.

Macroscopic images a), b) showing no compactness in outer sphere borders. Images c) and d) showing cell debris and “fluffy” cell material around the sphere borders. Images were taken with a Zeiss Axiocam. Scale bar: 100µm.

8.1.3 Testing rabbit cornea 3D model viability

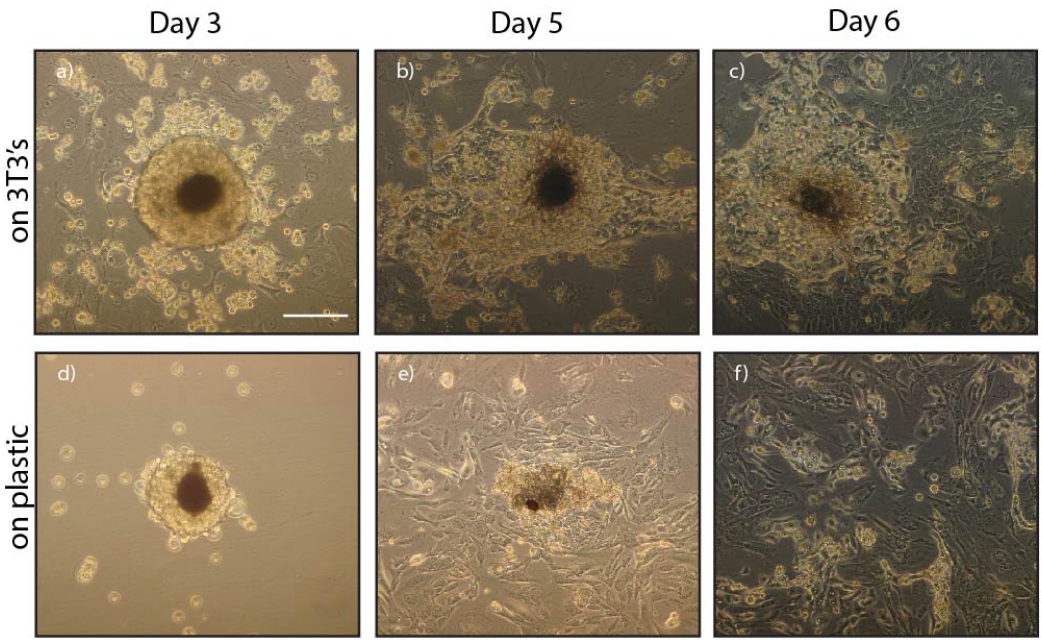

Figure 3: Rb cornea 3D model placed back into culture at culture day 5, on the 3T3 feeder layer and on plastic over 6 days.

Macroscopic images a), b) and c) showing models placed on a mitotically inactivated 3T3 feeder layer. d),e) and f) show models placed on plastic. Images were taken with a Zeiss Axiocam. Scale bar: 100µm.

Rabbit upper stromal (P6) spheres were double coated at culture day 4 with rabbit limbal CEC (P2) and the double layered model was allowed to form for 3 days. At culture day 5 a few models were placed back in culture, either on mitotically inactivated 3T3 mouse fibroblasts, or straight on plastic and cultured for 6 days. Figure 3 shows that models were viable, as cells grew out into the culture dishes when placed back in culture. Also, it showed that the 3T3 feeder layer maintained intact models for longer and cells growing onto the feeder layer were corneal epithelial cells (c), while model cultured on plastic exhibited fibroblastic growth (e,f).

8.2 Histology components

Reagent	Supplier
Haematoxylin	Fisher
Absolute Ethanol	Fisher
Eosin	Fisher
Histoclear	Fisher
DPX Mountant	Sigma-Aldrich
Acid Ethanol	For composition see Table 2

Table 1: Materials for H&E staining

Acid Ethanol	Composition	Supplier
Ethanol	350ml	Sigma-Aldrich
Hydrochloric Acid	15ml	Sigma-Aldrich
H_2O	150ml	Tap water

Table 2: Acid Ethanol components

8.3 Quantitative Real-time PCR raw data

8.3.1 Chapter 2 qRT-PCR Raw data & ANOVA analysis

<u>Data for donor 1:</u>

Non-wounded culture (control) raw data:

GAPDH	Mean GAPDH	ABCG2	CEBPdelta	p63alpha
15.71152401	15.84662596	25.61326408	26.2564888	37.03847122
15.00660324		24.93763733	26.72265816	35.96110535
16.82175064		24.48599874	28.03050613	40.21502304

p63gamma	deltaNp63	Ck12	BimS	p27
28.10512543	27.41012192	23.66277313	27.08543968	30.6491127
32.70676422	27.131073	22.99257851	23.98329163	31.80165863
30.38729875	28.36993599	22.64838997	26.79012489	31.39403725

Analysis for control:

ABCG2					
delta Ct	**Mean delta Ct**	deltadelta Ct	2-deltadelta Ct	**Mean 2-deltadelta Ct**	**SD 2-deltadelta Ct**
9.76663812	9.165674088	0.600964032	0.659313245	1.050886711	0.390464186
9.091011365		-0.074662723	1.053114807		
8.639372779		-0.526301309	1.440232082		
CEBPdelta					
delta Ct	**Mean delta Ct**	deltadelta Ct	2-deltadelta Ct	**Mean 2-deltadelta Ct**	**SD 2-deltadelta Ct**
10.40986284	11.15659173	-0.746728897	1.677983928	1.127760417	0.598427865
10.87603219		-0.28055954	1.214665893		
12.18388017		1.027288437	0.490631431		
p63alpha					
delta Ct	**Mean delta Ct**	deltadelta Ct	2-deltadelta Ct	**Mean 2-deltadelta Ct**	**SD 2-deltadelta Ct**
21.19184526	21.89157391	-0.699728648	1.624199273	1.743730393	1.627152549
20.11447938		-1.777094523	3.427352366		
24.36839708		2.476823171	0.179639539		
p63gamma					
delta Ct	**Mean delta Ct**	deltadelta Ct	2-deltadelta Ct	**Mean 2-deltadelta Ct**	**SD 2-deltadelta Ct**
12.25849946	14.5531035	-2.294604039	4.906193173	2.038974022	2.515621462
16.86013826		2.307034755	0.202075349		
14.54067279		-0.012430717	1.008653544		
deltaNp63					
delta Ct	**Mean delta Ct**	deltadelta Ct	2-deltadelta Ct	**Mean 2-deltadelta Ct**	**SD 2-deltadelta Ct**
11.56349595	11.79041767	-0.226921717	1.170335136	1.064036666	0.419418428
11.28444703		-0.505970637	1.420078456		
12.52331003		0.732892354	0.601696406		

Ck12					
delta Ct	**Mean delta Ct**	deltadelta Ct	2-deltadelta Ct	**Mean 2-deltadelta Ct**	**SD 2-deltadelta Ct**
7.816147168	7.25462124	0.561525928	0.677585108	1.041522086	0.347040943
7.145952543		-0.108668697	1.078232796		
6.801764009		-0.452857231	1.368748355		
BimS					
delta Ct	**Mean delta Ct**	deltadelta Ct	2-deltadelta Ct	**Mean 2-deltadelta Ct**	**SD 2-deltadelta Ct**
11.23881372	10.1063261	1.132487615	0.456128552	1.644209052	1.968767886
8.136665662		-1.969660441	3.916759217		
10.94349893		0.837172826	0.559739387		
p27					
delta Ct	**Mean delta Ct**	deltadelta Ct	2-deltadelta Ct	**Mean 2-deltadelta Ct**	**SD 2-deltadelta Ct**
14.80248674	15.4349769	-0.632490158	1.550238469	1.057536403	0.441617654
15.95503267		0.520055771	0.697344875		
15.54741128		0.112434387	0.925025866		

Wounded raw data:

GAPDH	Mean GAPDH	ABCG2	CEBPdelta	p63alpha	p63gamma
16.86194038	16.12828414	26.98597145	28.61003876	34.96444321	40.79607391
15.75132465		27.58801079	32.09441757	34.51088715	37.28300858
15.77158737		27.69672012	29.83439493	35.33662415	38.39284837

deltaNp63	Ck12	BimS	p27
33.34434509	21.65743637	31.51074791	34.88393021
31.30130577	21.26593208	26.20947456	46.97223663
29.02843094	22.81227112	27.32663345	44.00389244

Analysis for wounded:

ABCG2				
delta Ct	deltadelta Ct	2-deltadelta Ct	**Mean 2-deltadelta Ct**	**SD 2-deltadelta Ct**
10.85768731	1.428862571	0.37142361	0.281022198	0.078791978
11.45972665	2.030901909	0.24470205		
11.56843599	2.139611244	0.226940933		
CEBPdelta				
delta Ct	deltadelta Ct	2-deltadelta Ct	**Mean 2-deltadelta Ct**	**SD 2-deltadelta Ct**
12.48175462	1.325162891	0.399104129	0.217382161	0.256993672
15.96613344	4.809541706	0.035660192		
13.7061108	2.549519066	0.170811964		
p63alpha				
delta Ct	deltadelta Ct	2-deltadelta Ct	**Mean 2-deltadelta Ct**	**SD 2-deltadelta Ct**
18.83615907	-3.05541484	8.313262919	8.706827115	2.503974347
18.38260301	-3.5089709	11.38427806		
19.20834001	-2.683233901	6.422940362		

p63gamma				
delta Ct	deltadelta Ct	2-deltadelta Ct	**Mean 2-deltadelta Ct**	**SD 2-deltadelta Ct**
24.66778978	10.10847092	0.000905831	0.005623684	0.006672052
21.15472444	6.595405579	0.010341537		
22.26456424	7.705245376	0.004791704		
deltaNp63				
delta Ct	deltadelta Ct	2-deltadelta Ct	**Mean 2-deltadelta Ct**	**SD 2-deltadelta Ct**
17.21606096	5.425643286	0.023265834	0.194176113	0.235948555
15.17302163	3.382603964	0.095881483		
12.9001468	1.109729132	0.463381023		
Ck12				
delta Ct	deltadelta Ct	2-deltadelta Ct	**Mean 2-deltadelta Ct**	**SD 2-deltadelta Ct**
5.529152234	-1.951897622	3.868830764	3.560456686	1.689944526
5.137647947	-2.343401909	5.0749792		
6.683986982	-0.797062874	1.737560093		
BimS				
delta Ct	deltadelta Ct	2-deltadelta Ct	**Mean 2-deltadelta Ct**	**SD 2-deltadelta Ct**
15.38246377	5.276137673	0.025806214	0.504161548	0.496813188
10.08119043	-0.025135673	1.017575382		
11.19834932	1.092023217	0.469103049		
p27				
delta Ct	deltadelta Ct	2-deltadelta Ct	**Mean 2-deltadelta Ct**	**SD 2-deltadelta Ct**
18.75564607	3.32066917	0.1000873	0.050055142	0.070756156
30.8439525	15.4089756	2.29846E-05		
27.8756083	12.4406314	0.000179886		

50% healed raw data:

GAPDH	Mean GAPDH	ABCG2	CEBPdelta	p63alpha	p63gamma
15.22925186	14.81117249	27.82936287	25.12475967	34.24074554	29.57914543
14.92309284		27.72213745	25.65899277	33.27861023	27.90343857
14.28117275		27.8498493	26.69410896	33.39849388	30.00343704

deltaNp63	Ck12	BimS	p27
27.03566742	23.46702766	26.72786522	35.33680725
29.62273216	20.80186081	24.55535316	39.1184845
26.76453209	21.15447617	25.38473985	34.61133194

Analysis 50% healed:

ABCG2				
delta Ct	deltadelta Ct	2-deltadelta Ct	**Mean 2-deltadelta Ct**	**SD 2-deltadelta Ct**
13.01819038	3.589365641	0.083079386	0.086284367	0.004532528
12.91096497	3.482140223	0.089489348		
13.03867682	3.609852075	0.081907986		
CEBPdelta				
delta Ct	deltadelta Ct	2-deltadelta Ct	**Mean 2-deltadelta Ct**	**SD 2-deltadelta Ct**
10.31358719	-0.843004541	1.793781966	1.212289268	0.595112405
10.84782028	-0.308771448	1.238652455		
11.88293648	0.726344748	0.604433385		
p63alpha				
delta Ct	deltadelta Ct	2-deltadelta Ct	**Mean 2-deltadelta Ct**	**SD 2-deltadelta Ct**
19.42957306	-2.462000851	5.509803435	8.121977154	3.6941715
18.46743774	-3.424136166	10.73415087		
18.5873214	-3.304252512	9.878229673		
p63gamma				
delta Ct	deltadelta Ct	2-deltadelta Ct	**Mean 2-deltadelta Ct**	**SD 2-deltadelta Ct**
14.76797295	0.208654086	0.865344149	1.424922697	1.165390798
13.09226608	-1.467052777	2.764565546		
15.19226456	0.632945697	0.644858397		
deltaNp63				
delta Ct	deltadelta Ct	2-deltadelta Ct	**Mean 2-deltadelta Ct**	**SD 2-deltadelta Ct**
12.22449493	0.434077264	0.740167008	0.585516784	0.407639938
14.81155968	3.021142007	0.123181542		
11.9533596	0.162941934	0.893201802		

Ck12				
delta Ct	deltadelta Ct	2-deltadelta Ct	**Mean 2-deltadelta Ct**	**SD 2-deltadelta Ct**
8.655855179	1.174805323	0.442943526	1.817635772	1.228870396
5.990688324	-1.490361532	2.809593733		
6.34330368	-1.137746176	2.200370057		
BimS				
delta Ct	deltadelta Ct	2-deltadelta Ct	**Mean 2-deltadelta Ct**	**SD 2-deltadelta Ct**
11.91669273	1.810366634	0.285118462	0.785227176	0.707260526
9.744180679	-0.362145421	1.28533589		
10.57356736	0.467241264	0.723346467		

p27				
delta Ct	deltadelta Ct	2-deltadelta Ct	**Mean 2-deltadelta Ct**	**SD 2-deltadelta Ct**
20.52563477	5.090657866	0.029346701	0.0266679	0.023310393
24.30731201	8.872335112	0.002133836		
19.80015945	4.365182554	0.048523164		

Healed raw data:

GAPDH	Mean GAPDH	ABCG2	CEBPdelta	p63alpha	p63gamma
13.19111061	13.23246765	26.02472878	25.02882004	29.10360336	26.6499939
13.51416302		23.89722061	24.42762566	28.30142975	26.0422802
12.99212933		25.38748324	24.60324097	29.20869446	26.6535678

deltaNp63	Ck12	BimS	p27
25.4237442	19.25600624	25.84530258	31.00995445
27.64749527	19.44473076	27.97273064	30.91440964
26.49483985	19.8462677	26.1681881	29.86362648

Analysis healed:

ABCG2				
delta Ct	deltadelta Ct	2-deltadelta Ct	**Mean 2-deltadelta Ct**	**SD 2-deltadelta Ct**
12.79226112	3.363436381	0.09716386	0.224285858	0.23151057
10.66475296	1.235928217	0.424569248		
12.15501559	2.726190849	0.151124466		
CEBPdelta				
delta Ct	deltadelta Ct	2-deltadelta Ct	**Mean 2-deltadelta Ct**	**SD 2-deltadelta Ct**
11.79635239	0.639760656	0.641819418	0.825825497	0.168838954
11.195158	0.038566275	0.973622035		
11.37077332	0.214181585	0.862035038		
p63alpha				
delta Ct	deltadelta Ct	2-deltadelta Ct	**Mean 2-deltadelta Ct**	**SD 2-deltadelta Ct**
15.87113571	-6.020438198	64.91312016	79.4855215	29.27847945
15.0689621	-6.822611813	113.1907153		
15.97622681	-5.915347103	60.35272904		
p63gamma				
delta Ct	deltadelta Ct	2-deltadelta Ct	**Mean 2-deltadelta Ct**	**SD 2-deltadelta Ct**
13.41752625	-1.141792615	2.206550269	2.784492559	0.817333825
12.80981255	-1.749506314	3.362434849		
13.42110015	-1.138218711	2.201090877		

deltaNp63				
delta Ct	deltadelta Ct	2-deltadelta Ct	**Mean 2-deltadelta Ct**	**SD 2-deltadelta Ct**
12.19127655	0.40085888	0.757407241	0.459778009	0.420911296
14.41502762	2.624609948	0.162148777		
13.2623722	1.471954528	0.36049358		

Ck12				
delta Ct	deltadelta Ct	2-deltadelta Ct	**Mean 2-deltadelta Ct**	**SD 2-deltadelta Ct**
6.023538589	-1.457511267	2.746341947	2.326704182	0.466633705
6.212263107	-1.268786749	2.409588431		
6.613800049	-0.867249807	1.824182167		
BimS				
delta Ct	deltadelta Ct	2-deltadelta Ct	**Mean 2-deltadelta Ct**	**SD 2-deltadelta Ct**
12.61283493	2.50650883	0.17598095	0.11898276	0.070408863
14.74026299	4.633936885	0.040275969		
12.93572044	2.829394344	0.140691362		
p27				
delta Ct	deltadelta Ct	2-deltadelta Ct	**Mean 2-deltadelta Ct**	**SD 2-deltadelta Ct**
17.7774868	2.342509901	0.197167012	0.281420858	0.13441037
17.68194199	2.246965086	0.210666806		
16.63115883	1.196181929	0.436428757		

ANOVA:

ABCG2						
Anova: Single Factor						
SUMMARY						
Groups	*Count*	*Sum*	*Average*	*Variance*		
w0	3	3.152660133	1.050887	0.152462		
wound	3	0.843066593	0.281022	0.006208		
half healed	3	0.254476719	0.084826	1.67E-05		
confluent	3	0.672857574	0.224286	0.030813		
ANOVA						
Source of Variation	*SS*	*df*	*MS*	*F*	*P-value*	*F crit*
Between Groups	1.70279682	3	0.567599	11.98097	0.002498	4.066181
Within Groups	0.37900025	8	0.047375			
Total	2.08179707	11				

CEBPΔ

Anova: Single Factor

SUMMARY

Groups	*Count*	*Sum*	*Average*	*Variance*
w0	3	3.383281251	1.12776	0.358116
wound	3	0.605576285	0.201859	0.033746
half healed	3	3.636867805	1.212289	0.354159
confluent	3	2.477476491	0.825825	0.028507

ANOVA

Source of Variation	*SS*	*df*	*MS*	*F*	*P-value*	*F crit*
Between Groups	1.88644668	3	0.628816	3.247481	0.081202	4.066181
Within Groups	1.549054156	8	0.193632			
Total	3.435500836	11				

P63α

Anova: Single Factor

SUMMARY

Groups	*Count*	*Sum*	*Average*	*Variance*
w0	3	5.231191179	1.74373	2.647625
wound	3	26.12048135	8.706827	6.269888
half healed	3	26.12218398	8.707395	7.851593
confluent	3	238.4565645	79.48552	857.2294

ANOVA

Source of Variation	*SS*	*df*	*MS*	*F*	*P-value*	*F crit*
Between Groups	12119.94768	3	4039.983	18.48966	0.000589	4.066181
Within Groups	1747.996928	8	218.4996			
Total	13867.94461	11				

p63γ

Anova: Single Factor

SUMMARY

Groups	*Count*	*Sum*	*Average*	*Variance*
w0	3	6.116922065	2.038974	6.328351
wound	3	0.016039072	0.005346	2.25E-05
half healed	3	4.274768092	1.424923	1.358136
confluent	3	7.770075996	2.590025	0.44747

ANOVA

Source of Variation	*SS*	*df*	*MS*	*F*	*P-value*	*F crit*
Between Groups	11.15218844	3	3.717396	1.828082	0.22012	4.066181
Within Groups	16.26795868	8	2.033495			
Total	27.42014712	11				

ΔNp63

Anova: Single Factor

SUMMARY

Groups	*Count*	*Sum*	*Average*	*Variance*
w0	3	3.192109998	1.064037	0.175912
wound	3	0.58252834	0.194176	0.055672
half healed	3	1.756550351	0.585517	0.16617
confluent	3	1.280049599	0.426683	0.091869

ANOVA

Source of Variation	*SS*	*df*	*MS*	*F*	*P-value*	*F crit*
Between Groups	1.218219954	3	0.406073	3.317438	0.07773	4.066181
Within Groups	0.979245634	8	0.122406			
Total	2.197465588	11				

Ck12

Anova: Single Factor

SUMMARY

Groups	*Count*	*Sum*	*Average*	*Variance*
w0	3	3.124566259	1.041522	0.120437
wound	3	10.68137006	3.560457	2.855913
half healed	3	5.452907316	1.817636	1.510122
confluent	3	6.980112545	2.326704	0.217747

ANOVA

Source of Variation	*SS*	*df*	*MS*	*F*	*P-value*	*F crit*
Between Groups	10.06334821	3	3.354449	2.85229	0.104854	4.066181
Within Groups	9.408438764	8	1.176055			
Total	19.47178697	11				

BimS

Anova: Single Factor

SUMMARY

Groups	*Count*	*Sum*	*Average*	*Variance*
w0	3	4.932627155	1.644209	3.876047
wound	3	1.512484645	0.504162	0.246823
half healed	3	2.293800819	0.7646	0.251385
confluent	3	0.356948281	0.118983	0.004957

ANOVA

Source of Variation	*SS*	*df*	*MS*	*F*	*P-value*	*F crit*
Between Groups	3.774561116	3	1.258187	1.149236	0.386735	4.066181
Within Groups	8.75842575	8	1.094803			
Total	12.53298687	11				

p27						
Anova: Single Factor						
SUMMARY						
Groups	*Count*	*Sum*	*Average*	*Variance*		
w0	3	3.17260921	1.057536	0.195026		
wound	3	0.10029017	0.03343	0.003332		
half healed	3	0.080003701	0.026668	0.000543		
confluent	3	0.844262574	0.281421	0.018066		
ANOVA						
Source of Variation	*SS*	*df*	*MS*	*F*	*P-value*	*F crit*
Between Groups	2.13021244	3	0.710071	13.09079	0.001877	4.066181
Within Groups	0.43393614	8	0.054242			
Total	2.56414858	11				

Data for donor 2:

Non-wounded culture (control) raw data:

GAPDH	Mean GAPDH
18.58613396	18.10951805
17.89577866	
17.84664154	

ABCG2	CEBPdelta	p63alpha
26.43935776	32.40319061	31.20609283
25.85510063	32.89717865	32.37300491
26.05326653	31.9967804	30.23963165

p63gamma	deltaNp63
29.49778557	29.52791786
30.22332382	30.08560562
30.26508522	32.50690842

Ck12	BimS
24.52094841	29.81660652
24.51516533	29.26813889
25.01069641	29.83924833

p27
39.32569122
38.13455582
38.57292938

Analysis:

ABCG2					
delta Ct	**Mean delta Ct**	deltadelta Ct	2-deltadelta Ct	**Mean 2-deltadelta Ct**	**SD 2-deltadelta Ct**
8.329839706	8.006390254	0.323449453	0.799156825	1.013894174	0.201235238
7.745582581		-0.260807673	1.198149284		
7.943748474		-0.06264178	1.044376413		

CEBPdelta					
delta Ct	**Mean delta Ct**	deltadelta Ct	2-deltadelta Ct	**Mean 2-deltadelta Ct**	**SD 2-deltadelta Ct**
14.29367256	14.32286517	-0.029192607	1.020440884	1.032496846	0.314124576
14.7876606		0.464795431	0.724573812		
13.88726234		-0.435602824	1.352475841		
p63alpha					
delta Ct	**Mean delta Ct**	deltadelta Ct	2-deltadelta Ct	**Mean 2-deltadelta Ct**	**SD 2-deltadelta Ct**
13.09657478	13.16339175	-0.066816966	1.047403235	1.186852823	0.799268299
14.26348686		1.100095113	0.466485741		
12.1301136		-1.033278147	2.046669493		
p63gamma					
delta Ct	**Mean delta Ct**	deltadelta Ct	2-deltadelta Ct	**Mean 2-deltadelta Ct**	**SD 2-deltadelta Ct**
11.38826752	11.88588015	-0.497612635	1.411875264	1.031745494	0.329427324
12.11380577		0.227925618	0.853861736		
12.15556717		0.269687017	0.829499481		
deltaNp63					
delta Ct	**Mean delta Ct**	deltadelta Ct	2-deltadelta Ct	**Mean 2-deltadelta Ct**	**SD 2-deltadelta Ct**
11.41839981	12.59729258	-1.178892771	2.264029524	1.363114681	0.999994293
11.97608757		-0.621205012	1.538159394		
14.39739037		1.800097783	0.287155125		

Ck12					
delta Ct	**Mean delta Ct**	deltadelta Ct	2-deltadelta Ct	**Mean 2-deltadelta Ct**	**SD 2-deltadelta Ct**
6.411430359	6.572751999	-0.16132164	1.118311144	1.012506254	0.187162912
6.405647278		-0.167104721	1.12280292		
6.90117836		0.328426361	0.796404699		
BimS					
delta Ct	**Mean delta Ct**	deltadelta Ct	2-deltadelta Ct	**Mean 2-deltadelta Ct**	**SD 2-deltadelta Ct**
11.70708847	11.5318132	0.175275275	0.885598525	1.017540851	0.240572291
11.15862083		-0.373192361	1.295215684		
11.72973028		0.197917086	0.871808342		

p27					
delta Ct	**Mean delta Ct**	deltadelta Ct	2-deltadelta Ct	**Mean 2-deltadelta Ct**	**SD 2-deltadelta Ct**
21.21617317	20.56820742	0.647965749	0.638179535	1.056897464	0.409806902
20.02503777		-0.543169657	1.457170463		
20.46341133		-0.104796092	1.075342392		

Wounded raw data:

GAPDH	Mean GAPDH
13.42018795	13.70203082
13.78102398	
13.90488052	

ABCG2	CEBPdelta	p63alpha
22.95735931	25.00039864	24.92903709
21.7930851	25.49892235	25.05547714
23.42022324	25.4352932	26.25605392

p63gamma	deltaNp63	Ck12	BimS	p27
28.7677269	24.18338585	21.15625763	31.33760834	29.81208038
28.57177925	23.88863564	21.00122833	27.67073441	29.54041672
28.39927864	24.92903709	22.16982651	28.83372474	29.19572258

Analysis wounded:

ABCG2				
delta Ct	deltadelta Ct	2-deltadelta Ct	**Mean 2-deltadelta Ct**	**SD 2-deltadelta Ct**
9.2553285	1.248938242	0.420757752	0.556346785	0.33979668
8.0910543	0.084664027	0.943004116		
9.7181924	1.711802164	0.305278488		
CEBPdelta				
delta Ct	deltadelta Ct	2-deltadelta Ct	**Mean 2-deltadelta Ct**	**SD 2-deltadelta Ct**
11.298368	-3.024497352	8.137002037	6.638650521	1.304091714
11.796892	-2.52597364	5.759620036		
11.733262	-2.58960279	6.01932949		
p63alpha				
delta Ct	deltadelta Ct	2-deltadelta Ct	**Mean 2-deltadelta Ct**	**SD 2-deltadelta Ct**
11.227006	-1.936385474	3.827455153	2.953112276	1.246654945
11.353446	-1.809945425	3.506290246		
12.554023	-0.609368643	1.525591429		
p63gamma				
delta Ct	deltadelta Ct	2-deltadelta Ct	**Mean 2-deltadelta Ct**	**SD 2-deltadelta Ct**
15.065696	3.179815931	0.110351953	0.126405951	0.016054198
14.869748	2.983868283	0.12640555		
14.697248	2.811367673	0.142460348		

deltaNp63				
delta Ct	deltadelta Ct	2-deltadelta Ct	**Mean 2-deltadelta Ct**	**SD 2-deltadelta Ct**
10.481355	-2.115937549	4.334716222	4.079070793	1.383854162
10.186605	-2.410687762	5.317277507		
11.227006	-1.370286304	2.585218648		

Ck12				
delta Ct	deltadelta Ct	2-deltadelta Ct	**Mean 2-deltadelta Ct**	**SD 2-deltadelta Ct**
7.4542268	0.881474813	0.542812251	0.472022958	0.178613323
7.2991975	0.726445516	0.604391168		
8.4677957	1.895043691	0.268865455		
BimS				
delta Ct	deltadelta Ct	2-deltadelta Ct	**Mean 2-deltadelta Ct**	**SD 2-deltadelta Ct**
17.635578	6.20272287	0.013576704	0.087674444	0.079966016
13.968704	2.535848938	0.17243817		
15.131694	3.698839275	0.077008458		

p27				
delta Ct	deltadelta Ct	2-deltadelta Ct	**Mean 2-deltadelta Ct**	**SD 2-deltadelta Ct**
16.11005	-4.458157854	21.98058464	27.40392197	5.905970001
15.838386	-4.72982152	26.53494255		
15.493692	-5.074515658	33.69623873		

50% healed raw data:

GAPDH	Mean GAPDH	ABCG2	CEBPdelta	p63alpha	p63gamma
13.28953838	13.13968118	22.23909569	19.29657364	24.12453842	25.54275513
13.46803284		20.77712631	19.21193504	23.44725418	25.8501339
12.66147232		24.98608208	20.36277199	23.84492874	25.80484772

deltaNp63	Ck12	BimS	p27
22.69274712	23.25068092	25.77685928	28.59992218
22.71041298	21.3268795	27.58407402	28.36197853
22.63998413	19.39462471	27.38780975	28.23180008

Analysis 50% healed:

ABCG2				
delta Ct	deltadelta Ct	2-deltadelta Ct	**Mean 2-deltadelta Ct**	**SD 2-deltadelta Ct**
9.0994145	1.093024254	0.468777667	0.610005275	0.622914369
7.6374451	-0.368945122	1.291408226		
11.846401	3.840010643	0.069829931		

CEBPdelta				
delta Ct	deltadelta Ct	2-deltadelta Ct	**Mean 2-deltadelta Ct**	**SD 2-deltadelta Ct**
6.1568925	-8.165972711	287.2120983	242.9812312	92.0489482
6.0722539	-8.250611307	304.5660466		
7.2230908	-7.099774362	137.1655488		
p63alpha				
delta Ct	deltadelta Ct	2-deltadelta Ct	**Mean 2-deltadelta Ct**	**SD 2-deltadelta Ct**
10.984857	-2.178534509	4.526934739	5.753723672	1.374475981
10.307573	-2.855818749	7.239142168		
10.705248	-2.458144189	5.495094109		
p63gamma				
delta Ct	deltadelta Ct	2-deltadelta Ct	**Mean 2-deltadelta Ct**	**SD 2-deltadelta Ct**
12.403074	0.517193797	0.69872962	0.615344671	0.072772497
12.710453	0.824572566	0.564649469		
12.665167	0.779286387	0.582654926		
deltaNp63				
delta Ct	deltadelta Ct	2-deltadelta Ct	**Mean 2-deltadelta Ct**	**SD 2-deltadelta Ct**
9.5530659	-3.044226644	8.249042355	8.318001982	0.212402044
9.5707318	-3.026560781	8.148648394		
9.500303	-3.096989629	8.556315197		

Ck12				
delta Ct	deltadelta Ct	2-deltadelta Ct	**Mean 2-deltadelta Ct**	**SD 2-deltadelta Ct**
10.111	3.538247744	0.086075845	0.553033938	0.612426572
8.1871983	1.614446322	0.326590262		
6.2549435	-0.317808469	1.246435708		
BimS				
delta Ct	deltadelta Ct	2-deltadelta Ct	**Mean 2-deltadelta Ct**	**SD 2-deltadelta Ct**
12.637178	1.204323453	0.433972806	0.233350743	0.173978585
14.444393	3.01153819	0.124004279		
14.248129	2.815273923	0.142075143		

p27				
delta Ct	deltadelta Ct	2-deltadelta Ct	**Mean 2-deltadelta Ct**	**SD 2-deltadelta Ct**
15.460241	-5.10796642	34.48665793	39.88936361	5.057591739
15.222297	-5.345910069	40.67047878		
15.092119	-5.476088521	44.51095412		

Healed raw data:

GAPDH	Mean GAPDH	ABCG2	CEBPdelta	p63alpha
13.44355106	13.48117097	30.82522774	20.80845261	18.12671661
12.36354923		22.31615067	19.81593132	19.32828903
14.63641262		29.22387198	20.00676537	18.72050667

p63gamma	deltaNp63	Ck12	BimS	p27
23.86314201	22.62920952	21.76900673	23.15462	31.42677116
23.00895119	23.59481239	22.59270096	23.68616	30.95066643
23.98031998	23.47730827	20.64428902	23.73352	32.92338562

Analysis healed:

ABCG2				
delta Ct	deltadelta Ct	2-deltadelta Ct	**Mean 2-deltadelta Ct**	**SD 2-deltadelta Ct**
17.344057	9.337666511	0.001545547	0.189771562	0.323297989
8.8349797	0.828589439	0.563079511		
15.742701	7.736310754	0.004689628		
CEBPdelta				
delta Ct	deltadelta Ct	2-deltadelta Ct	**Mean 2-deltadelta Ct**	**SD 2-deltadelta Ct**
7.3272816	-6.995583536	127.6087579	201.3154775	65.74127119
6.3347603	-7.988104822	253.8979299		
6.5255944	-7.797270777	222.4397448		
p63alpha				
delta Ct	deltadelta Ct	2-deltadelta Ct	**Mean 2-deltadelta Ct**	**SD 2-deltadelta Ct**
4.6455456	-8.517846108	366.5448965	256.2638837	104.2325557
5.8471181	-7.31627369	159.3741337		
5.2393357	-7.924056054	242.872621		
p63gamma				
delta Ct	deltadelta Ct	2-deltadelta Ct	**Mean 2-deltadelta Ct**	**SD 2-deltadelta Ct**
10.381971	-1.503909109	2.836101388	3.525967858	1.390894567
9.5277802	-2.358099935	5.126946826		
10.499149	-1.386731145	2.614855358		

deltaNp63				
delta Ct	deltadelta Ct	2-deltadelta Ct	**Mean 2-deltadelta Ct**	**SD 2-deltadelta Ct**
9.1480385	-3.449254034	10.92267287	7.527835951	2.949576627
10.113641	-2.483651159	5.593111763		
9.9961373	-2.601155279	6.067723222		

Ck12				
delta Ct	deltadelta Ct	2-deltadelta Ct	**Mean 2-deltadelta Ct**	**SD 2-deltadelta Ct**
8.2878358	1.715083758	0.304584882	0.380282561	0.254626681
9.11153	2.538777987	0.17208843		
7.163118	0.590366046	0.664174369		
BimS				
delta Ct	deltadelta Ct	2-deltadelta Ct	**Mean 2-deltadelta Ct**	**SD 2-deltadelta Ct**
9.6734444	-1.75941022	3.38559692	2.664788839	0.62538304
10.204984	-1.227870303	2.34220979		
10.25235	-1.180504229	2.266559806		

p27				
delta Ct	deltadelta Ct	2-deltadelta Ct	**Mean 2-deltadelta Ct**	**SD 2-deltadelta Ct**
17.9456	-2.622607228	6.15862049	5.635891136	3.223950995
17.469495	-3.098711965	8.566536098		
19.442215	-1.125992772	2.18251682		

ANOVA:

ABCG2						
Anova: Single Factor						
SUMMARY						
Groups	*Count*	*Sum*	*Average*	*Variance*		
w0	3	3.041682522	1.013894	0.040496		
wound	3	1.669040356	0.556347	0.115462		
half healed	3	1.830015825	0.610005	0.388022		
confluent	3	0.569314686	0.189772	0.104522		
ANOVA						
Source of Variation	*SS*	*df*	*MS*	*F*	*P-value*	*F crit*
Between Groups	1.024130202	3	0.341377	2.105635	0.177839	4.066181
Within Groups	1.29700261	8	0.162125			
Total	2.321132812	11				

CEBPΔ

Anova: Single Factor

SUMMARY

Groups	*Count*	*Sum*	*Average*	*Variance*
w0	3	3.097491	1.032497	0.098674
wound	3	19.91595	6.638651	1.700655
half healed	3	728.9437	242.9812	8473.009
confluent	3	603.9464	201.3155	4321.915

ANOVA

Source of Variation	*SS*	*df*	*MS*	*F*	*P-value*	*F crit*
Between Groups	145632.6066	3	48544.2	15.17395	0.001152	4.066181
Within Groups	25593.44586	8	3199.181			
Total	171226.0525	11				

p63α

Anova: Single Factor

SUMMARY

Groups	*Count*	*Sum*	*Average*	*Variance*
w0	3	3.560558	1.186853	0.63883
wound	3	8.859337	2.953112	1.554149
half healed	3	17.26117	5.753724	1.889184
confluent	3	768.7917	256.2639	10864.43

ANOVA

Source of Variation	*SS*	*df*	*MS*	*F*	*P-value*	*F crit*
Between Groups	144013.3488	3	48004.45	17.66736	0.000689	4.066181
Within Groups	21737.01567	8	2717.127			
Total	165750.3644	11				

ΔNp63						
Anova: Single Factor						
SUMMARY						
Groups	*Count*	*Sum*	*Average*	*Variance*		
w0	3	4.089344042	1.363115	0.999989		
wound	3	12.23721238	4.079071	1.915052		
half healed	3	24.95400595	8.318002	0.045115		
confluent	3	22.58350785	7.527836	8.700002		
ANOVA						
Source of Variation	*SS*	*df*	*MS*	*F*	*P-value*	*F crit*
Between Groups	93.17815832	3	31.05939	10.65488	0.003621	4.066181
Within Groups	23.32031567	8	2.915039			
Total	116.498474	11				

Ck12						
Anova: Single Factor						
SUMMARY						
Groups	*Count*	*Sum*	*Average*	*Variance*		
w0	3	3.037518763	1.012506	0.03503		
wound	3	3.037518763	1.012506	0.03503		
half healed	3	1.659101815	0.553034	0.375066		
confluent	3	1.140847682	0.380283	0.064835		
ANOVA						
Source of Variation	*SS*	*df*	*MS*	*F*	*P-value*	*F crit*
Between Groups	0.938614691	3	0.312872	2.454082	0.13789	4.066181
Within Groups	1.019921929	8	0.12749			
Total	1.95853662	11				

BimS

Anova: Single Factor

SUMMARY

Groups	*Count*	*Sum*	*Average*	*Variance*
w0	3	3.052622552	1.017541	0.057875
wound	3	0.263023333	0.087674	0.006395
half healed	3	0.700052228	0.233351	0.030269
confluent	3	7.994366516	2.664789	0.391104

ANOVA

Source of Variation	*SS*	*df*	*MS*	*F*	*P-value*	*F crit*
Between Groups	12.57574725	3	4.191916	34.52679	6.31E-05	4.066181
Within Groups	0.971284173	8	0.121411			
Total	13.54703142	11				

p63γ

Anova: Single Factor

SUMMARY

Groups	*Count*	*Sum*	*Average*	*Variance*
w0	3	3.095236481	1.031745	0.108522
wound	3	0.379217852	0.126406	0.000258
half healed	3	1.846034014	0.615345	0.005296
confluent	3	10.57790357	3.525968	1.934588

ANOVA

Source of Variation	*SS*	*df*	*MS*	*F*	*P-value*	*F crit*
Between Groups	20.61148807	3	6.870496	13.41459	0.001733	4.066181
Within Groups	4.097327261	8	0.512166			
Total	24.70881533	11				

p27						
Anova: Single Factor						
SUMMARY						
Groups	*Count*	*Sum*	*Average*	*Variance*		
w0	3	3.170692391	1.056897	0.167942		
wound	3	82.21176592	27.40392	34.88048		
half healed	3	119.6680908	39.88936	25.57923		
confluent	3	16.90767341	5.635891	10.39386		
ANOVA						
Source of Variation	*SS*	*df*	*MS*	*F*	*P-value*	*F crit*
Between Groups	3019.59533	3	1006.532	56.68884	9.84E-06	4.066181
Within Groups	142.0430351	8	17.75538			
Total	3161.638365	11				

8.3.2 Chapter 3 qRT-PCR Raw Data

8.3.2.1 Raw data & analysis for LSC's

Uncultured LSC's (Reference) raw data:

Uncultured LSC (Ref)	GAPDH	Mean GAPDH	Ck3	Pax6	Ck4	Ck19
	11.294883	11.51845133	19.87919	16.952593	17.19843	15.512611
	11.041767		22.413948	17.17793	16.619234	14.149673
	12.218704		21.792038	17.08068	20.11831	13.933223

Uncultured LSC (Ref)	GAPDH	Mean GAPDH	P63	Ck12
	12.710369	12.54173	21.810772	20.16528
	12.875102		20.3055	20.675987
	12.039719		20.35039	20.61389

Uncultured LSC (Ref)	GAPDH	Mean GAPDH	CD200	Ck5	Ck10	Ck15	Ck17
	11.588602	11.38714533	20.650415	10.806277	26.736977	15.76636	10.696938
	11.357899		18.141293	11.570636	26.551245	15.842326	11.6679325
	11.214935		19.40515	11.012325	25.016508	15.38431	11.525779

Uncultured LSC (Ref)	GAPDH	Mean GAPDH	Integrin alpha 6
	12.710369	12.54173	16.434387
	12.875102		16.20072
	12.039719		16.630455

Analysis:

Unc. LSC P63		Unc. LSC Ck4		Unc. LSC Ck10	
delta Ct	Mean delta Ct	delta Ct	Mean delta Ct	delta Ct	Mean delta Ct
9.269042	8.280490667	5.679978667	6.460206667	15.34983167	14.71443133
7.76377		5.100782667		15.16409967	
7.80866		8.599858667		13.62936267	

Unc. LSC Ck3		Unc. LSC Ck19		Unc. LSC Ck15	
delta Ct	Mean delta Ct	delta Ct	Mean delta Ct	delta Ct	Mean delta Ct
8.360738667	9.843274	3.994159667	3.013384333	4.379214667	4.277186667
10.89549667		2.631221667		4.455180667	
10.27358667		2.414771667		3.997164667	

Unc. LSC Ck12		Unc. LSC CD200		Unc. LSC Ck17	
delta Ct	Mean delta Ct	delta Ct	Mean delta Ct	delta Ct	Mean delta Ct
7.62355	7.943322333	9.263269667	8.011807333	-0.690207333	-0.090262167
8.134257		6.754147667		0.280787167	
8.07216		8.018004667		0.138633667	

Unc. LSC Pax6		Unc. LSC Ck5		Unc. LSC Integrin alpha 6	
delta Ct	Mean delta Ct	delta Ct	Mean delta Ct	delta Ct	Mean delta Ct
5.434141667	5.551949667	-0.580868333	-0.257399333	3.892657	3.880124
5.659478667		0.183490667		3.65899	
5.562228667		-0.374820333		4.088725	

Analysis: Uncultured LSC's (HFC Primary Culture as Reference)

Unc. LSC Ck19				
delta Ct	deltadelta Ct	2-deltadelta Ct	Mean 2-deltadelta Ct	SD 2-deltadelta Ct
3.994159667	0.535473667	0.689932121	1.508769996	0.723532873
2.631221667	-0.827464333	1.774563664		
2.414771667	-1.043914333	2.061814204		
Unc. LSC CD200				
delta Ct	deltadelta Ct	2-deltadelta Ct	Mean 2-deltadelta Ct	SD 2-deltadelta Ct
11.050797	-3.26669633	9.624398174	11.54791766	1.982688806
10.553561	-3.76393233	13.58490272		
10.802178	-3.51531533	11.43445207		
Unc. LSC Ck5				
delta Ct	deltadelta Ct	2-deltadelta Ct	Mean 2-deltadelta Ct	SD 2-deltadelta Ct
-0.580868333	-0.951082	1.933322078	1.582503774	0.40573713
0.183490667	-0.186723	1.138175477		
-0.374820333	-0.745034	1.676013768		
Unc. LSC Ck10				
delta Ct	deltadelta Ct	2-deltadelta Ct	Mean 2-deltadelta Ct	SD 2-deltadelta Ct
15.34983167	13.18767667	0.00010718	0.000194097	0.000137988
15.16409967	13.00194467	0.000121906		
13.62936267	11.46720767	0.000353205		
Unc. LSC Ck15				
delta Ct	deltadelta Ct	2-deltadelta Ct	Mean 2-deltadelta Ct	SD 2-deltadelta Ct
4.379214667	1.208006167	0.432866433	0.469212638	0.082928415
4.455180667	1.283972167	0.410663273		
3.997164667	0.825956167	0.564108208		
Unc. LSC Ck17				
delta Ct	deltadelta Ct	2-deltadelta Ct	Mean 2-deltadelta Ct	SD 2-deltadelta Ct
-0.690207333	0.90253	0.534947791	0.369673105	0.143827829
0.280787167	1.8735245	0.272905902		
0.138633667	1.731371	0.301165622		
Unc. LSC Integrin alpha 6				
delta Ct	deltadelta Ct	2-deltadelta Ct	Mean 2-deltadelta Ct	SD 2-deltadelta Ct
3.892657	3.933482	0.065449138	0.066512605	0.00995475
3.65899	3.699815	0.076956393		
4.088725	4.12955	0.057132283		

LSC's Primary Culture raw data:

LSC Primary Culture	GAPDH	Mean GAPDH	P63	Ck3	Ck12	Pax6	Ck4	Ck19
	8.359078	8.599949667	13.246313	21.553282	14.655826	17.118187	14.14509	10.107184
	9.336709		13.66911	21.064655	12.877189	16.46544	12.438586	9.350341
	8.104062		13.163901	21.501343	13.474317	16.564478	12.313976	9.225476

LSC Primary Culture	GAPDH	Mean GAPDH	CD200	Ck5	Ck10	Ck15	Ck17	Integrin alpha 6
	7.1996164	7.947047933	26.398317	8.753448	22.20741	12.374764	9.483575	13.540519
	8.656573		26.575365	8.062856	21.904722	13.772566	9.627451	13.361993
	7.9849544		25.32438	8.848768	21.312513	13.285127	9.771328	13.092225

Analysis (Uncultured LSC's as reference):

LSC Primary C P63				
delta Ct	deltadelta Ct	2-deltadelta Ct	Mean 2-deltadelta Ct	SD 2-deltadelta Ct
4.646363333	-3.634127334	12.41598947	11.60797214	2.064152888
5.069160333	-3.211330334	9.262042222		
4.563951333	-3.716539334	13.14588472		
LSC Primary C Ck3				
delta Ct	deltadelta Ct	2-deltadelta Ct	Mean 2-deltadelta Ct	SD 2-deltadelta Ct
12.95333233	3.110058333	0.115818825	0.132796559	0.025816921
12.46470533	2.621431333	0.162506425		
12.90139333	3.058119333	0.120064426		
LSC Primary C Ck12				
delta Ct	deltadelta Ct	2-deltadelta Ct	Mean 2-deltadelta Ct	SD 2-deltadelta Ct
6.055876333	-1.887446	3.699796703	8.261840447	4.498542481
4.277239333	-3.666083	12.69407177		
4.874367333	-3.068955	8.391652865		
LSC Primary C Pax6				
delta Ct	deltadelta Ct	2-deltadelta Ct	Mean 2-deltadelta Ct	SD 2-deltadelta Ct
8.518237333	2.966287666	0.127955346	0.172313771	0.03899081
7.865490333	2.313540666	0.201166131		
7.964528333	2.412578666	0.187819835		
LSC Primary C Ck4				
delta Ct	deltadelta Ct	2-deltadelta Ct	Mean 2-deltadelta Ct	SD 2-deltadelta Ct
5.545140333	-0.915066334	1.88565577	4.916411868	2.639350377
3.838636333	-2.621570334	6.154195753		
3.714026333	-2.746180334	6.709384081		

LSC Primary C Ck19				
delta Ct	deltadelta Ct	2-deltadelta Ct	Mean 2-deltadelta Ct	SD 2-deltadelta Ct
1.507234333	-1.50615	2.840510035	4.291389796	1.275093694
0.750391333	-2.262993	4.799862239		
0.625526333	-2.387858	5.233797113		

LSC Primary C Ck15				
delta Ct	deltadelta Ct	2-deltadelta Ct	Mean 2-deltadelta Ct	SD 2-deltadelta Ct
4.427716067	0.1505294	0.900919808	0.574053518	0.291295284
5.825518067	1.5483314	0.341905278		
5.338079067	1.0608924	0.479335468		
LSC Primary C Integrin alpha 6				
delta Ct	deltadelta Ct	2-deltadelta Ct	Mean 2-deltadelta Ct	SD 2-deltadelta Ct
5.593471067	1.713347067	0.304951757	0.355385986	0.056272615
5.414945067	1.534821067	0.34512214		
5.145177067	1.265053067	0.416084062		

Analysis (HFC Primary Culture as reference):

LSC Primary C Ck19				
delta Ct	deltadelta Ct	2-deltadelta Ct	Mean 2-deltadelta Ct	SD 2-deltadelta Ct
1.507234333	-1.951451667	3.867635045	5.843151181	1.736166039
0.750391333	-2.708294667	6.535486649		
0.625526333	-2.833159667	7.12633185		
LSC Primary C CD200				
delta Ct	deltadelta Ct	2-deltadelta Ct	Mean 2-deltadelta Ct	SD 2-deltadelta Ct
18.45126907	4.133775737	0.056965184	0.075757645	0.038388143
18.62831707	4.310823737	0.050386333		
17.37733207	3.059838737	0.119921419		
LSC Primary C Ck5				
delta Ct	deltadelta Ct	2-deltadelta Ct	Mean 2-deltadelta Ct	SD 2-deltadelta Ct
0.806400067	0.4361864	0.739085718	0.874587292	0.276629382
0.115808067	-0.2544056	1.192844182		
0.901720067	0.5315064	0.691831976		
LSC Primary C Ck10				
delta Ct	deltadelta Ct	2-deltadelta Ct	Mean 2-deltadelta Ct	SD 2-deltadelta Ct
14.26036207	12.09820707	0.000228075	0.000311163	0.000101364
13.95767407	11.79551907	0.000281316		
13.36546507	11.20331007	0.000424099		
LSC Primary C Ck15				
delta Ct	deltadelta Ct	2-deltadelta Ct	Mean 2-deltadelta Ct	SD 2-deltadelta Ct
4.427716067	1.256507567	0.418555962	0.266698013	0.135332109
5.825518067	2.654309567	0.158844873		
5.338079067	2.166870567	0.222693203		
LSC Primary C Ck17				
delta Ct	deltadelta Ct	2-deltadelta Ct	Mean 2-deltadelta Ct	SD 2-deltadelta Ct
1.536527067	3.1292644	0.114287189	0.103782718	0.010337153
1.680403067	3.2731404	0.103439535		
1.824280067	3.4170174	0.093621429		
LSC Primary C Integrin alpha 6				
delta Ct	deltadelta Ct	2-deltadelta Ct	Mean 2-deltadelta Ct	SD 2-deltadelta Ct
5.593471067	5.634296067	0.020132972	0.023462649	0.003715128
5.414945067	5.455770067	0.022785028		
5.145177067	5.186002067	0.027469947		

LSC's Passage 1 raw data:

LSC P1	GAPDH	Mean GAPDH	Ck3	Ck12	Ck4	Ck19	CD200
	9.573734	9.312279333	18.907356	16.869528	12.550445	12.299691	28.146828
	9.30426		17.795135	17.991283	10.507486	11.258408	27.580507
	9.058844		17.837193	18.24982	11.687729	11.913637	27.863667

Ck5	Ck10	Ck15	Ck17
8.771126	16.11122	11.913637	10.999483
9.016165	16.778309	11.813983	9.560559
9.981883	16.554111	12.7439575	10.212807

Analysis (Uncultured LSC's as reference):

LSC P1 Ck3					
delta Ct		deltadelta Ct	2-deltadelta Ct	Mean 2-deltadelta Ct	SD 2-deltadelta Ct
	9.595076667	-0.248197333	1.187722113	2.083047832	0.776251666
	8.482855667	-1.360418333	2.567596204		
	8.524913667	-1.318360333	2.493825179		
LSC P1 Ck12					
delta Ct		deltadelta Ct	2-deltadelta Ct	Mean 2-deltadelta Ct	SD 2-deltadelta Ct
	7.557248667	-0.386073666	1.306831981	0.803124707	0.438996166
	8.679003667	0.735681334	0.600534347		
	8.937540667	0.994218334	0.502007793		
LSC P1 Ck4					
delta Ct		deltadelta Ct	2-deltadelta Ct	Mean 2-deltadelta Ct	SD 2-deltadelta Ct
	3.238165667	-3.222041	9.331060136	21.58385311	15.09937085
	1.195206667	-5.265	38.45235359		
	2.375449667	-4.084757	16.9681456		
LSC P1 Ck19					
delta Ct		deltadelta Ct	2-deltadelta Ct	Mean 2-deltadelta Ct	SD 2-deltadelta Ct
	2.987411667	-0.025972666	1.018165909	1.481387703	0.554251724
	1.946128667	-1.067255666	2.095443564		
	2.601357667	-0.412026666	1.330553634		
LSC P1 Ck15					
delta Ct		deltadelta Ct	2-deltadelta Ct	Mean 2-deltadelta Ct	SD 2-deltadelta Ct
	2.601357667	-1.675829	3.195028943	2.805150999	0.880615324
	2.501703667	-1.775483	3.423526074		
	3.431678167	-0.8455085	1.796897979		

Analysis (HFC Primary Culture as reference):

LSC P1 Ck19				
delta Ct	deltadelta Ct	2-deltadelta Ct	Mean 2-deltadelta Ct	SD 2-deltadelta Ct
2.987411667	-0.471274333	1.386333477	2.017055713	0.75466848
1.946128667	-1.512557333	2.853153435		
2.601357667	-0.857328333	1.811680227		

LSC P1 CD200				
delta Ct	deltadelta Ct	2-deltadelta Ct	Mean 2-deltadelta Ct	SD 2-deltadelta Ct
18.83454867	4.517055337	0.043674793	0.05383065	0.010514899
18.26822767	3.950734337	0.064671132		
18.55138767	4.233894337	0.053146027		

LSC P1 Ck5				
delta Ct	deltadelta Ct	2-deltadelta Ct	Mean 2-deltadelta Ct	SD 2-deltadelta Ct
-0.541153333	-0.911367	1.880826799	1.426817055	0.551842442
-0.296114333	-0.666328	1.58702846		
0.669603667	0.29939	0.812595906		

LSC P1 Ck10				
delta Ct	deltadelta Ct	2-deltadelta Ct	Mean 2-deltadelta Ct	SD 2-deltadelta Ct
6.798940667	4.636785667	0.040196518	0.031694084	0.00766467
7.466029667	5.303874667	0.025314808		
7.241831667	5.079676667	0.029570928		

LSC P1 Ck15				
delta Ct	deltadelta Ct	2-deltadelta Ct	Mean 2-deltadelta Ct	SD 2-deltadelta Ct
2.601357667	-0.569850833	1.484370087	1.303237719	0.409122756
2.501703667	-0.669504833	1.590526968		
3.431678167	0.260469667	0.834816102		

LSC P1 Ck17				
delta Ct	deltadelta Ct	2-deltadelta Ct	Mean 2-deltadelta Ct	SD 2-deltadelta Ct
1.687203667	3.279941	0.102953087	0.186560639	0.088426801
0.248279667	1.841017	0.279124951		
0.900527667	2.493265	0.177603879		

8.3.2.2 Raw data & analysis for HFC

HFC Primary Culture (Reference) raw data:

HFC Primary Culture	GAPDH	Mean GAPDH	P63	Ck3	Pax6
	12.499685	11.65712967	14.521938	29.347393	25.67796
	10.88298		14.819979	30.004017	25.638582
	11.588724		16.670238	29.88038	25.166569

HFC Primary Culture	GAPDH	Mean GAPDH	CD200	Ck5	Ck10	Ck15	Ck17
	10.746106	10.85057267	24.932955	10.536768	12.612616	14.741912	9.958075
	11.149752		25.759678	11.726547	12.985474	13.7867365	8.420468
	10.65586		24.811565	11.399044	13.440093	13.536695	9.394963

HFC Primary Culture	GAPDH	Mean GAPDH	Ck12	Ck4	Ck19	Integrin alpha 6
	13.554301	13.42983333	25.72801	21.823935	18.288239	13.8985
	13.042395		25.691408	20.192982	16.630455	13.995594
	13.692804		24.517683	23.19751	15.746864	12.272931

Analysis:

HFC PC P63		
delta Ct		Mean delta Ct
	2.864808333	3.680255333
	3.162849333	
	5.013108333	
HFC PC Ck3		
delta Ct		Mean delta Ct
	17.69026333	18.08680033
	18.34688733	
	18.22325033	
HFC PC Ck12		
delta Ct		Mean delta Ct
	12.29817667	11.88253367
	12.26157467	
	11.08784967	
HFC PC Pax6		
delta Ct		Mean delta Ct
	14.02083033	13.83724067
	13.98145233	
	13.50943933	
HFC PC Ck4		
delta Ct		Mean delta Ct
	8.394101667	8.308309
	6.763148667	
	9.767676667	
HFC PC Ck19		
delta Ct		Mean delta Ct
	4.858405667	3.458686
	3.200621667	
	2.317030667	

HFC PC CD200	
delta Ct	Mean delta Ct
14.08238233	14.31749333
14.90910533	
13.96099233	

HFC PC Ck5	
delta Ct	Mean delta Ct
-0.313804667	0.370213667
0.875974333	
0.548471333	
HFC PC Ck10	
delta Ct	Mean delta Ct
1.762043333	2.162155
2.134901333	
2.589520333	
HFC PC Ck15	
delta Ct	Mean delta Ct
3.891339333	3.1712085
2.936163833	
2.686122333	
HFC PC Ck17	
delta Ct	Mean delta Ct
-0.892497667	-1.592737333
-2.430104667	
-1.455609667	
HFC PC Integrin alpha 6	
delta Ct	Mean delta Ct
0.468666667	-0.040825
0.565760667	
-1.156902333	

Analysis (Uncultured LSC's as reference):

HFC PC P63				
delta Ct	deltadelta Ct	2-deltadelta Ct	Mean 2-deltadelta Ct	SD 2-deltadelta Ct
2.864808333	-5.415682334	42.68574144	29.01114153	17.25165709
3.162849333	-5.117641334	34.71870746		
5.013108333	-3.267382334	9.628975678		
HFC PC Ck3				
delta Ct	deltadelta Ct	2-deltadelta Ct	Mean 2-deltadelta Ct	SD 2-deltadelta Ct
17.69026333	7.846989333	0.00434331	0.003366765	0.000854649
18.34688733	8.503613333	0.002755227		
18.22325033	8.379976333	0.003001759		
HFC PC Ck12				
delta Ct	deltadelta Ct	2-deltadelta Ct	Mean 2-deltadelta Ct	SD 2-deltadelta Ct
12.29817667	4.354854334	0.048871787	0.070694602	0.036716068
12.26157467	4.318252334	0.050127555		
11.08784967	3.144527334	0.113084466		
HFC PC Pax6				
delta Ct	deltadelta Ct	2-deltadelta Ct	Mean 2-deltadelta Ct	SD 2-deltadelta Ct
14.02083033	8.468880666	0.002822363	0.003248629	0.000671816
13.98145233	8.429502666	0.00290046		
13.50943933	7.957489666	0.004023064		
HFC PC Ck4				
delta Ct	deltadelta Ct	2-deltadelta Ct	Mean 2-deltadelta Ct	SD 2-deltadelta Ct
8.394101667	1.933895	0.261721618	0.391108841	0.372069164
6.763148667	0.302942	0.810597708		
9.767676667	3.30747	0.101007197		
HFC PC Ck19				
delta Ct	deltadelta Ct	2-deltadelta Ct	Mean 2-deltadelta Ct	SD 2-deltadelta Ct
4.858405667	1.845021334	0.278351288	0.925680463	0.672280548
3.200621667	0.187237334	0.878285972		
2.317030667	-0.696353666	1.620404129		
HFC PC Ck15				
delta Ct	deltadelta Ct	2-deltadelta Ct	Mean 2-deltadelta Ct	SD 2-deltadelta Ct
3.891339333	-0.385847334	1.306626979	2.284216952	0.879897327
2.936163833	-1.341022834	2.533308602		
2.686122333	-1.591064334	3.012715275		
HFC PC Integrin alpha 6				
delta Ct	deltadelta Ct	2-deltadelta Ct	Mean 2-deltadelta Ct	SD 2-deltadelta Ct
0.468666667	-3.411457333	10.64022928	17.8066105	13.01688865
0.565760667	-3.314363333	9.9477023		
-1.156902333	-5.037026333	32.83189992		

HFC Passage 1 raw data:

HFC P1	GAPDH	Mean GAPDH	Ck12	Pax6	Ck4	Ck19
	8.855484	10.64027933	31.47055	25.794199	22.263073	19.857054
	11.227261		32.134106	25.438528	21.479464	20.292559
	11.838093		31.070105	25.585598	21.760546	20.549868

HFC P1	GAPDH	Mean GAPDH	CD200	Ck5	Ck15	Ck17	Integrin alpha 6
	11.050922	11.02479633	24.639254	11.17292	15.904392	10.242707	15.214582
	11.537326		24.631548	11.378112	15.67127	10.626658	14.851313
	10.486141		24.935446	11.050922	15.927067	10.486141	16.711315

HFC P1	GAPDH	Mean GAPDH	P63	Ck3	Ck10
	10.187325	11.14463267	17.322968	25.26475	17.68278
	10.91754		18.442383	24.57613	15.56923
	12.329033		18.51351	24.476488	16.41226

Analysis (HFC Primary Culture as reference):

HFC P1 Ck19				
delta Ct	deltadelta Ct	2-deltadelta Ct	Mean 2-deltadelta Ct	SD 2-deltadelta Ct
9.216774667	5.758088667	0.018477474	0.014523792	0.003601251
9.652279667	6.193593667	0.013662889		
9.909588667	6.450902667	0.011431015		
HFC P1 CD200				
delta Ct	deltadelta Ct	2-deltadelta Ct	Mean 2-deltadelta Ct	SD 2-deltadelta Ct
13.61445767	-0.703035663	1.627926612	1.530117989	0.177013771
13.60675167	-0.710741663	1.636645271		
13.91064967	-0.406843663	1.325782085		
HFC P1 Ck5				
delta Ct	deltadelta Ct	2-deltadelta Ct	Mean 2-deltadelta Ct	SD 2-deltadelta Ct
0.148123667	-0.22209	1.166422133	1.149184036	0.129645703
0.353315667	-0.016898	1.011781665		
0.026125667	-0.344088	1.26934831		
HFC P1 Ck10				
delta Ct	deltadelta Ct	2-deltadelta Ct	Mean 2-deltadelta Ct	SD 2-deltadelta Ct
6.538147333	4.375992333	0.04816095	0.124255791	0.08043302
4.424597333	2.262442333	0.20841885		
5.267627333	3.105472333	0.116187572		
HFC P1 Ck15				
delta Ct	deltadelta Ct	2-deltadelta Ct	Mean 2-deltadelta Ct	SD 2-deltadelta Ct
4.879595667	1.708387167	0.306001967	0.322299783	0.03244904
4.646473667	1.475265167	0.359667282		
4.902270667	1.731062167	0.301230098		
HFC P1 Ck17				
delta Ct	deltadelta Ct	2-deltadelta Ct	Mean 2-deltadelta Ct	SD 2-deltadelta Ct
-0.782089333	0.810648	0.570125723	0.496212439	0.067799729
-0.398138833	1.1945985	0.436908022		
-0.538655333	1.054082	0.481603573		
HFC P1 Integrin alpha 6				
delta Ct	deltadelta Ct	2-deltadelta Ct	Mean 2-deltadelta Ct	SD 2-deltadelta Ct
4.189785667	4.230610667	0.053267129	0.046887365	0.025429478
3.826516667	3.867341667	0.068519495		
5.686518667	5.727343667	0.018875469		

Analysis (Uncultured LSC's as reference):

HFC P1 P63				
delta Ct	deltadelta Ct	2-deltadelta Ct	Mean 2-deltadelta Ct	SD 2-deltadelta Ct
6.178335333	-2.102155334	4.293503398	2.716955648	1.366157593
7.297750333	-0.982740334	1.976215578		
7.368877333	-0.911613334	1.881147968		
HFC P1 Ck3				
delta Ct	deltadelta Ct	2-deltadelta Ct	Mean 2-deltadelta Ct	SD 2-deltadelta Ct
14.12011733	4.276843333	0.05158719	0.074607695	0.020156761
13.43149733	3.588223333	0.083145193		
13.33185533	3.488581333	0.089090701		
HFC P1 Ck12				
delta Ct	deltadelta Ct	2-deltadelta Ct	Mean 2-deltadelta Ct	SD 2-deltadelta Ct
20.83027067	12.88694833	0.000132021	0.000129875	4.54924E-05
21.49382667	13.55050433	8.33473E-05		
20.42982567	12.48650333	0.000174256		
HFC P1 Pax6				
delta Ct	deltadelta Ct	2-deltadelta Ct	Mean 2-deltadelta Ct	SD 2-deltadelta Ct
15.15391967	9.60197	0.001286824	0.001473476	0.000180267
14.79824867	9.246299	0.001646594		
14.94531867	9.393369	0.001487011		
HFC P1 Ck4				
delta Ct	deltadelta Ct	2-deltadelta Ct	Mean 2-deltadelta Ct	SD 2-deltadelta Ct
11.62279367	5.162587	0.027919424	0.038511352	0.01011132
10.83918467	4.378978	0.048061384		
11.12026667	4.66006	0.039553249		
HFC P1 Ck19				
delta Ct	deltadelta Ct	2-deltadelta Ct	Mean 2-deltadelta Ct	SD 2-deltadelta Ct
9.216774667	6.203390334	0.013570425	0.01066672	0.00264487
9.652279667	6.638895334	0.010034445		
9.909588667	6.896204334	0.008395289		
HFC P1 Ck15				
delta Ct	deltadelta Ct	2-deltadelta Ct	Mean 2-deltadelta Ct	SD 2-deltadelta Ct
4.879595667	0.602409	0.658653223	0.693733418	0.069844861
4.646473667	0.369287	0.774165006		
4.902270667	0.625084	0.648382025		
HFC P1 Integrin alpha 6				
delta Ct	deltadelta Ct	2-deltadelta Ct	Mean 2-deltadelta Ct	SD 2-deltadelta Ct
4.189785667	0.309661667	0.806830951	0.710197408	0.385177324
3.826516667	-0.053607333	1.037856753		
5.686518667	1.806394667	0.28590452		

HFC Passage 2 raw data:

HFC P2	GAPDH	Mean GAPDH	Ck19	Ck10	Ck17
	12.710651	13.13383467	19.811657	16.312973	9.175393
	13.971031		20.13226	16.554111	10.25762
	12.719822		19.392366	17.623428	10.02461

HFC P2	GAPDH	Mean GAPDH	Ck5	Ck15
	12.710651	13.13383467	11.064633	14.680196
	13.971031		12.412788	14.823852
	12.719822		12.301066	15.973452

HFC P2	GAPDH	Mean GAPDH	Ck3	Ck12	Pax6	Ck4	Ck19
	12.710651	13.13383467	27.586485	23.739988	24.922926	20.28024	19.811657
	13.971031		24.934656	26.364153	25.674995	20.807514	20.13226
	12.719822		25.297516	25.05207	28.364243	18.695595	19.392366

Analysis (HFC Primary Culture as reference):

HFC P2 Ck19				
delta Ct	deltadelta Ct	2-deltadelta Ct	Mean 2-deltadelta Ct	SD 2-deltadelta Ct
6.677822333	3.219136333	0.107384946	0.112324844	0.029123818
6.998425333	3.539739333	0.085986898		
6.258531333	2.799845333	0.143602689		
HFC P2 Ck5				
delta Ct	deltadelta Ct	2-deltadelta Ct	Mean 2-deltadelta Ct	SD 2-deltadelta Ct
-2.069201667	-2.439415334	5.424218646	3.285656759	1.854034131
-0.721046667	-1.091260334	2.130600838		
-0.832768667	-1.202982334	2.302150792		
HFC P2 Ck10				
delta Ct	deltadelta Ct	2-deltadelta Ct	Mean 2-deltadelta Ct	SD 2-deltadelta Ct
3.179138333	1.016983333	0.494148534	0.370491382	0.153108457
3.420276333	1.258121333	0.418088036		
4.489593333	2.327438333	0.199237576		
HFC P2 Ck15				
delta Ct	deltadelta Ct	2-deltadelta Ct	Mean 2-deltadelta Ct	SD 2-deltadelta Ct
1.546361333	-1.624847167	3.084094917	2.378095622	0.98063662
1.690017333	-1.481191167	2.791791435		
2.839617333	-0.331591167	1.258400515		
HFC P2 Ck17				
delta Ct	deltadelta Ct	2-deltadelta Ct	Mean 2-deltadelta Ct	SD 2-deltadelta Ct
-3.958441667	-2.365704334	5.154042143	3.483078365	1.462738461
-2.876218667	-1.283481334	2.434256735		
-3.109224667	-1.516487334	2.860936216		

Analysis (Uncultured LSC's as reference):

HFC P2 Ck3					
delta Ct		deltadelta Ct	2-deltadelta Ct	Mean 2-deltadelta Ct	SD 2-deltadelta Ct
	14.45265033	4.609376333	0.0409675	0.166214742	0.112181475
	11.80082133	1.957547333	0.257465792		
	12.16368133	2.320407333	0.200210933		
HFC P2 Ck12					
delta Ct		deltadelta Ct	2-deltadelta Ct	Mean 2-deltadelta Ct	SD 2-deltadelta Ct
	10.60615333	2.662831	0.157909404	0.082372812	0.0681177
	13.23031833	5.286996	0.025612715		
	11.91823533	3.974913	0.063596316		
HFC P2 Pax6					
delta Ct		deltadelta Ct	2-deltadelta Ct	Mean 2-deltadelta Ct	SD 2-deltadelta Ct
	11.78909133	6.237141666	0.013256634	0.007449385	0.006029203
	12.54116033	6.989210666	0.007871146		
	15.23040833	9.678458666	0.001220376		
HFC P2 Ck4					
delta Ct		deltadelta Ct	2-deltadelta Ct	Mean 2-deltadelta Ct	SD 2-deltadelta Ct
	7.146405333	0.686198666	0.621489246	0.972258692	0.778157112
	7.673679333	1.213472666	0.431229367		
	5.561760333	-0.898446334	1.864057462		
HFC P2 Ck19					
delta Ct		deltadelta Ct	2-deltadelta Ct	Mean 2-deltadelta Ct	SD 2-deltadelta Ct
	6.677822333	3.664438	0.078866805	0.082494818	0.021389427
	6.998425333	3.985041	0.063151421		
	6.258531333	3.245147	0.105466228		
HFC P2 Ck15					
delta Ct		deltadelta Ct	2-deltadelta Ct	Mean 2-deltadelta Ct	SD 2-deltadelta Ct
	1.546361333	-2.730825334	6.638352934	5.118726394	2.110769013
	1.690017333	-2.587169334	6.009184983		
	2.839617333	-1.437569334	2.708641264		

8.3.3 Chapter 4 qRT-PCR Raw Data

8.3.3.1 Raw data for Upper 3D vs. 2D and stroma, n = 3

Stroma raw data (main reference):

In vivo stroma 1	beta actin	mean beta actin	Keratocan	Alpha smooth	GAPDH
	21	20.23333333	21	27.1	16.3
	19.7		21.3	27.3	16.6
	20		21.4	26.8	16.5

beta actin	mean beta actin	Lumican	Aldh1a1
20.4	20.03333333	20.6	18.1
20		19.6	18
19.7		19.2	19.2

Stroma raw data 1 (ref.):

beta actin	mean beta actin	Keratocan	Alpha smooth	GAPDH	beta actin	mean beta actin	Lumican	Aldh1a1
19.9	19.53333333	21.3	29.1	17.4	21.1	21.4	21.5	19
19.7		21	29.5	16.8	21.9		20.3	19.3
19		20	29.5	17	21.2		20.6	19.7

Stroma raw data 2 (ref.):

beta actin	mean beta actin	Keratocan	Alpha smooth	GAPDH	beta actin	mean beta actin	Lumican	Aldh1a1
24	23.36666667	24.4	30.4	20.5	21.9	22.9	23.4	18.2
23.8		25.5	32	20.3	24.6		19	18.5
22.3		25	30.5	19	22.2		20.8	18.3

Stroma raw data 3 (ref.):

beta actin	mean beta actin	Keratocan	Alpha smooth	GAPDH	beta actin	mean beta actin	Lumican	Aldh1a1
17.5	18.26666667	21.2	29.1	14.9	20.5	20.2	19.9	20.2
18.5		21.3	31.1	14.8	19.7		21.1	19.9
18.8		22.1	27.6	15.3	20.4		20.4	19.4

Upper 2D raw data 1:

Upper 2D	beta actin	mean beta actin	Keratocan	Alpha smooth	GAPDH
	16	15.56666667	25.7	19.4	15.4
	14.8		24.5	19.4	15.6
	15.9		24.7	19.2	15.7

Upper 2D	beta actin	mean beta actin	Lumican	Aldh1a1
	17.5	16.73333333	20.2	24
	15.4		19.2	23.6
	17.3		20	24.8

Upper 3D raw data 1:

Upper 3D	beta actin	mean beta actin	Keratocan	Alpha smooth	GAPDH
	17.4	17.26666667	30.4	26.2	14.8
	16.9		30.3	26.2	14.7
	17.5		31	26.5	14.7

Upper 3D	beta actin	mean beta actin	Lumican	Aldh1a1
	17	17.36666667	19.2	24.6
	17.9		20.1	24.1
	17.2		18.8	23.8

Upper 2D raw data 2:

Upper 2D	beta actin	mean beta actin	Keratocan	Alpha smooth	GAPDH
	14.9	15.16666667	19.8	17.3	16
	15.5		19.4	17.4	16.3
	15.1		20.9	17	16.7

Upper 2D	beta actin	mean beta actin	Lumican	Aldh1a1
	17.2	17.33333333	17.8	23.6
	17.8		16.9	22
	17		16.7	22.6

Upper 3D raw data 2:

Upper 3D	beta actin	mean beta actin	Keratocan	Alpha smooth	GAPDH
	16.1	16.7	29.2	25.5	14.3
	16.6		30	26.2	15.4
	17.4		31.6	25.3	14.7

Upper 3D	beta actin	mean beta actin	Lumican	Aldh1a1
	17.8	17	21.1	23.6
	16.8		21	24.2
	16.4		21.5	24.3

Upper 2D raw data 3:

Upper 2D	beta actin	mean beta actin	Keratocan	Alpha smooth	GAPDH
	19.2	19.23333333	26.6	23.5	17.4
	19.2		24.9	22.1	17.7
	19.3		23.4	22.7	17.4

Upper 2D	beta actin	mean beta actin	Lumican	Aldh1a1
	17.9	18.2	16	24.9
	18.8		16.5	25.8
	17.9		15.8	26.1

Upper 3D raw data 3:

Upper 3D	beta actin	mean beta actin	Keratocan	Alpha smooth	GAPDH
	18.1	18.23333333	33.7	29.7	15.9
	18.3		33.3	29	15.4
	18.3		31.3	28.7	15.9

Upper 3D	beta actin	mean beta actin	Lumican	Aldh1a1
	17.4	16.43333333	19	18.9
	16.1		19.5	20
	15.8		19.1	19.8

ANOVA single factor analysis:

Keratocan

Anova: Single Factor						
SUMMARY						
Groups	Count	Sum	Average	Variance		
In vivo stroma	3	1.827601818	0.609201	0.129147		
2D	3	0.18538628	0.061795	0.001641		
3D	3	0.001383433	0.000461	1.99E-07		
ANOVA						
Source of Variation	SS	df	MS	F	P-value	F crit
Between Groups	0.673978057	2	0.336989	7.729799	0.021856922	5.14325285
Within Groups	0.261576552	6	0.043596			
Total	0.935554609	8				

Alpha-smooth muscle actin

Anova: Single Factor						
SUMMARY						
Groups	Count	Sum	Average	Variance		
In vivo stroma	3	0.867729332	0.289243	0.101669		
2D	3	388.1887328	129.3962	10467.87		
3D	3	5.918601098	1.972867	3.65632		
ANOVA						
Source of Variation	SS	df	MS	F	P-value	F crit
Between Groups	32908.1694	2	16454.08	4.713905	0.058822	5.14325285
Within Groups	20943.2554	6	3490.543			
Total	53851.4248	8				

GAPDH

Anova: Single Factor						
SUMMARY						
Groups	Count	Sum	Average	Variance		
In vivo stroma	3	2.015963834	0.671988	0.058252		
2D	3	0.495697025	0.165232	0.015674		
3D	3	1.840735373	0.613578	0.00794		
ANOVA						
Source of Variation	SS	df	MS	F	P-value	F crit
Between Groups	0.461227149	2	0.230614	8.450884	0.017982	5.14325285
Within Groups	0.163732155	6	0.027289			
Total	0.624959304	8				

Lumican

Anova: Single Factor						
SUMMARY						
Groups	Count	Sum	Average	Variance		
In vivo stroma	3	7.763186031	2.587729	7.125008		
2D	3	2.175113408	0.725038	0.293843		
3D	3	0.399287968	0.133096	0.026577		
ANOVA						
Source of Variation	SS	df	MS	F	P-value	F crit
Between Groups	9.845234034	2	4.922617	1.983479	0.218155	5.14325285
Within Groups	14.8908574	6	2.48181			
Total	24.73609144	8				

Aldh1a1

Anova: Single Factor						
SUMMARY						
Groups	Count	Sum	Average	Variance		
In vivo stroma	3	9.692010904	3.23067	16.21363		
2D	3	0.011358357	0.003786	9.76E-06		
3D	3	0.014101136	0.0047	7.07E-06		
ANOVA						
Source of Variation	SS	df	MS	F	P-value	F crit
Between Groups	20.8196643	2	10.40983	1.926124	0.225864411	5.14325285
Within Groups	32.42729972	6	5.40455			
Total	53.24696402	8				

8.3.3.1 Raw data for Whole 3D vs. 2D, n=3

Whole 2D raw data 1:

Whole 2D	beta actin	mean beta actin	Keratocan	Alpha smooth	GAPDH
	17.3	17.06666667	20.7	23.8	14.6
	17		21.1	24.2	14.4
	16.9		21.1	23.5	14.5

Whole 2D	beta actin	mean beta actin	Lumican	Aldh1a1
	18.2	17.93333333	15.7	19.8
	17.8		17.3	19.6
	17.8		16.7	19.7

Whole 3D raw data 1:

Whole 2D	beta actin	mean beta actin	Keratocan	Alpha smooth	GAPDH
	17.3	17.06666667	20.7	23.8	14.6
	17		21.1	24.2	14.4
	16.9		21.1	23.5	14.5

Whole 2D	beta actin	mean beta actin	Lumican	Aldh1a1
	18.2	17.93333333	15.7	19.8
	17.8		17.3	19.6
	17.8		16.7	19.7

Whole 2D raw data 2:

Whole 2D	beta actin	mean beta actin	Keratocan	Alpha smooth	GAPDH
	16	16	20.1	22.5	14.4
	15.4		20.2	21.9	15
	16.6		21.4	22	14.8

Whole 2D	beta actin	mean beta actin	Lumican	Aldh1a1
	17	18.06666667	19.1	19.8
	18.5		20.9	19.6
	18.7		19.1	19.7

Whole 3D raw data 2:

Whole 3D	beta actin	mean beta actin	Keratocan	Alpha smooth	GAPDH
	15.6	15.93333333	24.4	24.3	13.3
	16.2		23.7	24.7	13.8
	16		24.1	25.8	13.4

Whole 3D	beta actin	mean beta actin	Lumican	Aldh1a1
	18.7	18.66666667	17.7	20.6
	17.7		17.9	20.5
	19.6		17.6	20.3

Whole 2D raw data 3:

Whole 2D	beta actin	mean beta actin	Keratocan	Alpha smooth	GAPDH
	19.8	19.83333333	25.7	23.9	20.3
	20		26.8	24.1	20.8
	19.7		26.5	24.1	20.6

Whole 2D	beta actin	mean beta actin	Lumican	Aldh1a1
	17.8	18.13333333	14.5	25.9
	18.5		15.8	25.9
	18.1		15.7	26.6

Whole 3D raw data 3:

Whole 3D	beta actin	mean beta actin	Keratocan	Alpha smooth	GAPDH
	20.8	20.7	29.8	29.9	18
	20.7		29.5	29.9	18
	20.6		29.8	29.9	18.4

Whole 3D	beta actin	mean beta actin	Lumican	Aldh1a1
	16.8	17.63333333	15.9	23.7
	17.8		15.4	25
	18.3		15.1	24.3

ANOVA single factor analysis:

Keratocan

Anova: Single Factor						
SUMMARY						
Groups	Count	Sum	Average	Variance		
In vivo stroma	3	1.827601818	0.609201	0.129147		
2D	3	2.355249886	0.785083	1.530501		
3D	3	0.207388494	0.069129	0.011491		
ANOVA						
Source of Variation	SS	df	MS	F	P-value	F crit
Between Groups	0.835201362	2	0.417601	0.74967	0.512135	5.143253
Within Groups	3.342276767	6	0.557046			
Total	4.17747813	8				

Alpha-smooth muscle actin

Anova: Single Factor						
SUMMARY						
Groups	Count	Sum	Average	Variance		
In vivo stroma	3	0.867729332	0.289243	0.101669		
2D	3	89.03853763	29.67951	950.9785		
3D	3	11.92352988	3.97451	24.79761		
ANOVA						
Source of Variation	SS	df	MS	F	P-value	F crit
Between Groups	1538.116287	2	769.0581	2.364204	0.174923	5.143253
Within Groups	1951.755478	6	325.2926			
Total	3489.871765	8				

GAPDH

Anova: Single Factor						
SUMMARY						
Groups	Count	Sum	Average	Variance		
In vivo stroma	3	2.015963834	0.671988	0.058252		
2D	3	2.596147473	0.865382	1.176596		
3D	3	2.683579559	0.894527	0.093504		
ANOVA						
Source of Variation	SS	df	MS	F	P-value	F crit
Between Groups	0.087774242	2	0.043887	0.099116	0.90709	5.143253
Within Groups	2.656705056	6	0.442784			
Total	2.744479299	8				

Lumican

Anova: Single Factor						
SUMMARY						
Groups	Count	Sum	Average	Variance		
In vivo stroma	3	7.763186031	2.587729	7.125008		
2D	3	5.833577831	1.944526	2.595416		
3D	3	3.262809867	1.087603	0.109478		
ANOVA						
Source of Variation	SS	df	MS	F	P-value	F crit
Between Groups	3.398402372	2	1.699201	0.518581	0.619813	5.143253
Within Groups	19.65980316	6	3.276634			
Total	23.05820553	8				

Aldh1a1

Anova: Single Factor						
SUMMARY						
Groups	Count	Sum	Average	Variance		
In vivo stroma	3	9.692010904	3.23067	16.21363		
2D	3	0.305534551	0.101845	0.013471		
3D	3	0.127371024	0.042457	0.001353		
ANOVA						
Source of Variation	SS	df	MS	F	P-value	F crit
Between Groups	19.95777962	2	9.97889	1.844702	0.237445	5.143253
Within Groups	32.45691373	6	5.409486			
Total	52.41469335	8				